Design, Synthesis and Biological Evaluation of 2,4-Disubstituted Pyrimidine Derivatives: Multifunctional Candidates as Potential Treatment Options for Alzheimer's Disease

by

Tarek Mohamed

A thesis
presented to the University of Waterloo
in fulfilment of the
thesis requirement for the degree of
Master of Science
in
Pharmacy

Waterloo, Ontario, Canada, 2011

AUTHOR'S DECLARATION

I hereby declare that I am the sole author of this thesis. This is a true copy of the thesis, including any required final revisions, as accepted by my examiners.

I understand that my thesis may be made electronically available to the public.

ABSTRACT

Alzheimer's disease (AD) is a highly complex and rapidly progressive neurodegenerative disorder characterized by the systemic collapse of cognitive function and formation of dense amyloid-β (Aβ) plaques and neurofibrillary tangles (NFTs). AD pathology is derived from the cholinergic, amyloid and tau hypotheses, respectively. Current pharmacotherapy with known anti-cholinesterases, such as Aricept ® and Exelon ®, only offer symptomatic relief without any disease-modifying effects (DMEs). It is now clear that in order to prevent the rapid progression of AD, new therapeutic treatments should target multiple AD pathways as opposed to the traditional "one drug, one target" approach. This research project employed medicinal chemistry tools to develop multifunctional small organic molecules against three key targets of AD pathology – the cholinesterases (AChE and BuChE), AChE-induced and self-induced $A\beta_{1\text{-}40}$ aggregation and generation (β-secretase). A chemical library composed of 112 derivatives was generated to gather structure-activity relationship (SAR) data. The derivatives were based on a novel, non-fused, 2,4-disubstituted pyrimidine ring (2,4-DPR) template with substituents at the C-2 and C-4 position varying in size, steric and electronic properties. Molecular modeling was utilized to investigate their binding modes within the target enzymes and along with the acquired SAR, the chemical library was screened to identify lead multifunctional candidates.

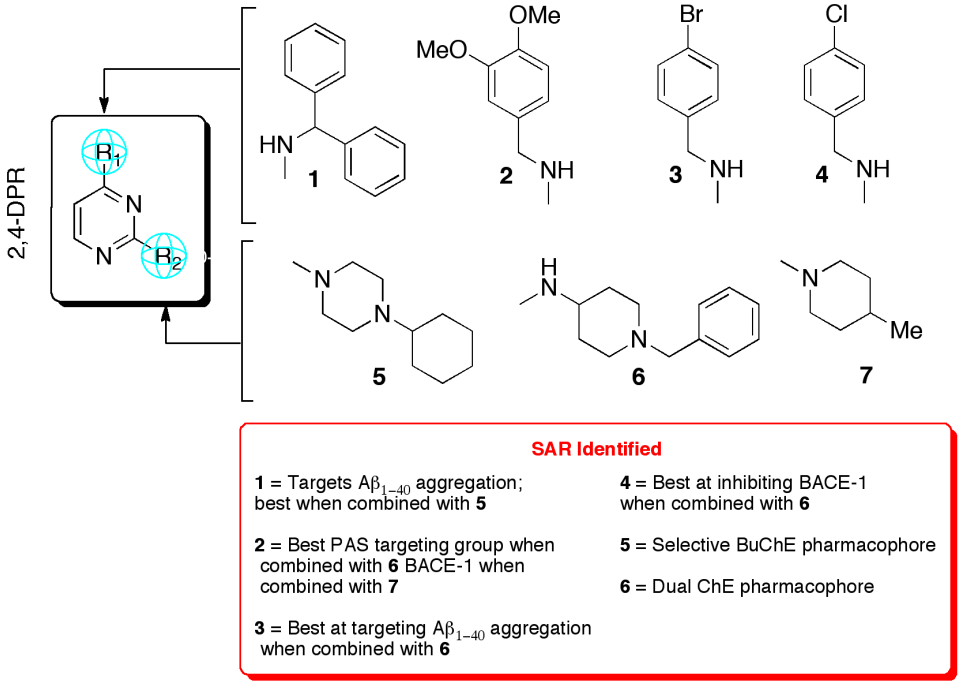

ACKNOWLEDGEMENTS

I would like to thank the School of Pharmacy and Department of Biology at the University of Waterloo for supporting the presented work. This work was also partially supported by the Alzheimer's Association (NIRG-08-91651) and the Alzheimer's Disease Research Center (NIH 3P50 AG005131). The NSF is also acknowledged for a CAREER Award to Dr. Jerry Yang (CHE-0847530).

I also acknowledge Jacky C. K. Yeung for his assistance with the project during his time with our research group as a volunteer RA. Collaborators involved with this project include: 1) Dr. Jerry Yang, X. Zhao, and L. K. Habib, University of California, San Diego (ran Aβ-aggregation and cell viability assays for some derivatives; 2) Dr. Michael Beazely and S. M. Vasefi, University of Waterloo (ran cell viability assay for some derivatives).

DEDICATION

I would like to dedicate the efforts presented here to my parents, Abeir and Mostafa, my younger sister, Yosra and my support network both close to and far from home. I also would like to extend my appreciation and thanks to my supervisor, Dr. Praveen N. Rao and my committee advisors, Drs. Michael Beazely and David R. Rose for their patience and support over the past two years.

TABLE OF CONTENTS

TABLE OF CONTENTS – cont'd

TABLE OF CONTENTS – cont'd

LIST OF FIGURES

LIST OF FIGURES – cont'd

LIST OF FIGURES – cont'd

LIST OF FIGURES – cont'd

LIST OF TABLES

LIST OF ABBREVIATIONS

2,4-DPR = 2,4-disubstituted pyrimidine ring

Aβ = Amyloid-β

ACh = Acetylcholine

AChE = Acetylcholinesterase

AChEI = Acetylcholinesterase inhibitor

ACID = APP intracellular domain

AD = Alzheimer's disease

ADAM = A disintegrin and metalloprotease

Aph-1 = Anterior pharynx-defective 1

Apo ε4 = Apolpoprotein ε4

APP = Amyloid precursor protein

ATCh = Acetylthiocholine

BACE = Beta-site APP cleaving enzyme

BuCh = Butyrylcholine

BuChE = Butyrylcholinesterase

BuChEI = Butyrylcholinesterase inhibitor

BuOH = Butanol

BuTCh = Butyrylthiocholine

CAS = Cationic active site

ChAT = Choline acetyltransferase

ChE = Cholinesterase

ChEI = Cholinesterase inhibitor

ClogP = Partition coefficient

CT = Catalytic triad

CTF = C-terminal fragment

LIST OF ABBREVIATIONS – cont'd

DCM = Dichloromethane

DIPEA = Diisopropylethylamine

DM = Diabetes mellitus

DMA = Disease-modifying agent

DME = Disease-modifying effect

DMP = Differential melting point

DTNB = dithiobis-(2-nitrobenzoic acid)

EDG: Electron-donating groups

EWG: Electron-withdrawing groups

EtOAc = Ethyl acetate

EtOH = Ethanol

FAD = Familial Alzheimer's disease

FRET = Fluorescence resonance energy transfer

HPLC = High-performance liquid chromatography

HREIMS = High-resolution electron ionization mass spectroscopy

IC_{50} = Concentration required for 50% inhibition

IMP = Integral membrane protein

IR = Infrared

$KMnO_4$ = Potassium permanganate

KPI = Kunitz-type serine protease inhibitor

mAChR = Muscarinic acetylcholine receptor

MAO = Monoamine oxidase

*m*CPBA = *meta*-chloroperoxybenzoic acid

MeOH = Methanol

$MgSO_4$ = Magnesium sulfate

MTT = 3-(4,5-dimethylthiazol-2-yl)-2,5-diphenyltetrazolium bromide

LIST OF ABBREVIATIONS – cont'd

MV = Molecular volume

nAChR = Nicotinic acetylcholine receptor

NAS = Nucleophilic aromatic substitution

NFTs = Neurofibrillary tangles

NMDA = *N*-methyl-D-aspartate

NTB = 2-nitro-5-thiobenzoic acid

PAS = Peripheral anionic site

PKC = Protein kinase C

PV = Pressure vial

RFUs = Relative fluorescence units

ROS = Reactive oxygen species

r.t = Room temperature

$sAPP_{\alpha/\beta}$ = Soluble APP fragment α/β

SAR = Structure-activity relationship

SGCC = Silica gel column chromatography

SI = Selectivity index

SODS = Superimposition of docked structures

TFA = Trifluoroacetic acid

TLC = Thin-layer chromatography

ThT = Thioflavin T

TNF = Tumor necrosis factor

NOMENCLATURE

Ac = Acetyl

Ar = Aryl

Bn = Benzyl

Boc = *t*-butoxylcarbonyl

Et = Ethyl

*i*Pr = *iso*Propyl

Me = Methyl

*n*Pr = normal Propyl

OMe = Methoxy

Ph = Phenyl

CHAPTER I

• Introduction •

1.1. Background on Alzheimer's Disease

Neurodegenerative diseases have a large socioeconomic impact on healthcare costs, patients and their care-providers. Alzheimer's disease (AD) is a rapidly progressive, neurodegenerative disease first described by Alois Alzheimer in 1907 [1-3]. Its demoralizing pathophysiology primarily affects elderly populations; however, genetic predispositions associated with the apolipoprotein ε4 (Apo ε4) allele are linked to its prevalence in middle-aged patients [4,5]. According to the Alzheimer's Association, the epidemiology of AD shows a doubling in the rate of disease development by 2050 with a current patient load of 5.4 million in the United States alone. Along with an estimated care cost of $202 billion in 2010, these factors collectively build on the unmet need to develop a safe and effective cure to AD [6].

Ever since the manifestation of Mrs. Auguste Deter's case in 1901 and the subsequent characterization of AD pathology in 1906, various hypotheses outlining its pathogenesis have been described [7]. These hypotheses branch off of the common physical and behavioral observations seen in AD patients such as cognitive impairment, dense amyloid-β (Aβ) plaques and neurofibrillary tangles (NFTs) leading to memory loss, depression, loss of independence and eventually death [6,8]. Although AD pathogenesis is mainly described by the cholinergic, Aβ and tau (τ) protein hypotheses, other subsequent mechanisms have emerged over the past few years expanding on its complex pathology (Fig. **1**). Of those mechanisms, pathways generating reactive oxygen species (ROS), neuroinflammatory responses and complications of diabetes mellitus (DM) have sparked keen interests in multi-disciplinary areas of AD research [1,9-17].

Most of the current AD pharmacotherapies on the market (Fig. **2**) are considered examples of a mono-targeted approach, where the end result is mild symptom relief and cognitive improvement, but lack an overall disease-modifying effect (DME). Galantamine (Fig. **2**) on the other hand, is an example of a disease-modifying agent (DMA) as it is a dual cholinesterase inhibitor (ChEI) and an allosteric enhancer of nicotinic acetylcholine receptors (nAChR) – collectively improving cholinergic neurotransmission [2,18].

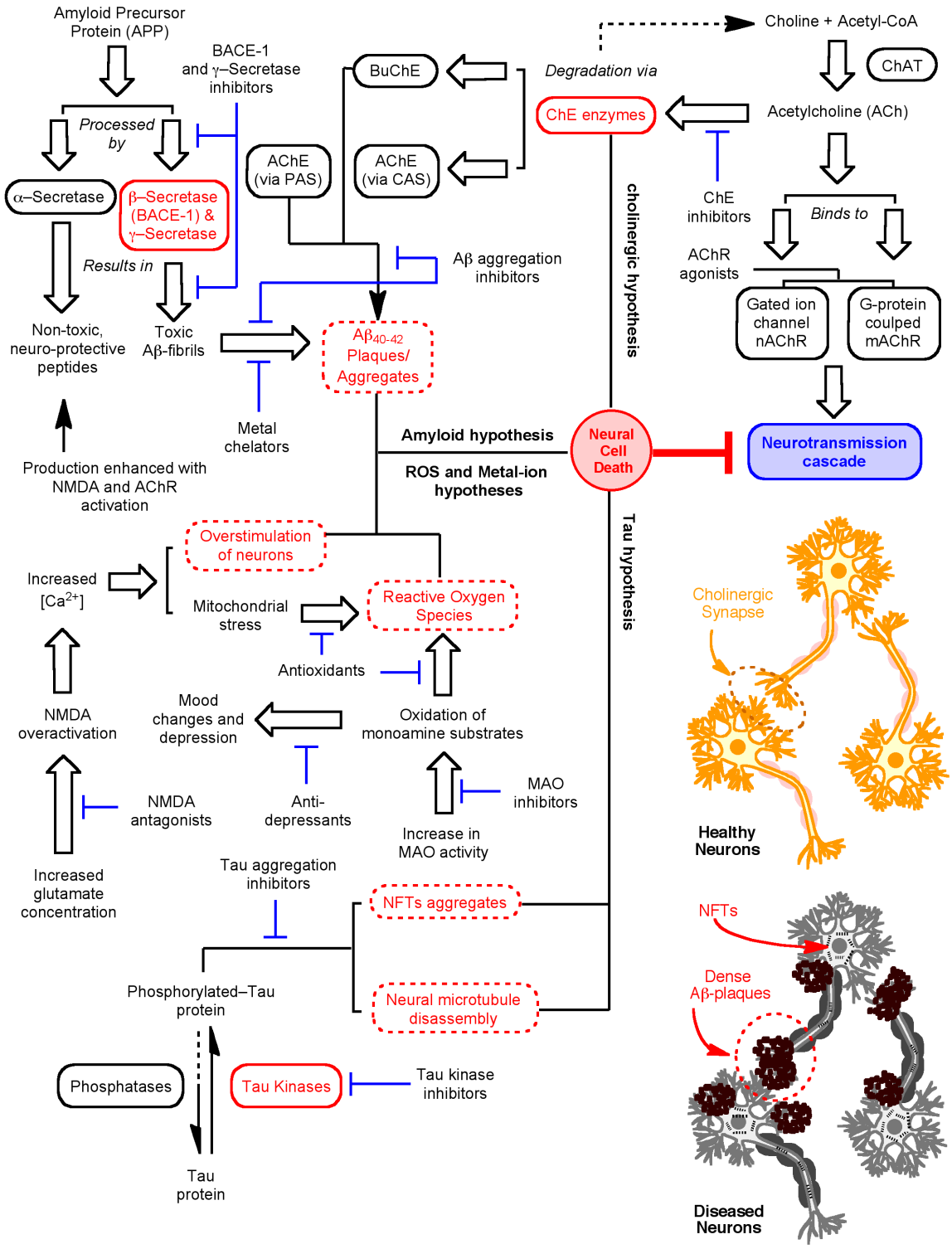

Fig. (**1**): Outline of AD pathophysiology.

A recent study also demonstrated galantamine's ability to inhibit self-induced aggregation of Aβ-fibrils and its respective cytotoxicity [19]. Supported by recent studies, current research efforts are abstaining from the "one drug, one target" approach in favour of generating multifunctional candidates in order to attain DMAs: a key step in halting the rapid progression of AD [20-24].

The thesis presented here is aimed at examining the potential of a novel class of small organic molecules, based on a 2,4-disubstituted pyrimidine ring (2,4-DPR) template, to act as DMAs for the treatment of AD: primarily evaluating anti-cholinesterase (ChE) and anti-Aβ dual activities. The template design concept is discussed in CHAPTER II.

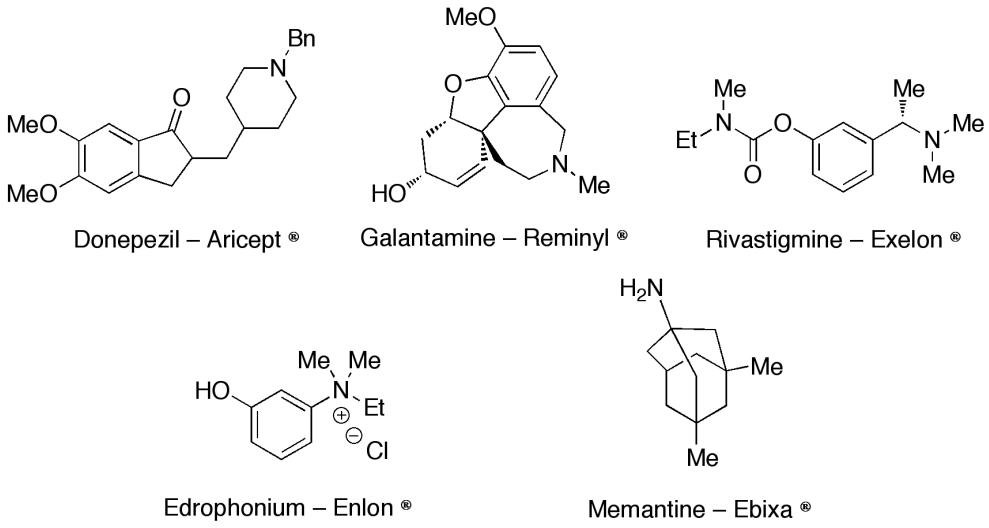

Fig. (**2**): Marketed AD pharmacotherapies.

1.2. The Cholinergic Hypothesis

This is one of the oldest and most studied hypotheses outlining the pathogenesis of AD. The hypothesis suggests that impairments in cholinergic neurotransmission, dependent on the neurotransmitter acetylcholine (ACh), are to blame for the rapid decline in cognitive ability of AD patients. The cholinergic branch of the CNS, primarily allocated within the cerebrum and cerebellum, is associated with cognitive function and overall physical awareness. Besides ACh, other key players in the cholinergic hypothesis are the ChE enzymes: Acetylcholinesterase (AChE) and butyrylcholinesterase (BuChE) – ACh degrading enzymes [1,3,8].

1.2.1. Cholinergic Neurotransmission

The cholinergic branches of the nervous system rely on ACh to initiate and transmit a neuronal impulse. This neurotransmitter is synthesized by choline acetyltransferase (ChAT) within cholinergic neurons by coupling choline and acetyl-CoA using an active site histidine residue [25]. Once released from storage vesicles into the synapse, ACh binds to nAChR or muscarinic G-protein coupled receptors (mAChR) to initiate a neurotransmission cascade [8,9,26]. Nicotinic receptors are mostly associated with the CNS, PNS and neuromuscular junctions, while mAChRs are mostly associated with the PNS but are also more widely distributed throughout the body [9]. Degradative ChE enzymes hydrolyze ACh to acetate and choline where the latter enters a high affinity re-uptake mechanism to be re-used for ACh synthesis in the presynaptic neuron [27].

With AD, the concentration of ACh is significantly reduced compared to that of non-AD patients due to the ChEs' rapid hydrolysis rate and impairments in ChAT's activity [26-28]. Without swift intervention, AD patients start to encounter difficulties with learning, memory recall and self-care. This ultimately leads to the systemic collapse of cognitive function within the CNS. Thus, pharmacotherapy targets to improve cognitive function in AD patients would include AChR agonists or ChEIs, where the majority of currently marketed therapies are derived from the latter class of agents (Table **1**, Fig. **2**).

Table (**1**): Comparison of currently marketed cholinergic pharmacotherapies.

Therapeutic Agent	Trade Name + Route of Administration	Mode of Action	Main Advantage	Main Disadvantage	Ref.
Donepezil	Aricept ® Oral	Potent AChEI	Long half-life (70 hours)	Mild-moderate side effects	[2]
Rivastigmine	Exelon ® Oral/transdermal patch	Dual ChEI	High brain selectivity	Short half-life and moderate side effects	[2]
Galantamine	Reminyl ® Oral	Selective AChEI	DMA (AChEI + nAChR agonist)	Potency and short half-life	[2]

On the other hand, a number of nAChR agonists are enrolled in clinical trials to assess their efficacy on improving cognitive function including the FDA-approved treatment for smoking addiction, varenicline (Chantex ®) [29,30]. Positive outcomes from those trials would be beneficial considering that the risk of developing AD amongst current smokers is higher than that of past and non-smokers [31].

1.2.2. The Cholinesterase (ChE) Enzymes

Classified as α/β hydrolase enzymes, the ChEs' primary role is to terminate the stimulatory action of ACh in the synapse; however, they are also involved in other cellular functions including cell-adhesion and embryonic development [32-35]. The two isoforms (AChE and BuChE) share a high degree of structural homology and around 51-54% sequence identity [32]. Once ACh binds within the enzyme catalytic site (CT), active site residues rapidly degrade the neurotransmitter to release choline and acetate (Fig. **3**).

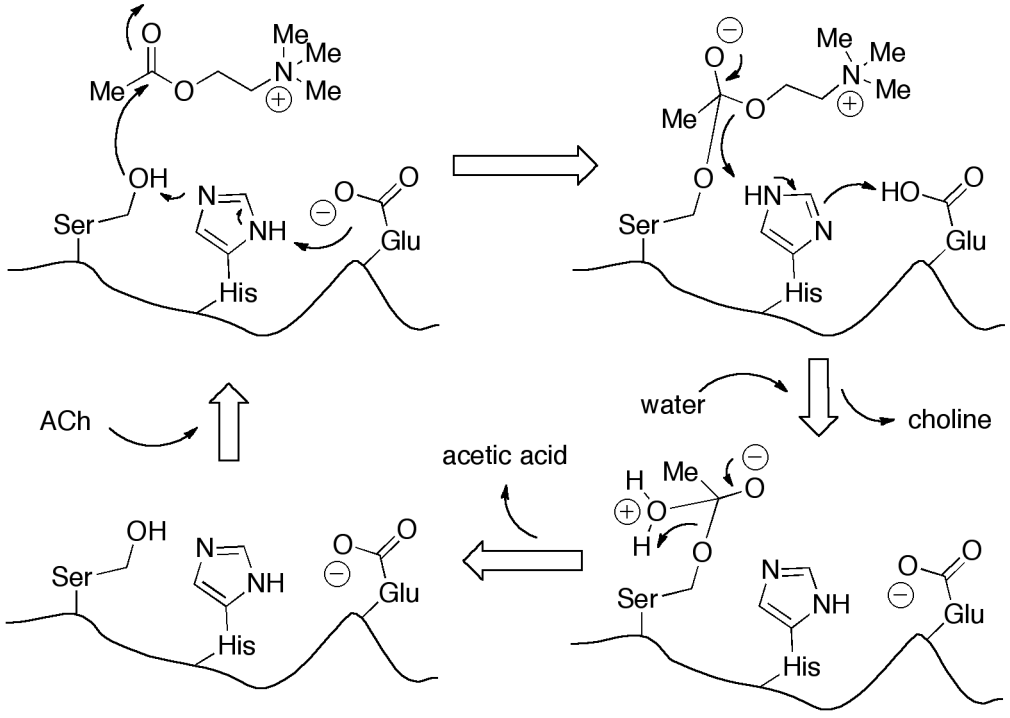

Fig. (**3**): ACh hydrolysis by the ChEs.

Due to the dynamic imbalance between the generation and degradation of ACh, the ChE isoforms are well-known targets for AD pharmacotherapies as they play a vital role in the pathology of AD. In fact, early marketed therapeutic agents against AD (e.g. Tacrine, Cognex ®) were derived from research into anti-cholinesterases [2].

The development of safe and effective ChEIs requires employing the key architectural differences and similarities associated with AChE and BuChE leading to their ligand specificity (Fig. **4**) [36]. Because AChE is primarily synthesized and localized within the cholinergic regions of the CNS, its concentration and actions there quickly dissipate after the onset of AD. On the other hand, BuChE is more widely

distributed within the body and with disease progression, the ratio of BuChE to AChE increases aiding in the transfer of AChE's degradative duties to the secondary/pseudocholinesterase [37-39]. This shift in the ChE ratio with disease progression constitutes the urgency in developing dual ChEIs in an effort to better manage patient symptoms at various stages of AD.

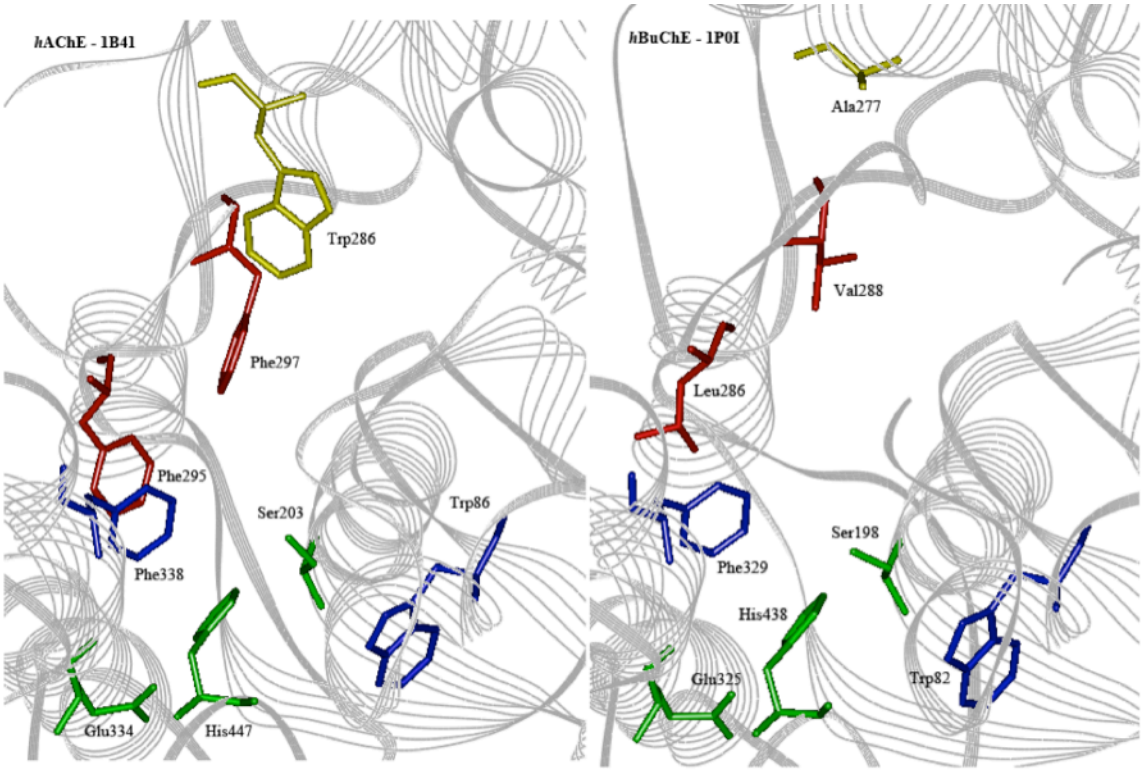

Fig. (**4**): Active site comparison between *h*AChE (PDB:1B41) and *h*BuChE (PDB:1P0I). *Green*: CT; *Red*: Acyl pocket; *Blue*: Hydrophobic stabilizing residues; *Yellow*: gorge entry (PAS – AChE).

1.2.2.1. Acetylcholinesterase (AChE)

With ACh as its natural substrate, AChE (EC 3.1.1.7) is widely recognized as the primary ChE enzyme, thus main inhibitory target of the cholinergic hypothesis [40,41]. As a serine hydrolase enzyme, AChE utilizes the commonly associated CT residues, histidine and serine, with the typical aspartic acid residue substituted for a glutamic acid [33,41]. These triad residues work systematically to activate the side chain hydroxyl group of serine to initiate the degradation of ACh (Fig. **3**).

This ChE isoform predominately exists in the CNS but is also found on the surface of erythrocytes and muscle tissue. Although the enzyme is encoded from a single gene on chromosome 7 in humans,

alternative mRNA splicing yields a variety of physiological forms ranging from monomers to sets of tetramers [41,42]. The more prominent form within the CNS is the amphiphilic membrane-bound tetramer [32]. The molecular architecture of AChE is unique in that its active site is located at the bottom of a 20 Å gorge with a secondary "back-door" channel believed to aid in the displacement of water molecules. The entry to the main gorge resembles a bottleneck, where aromatic residues (like tryptophan and tyrosine) line up the entry and contribute to its specificity [42]. Other important features of AChE include: i) the key stabilizing aromatic residues (Trp86 and Phe338 – *human* enzyme numbering) as part of the hydrophobic pocket; ii) Phe295 and Phe297 that form the acyl pocket that stabilizes the acetyl end of ACh and iii) Gly120, Gly121 and Ala204 that form the oxyanion hole used to stabilize the transition-state intermediate [43]. In addition, a peripheral anionic site (PAS) is located near the entry to the active site gorge and it is mainly marked with Tyr72, Tyr124 and more importantly, Trp286. Numerous studies implicate the PAS with AChE-induced aggregation of the Aβ fibrils, thus creating a highly neurotoxic AChE-Aβ complex [3,9,33, 44-48]. Highlights of human AChE's key features are presented in (Fig. **4**, left panel).

1.2.2.2. Butyrylcholinesterase (BuChE)

This secondary/pseudocholinesterase (BuChE, EC 3.1.1.8) is capable of hydrolyzing the cholinergic neurotransmitter ACh, although it is not its natural substrate. While it attains similar properties of the primary isoform, BuChE is unique in its ability to hydrolyze various types of natural and toxic esters such as the recreational alkaloid cocaine [49]. As a serine hydrolase, BuChE utilizes the same CT elements found in AChE – serine, histidine and glutamic acid – and follows the same hydrolysis mechanism described above (Fig. **3**) with varying kinetic parameters based on the concentration of ACh [50]. In contrast to AChE's localization, BuChE is more widely distributed throughout the body and is associated with the plasma, liver and various components of the nervous system [36,51]. The pseudocholinesterase is encoded from a single gene on chromosome 3 in humans and, as with AChE, variable splicing yields different physiological forms ranging from monomers to sets of tetramers [32,52]. In human plasma, the most prominent form is the soluble G4 tetramer, while variable dimers and tetramers occur within glial cells and the CNS [53].

The architecture of BuChE attains certain aspects seen in AChE; however, it is unique in other key areas as well. Although the active site gorge is also 20 Å below the enzyme surface, the entry to that gorge is far less restrictive as the number of aromatic residues in that region is lower than that found in AChE's gorge entry [51]. The key ligand-stabilizing aromatic residues found in the primary ChE are also present here (Trp82 and Phe329); however, smaller residues (Leu286 and Val288) replace Phe288 and Phe290 in the acyl pocket accounting for BuChE's wider substrate pool [54]. Since the gorge of BuChE contains fewer aromatic residues at both the entry and the active sites, the overall volume capacity of BuChE is approximately 200 $Å^3$ larger than that of AChE [55]. Another key feature of BuChE is the lack of a PAS at its gorge entry – Nonetheless, various studies suggested its association with neurotoxic aggregates in the brain via an undetermined mechanism [50,51]. Highlights of human BuChE's key features are presented in (Fig. **4**, right panel).

1.2.3. Summary

The cholinergic hypothesis is centered around ACh and its perspective neurotransmission cascades. Key aspects include the generation and degradation of ACh (ChAT and the ChEs, respectively) and the cascade receptors (nAChRs and mAChRs). Of all the hypotheses that describe AD pathogenesis, cholinergic dysfunction is the core physiological failure that occurs within the CNS. That said, it has been linked to the amyloid hypothesis (discussed next, *Section 1.3*) and that in itself, strengthens recent ideologies that AD is a highly complex neurodegenerative disease that can't be defined by nor limited to a single pathological mechanism. As discussed above, most of the currently marketed pharmacotherapies were derived from cholinergic research – specifically, anti-ChEs. Although those agents offer symptomatic relief, they lack DMEs to stop and reverse the progression of AD. Current research efforts are attempting to combine anti-ChE function with other pharmacotherapy targets to steer away from the "one drug, one target" approach.

1.3. The Amyloid-β Hypothesis

Medical complications involving the misfolding and aggregation of amyloid peptides have sparked exponential interest over the past few years. Several studies have implicated these insoluble aggregates in the direct and indirect pathologies of neurodegenerative diseases, various cancers and organ failures [9,56-60].

With respect to AD, the amyloid-β hypothesis is centered around the pathology of notorious amyloid-β aggregates. These insoluble plaques wreak havoc on internal and external cellular mechanisms leading to neuronal cell death and corroborating cognitive dysfunction. Key aspects here include the amyloid precursor protein (APP), the APP processing secretase enzymes and the aggregation mechanisms that produce these neurotoxic proteinaceous Aβ-plaques (Fig. **1**).

1.3.1. Amyloid Precursor Protein

As its name suggests, APP is the precursor substrate to amyloid-β peptides. The APP is a large, integral membrane protein (IMP) that is ubiquitously expressed in mammalian cells and concentrated in the CNS [61-63]. Although it plays a fundamental role in the amyloid-β hypothesis, various studies report putative physiological roles for APP including: i) cell adhesion; ii) metal-ion homeostasis; iii) cell signaling and iv) synapse formation, function and elasticity [61,64,65]. A single gene (~ 240 kbps) on chromosome 21 encodes human APP. Alternative splicing generates various isoforms of APP ranging from 365-770 amino acids in length. Isoforms encoding the Aβ-peptide are dubbed APP695, APP751 and APP770, where the foremost is mainly expressed in neuronal tissues [61].

The architecture of APP is quite interesting (Fig. **5**). Its extracellular domain accounts for the bulk (~90%) of this IMP and is comprised of the E1 and E2 domains, where the former contains a conserved metal binding motif and a growth factor-like domain. A Kunitz-type serine protease inhibitor (KPI) domain divides the E1 and E2 domains but it is only present in the APP751 and APP770 isoforms and two key glycosylation sites are located downstream of the E2 domain. With respect to the embedded Aβ-peptide, the bulk of its sequence (~70%) is part of extracellular domain with the remaining 30% belonging to the transmembrane domain [1,61-63,66,67]. The intracellular domain (AICD) is highly conserved and is believed to act as a transcriptional regulator as it is translocated to the nucleus after APP has been

processed by the secretase enzymes [68]. The AICD also contains a key Thr668 residue that is susceptible to phosphorylation by various kinases that allow for APP to interact with different adaptor proteins and the phosphorylation state of this residue also plays an important role in APP localization. Recent studies also discovered high levels of phosphorylated Thr668-APP compared to healthy/control groups suggesting a role for this residue in AD pathology [61].

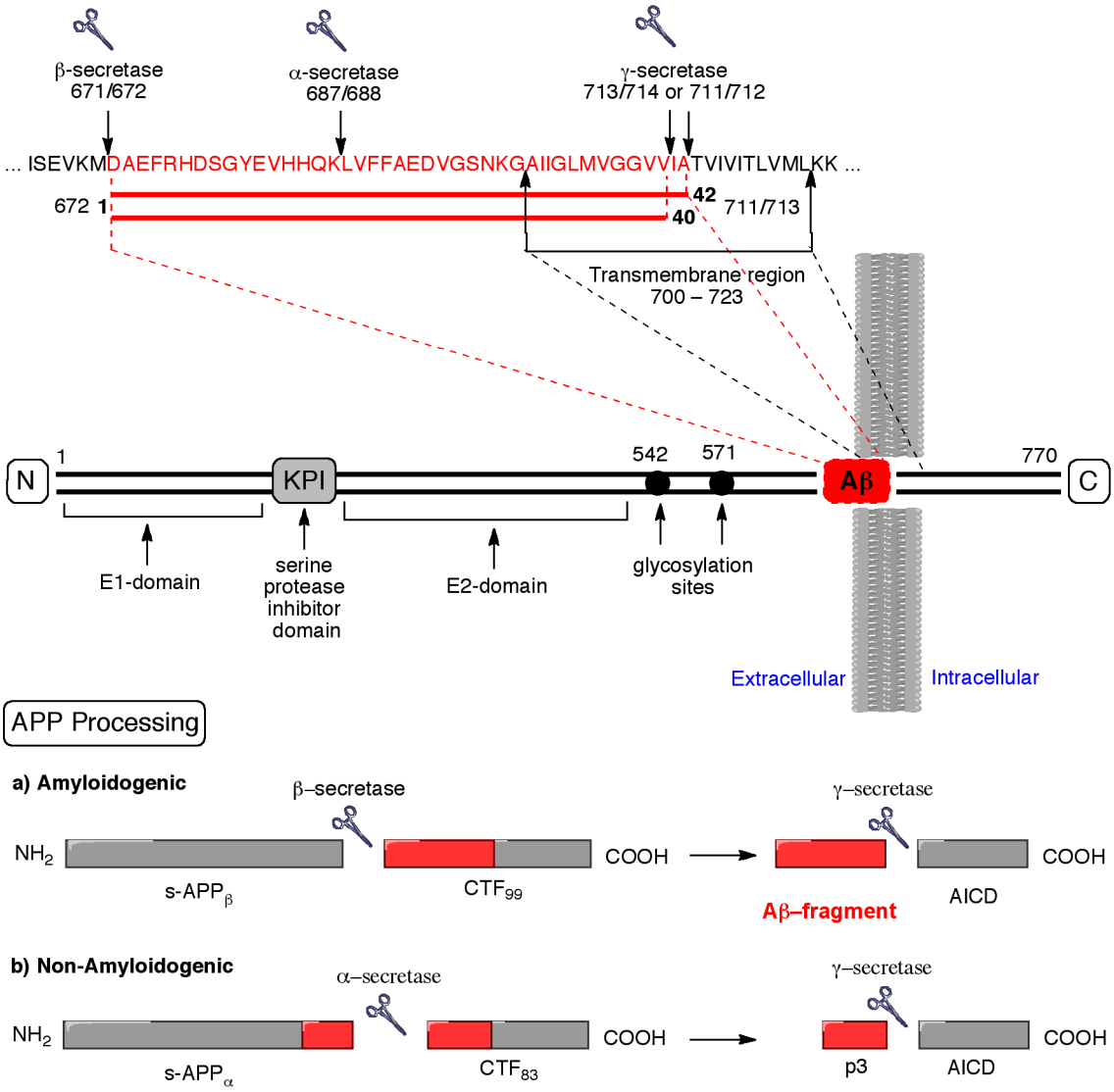

Fig. (**5**): APP architecture and processing. ** Numbering based on the APP770 isoform*

Mutations in the critical regions of the APP gene can potentiate the development of AD by increasing the overall production of Aβ-peptides. Some mutations occur within and some occur outside the Aβ-peptide sequence. The most studied mutations of the APP gene are the Swedish, Flemish, Dutch, Florida and London (Table **2**). These mutations don't include other factors such as Down's syndrome and Presenilin-1 and -2 (PS1, PS2) mutations that are also linked to disrupting the APP processing balance [69].

Table (**2**): APP mutations leading to the overall increase in Aβ-peptide liberation.

Name	Location	Mutation	Biochemical Effect	Molecular Effect	Ref.
Swedish	Upstream Aβ-Sequence	Lys670Asn Met671Leu	Enhance β-secretase	Increase toward amyloidogenic APP processing	[69]
Flemish	Within Aβ-Sequence	Ala692Gly	Inhibit α-secretase	Increase toward amyloidogenic APP processing	[69]
Dutch	Within Aβ-Sequence	Glu693Gln	Enhanced fibrillogenesis	Hereditary cerebral hemorrhage w/ amyloidosis	[63]
Florida	Downstream Aβ-Sequence	Ile716Val	Alter γ-secretase cleavage	Increase the amount of $A\beta_{1-42}$ liberated	[69]
London	Downstream Aβ-Sequence	Val717Phe, Gly or Ile	Alter γ-secretase cleavage	Increase the amount of $A\beta_{1-42}$ liberated	[69]

1.3.2. APP Metabolism and Processing Pathways

Although APP is involved in many cellular functions, it exhibits a short half-life and thus, is under a constitutive secretory pathway [61]. Its processing is governed by the activity of the secretase enzymes (α-, β- and γ-secretases) and interestingly, is influenced by AChRs – a link between the cholinergic and amyloid hypotheses. [70]. The proteolytic cleavage of APP can be divided into two main branches based on the secretases involved: amyloidogenic and non-amyloidogenic.

The amyloidogenic pathway is of greater interest with respect to AD pathology as the resulting APP products include the $A\beta_{1-40}$ or $A\beta_{1-42}$ peptide that constitutes a major role in the amyloid hypothesis. In this metabolic pathway, β-secretase or β-site APP cleaving enzyme (BACE) is the primary protease acting on APP. The cleavage between Met671 and Asp672 generates a large soluble peptide ($sAPP_{\beta}$) and a 99-amino acid C-terminal fragment (CTF_{99}) carrying the Aβ-fragment. γ-secretase cleaves the CTF_{99} between Ala713 and Trp714 or Val711 and Ile712 to release the $A\beta_{1-42}$ or $A\beta_{1-40}$ peptide, respectively along with the AICD [62,71-73] (Fig. **5**). In contrast, the non-amyloidogenic pathway is initiated by α-secretase. The cleavage between Lys687 and Leu688 generates a larger soluble peptide ($sAPP_{\alpha}$) with neuroprotective properties and an 83-amino acid C-terminal fragment (CTF_{83}) [74,75]. Because α-secretase's cleavage pattern occurs

within the Aβ-fragment, the resulting CTF_{83} does not carry a complete and functional Aβ-fragment. γ-secretase cleaves the CTF_{83} to release a small p3 peptide and the AICD [61-63] (Fig. **5**).

It is noteworthy that both metabolic pathways occur in healthy individuals and that suggests that the liberation of Aβ-peptides itself is not an AD characteristic. The non-amyloidogenic branch is the most common metabolic pathway but when the amyloidogenic pathway does occur, efficient clearance mechanisms are in place to remove the Aβ-peptides [63,76]. In the amyloid hypothesis, AD pathogenesis emerges when the balance between the APP metabolism and processing pathways, in addition to the generation and clearance of Aβ-peptides, is disrupted resulting in the rapid accumulation of Aβ-peptides that aggregate to form insoluble and neurotoxic species in the CNS.

1.3.3. The Secretase Enzymes

These are transmembrane protease enzymes involved in the metabolism and processing of APP via the amyloidogenic pathway to generate either $A\beta_{1-40}$ or $A\beta_{1-42}$ peptides (BACE-1 and γ-secretase metabolic pathway) or the non-amyloidogenic pathway to generate a neuroprotective soluble peptide (α- and γ-secretase metabolic pathway) (Fig. **5**). Key features of the secretases will be briefly discussed below.

As the initiator of the amyloidogenic metabolic pathway of APP, BACE-1 (EC 3.4.23.66) is a key pharmacotherapy target in an effort to reduce the overall generation of the pro-Aβ-peptide CTF_{99}. This is a membrane bound, aspartic protease where optimal activity is observed in acidic environments – a typical protease property [77,78]. Interestingly, two BACE homologues exist sharing ~ 45% sequence identity and ~ 75% structural homology. The key isoform, BACE-1, is encoded by a single gene on chromosome 11 and is mainly expressed in neuronal tissue – more notably the hippocampus, cortex and cerebellum [79]. On the other hand the secondary isoform, BACE-2, is mapped on chromosome 21 and, unlike BACE-1, is expressed in various tissues but is barely detectable in the brain and recent studies suggest BACE-2 acting as an antagonist to BACE-1 or an alternative α-secretase [62,78,80,81]. In terms of its architecture, the narrow cleft-like active site is located in the center of the enzyme between the extracellular N-terminal and intracellular C-terminal lobes. The active site is sealable with a flexible, 10-residue hairpin loop or 'flap' with Tyr71 playing a key role in controlling the dynamics and conformations of that flap [82,83]. Upon substrate binding, the flap closes down on the active site entry and re-opens to release hydrolysis products;

the overall variance in the position of the flap ranges between 5-7 Å [83,84]. The catalytic residues, Asp32 and Asp228 are part of a large hydrogen-bond network mainly comprised of polar residues (e.g. Thr232, Ser35) and water molecules, where the latter is an essential part of the proteolytic mechanism (Fig. **6**) [84,85].

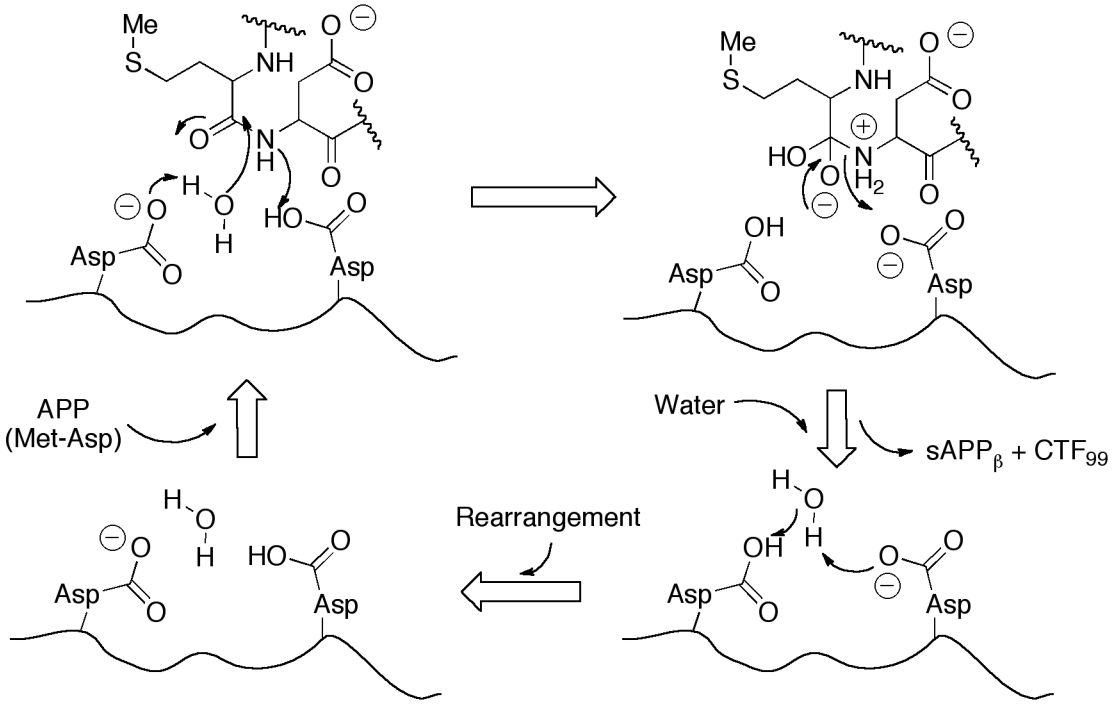

Fig. (**6**): BACE-1 proteolytic mechanism of APP. **Substrate shown reflects the peptide bond between Met671 and Asp672 of APP770 isoform*

In its unbound form, studies suggest that the protonation state of the aspartic acids is di-deprotonated (*not depicted above*), while it maintains a mono-protonated state with a bound substrate; these conformations are affected by pH and water networks within the enzyme [82]. Besides the catalytic site, several sub-site pockets have been identified and their primary goal is to stabilize and orient incoming substrates. Some of these sub-site pockets include: i) S_1 and S_3 – mainly consist of hydrophobic residues; ii) S_2 and S_4 – mainly consist of hydrophilic residues and iii) S_5 to S_7 – localize near the insertion helix and are primarily used for substrate recognition [84,86]. Highlights of human BACE-1's key features are presented in (Fig. **7**).

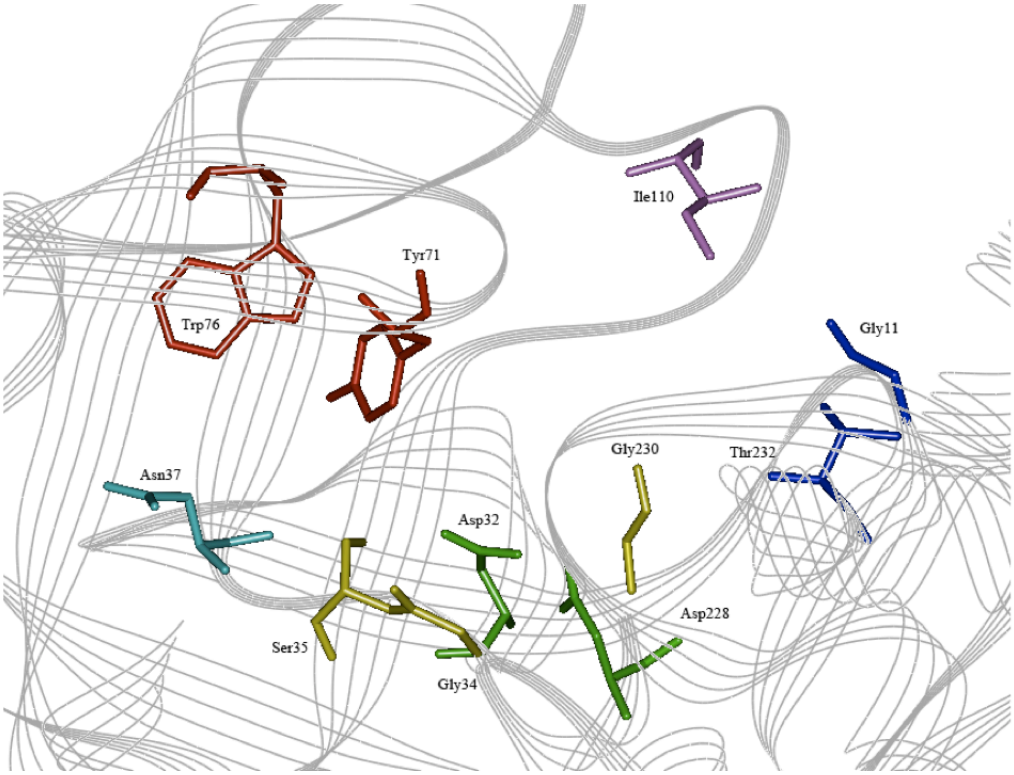

Fig. (**7**): Active site of *h*BACE-1 (PDB:1FKN). *Green*: Catalytic site; *Red*: Flap; *Purple*, *Turquoise* and *Blue*: Some hydrophobic and hydrophilic residues of the various sub-site pockets in BACE-1; *Yellow*: Other key residues - part of the hydrogen-bond network.

In contrast, α-secretase is the initiator of the more dominant, non-amyloidogenic pathway of APP. Classified as a disintegrin and metalloprotease (ADAM – EC 3.4.24.81), α-secretase isoforms include ADAM10 and ADAM17/TACE, with the latter being involved in the processing of a variety of type-1 membrane glycoproteins such as pro-tumor necrosis factor-α (pro-TNF-α). The more prominent zinc-metalloprotease isoform, ADAM10, is encoded on chromosome 15 and its activity is regulated through constitutive and inducible components, where the latter is under the control of protein kinase C (PKC) [62,74,87]. As discussed earlier, the non-amyloidogenic metabolic pathway disrupts the Aβ-fragment and generates s-APPα with neurotrophic and neuroprotective properties, which supports the hypothesis that over-activation/stimulation of α-secretase should reduce amyloidogenesis [74,75,87] (Fig. **5**).

As the final protease involved in APP processing, the end products of γ-secretase's activity depends on the competition between BACE-1 and α-secretase for the APP substrate and the resulting CTF: amyloidogenic CTF_{99} or non-amyloidogenic CTF_{83} (Fig. **5**). Compared to the preceding proteases, γ-secretase is a larger, multi-complex aspartyl protease comprised of PS1, nicastrin, anterior pharynx-

defective 1 (Aph-1) and PS2 with numerous studies linking certain mutations in the presenilin genes (*PSEN1* on chromosome 14 and *PSEN2* on chromosome 1) to early on-set and familial Alzheimer's disease (FAD) cases [62,69,88]. Similar to α- and β-secretases' range of substrates, γ-secretase is known to act on a wide range of glycoproteins and other substrates, including the Notch protein – a vital component in the cell signaling pathway [89-94]. In most cases, γ-secretase generates the $A\beta_{1-40}$ fragment with the generation of the $A\beta_{1-42}$ being less frequent. However, it is noteworthy that the $A\beta_{1-42}$ peptide is more hydrophobic and is more susceptible to aggregation leading to the insoluble neurotoxic plaques [62]. On the other hand, some studies suggest that the AChE-$A\beta_{1-40}$ complexes are more neurotoxic compared to other aggregates [95].

1.3.4. Aggregation and Toxicity Mechanisms

As Aβ elimination mechanisms start to deteriorate, Aβ-peptides accumulate in the CNS where their neurotoxic properties take affect. Aβ-peptides can take on many forms – oligomers, fibrils and aggregates/plaques –, each having a unique biochemical formation mechanism but all start with the monomeric Aβ-fragment released by γ-secretase (Fig. **8**). Factors implicated in turning monomeric Aβ to neurotoxic species include: i) biophysical properties of Aβ itself; ii) AChE PAS and iii) certain metal-ions.

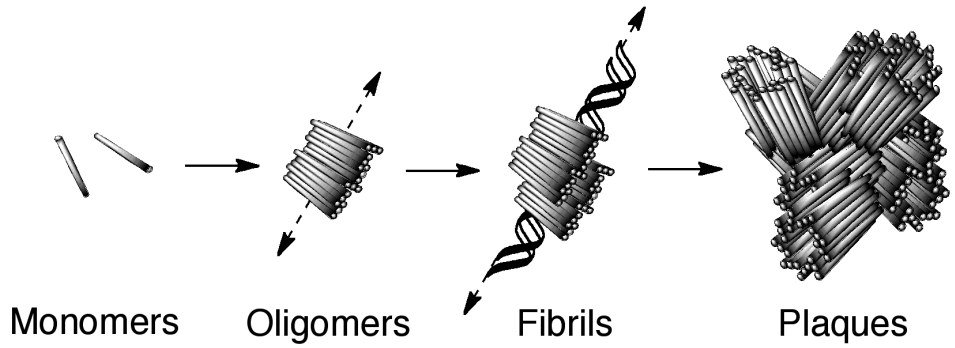

Fig. (**8**): Transformation of Aβ-monomers into various soluble and insoluble forms.

The biophysical properties of Aβ allow it to self assemble at high concentrations (μM range) and acidic conditions. With disease progression, the transport of Aβ monomers to the lysosome for degradation is hindered thus the extracellular concentration of Aβ increases facilitating self-assembly and oligomerization [96]. As this patterns continues, these small oligomers grow in size, taking on a cross-β-

sheet assembly conformation, to generate Aβ-protofilaments and two protofilaments intertwine to form an Aβ-fibril. These structures can continue to grow in size, aggregate and form dense, insoluble plaques [97]. In connection to the cholinergic hypothesis, numerous studies have demonstrated the role of the PAS of AChE in promoting Aβ aggregation. The architecture of the PAS (mainly aromatic residues) is believed to provide suitable conditions for monomeric or small oligomeric forms of Aβ to assemble into larger, insoluble aggregates [3,9,33, 44-48]. Similarly, metal ions, especially copper (Cu^{2+}), iron (Fe^{3+}) and zinc (Zn^{2+}), are known to facilitate the aggregation of Aβ-peptides through the metal-ion coordinating domain at the N-terminal end. Three conserved histidine residues (His6, His13 and His14) play an essential role in the coordination of the bound metal-ion and it is noteworthy that APP itself has a highly conserved metal-ion binding domain at its N-terminal end [98-105]. In its interactions with the above metal species, these Aβ-metal ion complexes engage in various redox reactions leading to the generation of reactive oxygen species (ROS) [106].

1.3.5. Summary

The amyloid-β hypothesis is mainly centered around Aβ-peptides. It is evident that the mechanisms involved are very complex with numerous factors leading to the disruption in the balance between the generation and clearance of Aβ-peptides. Various studies have demonstrated the impact of Aβ-species on cellular structure and function; these impacts include the disruption of membrane integrity, transport and ion channels and the decrease in cholinergic efficiency, among others. As mentioned earlier, the cholinergic and amyloid hypotheses cross paths with AChE implicated in the facilitation of Aβ aggregates as well as AChRs influencing APP processing mechanisms.

Anti-amyloid strategies are directed at reducing the generation or aggregation of Aβ-peptides – those include the development of: i) BACE-1 inhibitors; ii) γ-secretase inhibitors; iii) metal-ion chelators; iv) AChE-PAS blockers and v) Aβ anti-bodies. Although, there has yet to be an approved treatment option listed under one of the above strategies, a number are undergoing clinical trials to assess safety and efficacy. It is noteworthy that developing an agent capable of blocking the generation and/or aggregation of Aβ-peptides possesses a DME and along with an anti-cholinesterase profile, a candidate multifunctional pharmacotherapy option is within reach.

1.4. Other Factors in AD Pathology

The cholinergic and amyloid hypotheses govern this research project; however, it is important to address other key factors in AD pathology. Of those, the pathological mechanism involving tau (τ) is of great interest in AD research. Unlike extracellular amyloid plaques, neurofibrillary tangles (NFTs) cause significant internal damage to the neuron. Complications involving tau (τ) protein arise when the balance between tau (τ) kinases and phosphatases are disrupted resulting in hyperphosphorylation of the tau (τ) protein. In such a state, tau (τ) protein dissociates from microtubules, in turn distorting cellular integrity, and aggregate to form NFTs. Targeting tau abnormalities is challenging considering its regulatory mechanism involves a wide range of protein kinases (including Cdk5 and GSK-3β) and phosphatases that are crucial to other biological pathways [107-111]. Secondary hypotheses involve *N*-methly-D-aspartate (NMDA) excitotoxicty, monoamine oxidase (MAO) enzymes and neuroinflammatory pathways (Fig. **1**). With NMDA excitotoxicty, the elevated levels of glutamate result in over-activation of NMDA receptors leading to a large influx of Ca^{2+} ions and this leads to excitotoxicity and neuronal degeneration [112]. Along with the generation of peroxides as part of its oxidation mechanism, recent studies have reported elevated levels of MAO activity in AD patients, sparking a potentially new pathological hypothesis for AD. Neuroinflammatory responses have been linked with the formation of Aβ-plaques and NFTs and recent studies have implicated the COX-1 isoform of the cyclooxygenases, the 12-/15-LOX isoforms of the lipooxygenases as well as the pro-inflammatory cytokine TNF-α [113-117]. Interestingly, promising results were observed with the long-term use of non-steroidal anti-inflammatory drugs (NSAIDs) – selective COX-1 inhibitors – but not with the use of coxibs – selective COX-2 inhibitors –, suggesting the localization of those isoforms is important to the pathology of AD [2,113,117].

1.5. Chapter Conclusion

It is evident that AD pathology is complex. Numerous factors are involved and the end result is systemic collapse of cholinergic neurotransmission along with neuronal cell death, collectively leading to dementia symptoms (Fig. **1** and **9**). With the majority of current pharmacotherapy options only offering symptomatic relief, it is crucial to enroll more candidate agents in clinical trials to assess their safety and

efficacy. These up and coming agents need to possess DMEs and act as multifunctional pharmacotherapy options.

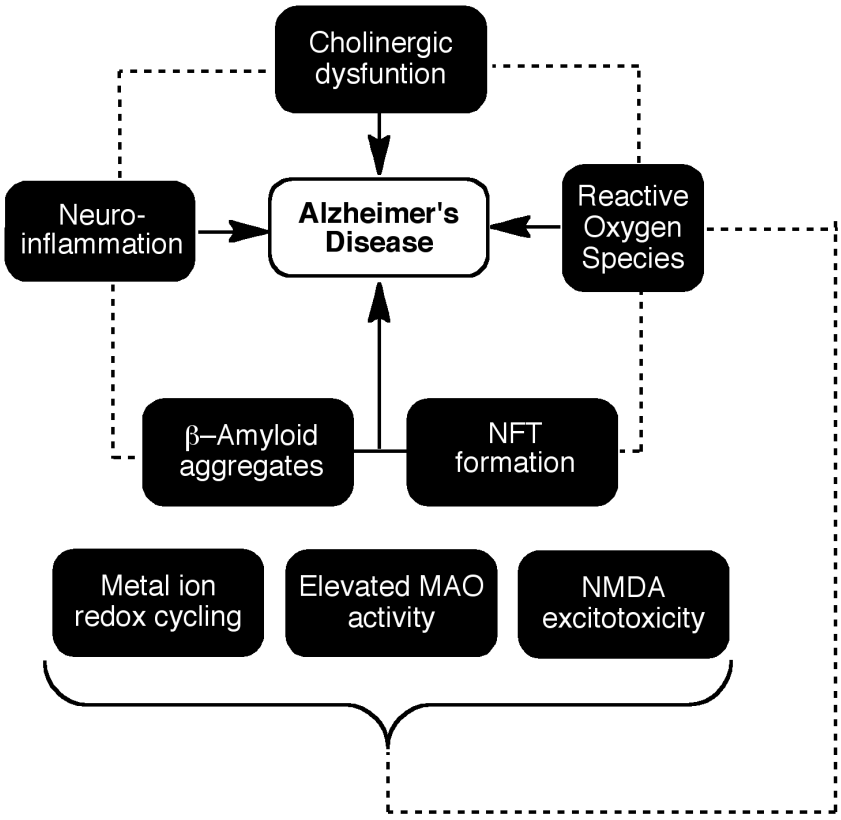

Fig. (**9**): Summary of pathological routes to AD

CHAPTER II

• Hypothesis and Design Rationale •

2.1. Template Design

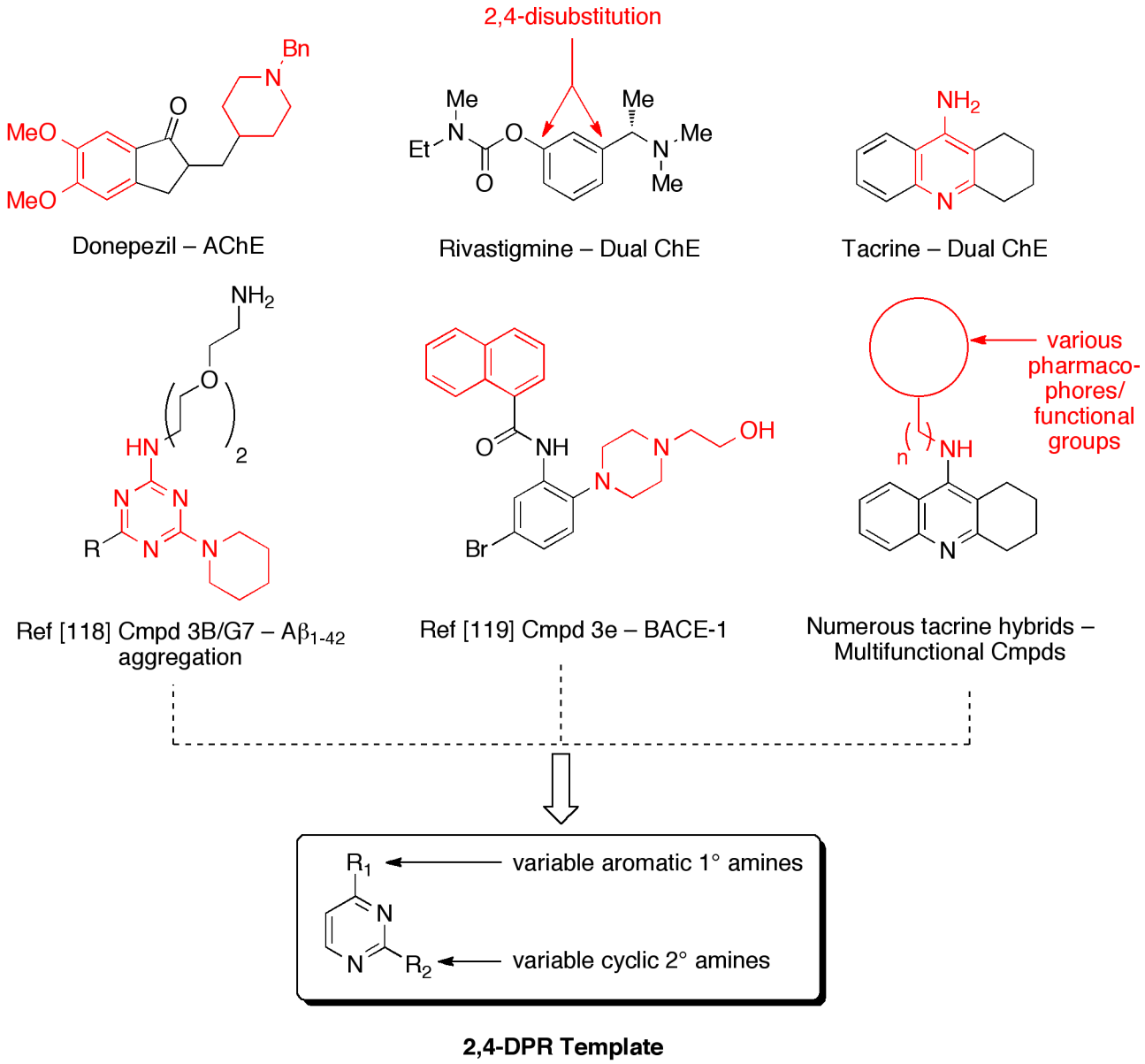

Fig. (**10**): 2,4-DPR template design concept based on key functional groups of marketed pharmacotherapies and other research candidates.

The goal of this research project was to develop a novel template that can be used to generate a chemical library capable of targeting multiple pathological mechanisms leading to AD. The novel template

design concept was attained by assessing recent research efforts, current therapeutic agents and molecular modeling studies. Key functional groups were identified (*red*, Fig. **10**) and collectively, a 2,4-DPR was hypothesized to serve as a suitable template to generate a chemical library capable of targeting the ChEs and amyloid-β parameters.

2.2. Target Derivatives

The basis of the chemical library is based on generating compounds with varying steric and electronic properties to assess those impacts on the biological profile of the derivative and aquire SAR data (Fig. **11**). Examples of such comparisons include evaluating: i) bioisosteres (e.g. piperidine vs. piperazine); ii) steric effects (e.g.: *i*Pr vs. *n*Pr); iii) positional isomers (*para*- vs. *meta*- vs. *ortho*) and iv) effect of electron-donating and withdrawing groups (EDGs and EWGs; respectively).

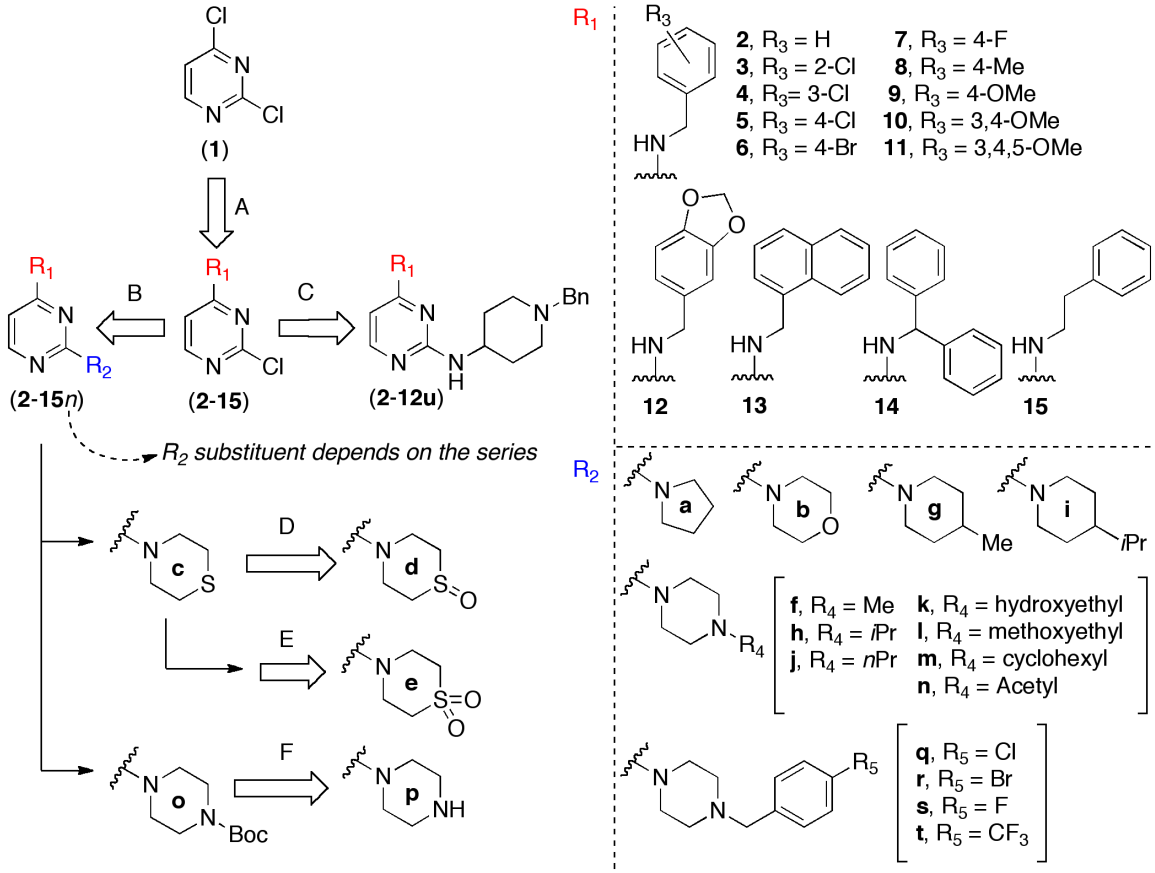

Fig. (**11**): Overview of the synthetic routes to target derivatives.

CHAPTER III

• Setup and Methodology •

3.1. Synthetic Chemistry

The synthetic routes to target derivatives were relatively simple and efficient, requiring a maximum of three steps to achieve the required coupling or modification.

3.1.1. Intermediate Product Synthesis – *Step A*

Necessary intermediates were synthesized via a nucleophilic aromatic substitution (NAS) reaction at the C-4 position of the ring system as shown in Fig. **12**.

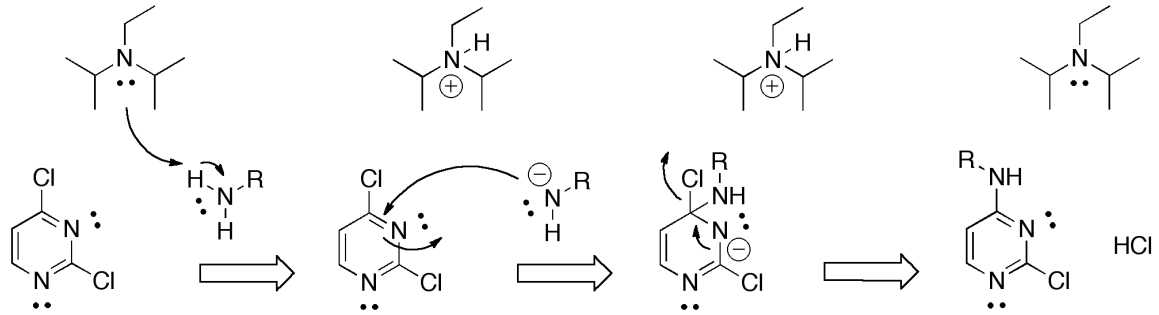

Fig. (**12**): NAS mechanism used to generate target intermediates with primary amines at C-4 position.

The 2,4-dichloropyrimidine starting material (**1**, Fig. **11**) was converted to the 2-chloro-4-substituted-pyrimidine intermediates (**2-15**, Fig. **11**) in the presence of diisopropylethylamine (DIPEA, a base) to activate the respective primary amine used (R_1 = benzylamine, 2-, 3-, 4-chloro, 4-bromo, 4-fluoro, 4-methyl, 4-methoxy, 3,4-dimethoxy, 3,4,5-trimethoxybenzylamines, benzo[*d*][1,3]dioxol-5-methylamine, naphthalen-1ylmethylamine, diphenylmethylamine or phenylethylamine; respectively).

This reaction (*Step A*, Fig. **11**) was run in ethanol (EtOH) and typically refluxed for 4-5 hrs with stirring. The resulting solution is evaporated in vacuo, re-dissolved in ethyl acetate (EtOAc), neutralized using 0.5M hydrochloric acid solution and washed with concentrated brine solution (3x15 mL). Collected organic fractions were dehydrated using anhydrous magnesium sulfate ($MgSO_4$), filtered and re-evaporated

in vacuo to afford a crude solid or semi-solid intermediate. Purification was performed using a differential melting point (DMP) technique and/or silica gel column chromatography (SGCC) with a suitable carrier solvent (Fig. **13**). Intermediate product yields ranged from 55-75% [120-122].

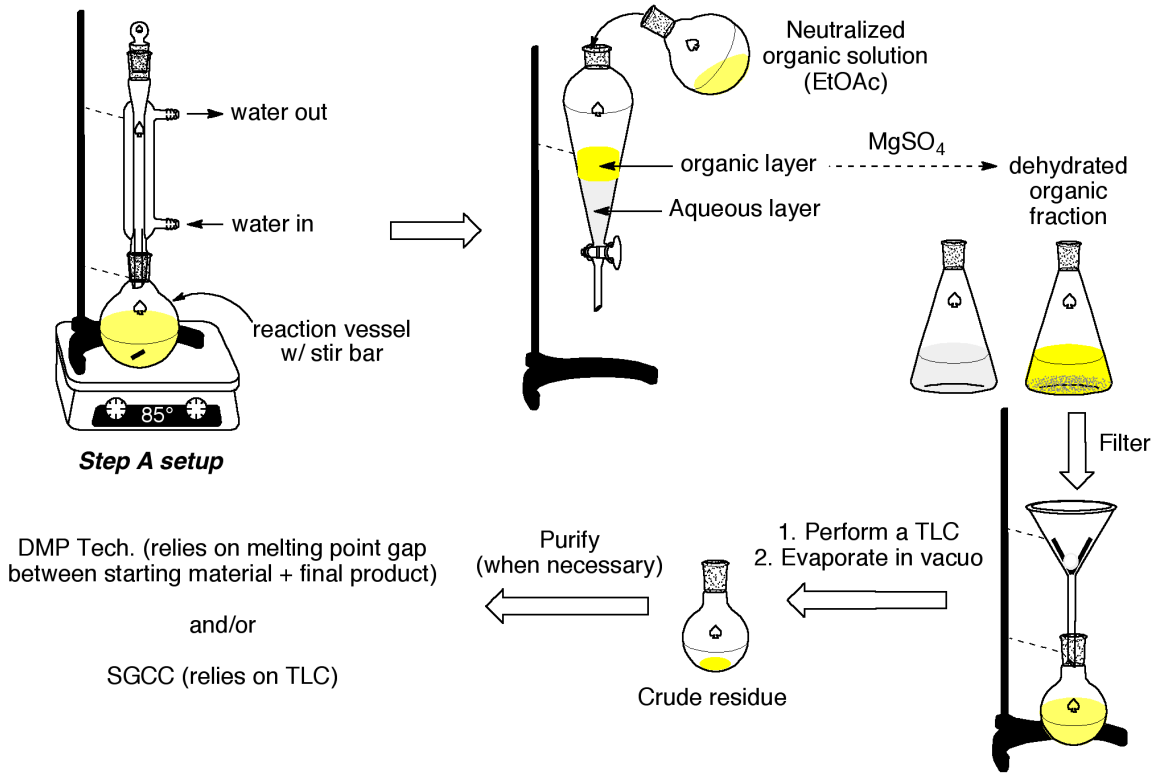

Fig. (**13**): Overview of –Step A– setup

3.1.2. Final Product Synthesis – *Step B* + *C*

To obtain the desired final products, intermediates **2**-**15** were coupled with the respective secondary cyclic amines (*Step B*, R_2 = pyrrolidine, morpholine, thiomorpholine, methylpiperazine, methylpiperidine, isopropylpiperazine, isopropylpiperidine, propyl-, hydroxyethyl-, methoxyethyl-, cyclohexyl-, acetyl-, Boc-piperazine, 4-chloro, 4-bromo, 4-fluoro or 4-trifluoromethylbenzylpiperazine; respectively) or 4-aminobenzylpiperidine (*Step C*). These were also NAS reactions that occur at the C-2 position of the ring system as shown in Fig. **14**.

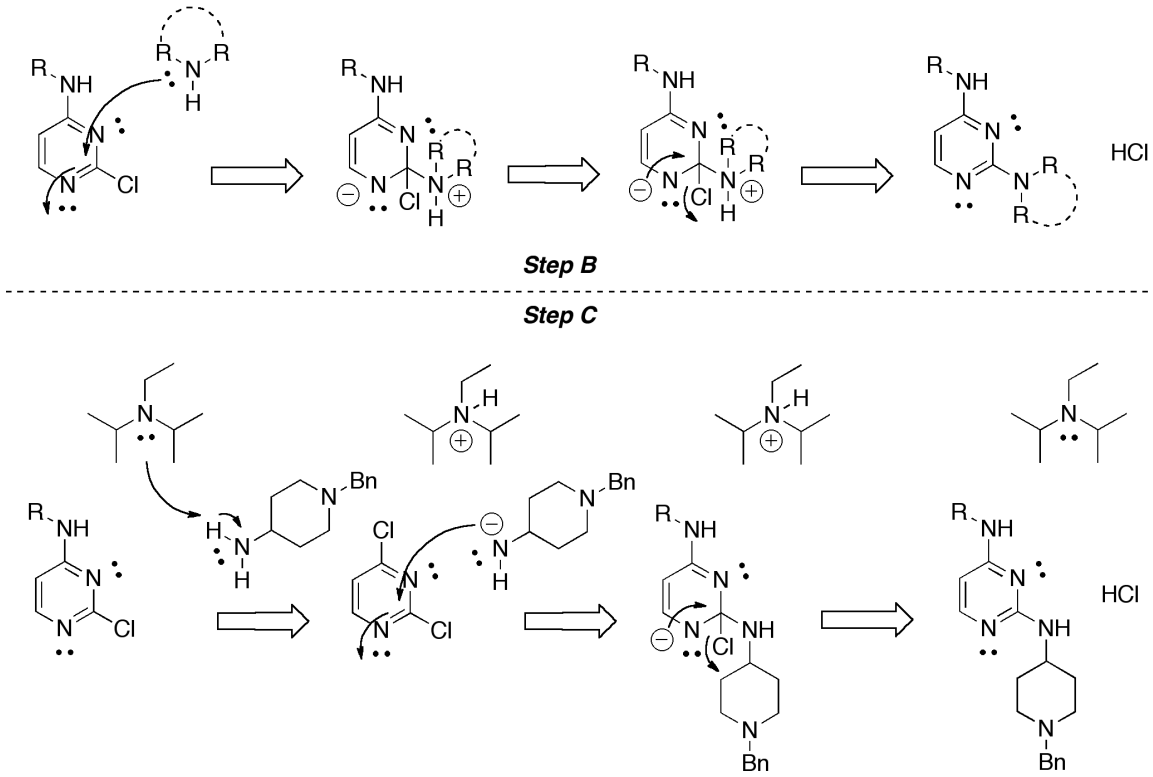

Fig. (**14**): NAS mechanism used to generate target products with secondary cyclic amines or 4-aminobenzylpiperidine at C-2 position.

Step B (Fig. **11**) was setup in a sealed pressure vial (PV) with butanol (BuOH) as the solvent and immersed in an oil bath (150-155 °C) for 1 hr. with stirring. *Step C* (Fig. **11**) was also setup in a sealed PV with DIPEA and BuOH as the solvent and immersed in an oil bath (190-195 °C) for 14-16 hrs. with stirring. The resulting solutions were evaporated in vacuo, re-dissolved in EtOAc, neutralized using 0.5M hydrochloric acid solution (*Step C* only) and washed with concentrated brine solution (3x15 mL). Collected organic fractions were dehydrated using anhydrous $MgSO_4$, filtered and re-evaporated in vacuo to afford a crude solid or semi-solid product. Purification was performed using SGCC or high-performance liquid chromatography (HPLC) with a suitable carrier solvent to achieve a final compound purity of 95% or higher for biological screening (Fig. **15**). Final product yields ranged from 45-90% [120-122].

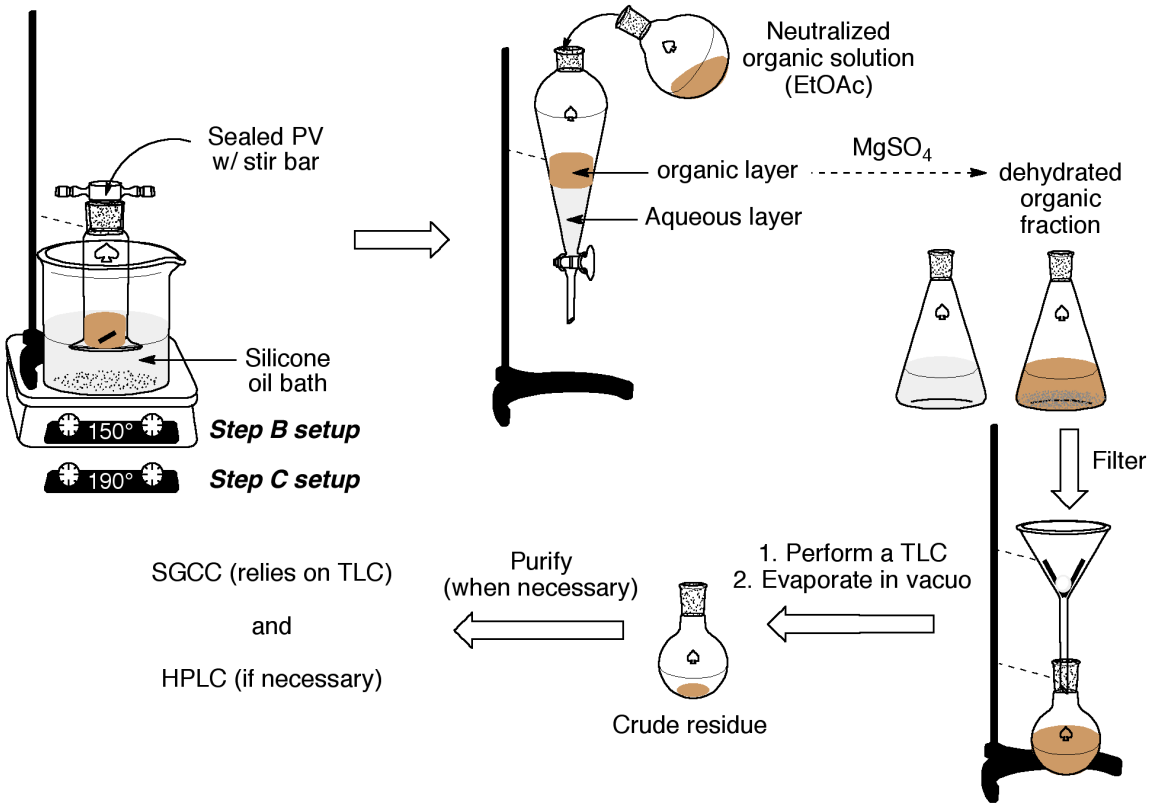

Fig. (**15**): Overview of –Step B/C– setup

3.1.3. Post-Synthesis Modifications – *Step D + E + F*

The thiomorpholine ring (*grp C*, Fig. **11**) is susceptible to oxidation by liver cytochrome enzymes. Therefore, to replicate this modification, peroxide reagents were used to oxidize *grp C* to the sulfoxide (SO) and sulfone (SO_2) analogs (*Step D + E*) (Fig. **16**). The conversion of *grp C* to *grp D* was accomplished using *meta*-chloroperoxybenzoic acid (*m*CPBA) in methanol (MeOH) and the reaction was run at room temperature (r.t) for 3 hrs. Conversely, the conversion of *grp C* to *grp E* was accomplished using potassium peroxymonosulfate (Oxone®) in a MeOH/water/dioxane cocktail and the reaction was refluxed for 1 hr. then moved to r.t for 4 hrs. The resulting solutions were diluted with EtOAc and washed with concentrated brine solution (3x15 mL). Collected organic fractions were dehydrated using anhydrous $MgSO_4$, filtered and re-evaporated in vacuo to afford a crude solid product. Purification was performed using SGCC with a suitable carrier solvent to achieve a final compound purity of 95% or higher for biological screening. Oxidized analogs were generated with yields of ~ 75% [120-122].

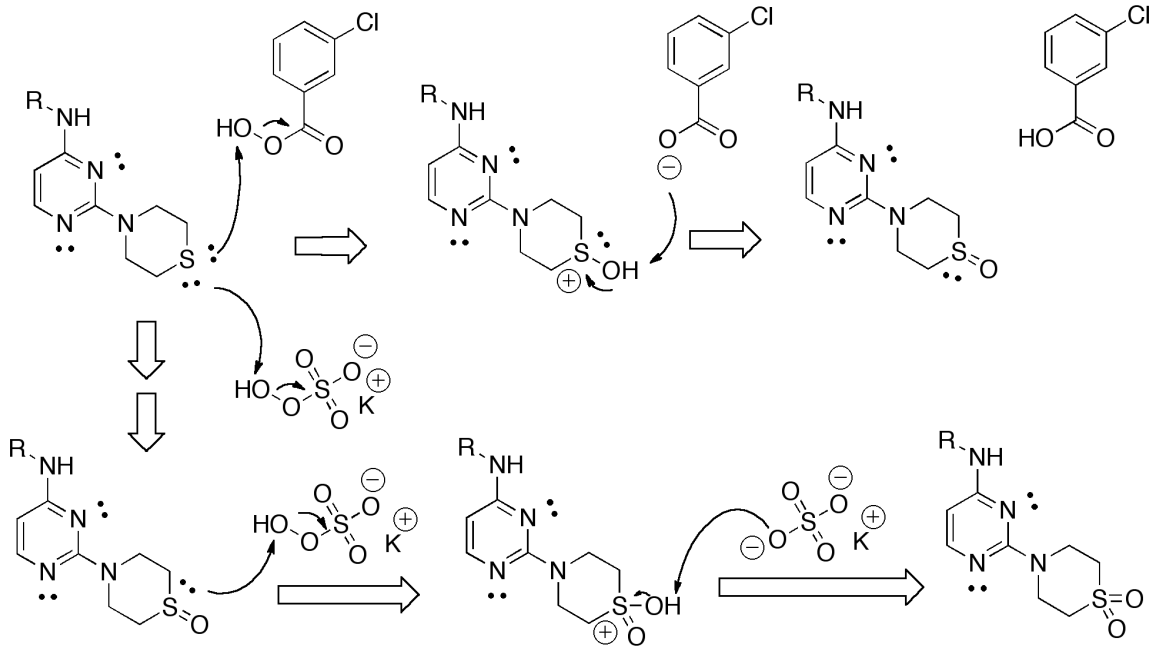

Fig. (**16**): Oxidation mechanisms used to generate the sulfoxide and sulfone analogs using peroxide reagents.

The *t*-butoxycarbonyl (Boc) functionality present in *grp O* (Fig. **11**) is susceptible to in vivo hydrolysis. Therefore, to replicate this modification, trifluoroacetic acid (TFA) was used to hydrolyze the Boc functionality present in *grp O* to generate the free-piperazine analog (*Step F*) (Fig. **17**).

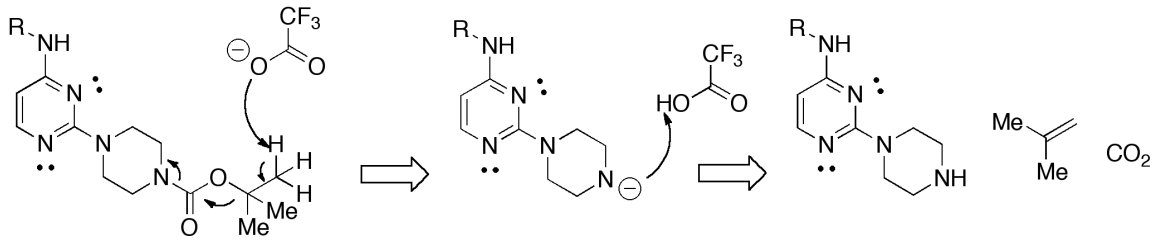

Fig. (**17**): Hydrolysis mechanisms used to generate free-piperazine analogs using TFA.

The reaction was setup using dichloromethane (DCM) and run at r.t for 2 hrs. The resulting solution was evaporated in vacuo with the aid of toluene then re-dissolved in EtOAc and DCM and washed with concentrated brine solution (3x15 mL). Collected organic fractions were dehydrated using anhydrous

$MgSO_4$, filtered and re-evaporated in vacuo to afford a solid product. Purification was usually not required for this hydrolysis reaction and yields were ~ 70-75% [120-122].

3.2. Biological Assays

Establishing a biological profile for the synthesized derivatives constitutes a large aspect of this research project. Derivative screening was coincident on the following parameters: i) ChEs; ii) AChE-induced $A\beta_{1-40}$ aggregation; iii) Self-induced $A\beta_{1-40}$ aggregation; iv) BACE-1 and v) cell toxicity of select derivatives (Fig. **18**).

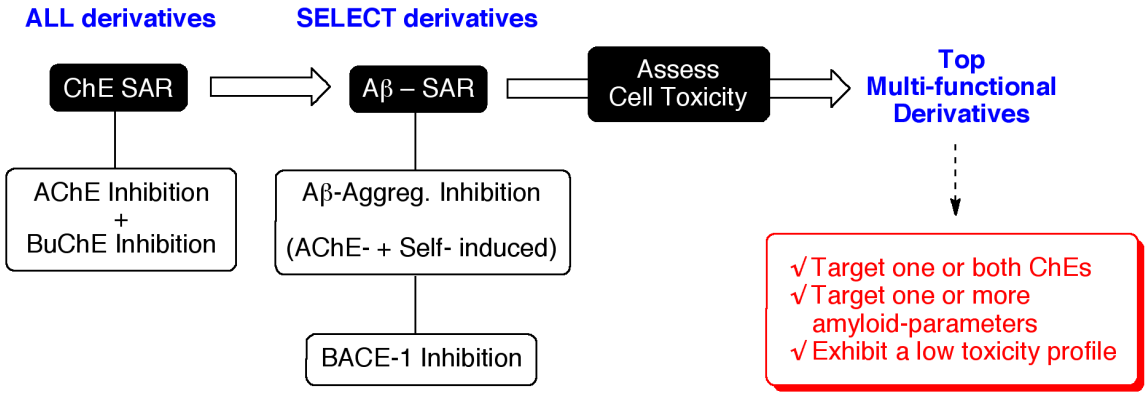

Fig. (**18**): Using SAR data to identify lead/top multifunctional derivatives.

3.2.1. Cholinesterase

The ChE screening assay is based on the Ellman method described in 1961 [123]. Thio-analogs of ACh (ATCh) and BuCh (BuTCh) are used as enzyme substrates and once degraded by the respective ChE, the thiocholine product reacts, non-enzymatically, with a pro-chromophore (dithiobis-(2-nitrobenzoic acid) or DTNB) to release 2-nitro-5-thiobenzoic acid (NTB – a yellow chromophore detected at wavelengths of 405-412 nm). With derivative screening, the ChE inhibition profile is obtained by monitoring the generation of NTB – as its concentration increases, the ability of the derivative to inhibit the ChEs decreases (Fig. **19**).

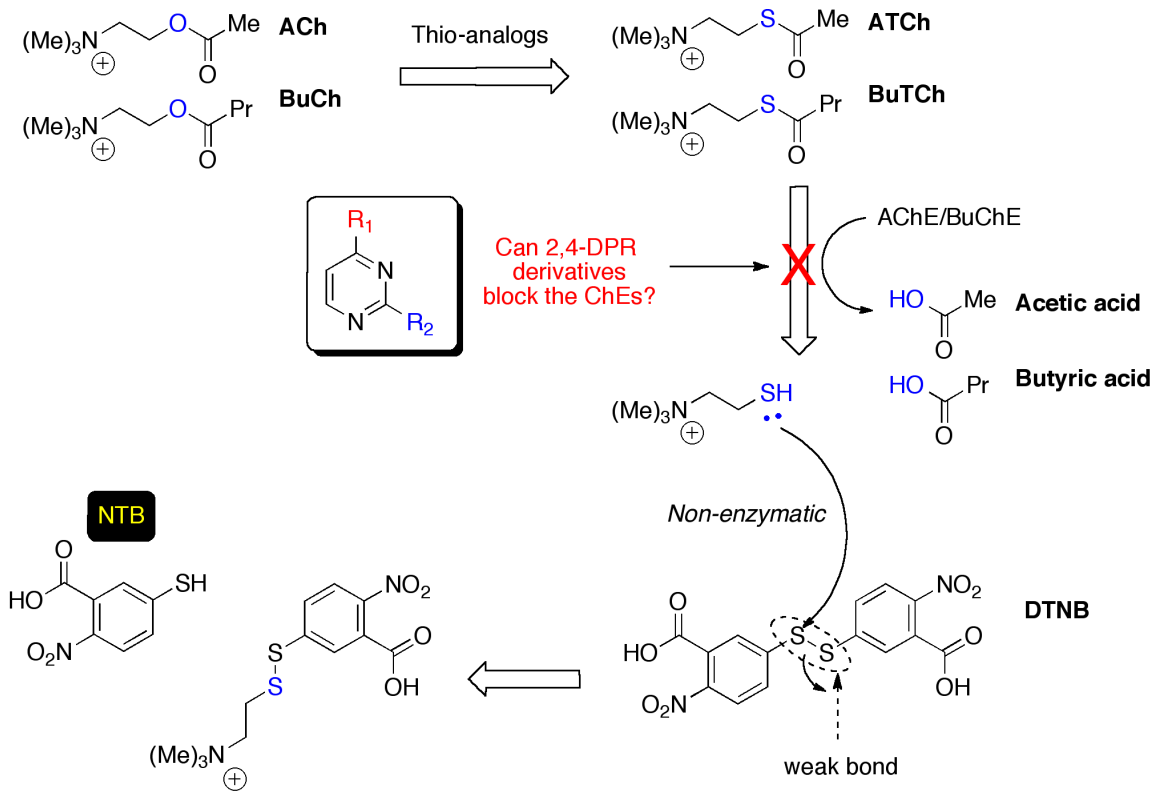

Fig. (**19**): The ChE biological assay based on the Ellman method.

3.2.2. AChE-induced and Self-induced $A\beta_{1-40}$ Aggregation

The $A\beta_{1-40}$ aggregation screening assay is based on the biophysical properties of Aβ-peptides and the significant change in thioflavin T (ThT) fluorescence in the presence of Aβ-oligomers and fibrils (excitation-emission from 385-445 nm to 450-482 nm). This is a linear relationship that can be applied to quantify self-induced and AChE-induced aggregation of $A\beta_{1-40}$ monomers. The mechanism involves the cross-β-sheets of oligomerizing Aβ-monomers and the ThT conformational changes upon binding to those secondary structures [118,124-126]. With derivative screening, the $A\beta_{1-40}$ aggregation inhibition profile is obtained by monitoring the change in relative fluorescence units (RFUs) after a 24 hrs incubation period and ThT addition – higher RFUs indicate the inability of the derivative to slow and/or halt the oligomerization and fibril-formation process (Fig. **20**).

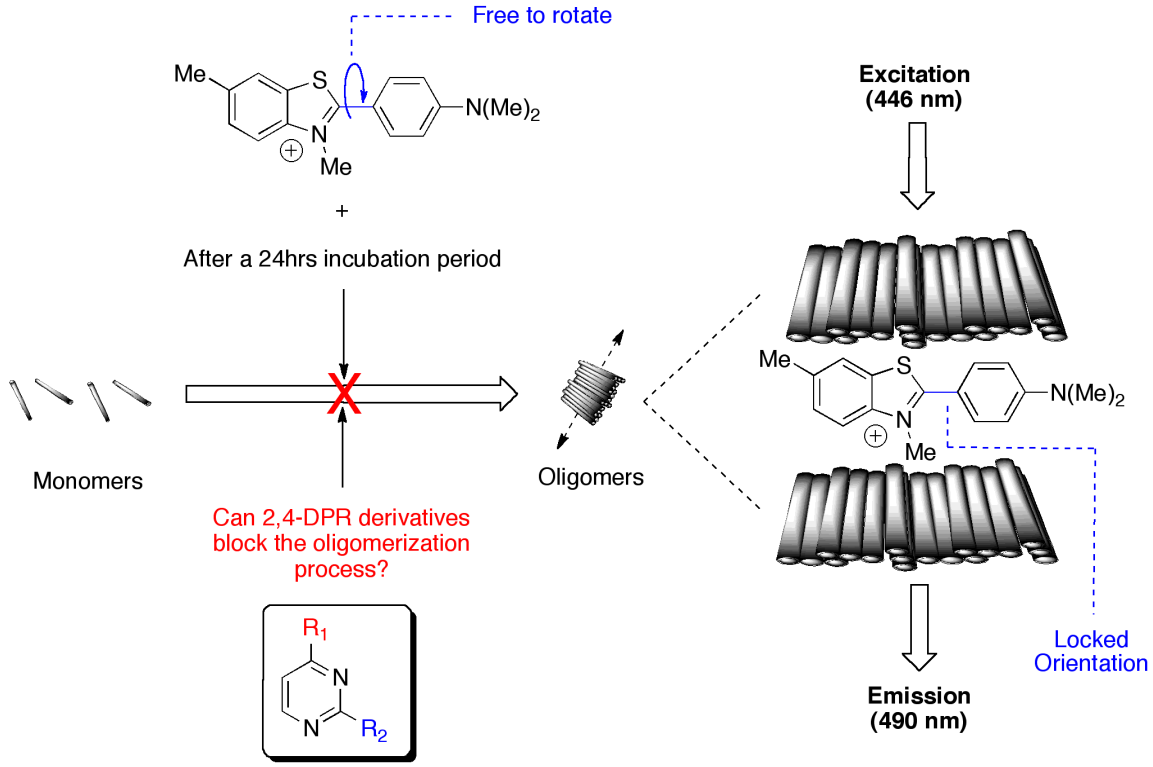

Fig. (**20**): The ThT Aβ-oligomers/fibrils quantification assay.

3.2.3. β-secretase

The BACE-1 screening assay is based on the fluorescence resonance energy transfer (FRET) method developed by PanVera ®. The peptide sequence uses the APP Swedish mutation (Table **2**) linked to enhanced BACE-1 cleavage and is capped by a fluorescence donor (Rhodamine derivative) and fluorescence quencher on either end. Upon cleavage of the labeled peptide, fluorescence is restored and detectable at 530-590 nm (excitation-emission). This relationship can be applied to quantify the rate of peptide cleavage by BACE-1. With derivative screening, the BACE-1 inhibition profile is obtained by monitoring the change in relative fluorescence units (RFUs) – higher RFUs indicate the inability of the derivative to inhibit BACE-1 (Fig. **21**).

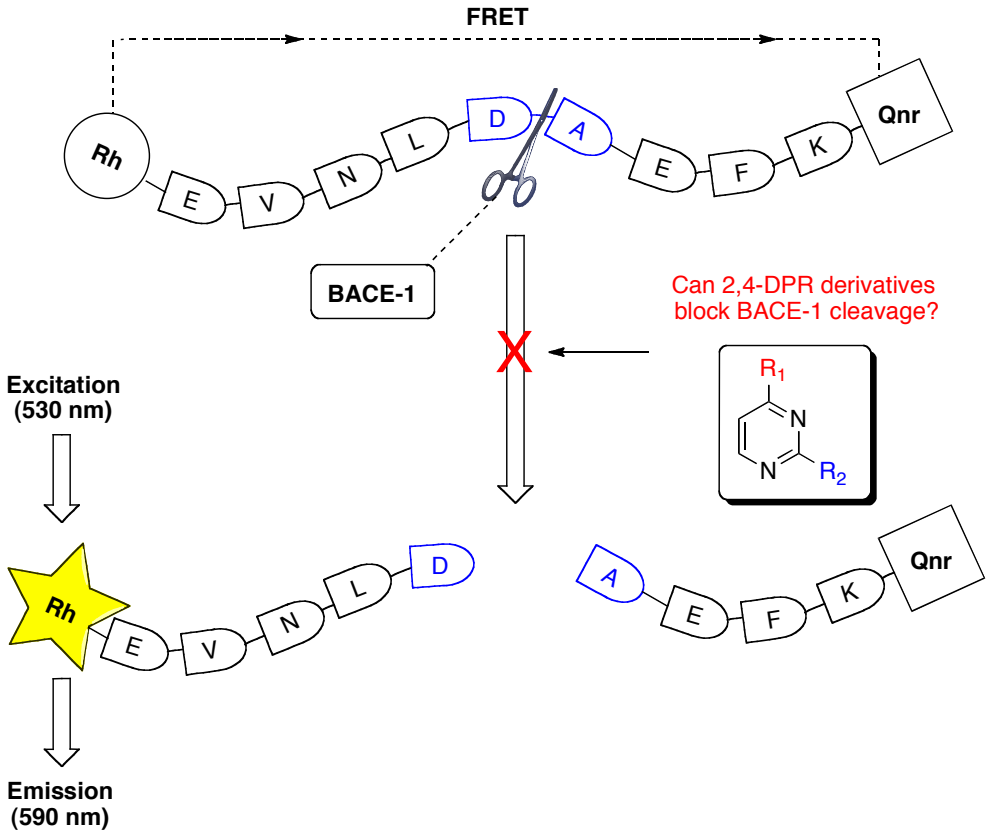

Fig. (**21**): PanVera® BACE-1 FRET assay.

3.2.4. Cell Viability

The cell viability screening assay is based on the MTT assay using 3-(4,5-dimethylthiazol-2-yl)-2,5-diphenyltetrazolium bromide (MTT reagent). This yellow tetrazole is reduced by the mitochondrial reductase enzymes of metabolically active cells to a purple formazan whose absorbance is detected between 500-600 nm [127]. This relationship can be applied to quantify the cytotoxic effects of a test sample. With derivative screening, the toxicity profile is obtained by monitoring the absorbance at 570 nm to detect the reduction of MTT – higher MTT reduction correlates to low cell toxicity or high cell viability (Fig. **22**).

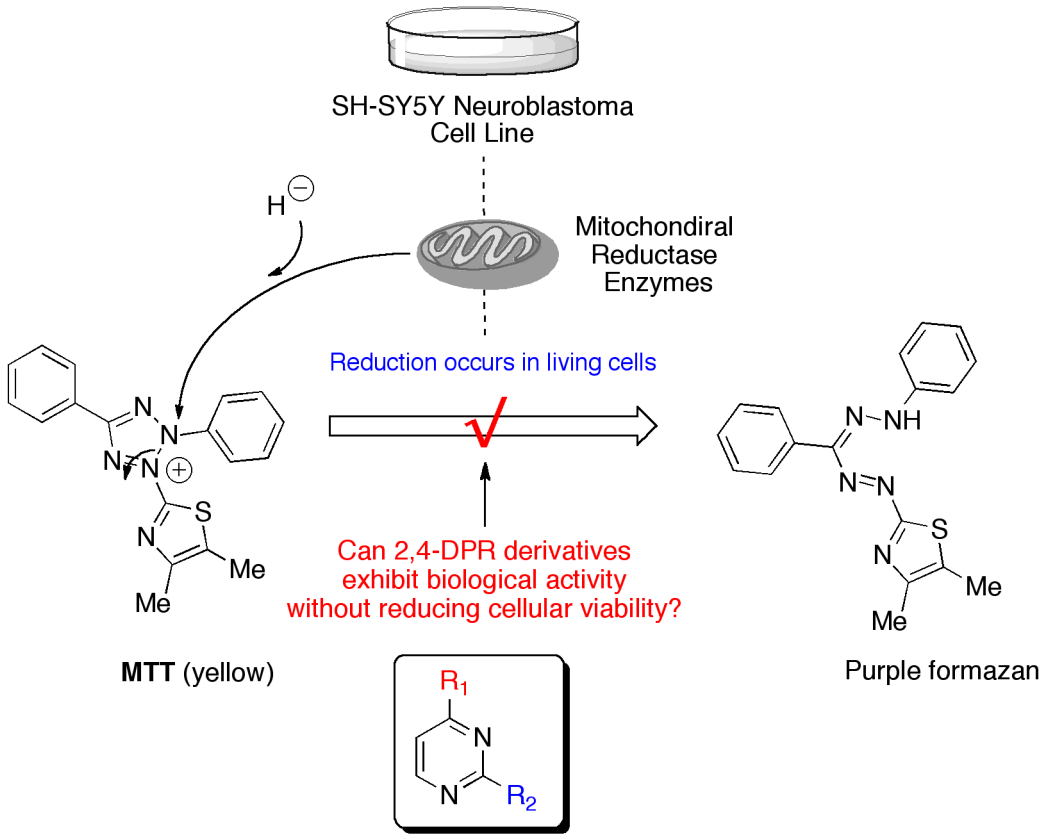

Fig. (**22**): MTT cell viability assay.

CHAPTER IV

• Results and Discussion •

4.1. Structure-Activity Relationship (SAR) Studies

Obtaining SAR data is an essential component of medicinal chemistry research. On the 2,4-DPR template, SAR studies investigate the role of the substituents at the C-2 and C-4 positions in mediating each derivative's biological profile (Fig. **23**). The breakdown of the synthesized small molecule chemical library is outlined in Table **3**.

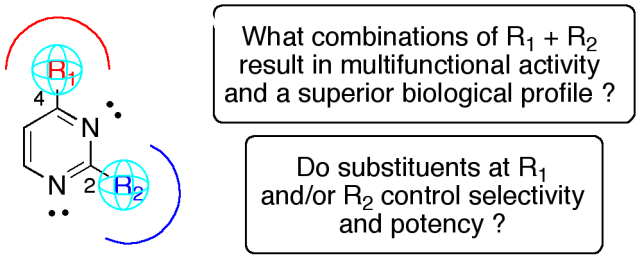

Fig. (**23**): Investigating the role of the substituents at the C-2 and C-4 positions through SAR studies.

Table (**3**): Breakdown of the small molecule chemical library.

Series	**Benzylamine and substituted benzylamines**										
C-4 group *	*2*	*3*	*4*	*5*	*6*	*7*	*8*	*9*	*10*	*11*	*12*
# of derivatives	21	6	6	6	6	6	6	6	6	6	6
	81										
Series	**Naphthalen-1-methylamine**			**Diphenylmethylamine**			**Phenylethylamine**				
C-4 group *	*13*			*14*			*15*				
# of derivatives	**14**			**11**			**6**				

* refer to Fig. **11** (R_1)

4.1.1. Anti-cholinesterase Evaluation

Anti-ChE SAR studies encompass the largest of the biological parameters assessed. This section is divided into four main classes: i) benzylamine and substituted benzylamines; ii) naphthalen-1-methyl-amine; iii) diphenylmethylamine and iv) phenylethylamine series.

4.1.1.1. Benzylamine and Substituted Benzylamine Series

The anti-ChE values for series **2–12** derivatives are expressed as the concentration required to inhibit 50% of this activity (IC_{50}) [a], along with the selectivity index (SI) [b], partition coefficient (ClogP) [c] and molecular volume (M.V - $Å^3$) [d] in Table **4**.

Table (**4**): ChE IC_{50} values for derivatives **2–12a-u** along with SI, ClogP and MV values.

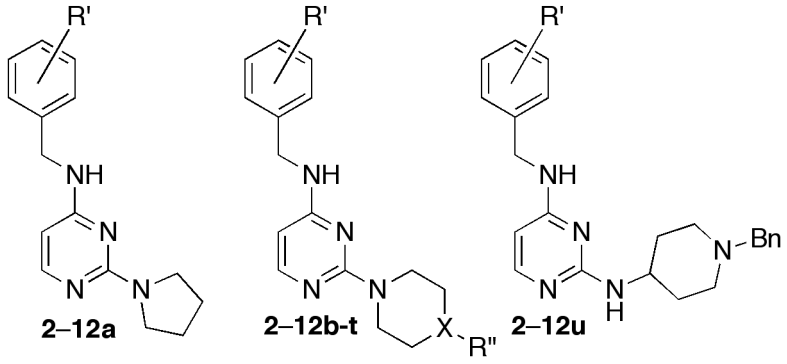

Cpd.	R'	X	R"	ChE IC_{50} (µM)		SI	ClogP	MV ($Å^3$)
				AChE	BuChE			
2a	*n/a*	*n/a*	*n/a*	8.70	26.40	0.3	2.97	174.9
2b	*n/a*	O	*n/a*	14.00	68.30	0.2	2.14	183.8
2c	*n/a*	S	*n/a*	23.20	6.10	3.8	2.98	193.5
2d	*n/a*	S	O	12.60	> 100	/	1.26	197.9
2e	*n/a*	S	O_2	24.20	> 100	/	1.18	202.4
2f	*n/a*	N	Me	24.90	> 100	/	2.71	199.6
2g	*n/a*	CH	Me	18.40	3.40	5.4	4.05	202.4
2h	*n/a*	N	*i*Pr	25.00	3.40	7.4	3.54	225.7
2i	*n/a*	CH	*i*Pr	14.20	6.50	2.2	4.97	225.7
2j	*n/a*	N	*n*Pr	15.30	59.90	0.3	3.76	224.7
2k	*n/a*	N	EtOH	26.40	> 100	/	2.13	217.5
2l	*n/a*	N	EtOMe	26.70	> 100	/	2.89	232.9
2m	*n/a*	N	Cyclohexyl	22.90	7.60	3.0	4.65	252.8
2n	*n/a*	N	Ac	16.60	> 100	/	1.73	211.3
2o	*n/a*	N	Boc	18.80	> 100	/	4.12	258.6
2p	*n/a*	N	H	15.50	> 100	/	2.13	185.6
2q	*n/a*	N	*p*-Cl-Bn	20.20	10.70	1.9	5.14	262.0
2r	*n/a*	N	*p*-Br-Bn	25.50	14.30	1.8	5.29	277.1
2s	*n/a*	N	*p*-F-Bn	21.60	7.30	3.0	4.57	250.7
2t	*n/a*	N	*p*-CF_3-Bn	28.80	>100	/	5.31	276.5
2u	*n/a*	*n/a*	*n/a*	12.40	8.20	1.5	4.60	261.0
3a	2-Cl	*n/a*	*n/a*	14.50	14.30	1.0	3.68	193.8
3f	2-Cl	N	Me	17.10	16.70	1.0	3.42	213.3
3g	2-Cl	CH	Me	13.20	8.80	1.5	4.75	216.1

Derv	R'	X	R"	ChE IC_{50} (µM)		SI	ClogP	MV (Å^3)
				AChE	BuChE			
3h	2-Cl	N	*i*Pr	14.60	4.70	3.1	4.26	239.4
3m	2-Cl	N	Cyclohexyl	14.00	3.00	4.7	5.24	266.9
3u	2-Cl	*n/a*	*n/a*	7.70	2.40	3.2	5.32	276.5
4a	3-Cl	*n/a*	*n/a*	15.20	12.80	1.2	3.68	195.2
4f	3-Cl	N	Me	16.80	11.30	1.5	3.42	216.4
4g	3-Cl	CH	Me	22.80	12.00	1.9	4.75	218.1
4h	3-Cl	N	*i*Pr	25.60	5.90	4.3	4.26	241.5
4m	3-Cl	N	Cyclohexyl	19.20	3.60	5.3	5.24	271.0
4u	3-Cl	*n/a*	*n/a*	7.70	2.50	3.1	5.32	271.7
5a	4-Cl	*n/a*	*n/a*	18.90	21.40	0.9	3.68	193.5
5f	4-Cl	N	Me	18.80	10.70	1.8	3.42	214.7
5g	4-Cl	CH	Me	16.00	9.20	1.7	4.75	218.5
5h	4-Cl	N	*i*Pr	25.20	6.70	3.8	4.26	241.5
5m	4-Cl	N	Cyclohexyl	20.70	3.00	6.9	5.24	270.5
5u	4-Cl	*n/a*	*n/a*	8.80	2.80	3.1	5.32	277.8
6a	4-Br	*n/a*	*n/a*	13.70	16.50	0.8	3.83	203.4
6f	4-Br	N	Me	14.70	15.50	0.9	3.57	223.3
6g	4-Br	CH	Me	10.10	8.10	1.3	4.91	225.7
6h	4-Br	N	*i*Pr	29.50	4.70	6.3	4.41	250.4
6m	4-Br	N	Cyclohexyl	22.70	3.70	6.1	5.39	277.8
6u	4-Br	*n/a*	*n/a*	9.90	4.10	2.4	5.48	287.1
7a	4-F	*n/a*	*n/a*	24.50	36.00	0.7	3.11	184.9
7f	4-F	N	Me	21.50	25.20	0.9	2.85	203.1
7g	4-F	CH	Me	27.30	14.30	1.9	4.18	207.5
7h	4-F	N	*i*Pr	33.40	11.80	2.8	3.69	229.5
7m	4-F	N	Cyclohexyl	23.20	4.10	5.7	4.67	257.2
7u	4-F	*n/a*	*n/a*	7.70	2.20	3.5	4.74	263.1
8a	4-Me	*n/a*	*n/a*	18.70	16.40	1.1	3.42	194.5
8f	4-Me	N	Me	30.10	25.40	1.2	3.20	213.7
8g	4-Me	CH	Me	27.20	12.10	2.2	4.54	214.0
8h	4-Me	N	*i*Pr	35.40	10.0	3.5	4.04	233.2
8m	4-Me	N	Cyclohexyl	16.80	1.70	9.9	5.03	264.1
8u	4-Me	*n/a*	*n/a*	12.90	2.50	5.2	5.10	272.7
9a	4-OMe	*n/a*	*n/a*	21.70	24.00	0.9	2.89	198.9
9f	4-OMe	N	Me	44.10	92.10	0.5	2.51	220.5
9g	4-OMe	CH	Me	21.00	7.10	3.0	3.96	224.0
9h	4-OMe	N	*i*Pr	29.70	20.70	1.4	3.34	249.4
9m	4-OMe	N	Cyclohexyl	17.70	3.10	5.7	4.45	274.7
9u	4-OMe	*n/a*	*n/a*	9.40	4.90	1.9	4.52	281.3
10a	3,4-OMe	*n/a*	*n/a*	18.10	71.70	0.3	2.62	217.5
10f	3,4-OMe	N	Me	21.50	> 100	/	3.70	240.1
10g	3,4-OMe	CH	Me	28.40	7.80	3.6	2.24	242.5
10h	3,4-OMe	N	*i*Pr	26.00	11.40	2.3	3.08	266.9
10m	3,4-OMe	N	Cyclohexyl	19.80	15.40	1.3	4.19	295.0

Derv	R'	X	R"	ChE IC_{50} (μM)		SI	ClogP	MV ($Å^3$)
				AChE	BuChE			
10u	3,4-OMe	*n/a*	*n/a*	9.90	11.40	0.9	4.26	240.1
11a	3,4,5-OMe	*n/a*	*n/a*	9.40	> 100	/	2.26	238.0
11f	3,4,5-OMe	N	Me	43.10	> 100	/	1.89	262.4
11g	3,4,5-OMe	CH	Me	26.70	28.30	0.9	3.35	260.7
11h	3,4,5-OMe	N	*i*Pr	28.40	80.20	0.4	2.72	283.3
11m	3,4,5-OMe	N	Cyclohexyl	25.90	13.00	2.0	3.83	319.3
11u	3,4,5-OMe	*n/a*	*n/a*	10.30	7.70	1.3	3.90	319.3
12a	[3,4]dioxole	*n/a*	*n/a*	21.80	25.70	0.9	2.93	200.0
12f	[3,4]dioxole	N	Me	31.10	22.20	1.4	2.67	219.5
12g	[3,4]dioxole	CH	Me	22.30	6.90	3.2	4.01	222.6
12h	[3,4]dioxole	N	*i*Pr	17.80	7.80	2.3	3.51	247.0
12m	[3,4]dioxole	N	Cyclohexyl	16.30	7.30	2.2	4.61	275.4
12u	[3,4]dioxole	*n/a*	*n/a*	12.60	3.90	3.2	4.57	280.9
Donepezil – Aricept ® (Fig.1)				0.03	3.60	0.009	4.60	271.0
Galantamine – Reminyl ® (Fig. 1)				3.20	12.60	0.3	1.00	179.2

[a] The result (IC_{50}) is the mean of two separate experiments (n = 4) and the deviation from the mean is < 10% of the mean value. [b] SI = *h*AChE IC_{50}/BuChE IC_{50}. [c] ClogP was determined using *ChemDraw Ultra 12.0.* CambridgeSoft Company. [d] MV was calculated after a minimization protocol using the molecular properties calculator in the *Discovery Studio* program from Accelrys Inc (San Diego, CA).

This class of derivatives offered a wide range of anti-ChE activity ranging from 7.70 to 44.10 μM (AChE) and 1.70 to >100 μM (BuChE) (Table **4**). The presence of the smaller, 5-membered pyrrolidine ring (group **a**, Fig. **11**) generally led to non-selective ChE inhibition, with the exception of **10a** and **11a** whose activity toward BuChE was or near non-existent (BuChE IC_{50} >100 or 71.70 μM; respectively). Of the 11 derivatives featuring this group at the C-2 position, **2a**, with the unsubstituted C-4 benzylamine, was the most potent AChEI (IC_{50} = 8.70 μM) while **11a**, with the tri-OMe-benzylamine C-4, was a close second (IC_{50} = 9.40 μM). In contrast, BuChE inhibition was directed by more hydrophobic C-4 substituted benzylamines like **3a** (2-Cl, IC_{50} = 14.30 μM) and **4a** (3-Cl, IC_{50} = 12.80 μM). Interestingly, the 4-Cl substituted C-4 benzylamine derivative (**5a**, IC_{50} = 21.40 μM) was ~ 1.6-fold less potent compared to its regioisomers. It is also noteworthy that the 4-F substituted C-4 benzylamine derivative (**7a**, BuChE IC_{50} = 36.00 μM) exhibited anti-BuChE activity similar to moderately hydrophilic C-4 derivatives (**9** and **12a**) and was a less potent BuChEI when compared to other halogen-substituted bioisosteres (**3**-**6a**).

The effects of increasing the ring size at the C-2 position were investigated by using piperazine-based substituents. Starting with alkyl piperazines, the smaller Me-piperazine substituent (group **f**, Fig. **11**)

generally led to non-selective ChE inhibition, with the exception of the unsubstituted benzylamine derivative (**2f**) and the OMe-substituted derivatives **9f** and **11f** whose activities toward BuChE were non-existent (BuChE IC_{50} ~ 92 to >100 μM). The common factor leading to this observation is likely the hydrophilic properties of these derivatives, leading to the suggestion that more hydrophobic substituents are required to target BuChE. In terms of AChE inhibition, the C-4 halogen-based benzylamine derivatives (**3f**-**7f**) exhibited activity in the range of ~ 15 to 22 μM, compared to the more hydrophilic C-4 substituted derivatives (**8f**, **9f**, **11f** and **12f**; ~ 30 to 45 μM). Interestingly, the di-OMe-benzylamine derivative (**10f**) exhibited similar activity to the 4-F substituted C-4 benzylamine derivative (**7f**, AChE IC_{50} = 21.50 μM) and the unsubstituted benzylamine derivative (**2f**) exhibited intermediate activity (AChE IC_{50} = 24.90 μM). The bioisosteric Me-piperidine substituent (group **g**, Fig. **11**) showcased a more unanimous inhibitory pattern. Due to its hydrophobic properties, derivatives with that C-2 group tend to be selective BuChEIs as seen with all the derivatives here (**2g**-**10g** and **12g**) with the exception of **11g** (AChE IC_{50} = 26.70 μM, BuChE IC_{50} = 28.30 μM) that exhibited a non-selective inhibitory profile. Of those derivatives, **2g** was the most potent (BuChE IC_{50} = 3.40 μM) while the others exhibited anti-BuChE activity within the range of ~ 7 to 14 μM and the anti-AChE range (~ 10 to 28 μM) is not far from that of the Me-piperazine substituent. With the larger/branched *i*Pr-piperazine (group **h**, Fig. **11**), selective BuChE inhibition was observed with all the derivatives except for **9h** (AChE IC_{50} = 29.70 μM, BuChE IC_{50} = 20.70 μM), showing non-selective inhibiton, and **11h** (AChE IC_{50} = 28.40 μM, BuChE IC_{50} = 80.20 μM) exhibiting selective AChEI with near loss of BuChEI. Interestingly, derivative **2h** demonstrated equipotent anti-BuChE activity to **2g** (IC_{50} = 3.40 μM). The halogen-based derivatives (**3h**-**7h**) were in second place in terms of BuChE inhibition (IC_{50} ranges from ~ 5 to 12 μM). With the bioisosteric *i*Pr-piperidine substituent (group **i**, Fig. **11**), **2i** exhibited an ~ 1.8-fold increase in AChEI and decrease in BuChEI (IC_{50} = 14.20 and 6.50 μM; respectively). The less sterically hindered, *n*Pr-piperazine isomer in **2j** exhibited an ~ 1.6-fold increase in AChE potency compared to **2f** and **2h**; however, it demonstrated weak BuChEI compared to its branched isomer (AChE IC_{50} = 15.30 μM, BuChE IC_{50} = 59.90 μM). This observation suggests the requirement for hydrophobic and branched/hindered substituents to target BuChE and additional support to that observation is seen with the derivatives featuring the cyclohexylpiperazine C-2 substituent (group **m**, Fig. **11**). Derivative **8m** exhibited superior BuChEI (AChE IC_{50} = 16.80 μM, BuChE IC_{50} = 1.70 μM), while the other derivatives ranged

from ~ 3 to 15 μM and considering the size and hydrophobic properties of group **m**, AChE activity ranges from ~ 14 to 23 μM.

With alkoxyl piperazines, the lack of steric hindrance and presence of polar moieties led to a complete loss of BuChEI regardless of the substituent (group **k** with a terminal OH or **l** with a terminal OMe). These derivatives (**2k** and **2l**) also exhibited an ~ 1.7-fold decrease in AChEI (IC_{50} ~ 26 μM) compared to the hydrophobic *n*Pr substituent in **2j**. A similar pattern was observed with carbonyl-based piperazines where the presence of an Ac-piperazine (group **n**) or a Boc-piperazine (group **o**) substituent at C-2 also led to a complete loss of BuChEI regardless of varying sterics. These derivatives (**2n** and **2o**) exhibited better (~ 1.6-fold) anti-AChE activity (IC_{50} = 16.60 and 18.80 μM; respectively) compared to **2k** and **2l**. The potential in vivo hydrolysis of **2o** to generate **2p** had no significant effect on the anti-ChE profile, which is surprising considering the 28% reduction in molecular volume and the overall variances in steric and electronic properties.

When a morpholine substituent (group **b**) is attached at C-2, derivative (**2b**) demonstrated moderate anti-AChE and weak anti-BuChE activity (IC_{50} = 14.00 and 68.30 μM). Interestingly, the thiomorpholine bioisostere (group **c**) had the opposite effect suggesting that the small differences between oxygen and sulfur atoms greatly influence anti-ChE activity (**2c**, AChE IC_{50} = 23.20 μM, BuChE IC_{50} = 6.10 μM). The potential in vivo oxidation of **2c** to generate **2d** (sulfoxide) or **2e** (sulfone) had significant effects on the anti-BuChE profile (IC_{50} > 100 μM), which correlates to the hypothesis that polar groups are not suitable to target BuChE.

Larger benzylpiperazine substituents (groups **q**-**t**) were investigated in an attempt to selectively target BuChE. Those attempts proved successful for derivatives **2q**-**s** as they selectively inhibited BuChE (IC_{50} ranges from ~ 7 to 11 μM) with moderate anti-AChE activity (IC_{50} ranges from ~ 20 to 26 μM). The trifluoromethyl group in **2t** didn't generate anti-BuChE activity and its AChE IC_{50} is inline with its bioisosteric derivatives. These observations denote the role of electronegativity in dictating anti-ChE activity. When the benzylpiperidine pharmacophore of donepezil (group **u**) is incorporated in a diamine template, dual anti-ChE activity is observed which can be attributed to the secondary amine found at C-2 that offers a degree of flexibility not present in derivatives **2q**-**t**. When compared to the unsubstituted benzylamine derivative (**2u**, AChE IC_{50} = 12.40 μM, BuChE IC_{50} = 8.20 μM), the majority of the

substituted derivatives enhanced BuChE inhibition (IC_{50} ranges from ~ 2 to 5 μM) except for **10u** offering non-selective inhibition (AChE IC_{50} = 9.90 μM, BuChE IC_{50} = 11.40 μM) and **11u** offering near equipotent activity (AChE IC_{50} = 10.40 μM, BuChE IC_{50} = 7.70 μM). In terms of AChE inhibition, most exhibited slight improvements (IC_{50} ranges from ~ 8 to 10 μM) while **8u** and **12u** offered equipotent activities compared to **2u** (IC_{50} = 12.90 and 12.60 μM; respectively).

The anti-ChE SAR data for derivatives **2**-**12a**, **f**, **g**, **h**, **m** and **u** are graphically summarized below (Fig. **24** – Panel A + B) by examining each C-2 group independently and comparing the activity across the 11 C-4 groups.

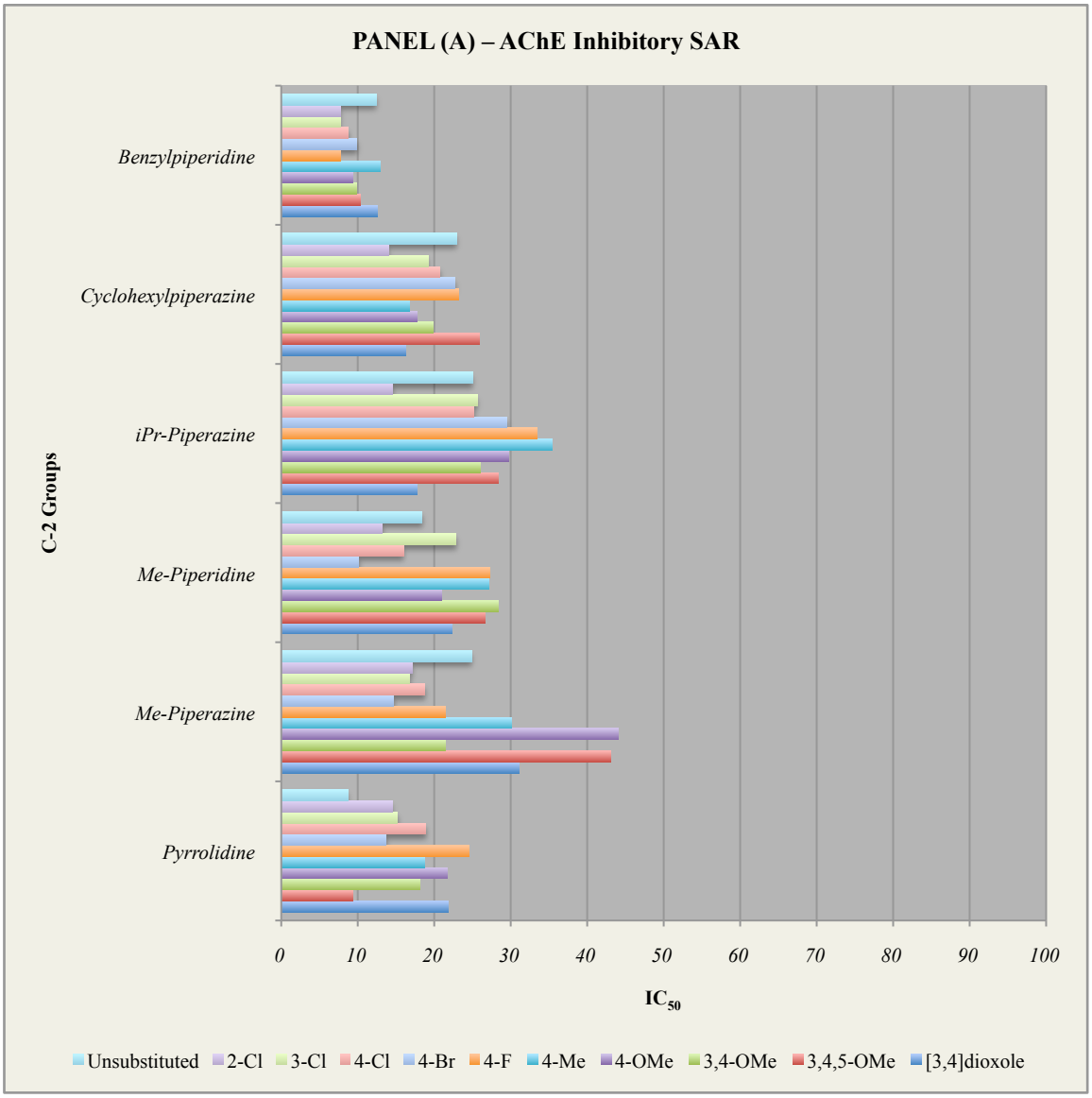

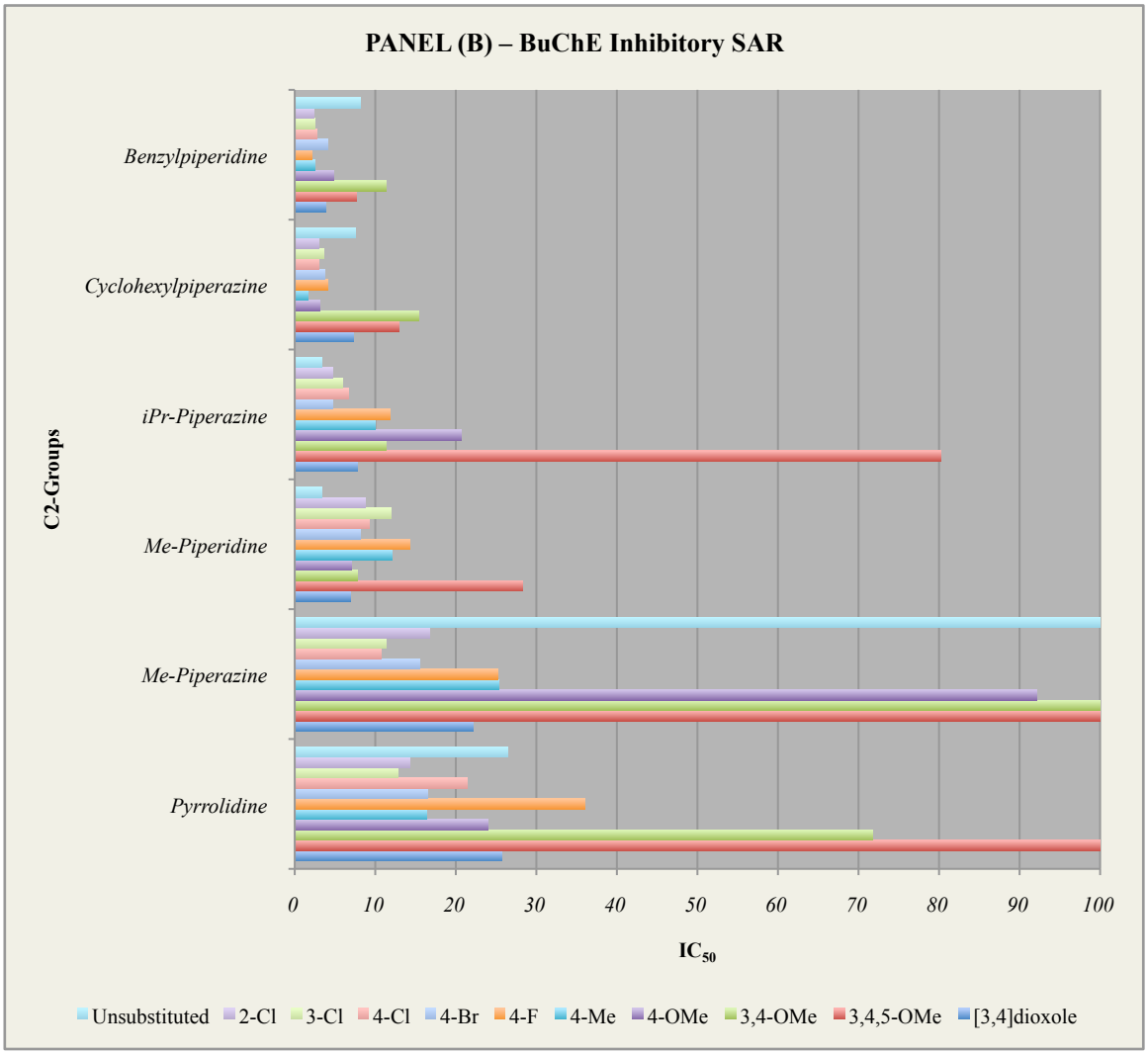

Fig. (**24**): Graphical summarization of anti-ChE SAR data from the benzylamine and related benzylamine series of derivatives. Panel (A): Anti-AChE; Panel (B): Anti-BuChE

Amongst the derivatives of these series, lead candidates were identified as follows: i) **11a** (AChE IC_{50} = 9.40 μM, BuChE IC_{50} > 100 μM) as the most potent, fully selective AChEI; ii) **7u** (AChE IC_{50} = 7.70 μM, BuChE IC_{50} = 2.20 μM) as the most potent, dual ChEI and iii) **8m** (AChE IC_{50} = 16.80 μM, BuChE IC_{50} = 1.70 μM) as the most potent, selective BuChEI (Fig. **25**).

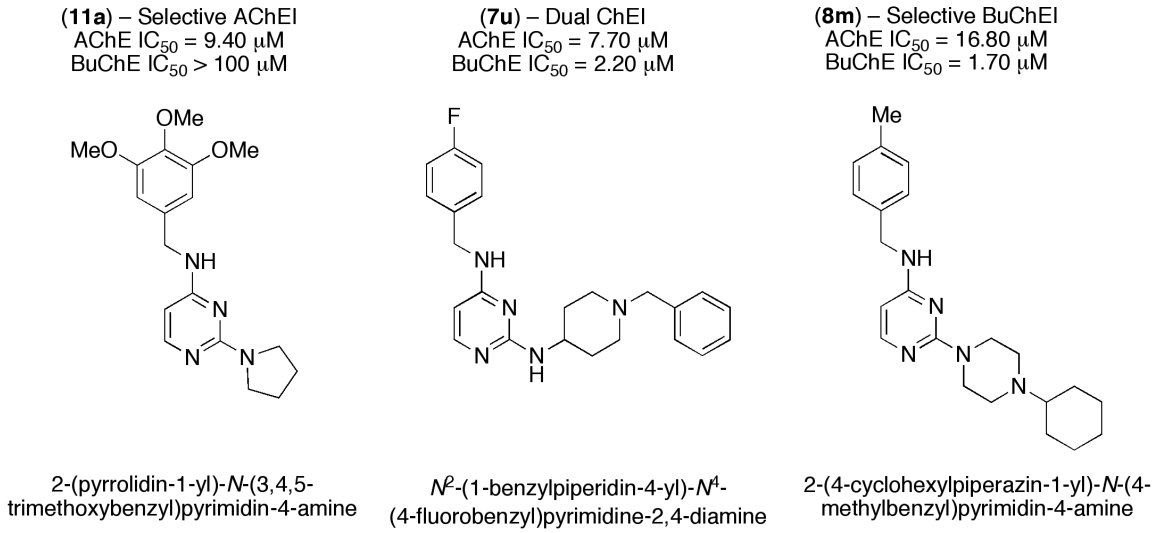

Fig. (**25**): Top candidates from the benzylamine and substituted benzylamine class of derivatives.

4.1.1.2. Naphthalen-1-ylmethylamine Series

The anti-ChE values for series **13** derivatives are expressed as IC_{50} [a], along with the selectivity index (SI) [b], partition coefficient (ClogP) [c] and molecular volume (M.V - $Å^3$) [d] in Table **5**. These derivatives were compared to the original, unsubstituted benzylamine series of derivatives to assess the impact of this planar, bulkier C-4 group (noted as Cprd).

This class of derivatives offered a wide range of anti-ChE activity ranging from 5.80 to 50.80 μM (AChE) and 2.20 to >100 μM (BuChE) (Table **5**).

Table (**5**): ChE IC_{50} values for derivatives **13a-c**,**f-p** along with SI, ClogP and MV values.

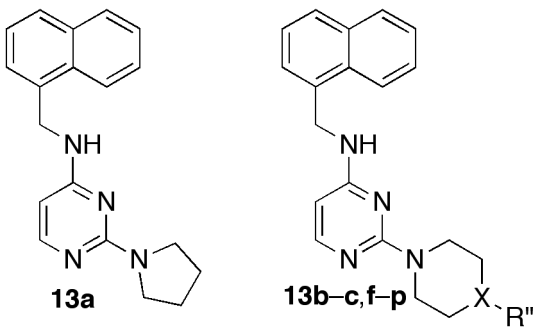

Cpd.	X	R"	ChE IC_{50} (μM)		SI	ClogP	MV (Å^3)	Cprd. to 2*x*
			AChE	BuChE				
13a	*n/a*	*n/a*	5.80	8.90	0.7	4.14	210.6	√ both ChEs
13b	O	*n/a*	14.70	28.00	0.5	3.32	218.5	√ BuChE
13c	S	*n/a*	12.80	34.70	0.4	4.15	227.4	√ AChE
13f	N	Me	17.50	2.60	6.7	3.88	229.8	√ both ChEs
13g	CH	Me	25.80	2.20	11.7	5.22	231.9	√ BuChE
13h	N	*i*Pr	15.80	7.60	2.1	4.70	255.1	√ AChE
13i	CH	*i*Pr	16.70	9.10	1.8	6.20	257.8	*not imprvt.*
13j	N	*n*Pr	19.00	18.10	1.1	4.91	256.2	√ BuChE
13k	N	EtOH	9.80	17.90	0.5	3.28	247.1	√ both ChEs
13l	N	EtOMe	11.70	26.50	0.4	4.11	260.2	√ both ChEs
13m	N	Cyclohexyl	8.00	3.90	2.1	5.76	284.0	√ both ChEs
13n	N	Ac	13.80	32.90	0.4	2.89	244.1	√ both ChEs
13o	N	Boc	50.80	>100	/	5.31	292.7	*not imprvt.*
13p	N	H	17.50	25.40	0.7	3.30	216.2	√ BuChE
Donepezil – Aricept ®			0.03	3.60	0.009	4.60	271.0	–
Galantamine – Reminyl ®			3.20	12.60	0.3	1.00	179.2	–

[a] The result (IC_{50}) is the mean of two separate experiments (n = 4) and the deviation from the mean is < 10% of the mean value. [b] SI = *h*AChE IC_{50}/BuChE IC_{50}. [c] ClogP was determined using *ChemDraw Ultra 12.0.* CambridgeSoft Company. [d] MV was calculated after a minimization protocol using the molecular properties calculator in the *Discovery Studio* program from Accelrys Inc (San Diego, CA).

The presence of the smaller, 5-membered pyrrolidine ring (group **a**, Fig. **11**) led to enhanced dual ChE inhibition, with the slight selectivity toward AChE (AChE IC_{50} = 5.80 μM, BuChE IC_{50} = 8.90 μM). The unsubstituted, polar 6-membered morpholine and thiomorpholine C-2 rings (group **b** and **c**, Fig. **11**) exhibited improvements to the anti-BuChE (**13b** – AChE IC_{50} = 14.70 μM, BuChE IC_{50} = 28.00 μM) and anti-AChE (**13c** – AChE IC_{50} = 12.80 μM, BuChE IC_{50} = 34.70 μM) profiles, respectively. The Me-piperazine, along with the piperidine bioisostere, derivatives were identified as near equipotent BuChEIs (BuChE IC_{50} = 2.60 and 2.20 μM; respectively) and **13f** also exhibited slight improvements to AChE inhibition (AChE IC_{50} = 17.50 μM). The *i*Pr bioisosteres and the *n*Pr isomeric derivatives (**13h**, **13i** and **13j**) exhibited similar anti-AChE activities (IC_{50} ranges from ~ 16 to 19 μM) and BuChE inhibition decreased sequentially from 7.60 μM to 18.10 μM. Derivative **13m** (with the bulkier cyclohexylpiperazine group) exhibited potent, dual ChE inhibition (AChE IC_{50} = 8.00 μM, BuChE IC_{50} = 3.90 μM) surpassing that of **2m**. The alkoxyl piperazine derivatives exhibited improvements to the anti-ChE profiles (**13k** – AChE IC_{50} = 9.80 μM, BuChE IC_{50} = 17.90 μM and **13l** – AChE IC_{50} = 11.70 μM, BuChE IC_{50} = 26.50 μM) suggesting a key role for the naphthalen-1-ylmethylamine C-4 group in balancing steric and

electrostatic properties of the less hindered and more polar C-2 groups. With the carbonyl-based piperazines, derivative **13n** demonstrated minor improvements to the anti-AChE activity and significant improvements to the anti-BuChE activity (AChE IC_{50} = 13.80 μM, BuChE IC_{50} = 32.90 μM), while **13o** didn't showcase a similar patter (AChE IC_{50} = 50.80 μM, BuChE IC_{50} > 100 μM). Derivative **13p** (with the free piperazine C-2 group) demonstrated similar anti-AChE activity to **2p** but exhibited significant improvements to the anti-BuChE activity (AChE IC_{50} = 17.50 μM, BuChE IC_{50} = 25.40 μM).

Overall, 12 of the 14 derivatives in this series exhibited some form of improvement in anti-ChE activity. Derivative **13a** (AChE IC_{50} = 5.80 μM, BuChE IC_{50} = 8.90 μM) was identified as the most potent AChEI, **13m** (AChE IC_{50} = 8.00 μM, BuChE IC_{50} = 3.90 μM) as the most potent dual ChEI and **13g** (AChE IC_{50} = 25.80 μM, BuChE IC_{50} = 2.20 μM) as the most potent BuChEI (Fig. **26**). This suggests that the bulkiness and hydrophobicity of this C-4 group is a key balancing factor and that is observed with both polar and non-polar C-2 groups.

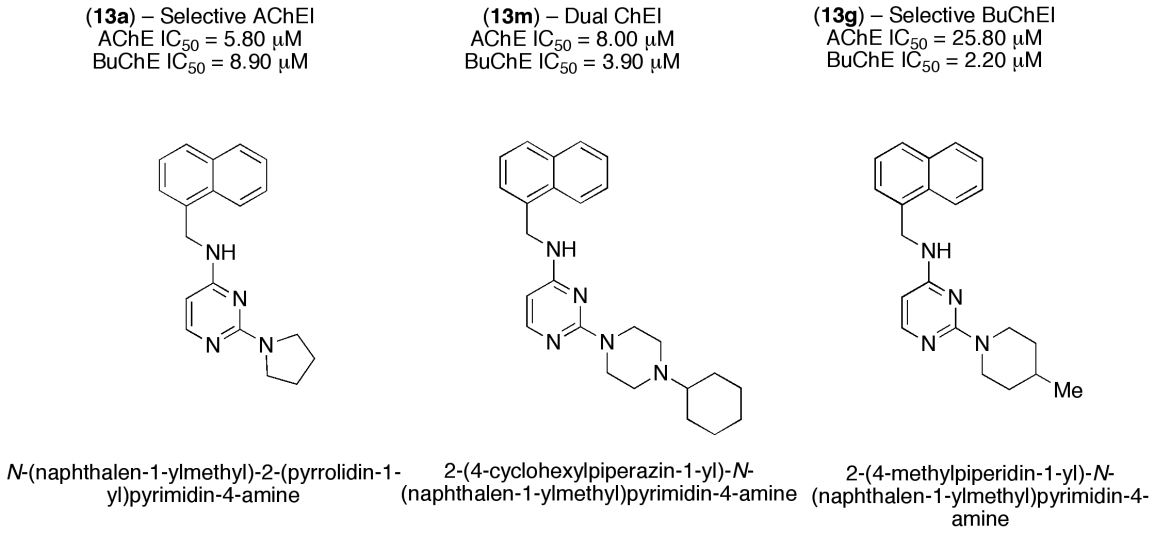

Fig. (**26**): Top candidates from the naphthalen-1ylmethylamine class of derivatives.

4.1.1.3. Diphenylmethylamine Series

The anti-ChE values for series **14** derivatives are expressed IC_{50} [a], along with the selectivity index (SI) [b], partition coefficient (ClogP) [c] and molecular volume (M.V - $Å^3$) [d] in Table **6**. These derivatives were

also compared to the original, unsubstituted benzylamine series of derivatives to assess the impact of this sterically hindered C-4 group (noted as Cprd).

This class of derivatives offered a wide range of anti-ChE activity ranging from 10.00 to >100 μM (AChE) and 7.60 to >100 μM (BuChE) (Table **5**). The Me-piperazine derivative (**14f** – AChE IC_{50} = 13.70 μM, BuChE IC_{50} = 23.80 μM) enhanced BuChE inhibition compared to **2f** but it was also 9-fold less potent compared to **13f**. In terms of AChE, it exhibited better activity compared to **2f** and **13f**. The bioisosteric derivative (**14g**) exhibited moderate, non-selective ChE inhibition (AChE IC_{50} = 32.30 μM, BuChE IC_{50} = 33.80 μM); however, it was far less potent compared to **2g** and **13g**.

In contrast to the benzylamine and naphthalen-1-ylmethlyamine series, the *i*Pr bioisosteric derivatives (**14h** and **14i**) exhibited a significant degree of variance in their anti-ChE activity profiles. Although **14h** exhibited selectivity toward BuChE (IC_{50} = 9.70 μM), it was ~ 2.9-fold less potent than **2h** but it also exhibited slight improvements to AChE inhibition (IC_{50} = 20.30 μM). On the other hand, **14i** exhibited weak anti-AChE activity (IC_{50} = 42.50 μM) and a near loss of BuChE inhibition (IC_{50} = 87.00 μM) compared to **2i**, **13i** and **14h**. Interestingly, **14m** offered good, non-selective ChE inhibitory activity similar to that of **13m** (AChE IC_{50} = 10.00 μM, BuChE IC_{50} = 7.60 μM) and its BuChE activity was near equipotent to that of **2m**. A similar pattern emerged with **14j** (with the *n*Pr isomer) where its AChE inhibitory profile (IC_{50} = 14.60 μM) was similar to that of **2j** and the BuChE inhibitory profile (IC_{50} = 17.50 μM) was close to that of **13j**. With the alkoxyl piperazines, the derivatives in this series (**14k** and **14l**) were less potent compared to their C-4 naphthyl analogs but they did improve BuChEI when compared to **2k** and **2l**. With the hydroxyethylpiperazine, derivative **14k** (AChE IC_{50} = 21.60 μM, BuChE IC_{50} = 59.50 μM) only improved BuChEI compared to **2k** but it was ~ 3.3-fold less potent compared to **13k**. In contrast, the methoxyethylpiperazine derivative (**14l** – AChE IC_{50} = 39.20 μM, BuChE IC_{50} = 28.40 μM) exhibited similar anti-BuChE activity similar to that of **13l** but it was also the least potent AChEI compared to **2l** and **13l**. The carbonyl-based and free piperazine group derivatives (**14n**-**p**) exhibited a complete loss of BuChE inhibition (IC_{50} >100 μM) and their anti-AChE activities (IC_{50} = 29.00, >100 and 31.30 μM; respectively) were also less potent compared to their benzylamine and naphthalen-1-ylmethylamine analogs.

Table (**6**): ChE IC_{50} values for derivatives **14f-p** along with SI, ClogP and MV values.

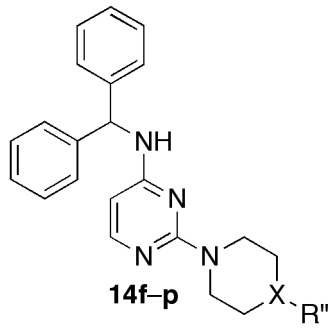

14f–p

Cpd.	X	R"	ChE IC_{50} (μM)		SI	ClogP	MV (Å^3)	Cprd. to 2*x*
			AChE	BuChE				
14f	N	Me	13.70	23.80	0.6	4.11	247.8	√ both ChEs
14g	CH	Me	32.20	33.80	0.9	5.40	251.1	*not imprvt.*
14h	N	*i*Pr	20.30	9.70	2.1	4.92	279.2	√ AChE
14i	CH	*i*Pr	42.50	87.00	0.5	6.33	282.0	*not imprvt.*
14j	N	*n*Pr	14.60	17.50	0.8	5.09	271.8	√ BuChE
14k	N	EtOH	21.60	59.50	0.4	3.47	264.9	√ both ChEs
14l	N	EtOMe	39.20	28.40	1.4	4.23	285.0	√ BuChE
14m	N	Cyclohexyl	10.00	7.60	1.3	6.01	303.2	√ AChE
14n	N	Ac	29.00	> 100	/	3.13	260.1	*not imprvt.*
14o	N	Boc	>100	> 100	/	5.51	260.2	*not imprvt.*
14p	N	H	31.30	> 100	/	3.52	235.3	*not imprvt.*
Donepezil – Aricept ®			0.03	3.60	0.009	4.60	271.0	–
Galantamine – Reminyl ®			3.20	12.60	0.3	1.00	179.2	–

[a] The result (IC_{50}) is the mean of two separate experiments (n = 4) and the deviation from the mean is < 10% of the mean value. [b] SI = *h*AChE IC_{50}/BuChE IC_{50}. [c] ClogP was determined using *ChemDraw Ultra 12.0.* CambridgeSoft Company. [d] MV was calculated after a minimization protocol using the molecular properties calculator in the *Discovery Studio* program from Accelrys Inc (San Diego, CA).

Overall, 6 of the 11 derivatives here offered moderate anti-ChE activity improvements compared to the unsubstituted benzylamine series. Also, variances were observed when comparing these derivatives with those from the naphthalen-1ylmethylamine series, indicating a key role in the steric differences between the linear/planar naphthyl ring system and the bulkier/branched diphenyl ring systems. From this series, derivative **14m** was identified as the most potent, dual ChEI with an IC_{50} value of 10.00 μM for AChE and 7.60 μM for BuChE (Fig. **28**).

(**13m**) – Dual ChEI
AChE IC_{50} = 10.00 μM
BuChE IC_{50} = 7.60 μM

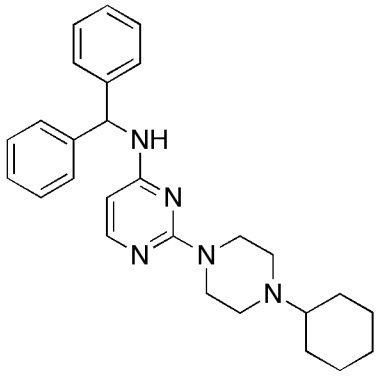

N-benzhydryl-2-(4-cyclohexylpiperazin-1-yl)pyrimidin-4-amine

Fig. (**27**): Top candidate from the diphenylmethylamine class of derivatives.

4.1.1.4. Phenylethylamine Series

The anti-ChE values for series **15** derivatives are expressed as inhibition concentration 50 (IC_{50}) [a], along with the selectivity index (SI) [b], partition coefficient (ClogP) [c] and molecular volume (M.V - $Å^3$) [d] in Table **7**. These derivatives were also compared to the unsubstituted benzylamine series of derivatives to assess the impact of the additional methylene (-CH_2-) group on the anti-ChE activities.

This was the least comprehensive series considering the preliminary results were not promising. Overall, anti-AChE activity (IC_{50}) ranges from 8.80 to 26.40 μM and anti-BuChE activity (IC_{50}) ranges from 13.80 to >100 μM. The presence of the smaller, 5-membered pyrrolidine ring (group **a**, Fig. **11**) led to dual ChE inhibition, with the slight selectivity toward AChE (**15a** – AChE IC_{50} = 9.80 μM, BuChE IC_{50} = 13.80 μM) and an improvement to BuChE inhibition compared to **2a**. The unsubstituted, 6-membered morpholine and thiomorpholine C-2 rings (group **b** and **c**, Fig. **11**) exhibited no improvements to the anti-ChE activities (**15b** – AChE IC_{50} = 19.70 μM, BuChE IC_{50} >100 μM; **15c** – AChE IC_{50} = 26.40 μM, BuChE IC_{50} >100 μM) compared to their benzylamine counterparts. The Me-piperazine derivative (**15f**) demonstrated slight improvements to the anti-AChE activity profile and a complete loss of BuChE inhibition (AChE IC_{50} = 20.40 μM, BuChE IC_{50} >100 μM). The piperidine bioisosteric derivative (**15g**) was identified as a selective AChEI (with improved activity compared to **2g**) but suffered (~ 5-fold) in

terms of BuChE inhibition (AChE IC_{50} = 8.80 μM, BuChE IC_{50} = 17.70 μM). With the Ac-piperazine derivative (**15n**), a minor decline in the anti-AChE activity was observed with no changes to the anti-BuChE activity (AChE IC_{50} = 19.90 μM, BuChE IC_{50} >100 μM).

Overall, this series was not pursued further as the majority of the synthesized derivatives exhibited no BuChE inhibition.

Table (**7**): ChE IC_{50} values for derivatives **15a-c**,**f-g**,**n** along with SI, ClogP and MV values.

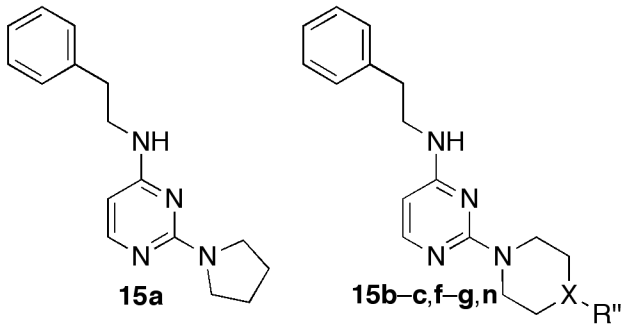

Derv	X	R"	ChE IC_{50} (μM)		SI	ClogP	MV (Å^3)	Cprd. to 2*x*
			AChE	BuChE				
15a	*n/a*	*n/a*	9.80	13.80	0.7	3.62	190.7	√ BuChE
15b	O	*n/a*	19.70	> 100	/	2.79	193.8	*n/a*
15c	S	*n/a*	26.40	> 100	/	3.63	206.5	*n/a*
15f	N	Me	20.40	> 100	/	3.35	211.3	√ AChE
15g	CH	Me	8.80	17.70	0.5	4.69	214.4	√ AChE
15n	N	Ac	19.90	> 100	/	2.37	220.9	*n/a*
Donepezil – Aricept ®			0.03	3.60	0.009	4.60	271.0	–
Galantamine – Reminyl ®			3.20	12.60	0.3	1.00	179.2	–

[a] The result (IC_{50}) is the mean of two separate experiments (n = 4) and the deviation from the mean is < 10% of the mean value. [b] SI = *h*AChE IC_{50}/BuChE IC_{50}. [c] ClogP was determined using *ChemDraw Ultra 12.0.* CambridgeSoft Company. [d] MV was calculated after a minimization protocol using the molecular properties calculator in the *Discovery Studio* program from Accelrys Inc (San Diego, CA).

4.1.1.5. Summary

The anti-ChE SAR studies examined a chemical library comprised of 112 2,4-DPR derivatives with varying steric and electronic properties at both the C-4 and C-2 positions of the pyrimidine ring.

Table (**8**): Recap chart of the anti-ChE IC_{50} values (*Red*: AChE, *Blue*: BuChE).

ChE DATA	Varying C-4 Substituents: 2	3	4	5	6	7	8	9	10	11	12	13	14	15
A	8.7 26.4	14.5 14.3	15.2 12.8	18.9 21.4	13.7 16.5	24.5 36.0	18.7 16.4	21.7 24.0	18.1 71.7	9.4 > 100	21.8 25.7	5.5 8.9		9.8 13.8
B	14.0 68.3											14.7 28.0		19.7 > 100
C	23.2 6.1											12.8 34.7		26.4 > 100
D	12.6 > 100													
E	24.2 > 100													
F	24.9 > 100	17.1 16.7	16.8 11.3	18.8 10.7	14.7 15.5	21.5 25.2	30.1 25.4	44.1 92.1	21.5 > 100	43.1 > 100	31.1 22.2	17.5 2.6	13.7 23.8	20.4 > 100
G	18.4 3.4	13.2 8.8	22.8 12.0	16.0 9.2	10.1 8.1	27.3 14.3	27.2 12.1	21.0 7.1	28.4 7.8	26.7 28.3	22.3 6.9	25.8 2.2	32.2 33.8	8.8 17.7
H	25.0 3.4	14.6 4.7	25.6 5.9	25.2 6.7	29.5 4.7	33.4 11.8	35.4 10.0	29.7 20.7	26.0 11.4	28.4 80.2	17.8 7.8	15.8 7.6	20.3 9.7	
I	14.2 6.5											16.7 9.1	42.5 87.0	
J	15.3 59.9											19.0 18.1	14.6 17.5	
K	26.4 > 100											9.8 17.9	21.6 59.5	
L	26.7 > 100											11.7 26.5	39.2 28.4	
M	22.9 7.6	14.0 3.0	19.2 3.6	20.7 3.0	22.7 3.7	23.2 4.1	16.8 1.7	17.7 3.1	19.8 15.4	25.9 13.0	16.3 7.3	8.0 3.9	10.0 7.6	
N	16.6 > 100											13.8 32.9	29.0 > 100	19.9 > 100
O	18.8 > 100											50.8 > 100	> 100 > 100	
P	15.5 > 100											17.5 25.4	31.3 > 100	
Q	20.2 10.7													
R	25.5 14.3													
S	21.6 7.3													
T	28.8 > 100													
U	12.4 8.2	7.7 2.4	7.7 2.5	8.8 2.8	9.9 4.1	7.7 2.2	12.9 2.5	9.4 4.9	9.9 11.4	10.3 7.7	12.6 3.9			

Varying C-2 Substituents

Table **8** summarizes all the anti-ChE IC_{50} values and the derivatives are graphically classified based on: i) their anti-ChE profile – selective AChEI (18), selective BuChEI (0), dual ChEI (86), and non-selective ChEI (18) – in Fig. **28a** and ii) their IC_{50} ranges in Fig. **28b**.

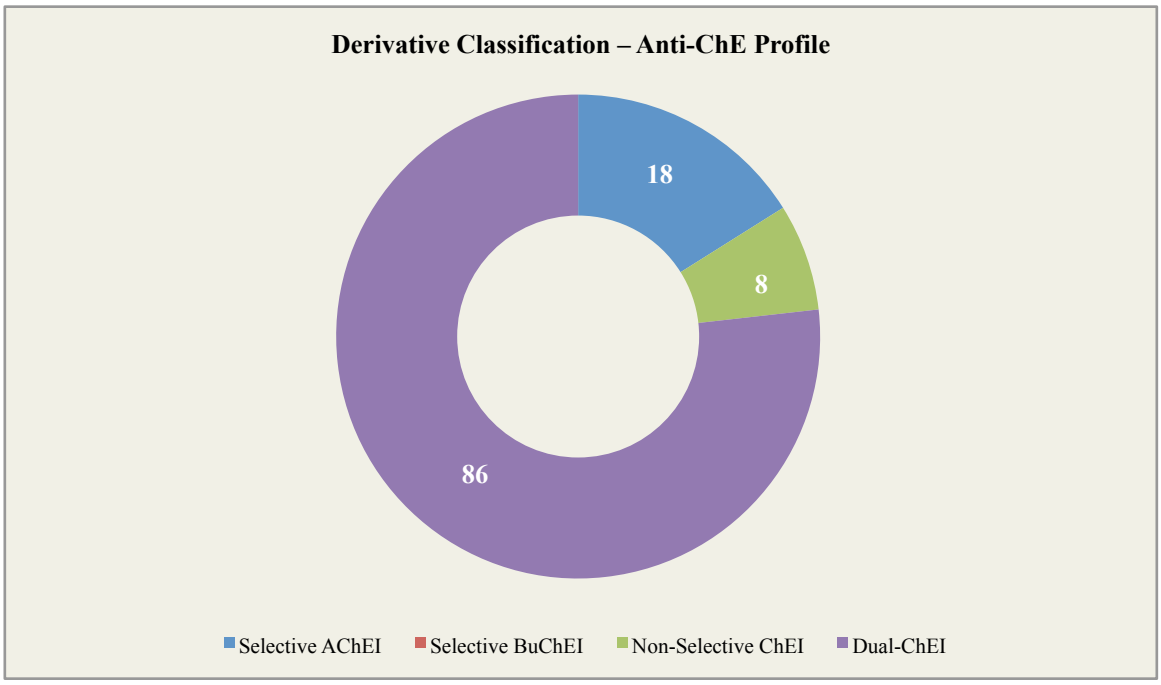

Fig. (**28a**): Derivative classification based on their anti-ChE activity profile allocated within one of the following categories: selective, non-selective, dual ChEI.

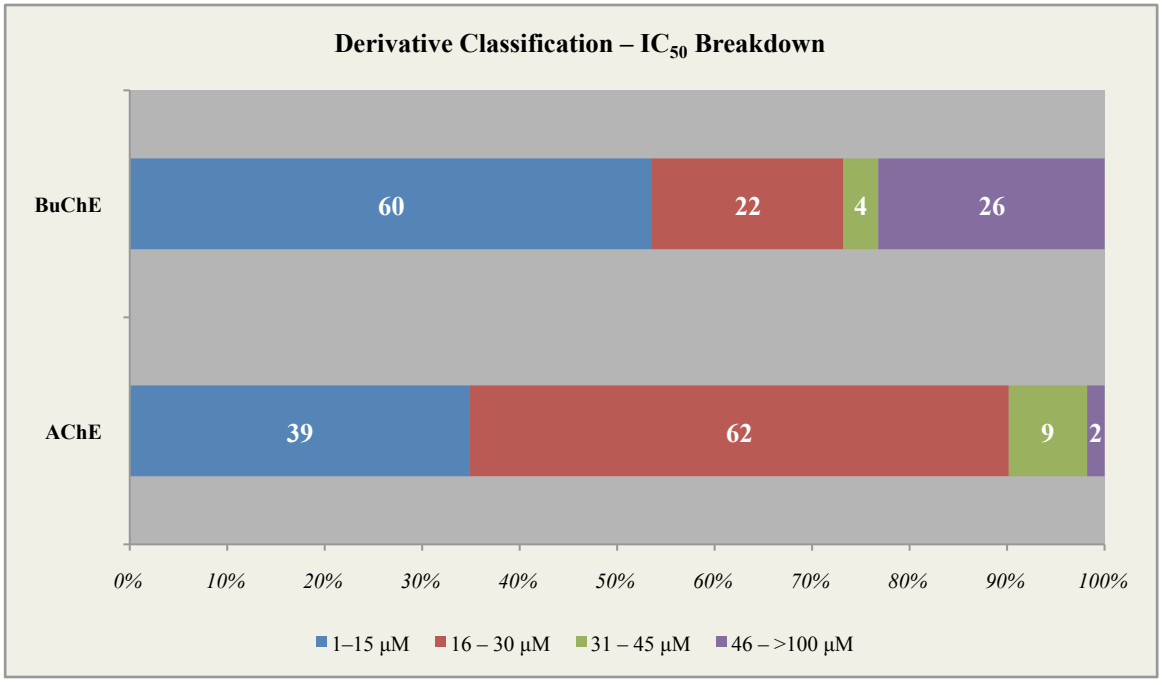

Fig. (**28b**): Derivative classification based on their IC_{50} values allocated within one of the following ranges: 1-15, 16-30, 31-45, 46->100 µM.

4.1.2. Anti-AChE-induced and Anti-Self-induced $A\beta_{1-40}$ Aggregation

Due to cost constraints, it was not feasible to screen all the derivatives for anti-$A\beta_{1-40}$ aggregation properties. The selection process was dependent on the anti-ChE profiles and preliminary ligand-docking studies in *h*AChE. The SAR data (% inhibition) [a] of select derivatives is presented collectively in Table **9**, along with the SI [b] value and mode of ChEI.

Table (**9**): Anti-$A\beta_{1-40}$ aggregation SAR data for select derivatives presented as % inhibition at 100 μM.

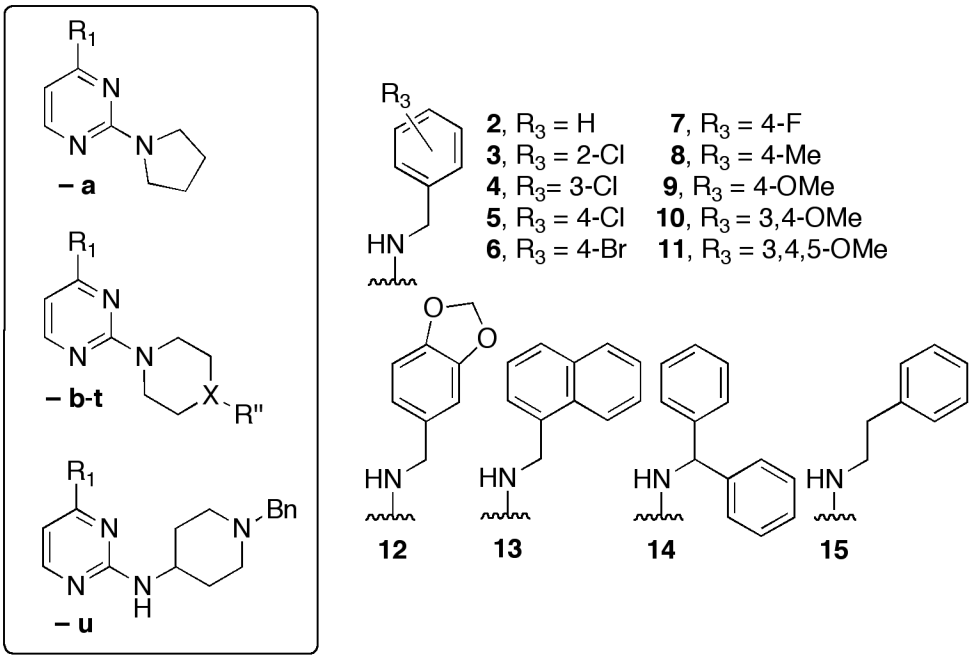

Derv	X	R"	Inhibition of $A\beta_{1-40}$ Aggreg. (%)		SI	Mode of ChEI
			AChE-induced	Self-induced		
2a[c]	*n/a*	*n/a*	Not active	*n/d*	/	Dual ChEI
2c[c]	S	*n/a*	Not active	*n/d*	/	Dual ChEI
2d[c]	S	O	56.00 ± 6.30	*n/d*	/	Selec. AChEI
2e[c]	S	O_2	44.00 ± 11.00	*n/d*	/	Selec. AChEI
2f[c]	N	Me	59.00 ± 3.00	*n/d*	/	Selec. AChEI
2o[c]	N	Boc	27.00 ± 17.00	*n/d*	/	Selec. AChEI
3m	N	Cyclohexyl	Not active	32.00 ± 3.20	/	Dual ChEI
3u	*n/a*	*n/a*	Not active	42.20 ± 4.20	/	Dual ChEI
4m	N	Cyclohexyl	Not active	39.30 ± 3.90	/	Dual ChEI
4u	*n/a*	*n/a*	27.20 ± 2.70	39.90 ± 4.00	0.70	Dual ChEI
5m	N	Cyclohexyl	Not active	36.30 ± 3.60	/	Dual ChEI
5u	*n/a*	*n/a*	Not active	42.60 ± 4.30	/	Dual ChEI
6f	N	Me	Not active	22.50 ± 2.30	/	Dual ChEI

Derv	X	R"	Inhibition of $A\beta_{1-40}$ Aggreg. (%)		SI	Mode of ChEI
			AChE-induced	Self-induced		
6m	N	Cyclohexyl	Not active	35.00 ± 3.50	/	Dual ChEI
6u	*n/a*	*n/a*	53.90 ± 5.40	48.40 ± 4.80	1.1	Dual ChEI
7f	N	Me	Not active	21.00 ± 2.10	/	Dual ChEI
7h	N	*i*Pr	Not active	Not active	/	Dual ChEI
7m	N	Cyclohexyl	Not active	35.80 ± 3.60	/	Dual ChEI
7u	*n/a*	*n/a*	38.10 ± 3.80	29.80 ± 3.00	1.3	Dual ChEI
8f	N	Me	Not active	21.60 ± 2.20	/	Dual ChEI
8g	CH	Me	Not active	24.40 ± 2.40	/	Dual ChEI
8m	N	Cyclohexyl	Not active	33.80 ± 3.40	/	Dual ChEI
8u	*n/a*	*n/a*	45.10 ± 4.50	21.90 ± 2.20	2.1	Dual ChEI
9a	*n/a*	*n/a*	Not active	39.40 ± 3.90	/	Dual ChEI
9g	CH	Me	20.70 ± 2.10	32.50 ± 3.30	0.6	Dual ChEI
9h	N	*i*Pr	Not active	Not active	/	Dual ChEI
9m	N	Cyclohexyl	Not active	38.40 ± 3.80	/	Dual ChEI
9u	*n/a*	*n/a*	36.20 ± 3.60	18.20 ± 1.80	2.0	Dual ChEI
10a	*n/a*	*n/a*	Not active	30.80 ± 3.10	/	Dual ChEI
10f	N	Me	Not active	28.30 ± 2.80	/	Selec. AChEI
10g	CH	Me	Not active	21.30 ± 2.10	/	Dual ChEI
10h	N	*i*Pr	Not active	Not active	/	Dual ChEI
10m	N	Cyclohexyl	Not active	31.70 ± 3.20	/	Dual ChEI
10u	*n/a*	*n/a*	59.30 ± 5.90	17.40 ± 1.70	3.4	Dual ChEI
11a	*n/a*	*n/a*	14.90 ± 1.50	35.40 ± 3.50	0.4	Selec. AChEI
11f	N	Me	Not active	32.60 ± 3.30	/	Selec. AChEI
11g	CH	Me	22.00 ± 2.20	37.40 ± 3.70	0.6	Dual ChEI
11h	N	*i*Pr	Not active	19.60 ± 2.00	/	Dual ChEI
11m	N	Cyclohexyl	Not active	36.40 ± 3.60	/	Dual ChEI
11u	*n/a*	*n/a*	32.70 ± 3.30	Not active	/	Dual ChEI
12h	N	*i*Pr	Not active	12.80 ± 1.30	/	Dual ChEI
12m	N	Cyclohexyl	Not active	36.70 ± 3.70	/	Dual ChEI
12u	*n/a*	*n/a*	50.20 ± 5.00	18.60 ± 1.90	2.7	Dual ChEI
13c[c]	S	*n/a*	38.00 ± 25.00	*n/d*	/	Dual ChEI
13f	N	Me	Not active	Not active	/	Dual ChEI
13g	CH	Me	Not active	Not active	/	Dual ChEI
13h	N	*i*Pr	17.10 ± 1.70	12.10 ± 1.20	1.4	Dual ChEI
13i	CH	*i*Pr	Not active	Not active	/	Dual ChEI
13j	N	*n*Pr	22.00 ± 2.20	Not active	/	Non-selec. ChEI
13k	N	EtOH	13.40 ± 1.30	Not active	/	Dual ChEI
13l	N	EtOMe	Not active	Not active	/	Dual ChEI
13m	N	Cyclohexyl	30.80 ± 3.10	Not active	/	Dual ChEI
13n	N	Ac	Not active	Not active	/	Dual ChEI
13o	N	Boc	11.10 ± 1.10	Not active	/	Selec. AChEI
13p	N	H	Not active	Not active	/	Dual ChEI
14f	N	Me	24.10 ± 2.40	24.80 ± 2.50	1.0	Dual ChEI

Derv	X	R"	Inhibition of $A\beta_{1-40}$ Aggreg. (%)		SI	Mode of ChEI
			AChE-induced	Self-induced		
14g	CH	Me	14.80 ± 1.50	18.90 ± 1.90	0.8	Non-selec. ChEI
14h	N	*i*Pr	20.80 ± 2.10	21.80 ± 2.20	1.4	Dual ChEI
14i	CH	*i*Pr	31.80 ± 3.20	11.80 ± 1.20	2.7	Dual ChEI
14j	N	*n*Pr	23.10 ± 2.30	18.20 ± 1.80	1.3	Non-selec. ChEI
14k	N	EtOH	18.80 ± 1.90	15.00 ± 1.50	1.3	Selec. AChEI
14l	N	EtOMe	10.40 ± 1.00	16.30 ± 1.60	0.6	Dual ChEI
14m	N	Cyclohexyl	32.00 ± 3.20	27.60 ± 2.80	1.2	Dual ChEI
14n	N	Ac	10.30 ± 1.00	15.80 ± 1.60	0.7	Selec. AChEI
14o	N	Boc	13.60 ± 1.40	11.40 ± 1.10	1.2	Not active
14p	N	H	Not active	20.80 ± 2.10	/	Selec. AChEI
15c[c]	S	*n/a*	Not active	*n/d*	/	Selec. AChEI
15g	CH	Me	Not active	26.30 ± 2.60	/	Dual ChEI
Propidium			82.00 ± 3.50	*n/d*	/	Not active
Donepezil – Aricept ®			17.00 ± 8.10	*n/d*	/	Potent AChEI
Galantamine – Reminyl ®			*n/d*	48 [*]		Dual ChEI

[a] The result (% inhibition) is the mean of two separate experiments (n = 4) ± SD. [b] SI = *h*AChE-induced/self-induced. *n/d* = not determined. [c] Derivative's anti-Aβ aggregation data obtained from the collaboration with Dr. Yang's group*; previously reported* [Ref. 121]. [*] Value retrieved from Ref. 128.

With 2,4-DPR derivatives, anti-$A\beta_{1-40}$ aggregation activity ranged from 0 up to 59% inhibition for *h*AChE-induced aggregation and from 0 up to 48% inhibition for self-induced aggregation. The benzyl derivative (**2a**) exhibited good AChE inhibition (IC_{50} = 8.90 μM); however, its smaller size (174.9 $Å^3$) could not allow it to span both the CAS and PAS, thus its activity toward anti-*h*AChE-induced aggregation is non-existent. Similarly, the methoxy-based derivatives (**9a**-**11a**) featuring the 5-membered heterocyclic C-2 group were inactive toward *h*AChE-induced aggregation (with **11a** showing very weak activity, ~ 15%) but they inhibited self-induced aggregation by ~ 30-40%. With the thiomorpholine analogs in the benzyl series (**2c**-**e**), an interesting pattern emerged, where the oxidation of the sulfur atom enabled derivatives **2d** and **2e** to exhibit good activity against *h*AChE-induced aggregation (56% and 44%; respectively) compared to the inactive parent derivative **2c**. The phenylethylamine analog (**15c**) was also inactive toward anti-*h*AChE-induced aggregation, but the naphthalen-1ylmethylamine (**13c**) analog exhibited a wide activity range (38.00% ± 25.00).

The selective AChEI (**2f** with the Me-piperazine C-2 group) exhibited superior activity against *h*AChE-induced aggregation (59%) regardless of its molecular volume (199.6 $Å^3$). Substituted variations of this derivative (bromo, fluoro, methyl, methoxy, dimethoxy or trimethoxy groups) were all inactive toward

*h*AChE-induced aggregation but they exhibited ~ 21-32% reduction in self-induced aggregation. Bulkier analogs, like the naphthalen-1ylmethylamine analog (**13f**) was inactive while the diphenylmethylamine analog (**14f**) was ~ 2.5-fold less active (24%). In terms of self-induced aggregation, **13f** was also inactive while **14f** exhibited comparable activity to *h*AChE-induced aggregation. The bioisosteric derivative (**13g**) was inactive on both fronts of $A\beta_{1-40}$ aggregation, whereas **14g** exhibited ~ 15% inhibition toward anti-*h*AChE-induced and ~ 19% inhibition toward self-induced aggregation. When coupled to a C-4 methylbenzylamine group, derivative (**8g**) exhibited activity toward self-induced aggregation only (~ 24%) and with stronger EDGs, the methoxy (**9g**) and trimethoxy (**11g**) derivatives were active toward both *h*AChE-induced and self-induced aggregation (~ 22% and 32-37%; respectively) while the dimethoxy derivative (**10g**) was only active toward self-induced aggregation (~ 21%). The *i*Pr-piperazine derivatives (**7h**, **9h**-**12h**) were all inactive toward *h*AChE-induced aggregation while **11h** and **12h** exhibited weak inhibition of self-induced aggregation (~ 20% and 12%; respectively). On the other hand, the bulkier derivatives (**13h** and **14h**), were active against both *h*AChE-induced and self-induced aggregation but **14h** exhibited better dual activity (17% and 12%, 21% and 22%; respectively). The bioisosteric derivative (**13i**) was inactive on both fronts of $A\beta_{1-40}$ aggregation, whereas **14i** exhibited ~ 32% inhibition toward *h*AChE-induced and ~ 12% inhibition toward self-induced aggregation. The *n*Pr-piperazine derivatives (**13j** and **14j**) exhibited comparable *h*AChE-induced inhibition (~ 22 to 23%); however, the latter also inhibited self-induced aggregation by 18%. The cyclohexylpiperazine derivatives exhibited an interesting pattern, where the substituted benzylamine derivatives (**3m**-**12m**) were all inactive toward anti-*h*AChE-induced aggregation, while the naphthalen-1ylmethylamine and diphenylmethylamine derivatives (**13m** and **14m**) exhibited comparable anti-*h*AChE-induced activity (~ 30-32%) corresponding to their overlapping binding modes in *h*AChE. On the other hand, derivatives **3m**-**12m** exhibited better anti-self-induced aggregation activity (~ 32-39%) compared to **14m** (~ 28%).

With the alkoxyl piperazines, derivatives **13k** and **14k** (with the hydroxyethyl group) exhibited 13% and 19% inhibition of *h*AChE-induced aggregation, while derivatives **13l** and **14l** (with the methoxyethyl group) exhibited 0% and 10% inhibition of *h*AChE-induced aggregation; respectively. In terms of self-induced aggregation, **14k** and **14l** provided 15% and 16% inhibition; respectively, while the naphthalen-1ylmethylamine analogs (**13k** and **13l**) were inactive. With an Ac-piperazine at C-2, **13n** was still inactive

toward both *h*AChE-induced activity and self-induced aggregation, while **14n** exhibited 10% and 16% inhibition; respectively. The bulkier C-2 group in **2o** (Boc-piperazine) was hypothesized to provide good activity considering the proximiety of the Boc-group to Trp286; however, this derivative exhibited weak to moderate activity against *h*AChE-induced aggregation (27%) suggesting other factors in play besides just the proximity to the crucial PAS residue in AChE. The naphthalen-1ylmethylamine and diphenylmethylamine analogs provided weak, equipotent values (~ 11 to 14%) for *h*AChE-induced aggregation and the latter (**14o**), also exhibited weak self-induced activity (11%). The hydrolyzed products of **13o** and **14o** were inactive toward both *h*AChE- (**13p** and **14p**) and self-induced (**13p**) aggregation but **14p** exhibited moderate activity against self-induced aggregation (21%).

All derivatives featuring the donepezil pharmacophore (benzylpiperidine, **3u**-**12u**) were able to reduce both *h*AChE-induced (except **3u** and **5u**) and self-induced aggregation of Aβ-peptides. Halogen/EWG-based derivatives exhibited a range of ~ 21-54% inhibition of *h*AChE-induced aggregation, while in self-induced aggregation, a range of ~ 22-48% was observed with the bromo bioisostere (**6u**) being the most active in both cases. This pattern is likely a result of the electron-withdrawing properties and sterics effects of the bromine atom. With regards to the EDG-based derivatives, anti-self-induced aggregation activity was lower than that observed with the EWG-based derivatives (range from 0-19%). With anti-*h*AChE-induced aggregation, activity ranged from ~ 33-59% with the methoxy (**9u**) and trimethoxy (**11u**) derivatives being less active than the similar dimethoxy (**10u**) and dioxolane (**12u**) derivatives, which correlates well with the molecular modeling studies.

Overall, it is evident that anti-$A\beta_{1-40}$ aggregation activity is mediated by the nature of the substituents at both the C-2 and C-4 positions of the 2,4-DPR template (Fig. **29**). Electronic and steric properties are important factors along with the derivative's proximity to the PAS of *h*AChE. In terms of self-induced aggregation, derivatives with the diphenylmethylamine C-4 group exhibited a broad range of activity where the majority of naphthalen-1ylmethylamine derivatives failed to do so. This observation is likely an effect of the aromatic structure at the C-4 position, where the branched diphenyl rings interact with $A\beta_{1-40}$ peptides and prevent them from stacking and aggregating while the planar naphthyl ring can be stacked along the β-sheet formations (Fig. **30**). The roles of EWGs and EDGs in the selectivity toward anti-$A\beta_{1-40}$ aggregation activity was evident in the profiles of derivatives **3u**-**7u** and **8u**-**12u**.

(**6u**)
AChE-induced = 53.90%
Self-induced = 48.40%

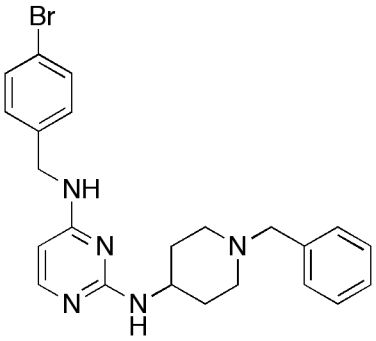

N^2-(1-benzylpiperidin-4-yl)-N^4-(4-bromobenzyl)pyrimidine-2,4-diamine

(**8u**)
AChE-induced = 45.10%
Self-induced = 21.90%

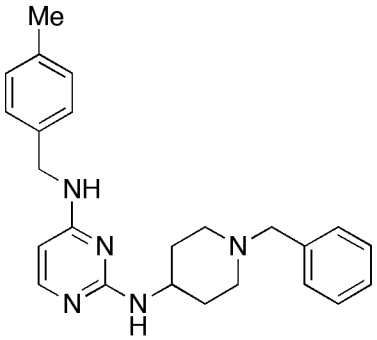

N^2-(1-benzylpiperidin-4-yl)-N^4-(4-methylbenzyl)pyrimidine-2,4-diamine

(**10u**)
AChE-induced = 59.30%
Self-induced = 17.40%

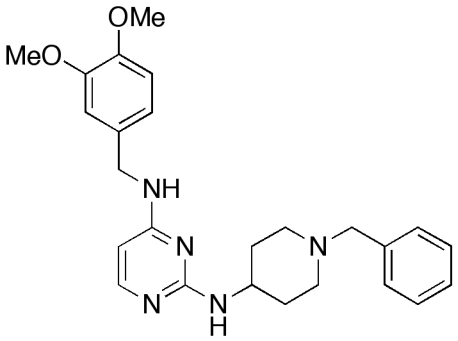

N^2-(1-benzylpiperidin-4-yl)-N^4-(3,4-dimethoxybenzyl)pyrimidine-2,4-diamine

(**12u**)
AChE-induced = 50.20%
Self-induced = 18.60%

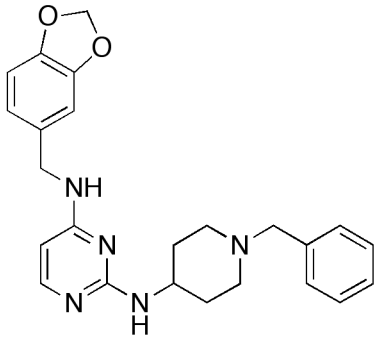

N^4-(benzo[*d*][1,3]dioxol-5-ylmethyl)-N^2-(1-benzylpiperidin-4-yl)pyrimidine-2,4-diamine

Fig. (**29**): Top dual (AChE-induced and self-induced) $A\beta_{1-40}$ aggregation inhibitors.

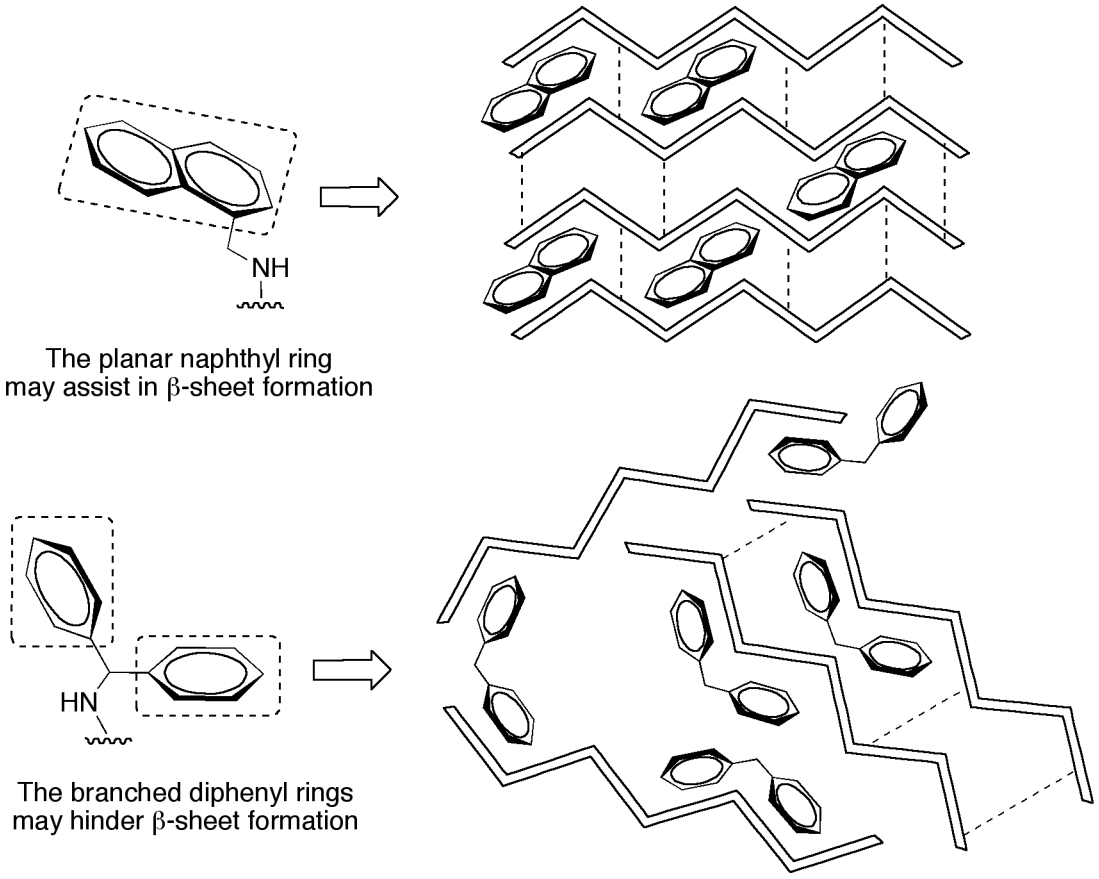

Fig. (**30**): Illustration of how the diphenyl rings in series **14** may hinder the aggregation of Aβ-peptides when compared to the stacking ability of the naphthyl ring in series **13**.

4.1.3. Anti-β-Secretase Evaluation

Due to cost constraints, it was not feasible to screen all the derivatives for anti-β-secretase activity. The selection process was dependent on the anti-ChE profiles, anti-Aβ-aggregation data (if applicable) and preliminary ligand-docking studies in *h*BACE-1. The SAR data (IC_{50}) [a] of selective derivatives is presented collectively in Table **10**, along with the mode of ChEI and anti-Aβ-activity (if applicable).

Table (**10**): Anti-β-secretase SAR data for select derivatives presented as IC_{50} values or % inhibition at their ChE IC_{50}

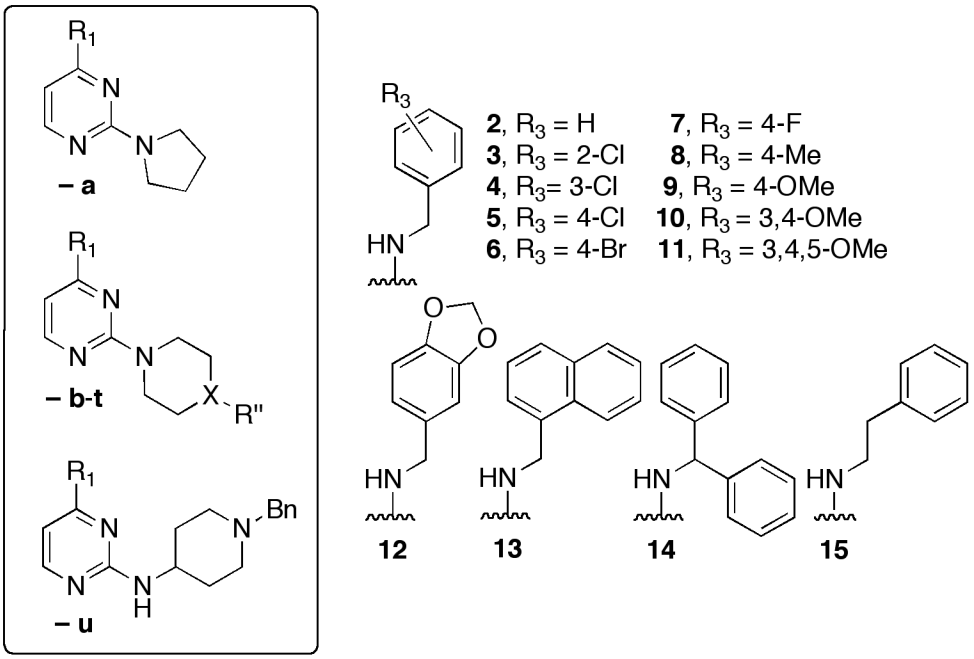

Cpd.	X	R"	IC_{50} (μM) [a]	Mode of ChEI	Mode of Anti-Aβ-activity
3m	N	Cyclohexyl	13.30	Dual ChEI	Selec. self-induced
3u	*n/a*	*n/a*	1.70	Dual ChEI	Selec. self-induced
4m	N	Cyclohexyl	2.60	Dual ChEI	Selec. self-induced
4u	*n/a*	*n/a*	0.60	Dual ChEI	Dual *h*AChE-/self-induced
5m	N	Cyclohexyl	1.30	Dual ChEI	Selec. self-induced
5u	*n/a*	*n/a*	3.20	Dual ChEI	Selec. self-induced
6f	N	Me	2.80	Dual ChEI	Selec. self-induced
6m	N	Cyclohexyl	2.40	Dual ChEI	Selec. self-induced
6u	*n/a*	*n/a*	> 50 (33%*)	Dual ChEI	Dual *h*AChE-/self-induced
7f	N	Me	2.60	Dual ChEI	Selec. self-induced
7h	N	*i*Pr	11.70	Dual ChEI	Not active
7m	N	Cyclohexyl	12.20	Dual ChEI	Selec. self-induced
7u	*n/a*	*n/a*	0.70	Dual ChEI	Dual *h*AChE-/self-induced
8f	N	Me	1.50	Dual ChEI	Selec. self-induced
8g	CH	Me	4.10	Dual ChEI	Selec. self-induced
8m	N	Cyclohexyl	3.10	Dual ChEI	Selec. self-induced
8u	*n/a*	*n/a*	11.10	Dual ChEI	Dual *h*AChE-/self-induced
9a	*n/a*	*n/a*	> 50 (34%*)	Dual ChEI	Selec. self-induced
9g	CH	Me	9.20	Dual ChEI	Dual *h*AChE-/self-induced
9h	N	*i*Pr	3.40	Dual ChEI	Not active
9m	N	Cyclohexyl	2.20	Dual ChEI	Selec. self-induced

Cpd.	X	R"	IC_{50} (μM) [a]	Mode of ChEI	Mode of Anti-Aβ-activity
9u	*n/a*	*n/a*	0.60	Dual ChEI	Dual *h*AChE-/self-induced
10a	*n/a*	*n/a*	5.20	Dual ChEI	Selec. self-induced
10f	N	Me	24.50	Selec. AChEI	Selec. self-induced
10g	CH	Me	0.60	Dual ChEI	Selec. self-induced
10h	N	*i*Pr	7.90	Dual ChEI	Not active
10m	N	Cyclohexyl	16.90	Dual ChEI	Selec. self-induced
10u	*n/a*	*n/a*	> 50 (34%*)	Dual ChEI	Dual *h*AChE-/self-induced
11a	*n/a*	*n/a*	1.30	Selec. AChEI	Dual *h*AChE-/self-induced
11f	N	Me	1.20	Selec. AChEI	Selec. self-induced
11g	CH	Me	2.90	Dual ChEI	Dual *h*AChE-/self-induced
11h	N	*i*Pr	4.60	Dual ChEI	Selec. self-induced
11m	N	Cyclohexyl	5.50	Dual ChEI	Selec. self-induced
11u	*n/a*	*n/a*	8.90	Dual ChEI	Selec. *h*AChE-induced
12h	N	*i*Pr	> 50 (12%*)	Dual ChEI	Selec. self-induced
12m	N	Cyclohexyl	0.70	Dual ChEI	Selec. self-induced
12u	*n/a*	*n/a*	1.40	Dual ChEI	Dual *h*AChE-/self-induced
15g	CH	Me	8.10	Dual ChEI	Selec. self-induced
Donepezil – Aricept ®			3.45	Potent AChEI	–
***N*-Benzyloxycarbonyl-Val-Leu-Leucinal**			14.00	–	–

[a] The results (IC_{50}) are the mean of duplicate readings (n = 2-4) with SD < 10%. *n/d* = Not determined. * % BACE-1 inhibition at the derivative's ChE IC_{50} (μM).

With 2,4-DPR derivatives, anti-β-secretase activity was relatively promising as it ranged from 0.60 to 24.50 μM with some exhibiting weak inhibition (> 50 μM). The methoxy-based derivatives with a small pyrrolidine C-2 group demonstrated that the number of OMe substituents at the C-4 phenyl was modulating activity in the order of **9a** < **10a** < **11a**. With a C-2 Me-piperazine, halogen-based derivatives (4-bromo and 4-fluorobenzylamine at C-4) exhibited equipotent activity (IC_{50} values between 2.60 and 2.80 μM) making them ~ 1.3-fold more potent than donepezil and ~ 5-fold more potent than the peptide-like BACE-1 inhibitor II (*N*-Benzyloxycarbonyl-Val-Leu-Leucinal). With EDGs at C-4, the methyl and tri-OMe derivatives (**8f** and **11f**) exhibited equipotent activity (IC_{50} ~ 1.20-1.50 μM), whereas the di-OMe derivative (**10f**) was ~ 16-fold less potent. With a C-2 Me-piperidine bioisostere, derivatives **8g** and **11g** were ~ 2.5-2.7-fold less potent compared to their piperazine relatives. This pattern was reversed for **10g**, where the bioisosteric replacement improved BACE-1 inhibition by ~ 41-fold (IC_{50} = 0.60 μM) and when compared

to the di-and trimethoxy derivatives, **9g** was the least active with an IC_{50} of 9.20 μM. Similarly, the phenylethylamine derivative also exhibited moderate activity (**15g**, IC_{50} = 8.10 μM) despite its extended C-4 group. With the branched *i*Pr-piperazine, the methoxy and tri-OMe derivatives (**9h** and **11h**) exhibited comparable potencies, while the presence of a highly EWG resulted in decrease in activity (**7h**, IC_{50} = 11.70 μM). Interestingly, the dioxolane derivative was not active (IC_{50} > 50 μM) despite it structural similarity to **10h**.

The SAR data involving the cyclohexylpiperazine C-2 group revealed an interesting pattern. With Cl-substituted benzylamine derivatives, the placement of the chlorine atom had a dramatic effect on BACE-1 inhibition and the order of potency was *p*-Cl > *m*-Cl > *o*-Cl. The bromo-substituted derivative was equipotent to the *m*-Cl analog (IC_{50} ~ 2-3 μM), while the fluoro-substituted derivative exhibited similar activity to that of the *o*-Cl analog (IC_{50} ~ 12-13 μM). With EDG-based derivatives, activity ranged from 0.70 μM (**12m**) to 16.90 μM (**10m**) with the methyl, methoxy and tri-OMe derivatives exhibiting low micromolar potency (IC_{50} ~ 2-5 μM).

Derivatives featuring the donepezil pharmacophore (benzylpiperidine, **3u**-**12u**) exhibited a wide range of inhibition (IC_{50} ~ 0.60 to > 50 μM). The EWG-based derivatives were potent inhibitors (IC_{50} ~ 0.60-3.20 μM) with the exception of the bromo-substituted analog (**6u**, IC_{50} > 50 μM). The EDG-based derivatives were moderate inhibitors with the exception of **9u** (IC_{50} = 0.60 μM, equipotent to **4u**). The second most potent inhibitor within this sub-group was **12u** (IC_{50} = 1.40 μM) and the methyl and tri-OMe analogs exhibited similar activities (IC_{50} = 8.90 and 11.10 μM; respectively). Surprisingly, the di-OMe analog (**10u**) was inactive up to 50 μM while **9u**, **11u** and **12u** (with the same C-2 pharmacophore) exhibited activity below 12 μM.

It is noteworthy that the 34 derivatives tested (~ 40% of the chemical library) generally exhibited potent BACE-1 inhibition with a few exceptions. Derivatives **4u**, **7u**, **9u**, **10g** and **12m** were indentified as promising compounds as they exhibited potent anti-BACE-1 activity (IC_{50} = 0.60 to 0.70 μM). The activity profile is sensitive to the nature of the substituents at both the C-2 and C-4 positions of the 2,4-DPR template but the overall design of these derivatives seem to be suitable to target BACE-1. Where AChE and BuChE have U-shaped active sites, BACE-1 has a more linear, cylindrical-type active site, which recognizes the linear and potential V-shaped conformations of 2,4-DPR derivatives.

4.1.4. Cell Viability *(data presented here is a result of collaborations with other groups)*

The results here represent the effects of select derivatives on the cell viability of neuroblastoma cells in the MTT assay. The SAR data (% cell viability at 40 μM) [a] of select derivatives is presented collectively in Table **11**.

Table (**11**): Percent SH-SY5Y neuroblastoma cell viability SAR data for select derivatives presented at 40 μM.

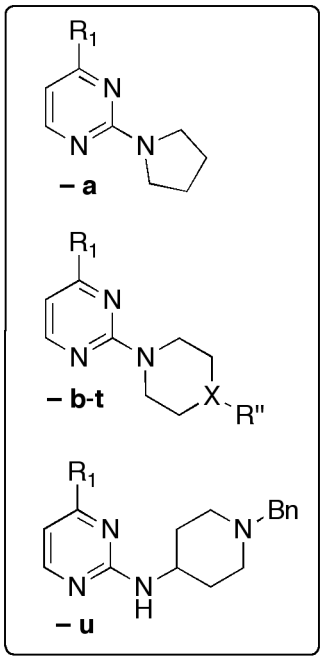

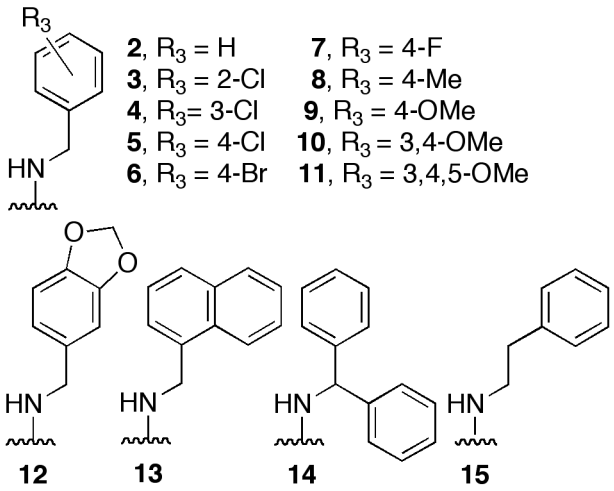

Cpd.	X	R"	Cell Viability (%)	Cpd.	X	R"	Cell Viability (%)
2a[b]	*n/a*	*n/a*	101.70 ± 16.40	**7u**[c]	*n/a*	*n/a*	8.90 ± 8.10
2b[b]	O	*n/a*	100.40 ± 6.00	**8m**[c]	N	Cyclohexyl	35.0 ± 1.00
2c[b]	S	*n/a*	97.80 ± 11.50	**8u**[c]	*n/a*	*n/a*	5.30 ± 2.60
2d[b]	S	O	89.70 ± 11.50	**9g**[c]	CH	Me	8.60 ± 3.40
2e[b]	S	O_2	91.80 ± 2.20	**9m**[c]	N	Cyclohexyl	53.40 ± 7.70
2f[b]	N	Me	98.30 ± 10.50	**9u**[c]	*n/a*	*n/a*	21.40 ± 18.00
2g[b]	CH	Me	89.50 ± 6.60	**10f**[c]	N	Me	60.30 ± 0.40
2h[b]	N	*i*Pr	81.00 ± 10.30	**10g**[c]	CH	Me	59.50 ± 9.00
2i[b]	CH	*i*Pr	45.20 ± 4.30	**10h**[c]	N	*i*Pr	61.90 ± 6.30
2j[b]	N	*n*Pr	87.90 ± 4.70	**10m**[c]	N	Cyclohexyl	67.10 ± 16.40
2k[b]	N	EtOH	81.20 ± 8.90	**10u**[c]	*n/a*	*n/a*	81.00 ± 7.20
2l[b]	N	EtOMe	78.60 ± 6.70	**11f**[c]	N	Me	60.50 ± 4.70
2n[b]	N	Ac	109.10 ± 4.60	**11g**[c]	CH	Me	69.10 ± 10.00
2o[b]	N	Boc	107.90 ± 0.50	**11m**[c]	N	Cyclohexyl	54.60 ± 7.20
2q[b]	N	*p*-Cl-Bn	74.90 ± 4.00	**11u**[c]	*n/a*	*n/a*	36.90 ± 5.50
2r[b]	N	*p*-Br-Bn	67.50 ± 3.40	**12g**[c]	CH	Me	42.00 ± 6.10
2s[b]	N	*p*-F-Bn	39.10 ± 4.20	**12h**[c]	N	*i*Pr	54.70 ± 6.50
2t[b]	N	*p*-CF_3-Bn	- 0.90 ± 7.40	**12m**[c]	N	Cyclohexyl	51.40 ± 8.60

Cpd.	X	R"	Cell Viability (%)	Cpd.	X	R"	Cell Viability (%)
2u[c]	*n/a*	*n/a*	44.20 ± 14.80	**12u**[c]	*n/a*	*n/a*	45.80 ± 20.20
3m[c]	N	Cyclohexyl	36.50 ± 4.70	**13b**[b]	O	*n/a*	95.00 ± 5.00
3u[c]	*n/a*	*n/a*	0.60 ± 0.30	**13c**[b]	S	*n/a*	89.30 ± 2.90
4f[c]	N	Me	72.00 ± 0.90	**13h**[c]	N	*i*Pr	70.80 ± 2.60
4u[c]	*n/a*	*n/a*	1.40 ± 1.00	**13j**[c]	N	*n*Pr	85.30 ± 17.90
5g[c]	CH	Me	0.20 ± 0.01	**13m**[c]	N	Cyclohexyl	30.80 ± 1.80
5u[c]	*n/a*	*n/a*	1.50 ± 0.60	**14h**[c]	N	*i*Pr	93.20 ± 6.30
6g[c]	CH	Me	0.50 ± 0.20	**14i**[c]	CH	*n*Pr	2.00 ± 0.50
6h[c]	N	*i*Pr	67.40 ± 8.20	**14m**[c]	N	Cyclohexyl	29.00 ± 5.30
6u[c]	*n/a*	*n/a*	1.30 ± 0.30	**15b**[b]	O	*n/a*	90.20 ± 10.80
7f[c]	N	Me	63.00 ± 6.70	**15c**[b]	S	*n/a*	116.10 ± 4.60
7m[c]	N	Cyclohexyl	45.40 ± 7.60	**15n**[b]	N	Ac	82.60 ± 6.70

[a] The results (% cell viability) are the mean of at least two separate experiments ($n = 4$) ± SD. [b] Derivative's cell viability data obtained from the collaboration with Dr. Yang's group. [c] Derivative's cell viability data obtained from the collaboration with Dr. Beazely's group.

Through the efforts of the collaborating groups, cell viability profiles were obtained for 60 of the 112 derivatives (~ 54% screened) and the results covered the entire spectrum ranging from 0 up to 100% cell viability. About 40% of the tested derivatives did not exhibit significant toxicity effects on neuroblastoma cell function (24 showed > 70% cell viability at 40 μM); however, an equal number were significantly harmful to the cells (23 showed < 50% + cell viability at 40 μM). The observations presented here suggest that the impact of 2,4-DPR derivatives on cell viability is dependent on the nature of the substituents at the C-2 and C-4 positions (ranges from 0 to 100%) and that ClogP values alone could not be used to predict cell viability. The tendency is for hydrophobic compounds to be more toxic compared to their more hydrophilic relatives/bioisosteres and this pattern is observed when comparing derivatives with a Me-piperazine or *i*Pr-piperazine C-2 group (**f** and **h**) with their respective bioisosteric relatives with a Me-piperidine or *i*Pr-piperidine C-2 group (**g** and **i**).

4.2. Molecular modeling studies

Computational chemistry plays an important role in understanding a derivative's biological profile and corroborating the acquired SAR. The proceeding sub-sections describe the binding modes of the lead cholinesterase and β-secretase inhibitors within their respective enzymes. The docking images were oriented to correspond to those in Section 1.2.2 and 1.3.3 and only the key residues within the active site

are highlighted. Hydrogen atoms were also removed to improve clarity and hydrogen-bonding interactions are depicted in solid green lines.

4.2.1. Lead acetylcholinesterase inhibitor

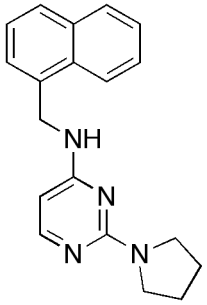

■ *N*-(Naphthalen-1-ylmethyl)-2-(pyrrolidin-1-yl)pyrimidin-4-amine

Designation: **13a**

Cholinesterase Profile: AChE IC_{50} = 5.50 µM, BuChE IC_{50} = 8.90 µM; S.I = 0.62

Amyloid Profile: β-secretase IC_{50} = *n/d*; $A\beta_{1\text{-}40}$-aggreg. (%) = *n/d*

SH-SY5Y Neuroblastoma Cell Viability (% at 40 µM)*: n/d*

Other Aspects: MW = 304.39 $gmol^{-1}$; MV = 210.60 $Å^3$; ClogP = 4.14

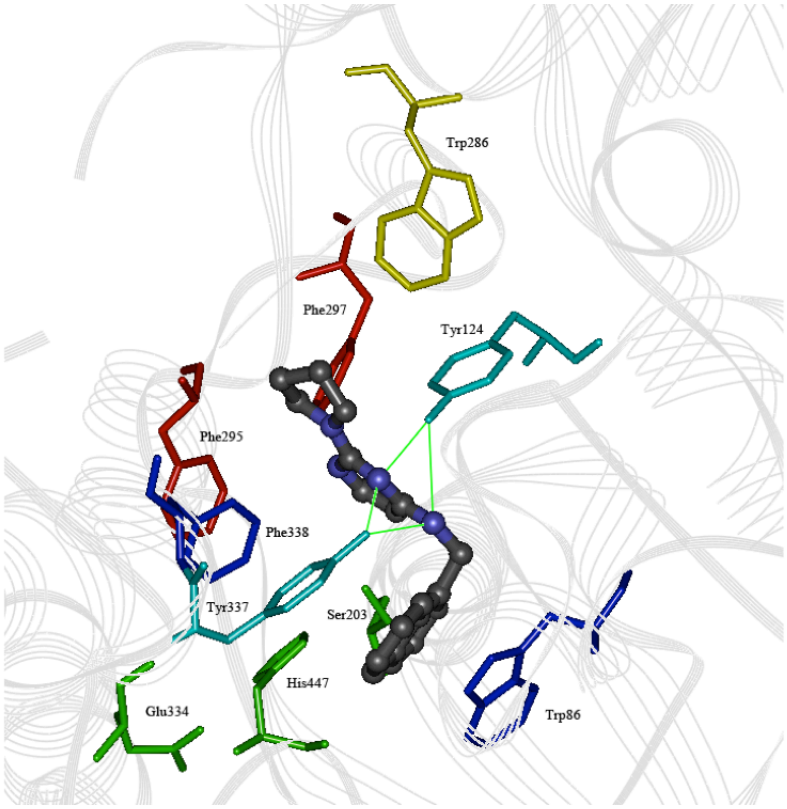

Fig. (**31**): Docking of *N*-(Naphthalen-1-ylmethyl)-2-(pyrrolidin-1-yl)pyrimidin-4-amine (**13a,** ball and stick) in the active site of *h*AChE. Green lines represent hydrogen bonding (distance < 3.5 Å). Hydrogen atoms are not shown for clarity. *Green*: CT; *Red*: Acyl pocket; *Blue*: Hydrophobic stabilizing residues; *Yellow*: gorge entry (PAS – AChE); *Turquoise*: hydrogen bonding residues.

The binding mode of **13a** in *h*AChE (PDB: 1B41) (Fig. **31**) indicated that the 2,4-DPR template was located midway through the active site gorge (~ 6 Å away from the catalytic triad His447 residue at the bottom of the active site and ~ 7 Å away from the PAS Trp286). The ring was also equidistantly suspended between Tyr124 and Tyr337 allowing for two hydrogen bonding interactions between the tyrosine hydroxyl groups and the C-4 N*H* along with two additional interactions between the tyrosine hydroxyl groups and the pyrimidine N-3 (distances < 3.5 Å). Hydrophobic interactions with a nearby glycine pocket (Gly120-122; ~ 5 Å away) assisted with template orientation. The naphthyl ring was tightly stacked between the aromatic segments of Tyr337 and Trp86 (distance ~ 3.5 Å) and the C-3/C-4 carbons of the naphthyl ring were in close proximity to His447 (distances 3.5-4 Å). The 5-membered pyrrolidine substituent was oriented toward an aromatic region close to the PAS and was ~ 4.5 Å away from Trp286 and ~ 3.5 Å from Tyr341. It is noteworthy that although the catalytic site is relatively exposed in this binding pattern (e.g. no close interactions with Ser203), the placement of the bulky, planar naphthyl ring at the C-4 position most likely attributed to this derivative's potency considering its close proximity to Trp86 (a key element in stabilizing ACh binding).

4.2.2. Lead butyrylcholinesterase inhibitor

■ 2-(4-cyclohexylpiperazin-1-yl)-*N*-(4-methylbenzyl)pyrimidin-4-amine

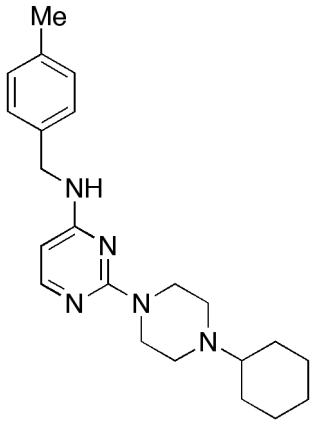

Designation: **8m**

Cholinesterase Profile: AChE IC_{50} = 16.80 μM, BuChE IC_{50} = 1.70 μM; S.I = 0.62

Amyloid Profile: β-secretase IC_{50} = 3.10 μM; $A\beta_{1\text{-}40}$-aggreg. (%) = Not active (*h*AChE-induced); 33.80 (self-induced)

SH-SY5Y Neuroblastoma Cell Viability (% at 40 μM)*:* 35.00

Other Aspects: MW = 365.52 $gmol^{-1}$; MV = 264.10 $Å^3$; ClogP = 5.03

The binding mode of **8m** in *h*BuChE (PDB: 1P0I) (Fig. **32**) indicated that the 2,4-DPR template was immersed closer to the active site (~ 7.5 Å away from the catalytic triad His438 residue at the bottom of the active site and ~ 17 Å away from the entry residue, Ala277). The ring stacked between Trp82 (~ 4.5 Å

away) and the tri-glycine pocket comprised of Gly115-117 (~ 3.8 Å away). The 4-methylphenyl ring at C-4 is perpendicularly stacked atop His438 (distance ~ 4.5 Å) with the methyl group pointed at Ala328, Met437 and Trp430 (distances ~ 3.8, 4.2 and 4.8 Å; respectively). The only hydrogen bonding interaction observed in this binding mode is that of the C-4 N*H* with the side chain of Glu197 (distance = 3.3 Å). Interestingly, the entire C-4 group (4-methylbenzylamine) and the 2,4-DPR template form a V-shaped conformation over Trp82, which is likely to hinder any interaction with ACh. The bulky and sterically demanding cyclohexylpiperazine C-2 substituent was oriented toward the entry site of BuChE and it exhibited an interesting Z-shaped conformation. The piperazine ring runs parallel along side a Thr120 residue (distance ~ 3-4 Å), while the cyclohexyl ring is hydrophobically interacting with Tyr332 and Asp70 (distances ~ 4-5 Å) and is ~ 10 Å away from Ala277. Although this binding mode doesn't offer much in terms of hydrogen bonding interactions, its orientation and proximity to the active site allowed for a great deal of hydrophobic interactions at either side of the ligand. The sterics and interactions offered by the C-2 cyclohexylpiperazine group and the V-shaped conformation atop Trp82 likely attributed to this derivative's potent anti-BuChE profile.

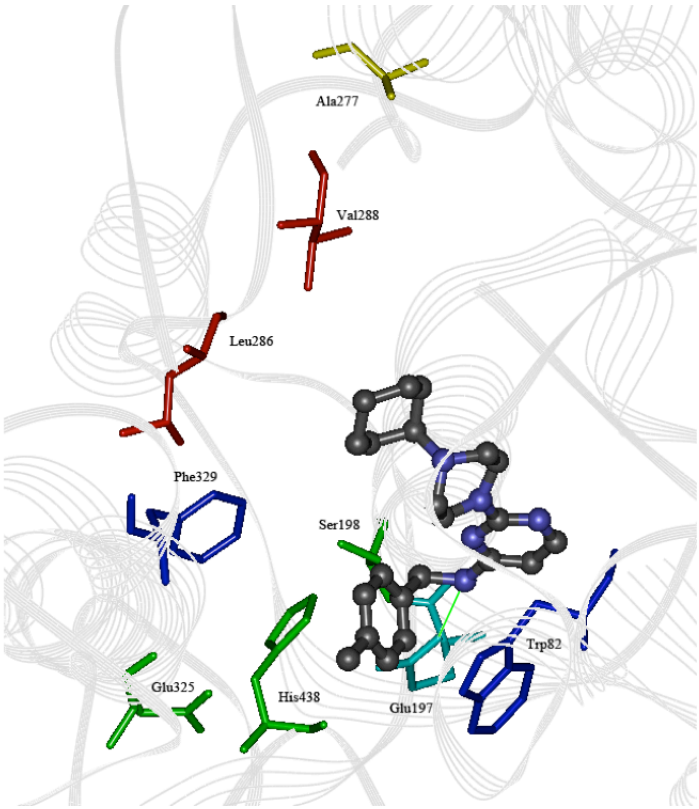

Fig. (**32**): Docking of 2-(4-cyclohexylpiperazin-1-yl)-*N*-(4-methylbenzyl)pyrimidin-4-amine (**8m,** ball and stick) in the active site of *h*BuChE. Green lines represent hydrogen bonding (distance < 3.5 Å). Hydrogen atoms are not shown for clarity. *Green*: CT; *Red*: Acyl pocket; *Blue*: Hydrophobic stabilizing residues; *Yellow*: gorge entry; *Turquoise*: hydrogen bonding residues.

4.2.3. Lead dual cholinesterase inhibitor

■ N^2-(1-Benzylpiperidin-4-yl)-N^4-(4-fluorobenzyl)pyrimidine-2,4-diamine

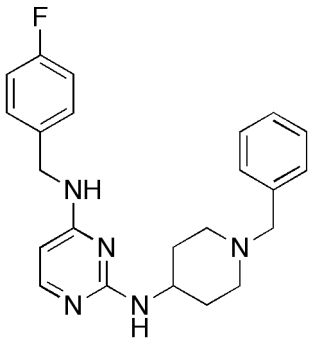

Designation: **7u**

Cholinesterase Profile: AChE IC_{50} = 7.70 µM, BuChE IC_{50} = 2.20 µM; S.I = 3.50

Amyloid Profile: β-secretase IC_{50} = 0.70 µM; $A\beta_{1\text{-}40}$-aggreg. (%) = 38.10 (*h*AChE-induced); 29.80 (self-induced)

SH-SY5Y Neuroblastoma Cell Viability (% at 40 µM)*:* 8.90

Other Aspects: MW = 391.48 $gmol^{-1}$; MV = 263.10 $Å^3$; ClogP = 4.75

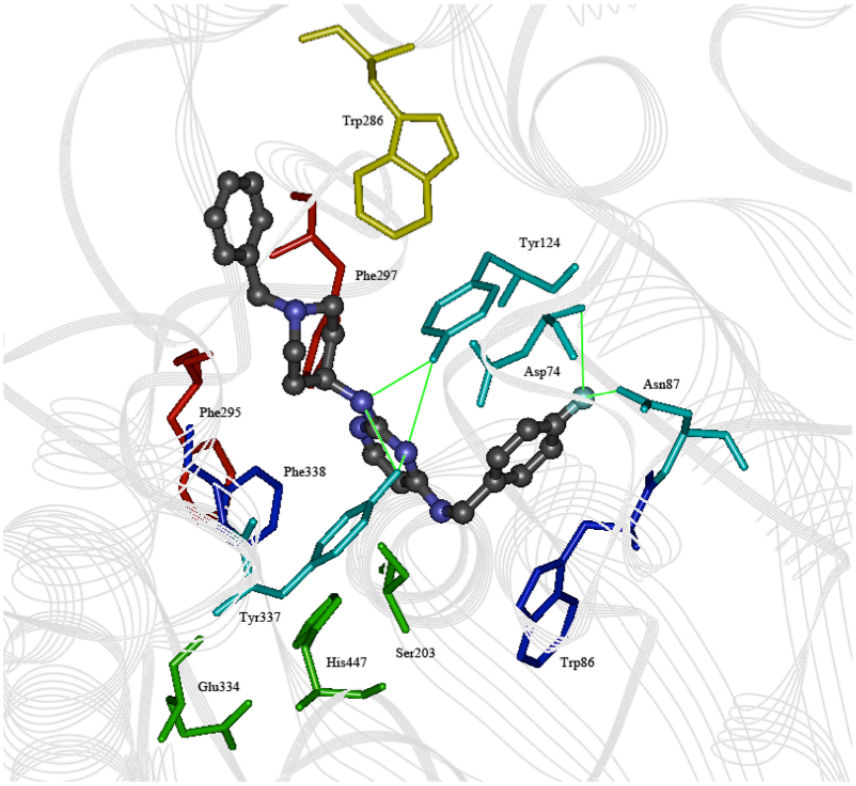

Fig. (**33**): Docking of N^2-(1-Benzylpiperidin-4-yl)-N^4-(4-fluorobenzyl)pyrimidine-2,4-diamine (**7u,** ball and stick) in the active site of *h*AChE. Green lines represent hydrogen bonding (distance < 3.5 Å). Hydrogen atoms are not shown for clarity. *Green*: CT; *Red*: Acyl pocket; *Blue*: Hydrophobic stabilizing residues; *Yellow*: gorge entry; *Turquoise*: hydrogen bonding residues.

The binding mode of **7u** in *h*AChE (PDB: 1B41) (Fig. **33**) indicated that the 2,4-DPR template was located midway through the active site gorge (~ 6.5 Å away from the catalytic triad His447 residue at the bottom of the active site and ~ 7 Å away from the PAS Trp286). The ring was also equidistantly suspended between Tyr124 and Tyr337 allowing for six hydrogen bonding interactions between the tyrosine hydroxyl groups and the C-2 NH and pyrimidine N-3 (3 hydrogen bonding interactions per Tyr residue; distances < 3.5 Å). Hydrophobic interactions with a nearby glycine pocket (Gly121 and 122; ~ 5 Å away) assisted with template orientation and C-5/6 of the ring are in close proximity to the catalytic residues (~ 4-6 Å). The entire C-4 group (4-fluorobenzylamine) was arched at a 90° angle off of the ligand's linear conformation to orient the fluorine atom in a polar pocket that allowed for two hydrogen bonding interactions to take place (Asp74 and Asn87 involved; distance ~ 3.5 Å). This arch conformation was supported by Trp86 that held the C-4 phenyl ring in place (distance ~ 4 Å). The donepezil pharmacophore (benzylpiperidine) was extended linearly from the C-2 amine group and was nestled by a large aromatic pocket comprised of Trp286, Tyr341 and Tyr337. Interestingly, the benzyl component of the pharmacophore was positioned at the posterior face of Trp286 and this prevents the C-2 group from fully interacting with the PAS. Overall, the ligand mainly exhibited a linear conformation spanning the CAS and PAS simultaneously. The arching conformation observed with the C-4 group was interesting as it denotes the unique properties offered by the small, yet highly electronegative halogen, fluorine.

On the other hand, the binding mode of **7u** in *h*BuChE (PDB: 1P0I) (Fig. **34**) indicated that the 2,4-DPR template was located almost midway through the active site gorge (~ 10 Å away from the catalytic triad His447 residue at the bottom of the active site and ~ 12 Å away from the entry site residue, Ala277). The ring was also stacked against Asp70 (distances ~ 4-5 Å) and perpendicularly suspended between Thr120 and Tyr332 (equidistant at ~ 4.5 Å). Similar to its *h*AChE binding mode, the entire C-4 group (4-fluorobenzylamine) was arched at a 90° angle off of the template's linear conformation to orient the fluorine atom toward His438 (hydrogen bonding interaction; distance ~ 3.5 Å) and Ser198. This arch conformation was supported by perpendicular stacking of the C-4 phenyl ring between Trp82 and Phe329 (distance ~ 4-6 Å). The donepezil pharmacophore (benzylpiperidine) was also arched at a 90° angle off of the template's linear conformation to run parallel to the orientation of the C-4 group. This placed the entire C-2 group in a hydrophobic region running along side Pro285 and the enzyme's acyl pocket (Leu286,

Ser287, Val288; distances ~ 4-5 Å) with the phenyl ring ~ 4 Å away from Trp231 and Phe398. Despite the fact that the ligand was oriented in an inverse U-shaped conformation, which is considered unfavourable, it was able to interact with various key residues and exhibit a good anti-BuChE profile.

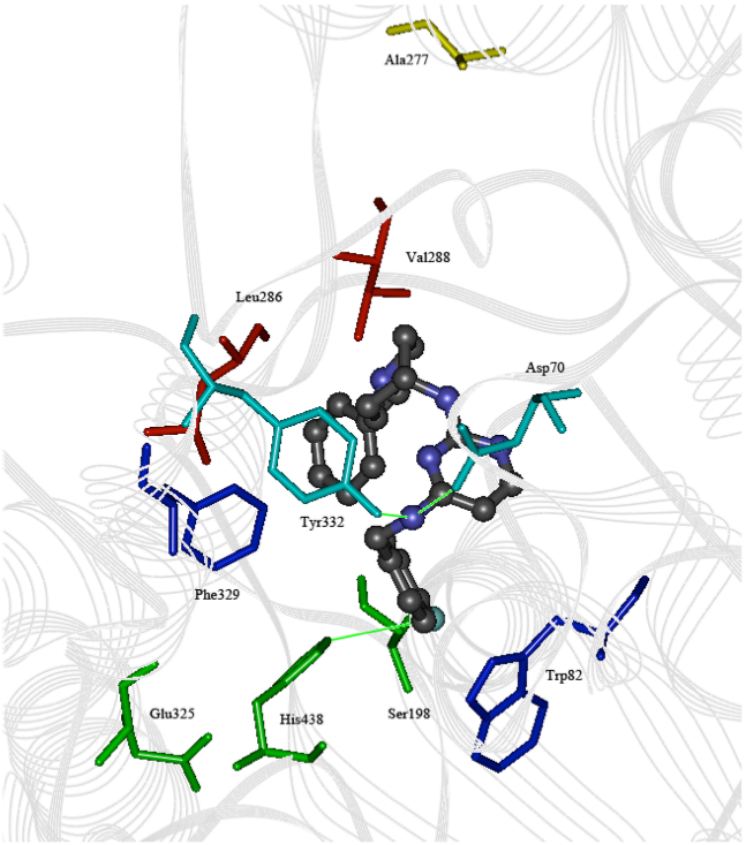

Fig. (**34**): Docking of N^2-(1-Benzylpiperidin-4-yl)-N^4-(4-fluorobenzyl)pyrimidine-2,4-diamine (**7u,** ball and stick) in the active site of *h*BuChE. Green lines represent hydrogen bonding (distance < 3.5 Å). Hydrogen atoms are not shown for clarity. *Green*: CT; *Red*: Acyl pocket; *Blue*: Hydrophobic stabilizing residues; *Yellow*: gorge entry; *Turquoise*: hydrogen bonding residues.

4.2.4. Lead β-secretase inhibitor

■ N^2-(1-benzylpiperidin-4-yl)-N^4-(4-chlorobenzyl)pyrimidin-2,4-diamine

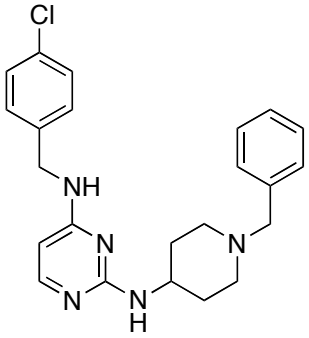

Designation: **4u**

Cholinesterase Profile: AChE IC_{50} = 7.70 µM, BuChE IC_{50} = 2.50 µM; S.I = 3.10

Amyloid Profile: β-secretase IC_{50} = 0.60 µM; $A\beta_{1\text{-}40}$-aggreg. (%) = 27.70 (*h*AChE-induced); 39.90 (self-induced)

SH-SY5Y Neuroblastoma Cell Viability (% at 40 µM)*:* 1.40

Other Aspects: MW = 407.94 gmol^{-1}; MV = 271.70 Å^3; ClogP = 5.32

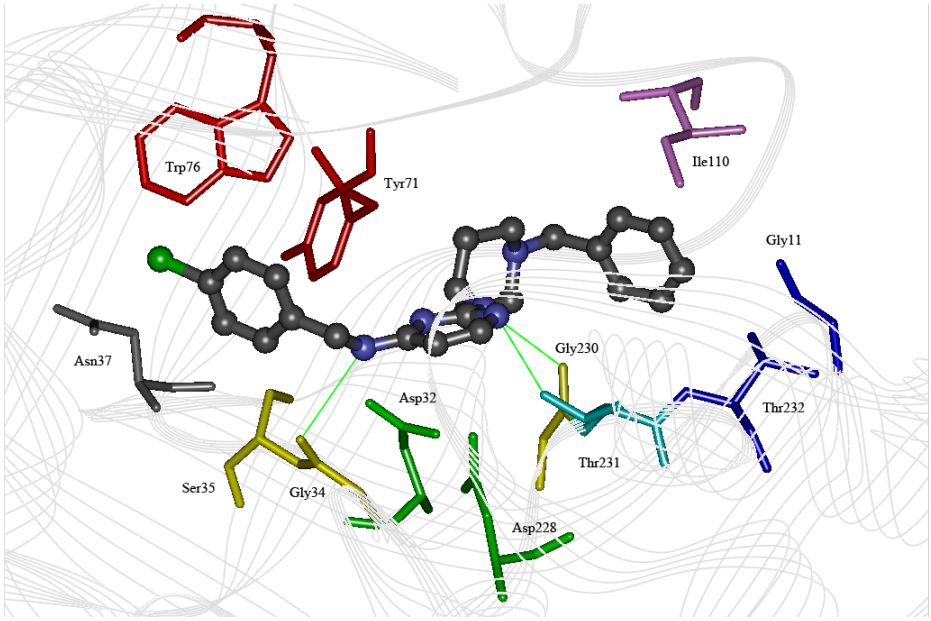

Fig. (**35**): Docking of N^2-(1-benzylpiperidin-4-yl)-N^4-(4-chlorobenzyl)pyrimidin-2,4-diamine (**4u,** ball and stick) in the active site of *h*BACE-1. Green lines represent hydrogen bonding (distance < 3.5 Å). Hydrogen atoms are not shown for clarity. *Green*: Catalytic site; *Red*: Flap; *Purple*, *grey* and *Blue*: Some hydrophobic and hydrophilic residues of the various sub-site pockets in BACE-1; *Yellow*: Other key residues - part of the hydrogen-bond network; *Turquoise*: hydrogen bonding residues.

The binding mode of **4u** in *h*BACE-1 (PDB: 1FKN) (Fig. **35**) indicated that the 2,4-DPR template was perpendicularly stacked between the active site Asp228 residue and Thr72 (distance ~ 3.5-5 Å) allowing for a hydrogen-bonding interaction between the pyrimidine N-1 and the Thr231 O*H* (distance < 2.5 Å). The 4-chlorobenzylamine substituent at the C-4 position was oriented toward a relatively hydrophobic pocket comprised of Val69, Pro70, Arg128, Tyr198 and Ile126 (distance ~ 6.5 Å) allowing for a strong hydrogen-bonding interaction between the C-4 N*H* and the backbone C=O of Gly34 (distance = 2.7 Å). The benzylpiperidine substituent at C-2 exhibited a V-shaped conformation as a result of its interactions within a hydrophobic region comprised of Tyr71, Phe108, Ile110 and Trp115 (distances ~ 6 Å). This conformation however, allowed for C-2 N*H* to undergo a strong hydrogen-bonding interaction with the C=O of Gly230 (distance < 2.3 Å). Overall this derivative exhibited an S-shaped binding mode in BACE-1; the balance of hydrogen-bonding and hydrophobic interactions at both the C-2 and C-4 positions allowed this derivative to exhibit potent BACE-1 inhibition.

4.2.5. Key Superimpositions

Investigating the binding modes of related ligands by superimposition of docked structures (SODS) is a fast and convenient method to correlate their binding modes with the biological profiles.

Fig. (**36**) – *h*AChE SODS of:

■ 2-(4-Cyclohexylpiperazin-1-yl)-*N*-(naphthalen-1-ylmethyl)pyrimidin-4-amine (**13m**):

AChE IC_{50} = 8.70 μM

■ *N*-Benzhydryl-2-(4-cyclohexylpiperazin-1-yl)pyrimidin-4-amine (**14m**):

AChE IC_{50} = 10.00 μM

The SODS of **13m** and **14m** elegantly corroborates the biological profiles of these derivatives in terms of their similar activity against *h*AChE (8.70 and 10.00 μM) and *h*AChE-induced aggregation of $A\beta_{1-40}$ peptide (~ 32% at 100 μM).

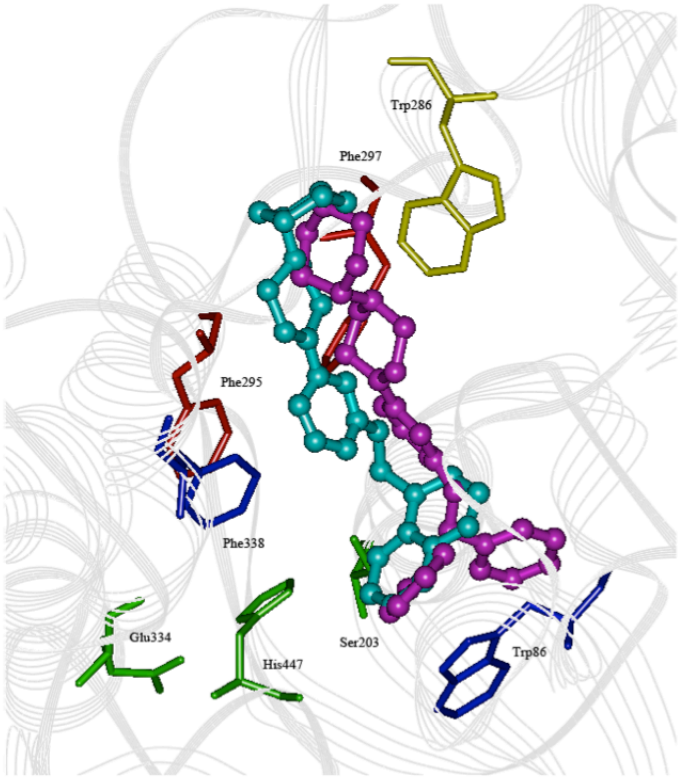

Fig. (**36**): SODS of **13m** (turquoise, ball and stick) and **14m** (fuchsia, ball and stick) in the active site of *h*BuChE. Hydrogen atoms are not shown for clarity. *Green*: CT; *Red*: Acyl pocket; *Blue*: Hydrophobic stabilizing residues; *Yellow*: gorge entry.

Fig. (**37**) – *h*AChE SODS of:

■ N^2-(1-Benzylpiperidin-4-yl)-N^4-(4-methoxybenzyl)pyrimidine-2,4-diamine (**9u**):

AChE IC_{50} = 9.40 μM

■ N^2-(1-Benzylpiperidin-4-yl)-N^4-(3,4-dimethoxybenzyl)pyrimidine-2,4-diamine (**10u**):

AChE IC_{50} = 9.90 μM

■ N^2-(1-Benzylpiperidin-4-yl)-N^4-(3,4,5-trimethoxybenzyl)pyrimidine-2,4-diamine (**11u**):

AChE IC_{50} = 10.30 μM

With donepezil for comparative purposes

The SODS of **9-11u** along with donepezil show how the 2,4-DPR derivatives extend further toward the PAS compared to donepezil correlating with the enhanced inhibition of *h*AChE-induced aggregation of $A\beta_{1-40}$ peptide. Interestingly, **10u** was completely blocking access to Trp286 compared to all the other

ligands shown. At the active site, the donepezil and 2,4-DPR derivative benzylpiperidine pharmacophores are all oriented toward Trp86 at varying angles.

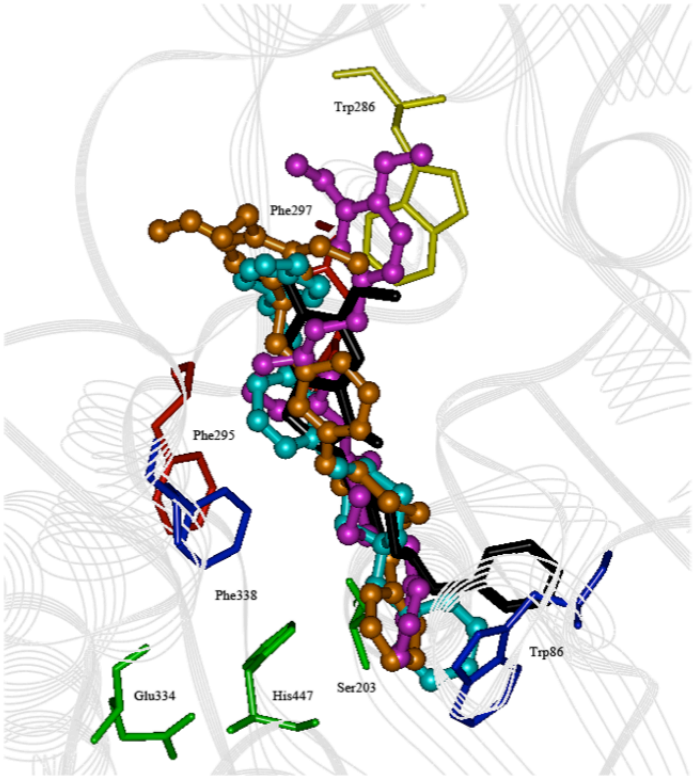

Fig. (**37**): SODS of **9u** (turquoise, ball and stick), **10u** (fuchsia, ball and stick) and **12u** (orange, ball and stick) in the active site of *h*AChE. Donepezil (black, stick) is shown for comparison. Hydrogen atoms are not shown for clarity. *Green*: CT; *Red*: Acyl pocket; *Blue*: Hydrophobic stabilizing residues; *Yellow*: gorge entry.

Fig. (**38**) – *h*BuChE SODS of:

■ 2-(4-Methylpiperazin-1-yl)-*N*-(naphthalen-1-ylmethyl)pyrimidin-4-amine (**13f**):

BuChE IC_{50} = 2.60 μM

■ 2-(4-Methylpiperidin-1-yl)-*N*-(naphthalen-1-ylmethyl)pyrimidin-4-amine (**13g**):

BuChE IC_{50} = 2.20 μM

■ *N*-Benzyl-2-(4-methylpiperidin-1-yl)pyrimidin-4-amine (**2g**):

BuChE IC_{50} = 3.40 μM

The SODS of **2g**, **13f** and **13g** corroborated the very similar anti-BuChE activities of these derivatives, regardless of the bioisosteric variances at either or both of the C-2 and C-4 positions. By interacting with Trp82 and the acyl pocket residues, these derivatives were able to provide potent BuChEI (IC_{50} < 4 μM).

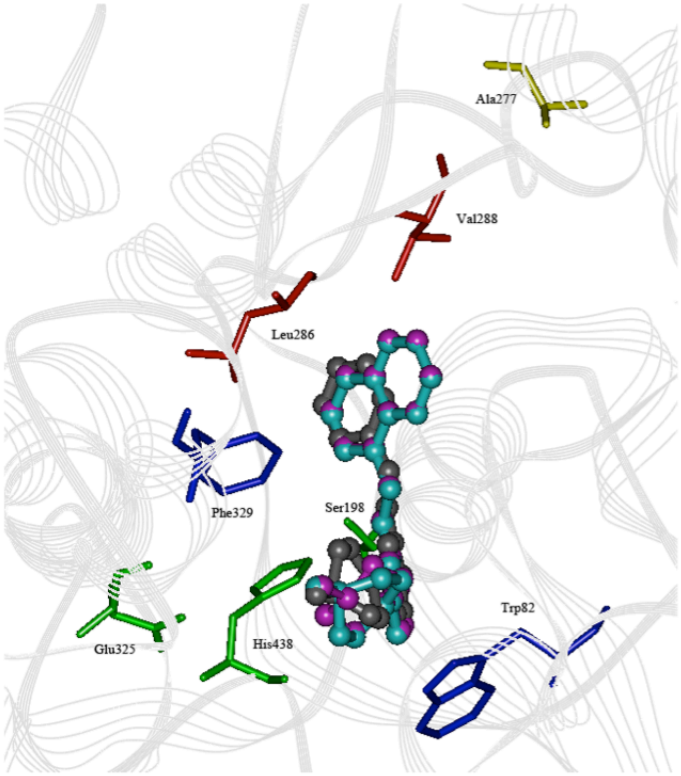

Fig. (**38**): SODS of **2g** (grey, ball and stick), **13f** (fuchsia, ball and stick) and **13g** (turquoise, ball and stick) in the active site of *h*BuChE. Hydrogen atoms are not shown for clarity. *Green*: CT; *Red*: Acyl pocket; *Blue*: Hydrophobic stabilizing residues; *Yellow*: gorge entry.

Fig. (**39**) – *h*BuChE SODS of:

■ *N*-(2-Chlorobenzyl)-2-(4-isopropylpiperazin-1-yl)pyrimidin-4-amine (**3h**):

BuChE IC_{50} = 4.70 μM

■ *N*-(3-Chlorobenzyl)-2-(4-isopropylpiperazin-1-yl)pyrimidin-4-amine (**4h**):

BuChE IC_{50} = 5.90 μM

■ *N*-(4-Chlorobenzyl)-2-(4-isopropylpiperazin-1-yl)pyrimidin-4-amine (**5h**):

BuChE IC_{50} = 6.70 μM

The SODS of **3**-**5h** corroborated the very similar anti-BuChE activities of these derivatives, regardless of the bioisosteric placement of the chlorine atom (2-, 3- or 4-position; respectively) on the C-4 benzylamine group. Interestingly, **3h** and **4h** were overlapping for most of their binding conformations (C-4 groups ran along side the acyl pocket), but **5h** was rotated 180° along the *x*-axis (C-4 group ran between Trp82 and Phe329).

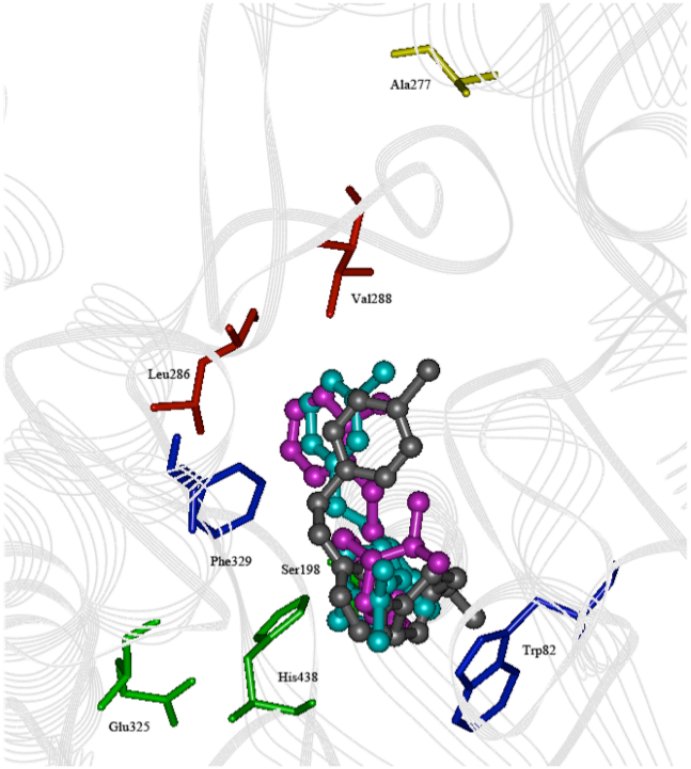

Fig. (**39**): SODS of **3**-**5h** (fuchsia, turquoise and grey, ball and stick; respectively) in the active site of *h*BuChE. Hydrogen atoms are not shown for clarity. *Green*: CT; *Red*: Acyl pocket; *Blue*: Hydrophobic stabilizing residues; *Yellow*: gorge entry.

Fig. (**40**) – *h*BACE-1 SODS of:

■ *N*-(2-Chlorobenzyl)-2-(4-cyclohexylpiperazin-1-yl)pyrimidin-4-amine (**3m**):

*h*BACE-1 IC_{50} = 13.30 µM

■ *N*-(3-Chlorobenzyl)-2-(4-cyclohexylpiperazin-1-yl)pyrimidin-4-amine (**4m**):

*h*BACE-1 IC_{50} = 2.60 µM

■ *N*-(4-Chlorobenzyl)-2-(4-cyclohexylpiperazin-1-yl)pyrimidin-4-amine (**5m**):

*h*BACE-1 IC_{50} = 1.30 µM

The SODS of **3-5m** corroborated the anti-BACE-1 inhibitory pattern of these derivatives, where the placement of the chlorine atom (2-, 3- or 4-position; respectively) impacted BACE-1 inhibition drastically. Interestingly, **3m** and **4m** had similar binding modes and orientation while **5m** was oriented in an opposite fashion with its C-4 group near the enzyme's mouth, allowing for the pyrimidine ring to lie suspended over the active site aspartic acid residues.

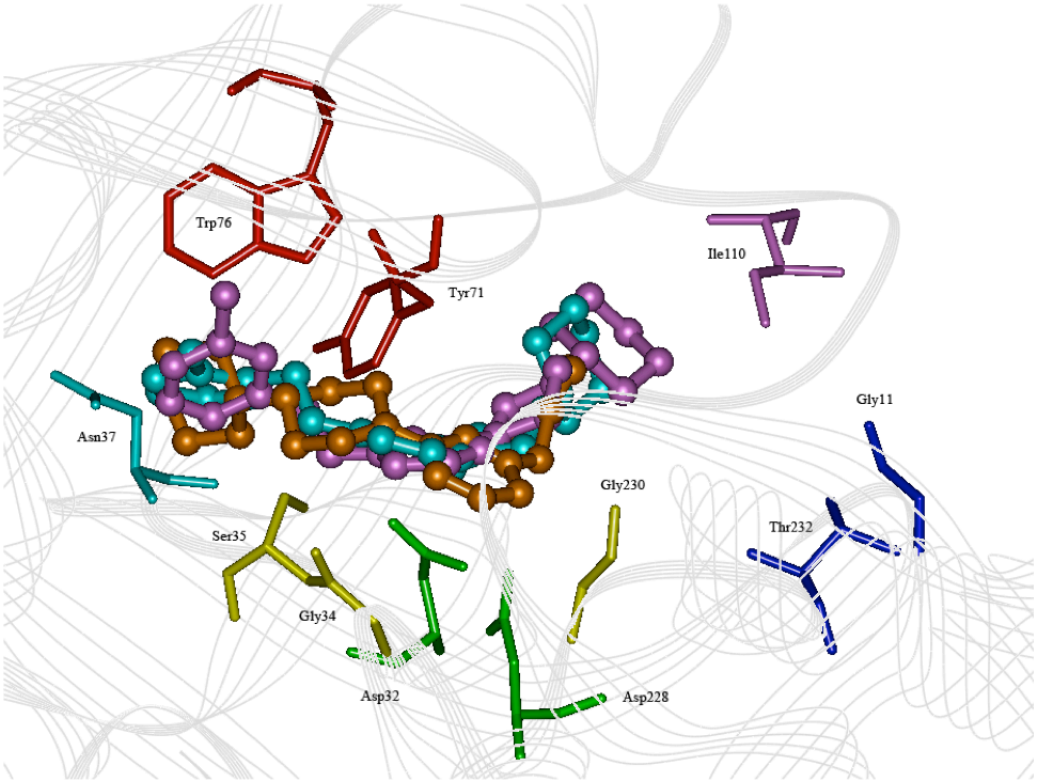

Fig. (**40**): SODS of **3-5m** (turquoise, fuchsia and orange, ball and stick; respectively) in the active site of *h*BACE-1. Hydrogen atoms are not shown for clarity. *Green*: Catalytic site; *Red*: Flap; *Purple*, turquoise and *Blue*: Some hydrophobic and hydrophilic residues of the various sub-site pockets in BACE-1; *Yellow*: Other key residues - part of the hydrogen-bond network.

CHAPTER V

• Conclusion and Future Outlook •

Over the course of the research program, a chemical library of 112 derivatives (series 2–12) based on a 2,4-DPR template were designed and synthesized using simple and efficient synthetic methods (2 or 3 step reactions) and screened against multiple pathways of AD (AChE, BuChE, AChE-induced $A\beta_{1-40}$-aggregation, self-induced $A\beta_{1-40}$-aggregation and β-secretase).

The design aspect of the project relied on the review of recent literature and preliminary molecular modeling studies to assess the potential of a 2,4-DPR template. The synthetic methods utilized (N.A.S, oxidation and hydrolysis) were successful and provided yields ranging from 45-90%. Biological screening was accomplished using previously established methods or commercially available assay kits to obtain SAR data. Molecular modeling studies were conducted to investigate the docking of lead derivatives within the target enzymes and to corroborate their biological profiles. A collective summary of the various parameters for library characterization is presented below:

- **Molecular Weights (MWs):** 254.33 – 463.57 $gmol^{-1}$
- **Molecular Volumes:** 174.90 – 319.30 $Å^3$
- **Partition Coefficients (ClogPs):** 1.18 – 6.32
- **AChE Inhibition Range (IC_{50}):** 5.50 – > 100 μM
- **BuChE Inhibition Range (IC_{50}):** 1.70 – > 100 μM
- **$A\beta_{1-40}$ Aggregation Inhibition (AChE-induced):** 0 – 59%
- **$A\beta_{1-40}$ Aggregation Inhibition (Self-induced):** 0 – 48%
- **BACE-1 Inhibition Range (IC_{50}):** 0.60 – > 50 μM
- **Neuroblastoma Cell Viability (at 40 μM):** 0 – 100%

The majority of 2,4-DPR derivatives (94 out of 112 or 84%) were classified as dual ChEI (Fig. **25**). With respect to AChE inhibition, the derivatives were not as potent as Aricept ® (donepezil; AChE IC_{50} of 32 nM) but the most potent derivative (**13a**, *N*-(Naphthalen-1-ylmethyl)-2-(pyrrolidin-1-yl)pyrimidin-4-amine;

AChE IC_{50} of 5.5 μM) exhibited an IC_{50} close to that of Reminyl ® (galantamine; AChE IC_{50} of 3.2 μM). A small fraction of 2,4-DPR derivatives (39 out of 112 or 35%) exhibited good activity ranging from 1-15 μM (Fig. **26**) and this highlights the challenge in designing potent AChE inhibitors with dual ChE activity. On the other hand, 60 out of 112 derivatives (~ 54%) exhibited good BuChEI ranging from 1-15 μM, despite the enzyme's larger and more open active site. Of those 60 derivatives, 13 exhibited better or equipotent activity compared to both Aricept ® (donepezil; BuChE IC_{50} of 3.2 μM) and Reminyl ® (galantamine; AChE IC_{50} of 13.2 μM) including the most potent BuChEI, **8m** (2-(4-cyclohexylpiperazin-1-yl)-*N*-(4-methylbenzyl)pyrimidin-4-amine; IC_{50} = 1.70 μM).

In an effort to identify novel and multifunctional candidates for the potential treatment of AD, select derivatives were screened for their ability to target some amyloid pathways of AD. In regards to $A\beta_{1-40}$ peptide aggregation, 2,4-DPR derivatives exhibited a wide range of activity toward both mechanisms of aggregation (AChE-induced – from 0 up to 59% and self-induced – from 0 up to 48%). With the first mechanism, derivatives that interacted with the PAS of AChE demonstrated good activity against peptide aggregation when compared to Aricept ® (donepezil; % inhibition at 100 μM = 17%) and Reminyl ® (galantamine; % inhibition at 100 μM = 0%). Top candidates included **2f (***N*-benzyl-2-(4-methylpiperazin-1-yl)pyrimidin-4-amine) and **10u** (N^2-(1-Benzylpiperidin-4-yl)-N^4-(3,4-dimethoxybenzyl)pyrimidine-2,4-diamine) that exhibited equipotent reduction in peptide aggregation (59%; ~ 3.5-fold more active compared to Aricept ® and ~ 1.4-fold less active compared to propidium) and of the derivatives tested, 23 out of 68 (~ 34%) surpassed the activity of Aricept ®. With the second mechanism, derivatives that disrupted β-sheet formation demonstrated good activity against peptide aggregation when compared to Reminyl ® (galantamine; % inhibition at 100 μM = 48%). Derivative **6u** (N^2-(1-benzylpiperidin-4-yl)-N^4-(4-bromobenzyl)pyrimidine-2,4-diamine) was the only equipotent inhibitor of self-induced $A\beta_{1-40}$ aggregates compared to Reminyl ® (% inhibition at 100 μM = 48%). To halt the generation of pro-Aβ peptides and to offer a degree of a DME, select derivatives were also screened for their ability to inhibit BACE-1. Of the 38 derivatives tested, 32 (~ 84%) exhibited superior activity toward BACE-1 compared to the peptide-like inhibitor (*N*-Benzyloxycarbonyl-Val-Leu-Leucinal; BACE-1 IC_{50} = 14 μM). Derivatives **4u**, **7u**, **9u**, **10g** and **12m** were the top candidate with a BACE-1 IC_{50} of 600-700 nM.

The neuroblastoma cell viability measurements in the presence and absence of test compounds was ranged from 0 to 100%. The data implied a relationship between lipophilicity parameters, bioisosteres and their impact on cell viability.

The SAR data acquired for dual ChE, $A\beta_{1\text{-}40}$ aggregation and BACE-1 inhibition supports the hypothesis that a 2,4-DPR can serve as a suitable template to develop multifunctional candidates for the potential treatment of AD. In this regard, a lead candidate from the chemical library generated (**10u**) was identified that fits the criteria of exhibiting multifunctional activity as shown below:

■ N^2-(1-benzylpiperidin-4-yl)-N^4-(3,4-dimethoxybenzyl)pyrimidine-2,4-diamine

Designation: **10u**

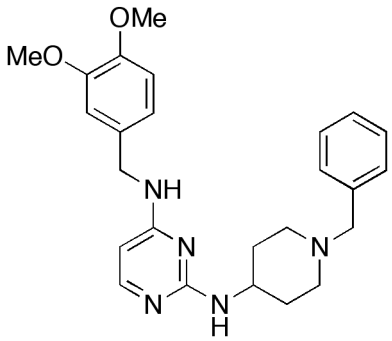

Cholinesterase Profile: AChE IC_{50} = 9.90 μM, BuChE IC_{50} = 11.40 μM; S.I = 0.90

Amyloid Profile: β-secretase IC_{50} = 34% inhibition at 10 μM; $A\beta_{1\text{-}40}$-aggreg. (%) = 59.30 (*h*AChE-induced); 17.10 (self-induced)

SH-SY5Y Neuroblastoma Cell Viability (% at 40 μM)*:* 81.00

Other Aspects: MW = 433.55 $gmol^{-1}$; MV = 240.10 $Å^3$; ClogP = 4.26

Future studies regarding this research program can be outlined as follows:

- Further examine lead derivatives such **10u** in other pathological parameters of AD such as metal chelation, anti-oxidant properties, inflammation and ability to prevent NFT formation.
- Modifications to structure could lead to an enhanced biological profile.
- Examine lead candidates in an AD animal model to assess in vivo potential.

Overall, the outcome of the research program was successful in providing some key insights into the development of novel pyrimidine-based templates as multifunctional small molecules to potentially treat AD. Current evidence supports the need to develop a multi-pronged approach to achieve the desired DMEs and potentially halt/reverse the rapid onset of AD as compared to the traditional "one drug, one target" approach.

CHAPTER VI

• Experimental •

6.1. Chemistry

All necessary solvents and reagents were obtained from various vendors (Acros Organics ®, Sigma-Aldrich ® and Alfa Aesar ®) with a minimum purity of 95% and were used without further purification. Melting points were determined on a Fisher-Johns apparatus and are uncorrected. Infrared (IR) spectra were obtained from microfilms on NaCl plates using a Perkin Elmer FT-IR spectrometer. ^{1}H-NMR spectra were recorded on a Bruker ® Avance 300 MHz series spectrometer using $CDCl_3$ or $MeOD_4$ as the solvent). Coupling constants (*J* values) were recorded in hertz (Hz) and the following abbreviations were used for multiplicity of NMR signals: s = singlet, d = doublet, t = triplet, m = multiplet, br = broad. High-resolution electron ionization mass spectral (HREIMS) analysis was obtained using a JEOL HX110 double focusing mass spectrometer. Residue purification was accomplished using i) SGCC using Merck 230-400 mesh silica gel 60 and, if necessary ii) HPLC. Combustion analysis was carried out by Midwest Microlab, LLC (Indianapolis, IN) and the % C, H, N of select compounds were within ± 0.4% of theoretical values for all elements listed indicating a purity of > 95%. All test derivatives showed single spot on thin-layer chromatography (TLC) performed on Merck 60F254 silica gel plates (0.2 mm) using three different solvent systems (9:1 EtOAc: MeOH; 3:1 EtOAc: hexanes and 3:1 EtOAc: DCM) and spots were visualized with UV 254 nm or stained with iodine or potassium permanganate ($KMnO_4$).

6.1.1. General Method to Prepare Intermediates 2-15

To a mixture of 2,4-dichloropyrimidine (**1**, Fig. **11**) (5.00 g, 33.60 mmol) and primary amines (R_1 = benzylamine, 2-, 3-, 4-chloro, 4-bromo, 4-fluoro, 4-methyl, 4-methoxy, 3,4-dimethoxy, 3,4,5-trimethoxy benzylamines, benzo[*d*][1,3]dioxol-5-methylamine, naphthalen-1ylmethylamine, diphenylmethylamine or phenylethylamine; respectively, 33.60 mmol) in 50-60 mL of EtOH, kept at 0 °C (ice-bath), DIPEA (6.08 mL, 36.80 mmol) was added. The reaction was stirred on the ice-bath for 5 minutes then refluxed at 80-85 °C for 4 hrs. After cooling to r.t, 15-20 mL of EtOAc was added and solution was neutralized with drop-

wise addition of ~ 6M HCl (pH = 7-7.5), washed with a saturated $NaHCO_3$ and NaCl solution (1:3, 1 x 50 mL). Aqueous layer was re-washed with EtOAc (2 x 25 mL) and the combined organic layer was dried over anhydrous $MgSO_4$ and filtered. The organic layer was evaporated in vacuo and the resulting residue was further purified using either one or both of the following methods: 1) Method A: SGCC using EtOAc: hexanes twice (3:1 and 1:3, respectively) or 9:1 DCM: EtOAc to afford solid products (60-65%) or 2) Method B: Differential melting point separation – The collected organic layers are evaporated in vacuo and the oily residue is vigorously mixed with a solution of hexanes to afford a precipitate that was filtered, washed with hexanes and dried on filter paper at 75-80 °C for ~ 2-3 hrs to afford solid products (60–89%). Some physical and spectroscopy data are provided below.

***N*-Benzyl-2-chloropyrimidin-4-amine** (**2**): The product was obtained as a white/light yellow solid after coupling with benzylamine (3.67 mL, 33.60 mmol). Method A – 4.78 g, 65%; Method B – 5.31 g, 72%. mp: 130-132 °C. IR (film, CH_2Cl_2): 3434 cm^{-1} (NH). ^{1}H-NMR (300 MHz, $CDCl_3$): δ 8.00 (d, J = 6.0 Hz, 1H), δ 7.28-7.34 (m, 5H), δ 6.20 (d, J = 6.0 Hz, 1H), δ 4.53 (br s, 2H). HREIMS Calcd for $C_{11}H_{10}ClN_3$ (M^+) *m/z* 219.6702, observed 219.0498. Anal. Calcd for: $C_{11}H_{10}ClN_3$•0.32 H_2O; C, 58.55; H, 4.43; N, 18.63. Found: C, 58.61; H, 4.76; N, 18.64.

2-Chloro-*N*-(2-chlorobenzyl)pyrimidin-4-amine (**3**): The product was obtained as a light yellow solid after coupling with 2-chlorobenzylamine (4.10 mL, 33.60 mmol). Method B – 5.97 g, 70%. mp: 95-97 °C. ^{1}H-NMR (300 MHz, $CDCl_3$): δ 8.00 (d, J = 6.0 Hz, 1H), δ 7.30-7.36 (m, 2H), δ 7.16-7.22 (m, 2H), δ 6.26 (d, J = 6.0 Hz, 1H), δ 5.80 (br s, 1H), δ 4.51 (br s, 2H). HREIMS Calcd for $C_{11}H_9Cl_2N_3$ 254.1153, observed 253.0196.

2-Chloro-*N*-(3-chlorobenzyl)pyrimidin-4-amine (**4**): The product was obtained as a yellow solid after coupling with 3-chlorobenzylamine (4.10 mL, 33.60 mmol). Method B – 5.98 g, 70%. mp: 128-130 °C. ^{1}H-NMR (300 MHz, $CDCl_3$) δ 7.99 (d, J = 6.0 Hz, 1H), δ 7.24-7.28 (m, 3H), δ 7.08-7.19 (m, 1H), δ 6.27 (d, J = 6.0 Hz, 1H), δ 5.81 (br s, 1H), δ 4.53 (br s, 2H). HREIMS Calcd for $C_{11}H_9Cl_2N_3$ 254.1153, observed 253.0168.

2-Chloro-*N*-(4-chlorobenzyl)pyrimidin-4-amine (**5**): The product was obtained as an off-white solid after coupling with 4-chlorobenzylamine (4.10 mL, 33.60 mmol). Method B – 5.13 g, 68%. mp: 138-140 °C. ^{1}H-NMR (300 MHz, $CDCl_3$) δ 8.00 (d, *J* = 6.0 Hz, 1H), δ 7.30-7.34 (m, 2H), δ 7.21-7.25 (m, 2H), δ 6.20 (d, *J* = 6.0 Hz, 1H), δ 5.54 (br s, 1H), δ 4.52 (br s, 2H). HREIMS Calcd for $C_{11}H_9Cl_2N_3$ 254.1153, observed 253.0176.

***N*-(4-bromobenzyl)-2-chloropyrimidin-4-amine** (**6**): The product was obtained as a yellow solid after coupling with 4-bromobenzylamine (5.39 mL, 33.60 mmol). Method B – 4.85 g, 66%. mp: 115-117 °C. ^{1}H-NMR (300 MHz, $CDCl_3$) δ 7.99 (d, *J* = 6.0 Hz, 1H), δ 7.45-7.48 (m, 2H), δ 7.17-7.20 (m, 2H), δ 6.25 (d, *J* = 6.0 Hz, 1H), δ 5.73 (br s, 1H), δ 4.51 (br s, 2H). HREIMS Calcd for $C_{11}H_9BrClN_3$ 298.5663, observed 296.9669.

2-Chloro-*N*-(4-fluorobenzyl)pyrimidin-4-amine (**7**): The product was obtained as an off-white solid after coupling with 4-fluorobenzylamine (3.86 mL, 33.60 mmol). Method B – 5.62 g, 71%. mp: 150-152 °C. ^{1}H-NMR (300 MHz, $CDCl_3$) δ 8.02 (d, *J* = 6.0 Hz, 1H), δ 7.25-7.30 (m, 2H), δ 7.00-7.05 (m, 2H), δ 6.22 (d, *J* = 6.0 Hz, 1H), δ 5.49 (br s, 1H), δ 4.51 (br s, 2H). HREIMS Calcd for $C_{11}H_9ClFN_3$ 237.6607, observed 237.0474.

2-Chloro-*N*-(4-methylbenzyl)pyrimidin-4-amine (**8**): The product was obtained as a yellow solid after coupling with 4-methylbenzylamine (4.29 mL, 33.60 mmol). Method B – 6.95 g, 88%. mp: 97-99 °C. ^{1}H-NMR (300 MHz, $CDCl_3$) δ 7.98 (d, *J* = 6.0 Hz, 1H), δ 7.16-7.22 (m, 2H), δ 7.10-7.15 (m, 2H), δ 6.21 (d, *J* = 6.0 Hz, 1H), δ 5.57 (s, 1H), δ 4.47 (br s, 2H), δ 2.33 (s, 3H). HREIMS Calcd for $C_{12}H_{12}ClN_3$ 233.6968, observed 233.0715.

2-Chloro-*N*-(4-methoxybenzyl)pyrimidin-4-amine (**9**): The product was obtained as a yellow solid after coupling with 4-methoxybenzylamine (4.39 mL, 33.60 mmol). Method B – 7.45 g, 89%. mp: 89-91 °C. ^{1}H-NMR (300 MHz, $CDCl_3$) δ 7.98 (d, *J* = 6.0 Hz, 1H), δ 7.23-7.26 (m, 2H), δ 6.86-6.89 (m, 2H), δ 6.23 (d, *J*

= 6.0 Hz, 1H), δ 5.64 (s, 1H), δ 4.45 (br s, 2H), δ 3.78 (s, 3H). HREIMS Calcd for $C_{12}H_{12}ClN_3O$ 249.6962, observed 249.0675.

2-Chloro-*N*-(3,4-dimethoxybenzyl)pyrimidin-4-amine (**10**): The product was obtained as a yellow solid after coupling with 3,4-dimethoxybenzylamine (5.11 mL, 33.60 mmol). Method B – 6.95 g, 88%. mp: 79-81 °C. ^{1}H-NMR (300 MHz, $CDCl_3$) δ 8.00 (d, *J* = 6.0 Hz, 1H), δ 6.79-6.84 (m, 3H), δ 6.21 (d, *J* = 6.0 Hz, 1H), δ 5.51 (s, 1H), δ 4.45 (br s, 2H), δ 3.86 (s, 3H), δ 3.85 (s, 3H). HREIMS Calcd for $C_{13}H_{14}ClN_3O_2$ 279.7222, observed 279.0778.

2-Chloro-*N*-(3,4,5-trimethoxybenzyl)pyrimidin-4-amine (**11**): The product was obtained as a beige solid after coupling with 3,4,5-trimethoxybenzylamine (5.71 mL, 33.60 mmol). Method B – 4.33 g, 60%. mp: 93-95 °C. ^{1}H-NMR (300 MHz, $CDCl_3$) δ 8.00 (d, *J* = 6.0 Hz, 1H), δ 6.53 (br s, 2H), δ 6.29 (d, *J* = 6.0 Hz, 1H), δ 5.78 (br s, 1H), δ 4.46 (br s, 2H), δ 3.84 (s, 6H), δ 3.82 (s, 3H). HREIMS Calcd for $C_{14}H_{16}ClN_3O_3$ 309.7481, observed 309.0880.

***N*-(benzo[*d*][1,3]dioxol-5-ylmethyl)-2-chloropyrimidin-4-amine** (**12**): The product was obtained as a light orange/brown solid after coupling with benzo[*d*][1,3]dioxol-5-ylmethylamine (4.23 mL, 33.60 mmol). Method B – 7.07 g, 80%. mp: 110-112 °C. ^{1}H-NMR (300 MHz, $CDCl_3$) δ 7.99 (d, *J* = 6.0 Hz, 1H), δ 6.81 (br s, 1H), δ 6.76 (br s, 2H), δ 6.20 (d, *J* = 6.0 Hz, 1H), δ 5.94 (s, 2H), δ 4.42 (br s, 2H). HREIMS Calcd for $C_{12}H_{10}ClN_3O_2$ 263.6797 , observed 263.0462.

2-Chloro-*N*-(naphthalen-1-ylmethyl)pyrimidin-4-amine (**13**): The product was obtained after coupling with naphthalen-1-ylmethylamine (4.95 mL, 33.60 mmol) and was a light orange/brown solid (Method A – 5.43 g, 60%; Method B – 6.83 g, 75%): mp: 158-160 °C. IR (film, CH_2Cl_2): 3432 cm^{-1} (NH). ^{1}H-NMR (300 MHz, $CDCl_3$): δ 8.01 (d, *J* = 6.0 Hz, 1H), δ 7.82-7.96 (m, 3H), δ 7.40-7.56 (m, 4H), δ 6.23 (d, *J* = 6.0 Hz, 1H) δ 4.70 (br s, 2H). HREIMS Calcd for $C_{15}H_{12}ClN_3$ (M^+) *m/z* 269.7289, observed 269.0737. Anal. Calcd for: $C_{15}H_{12}ClN_3 \bullet 0.17\ H_2O$: C, 66.79; H, 4.48; N, 15.58. Found: C, 66.04; H, 4.56; N, 15.40.

***N*-Benzhydryl-2-chloropyrimidin-4-amine (14)**: The product was obtained after coupling with diphenylmethylamine (5.81 mL, 33.60 mmol) and was a light yellow solid (Method A using 9:1 DCM: EtOAc followed by Method B – 5.46 g, 55%): mp: 133-135 °C. IR (film, $CDCl_3$): 3412 cm^{-1} (NH). ^{1}H-NMR (300 MHz, $CDCl_3$) δ 7.98 (d, *J* = 6.0 Hz, 1H), δ 7.27-7.36 (m, 10H), δ 6.12 (d, *J* = 6.0 Hz, 1H), δ 5.78 (br s, 2H). HREIMS Calcd for $C_{17}H_{14}ClN_3$ (M^+) *m/z* 295.7662, found 295.0871.

2-Chloro-*N*-phenethylpyrimidin-4-amine (**15**): The product was synthesized after coupling with 2-phenylethylamine (4.35 mL, 33.60 mmol). The residue was re-dissolved in a solvent mixture of EtOAc, DCM and MeOH in ~ 4:2:1 ratio. The resulting oily residue was further purified by SGCC (Method A) to afford a white/off-white solid (4.70 g, 60%): mp: 75-77 °C. IR (film, CH_2Cl_2): 3433 cm^{-1} (NH). ^{1}H-NMR (300 MHz, $CDCl_3$): δ 7.98 (d, *J* = 6.0 Hz, 1H), δ 7.17-7.33 (m, 5H), δ 6.16 (d, *J* = 6.0 Hz, 1H), δ 3.60 (br s, 2H), δ 2.88-2.92 (m, 2H). HREIMS Calcd for $C_{12}H_{12}ClN_3$ (M^+) *m/z* 233.6968, observed 233.0606.

6.1.2. General Method to Prepare Derivatives 2a-c,f-o,q-t, 3-12a,f-h,m, 13a-c,f-o, 14f-o, 15a-c,f,g,n

To a solution of **2-15** (0.20 g, 0.65-0.91 mmol) in 3 mL of *n*-BuOH kept in a PV with stirring, a cyclic amine (R_2 = pyrrolidine, morpholine, thiomorpholine, methylpiperazine, methylpiperidine, isopropyl piperazine, isopropylpiperidine, propyl-, hydroxyethyl-, methoxyethyl-, cyclohexyl-, acetyl-, Boc-piperazine, 4-chloro, 4-bromo, 4-fluoro or 4-trifluoromethylbenzylpiperazine – 0.85-1.18 mmol) was added. The sealed PV was placed in an oil bath at 150-155 °C and stirred for 1 hr. *n*-BuOH was evaporated in vacuo and the residue was re-dissolved in 3:1 EtOAc: DCM (15 mL) and washed successively with saturated $NaHCO_3$ and NaCl solution (1:2, 1 x 15 mL). The aqueous layer was washed with EtOAc (2 x 5 mL) and the organic layer was dried over anhydrous $MgSO_4$ then filtered. The solution was evaporated in vacuo to afford either solid or semisolid product. Some physical and spectroscopy data are provided below.

6.1.2.1. Benzylamines (2a-c,f-o,q-t)

***N*-Benzyl-2-(pyrrolidin-1-yl)pyrimidin-4-amine** (**2a**): The product was obtained after coupling **2** with pyrrolidine (0.10 mL, 1.18 mmol) to afford a light brown solid (0.15 g, 65%). mp: 103-105 °C. IR (film, CH_2Cl_2): 3435 cm^{-1} (NH). ^{1}H-NMR (300 MHz, $CDCl_3$): δ 7.87 (d, *J* = 6.0 Hz, 1H), δ 7.26-7.32 (m, 5H), δ 5.62 (d, *J* = 6.0 Hz, 1H), δ 4.86 (br s, 1H), δ 4.51 (d, *J* = 6.0 Hz, 2H), δ 3.49-3.53 (m, 4H), δ 1.90-1.94 (m, 4H). HREIMS Calcd for $C_{15}H_{18}N_4$ (M^+) *m/z* 254.3302, observed 254.1964. Anal. Calcd for: $C_{15}H_{18}N_4 \bullet H_2O$; C, 66.15; H, 7.40; N, 20.57. Found: C, 66.15; H, 7.40; N, 20.57.

***N*-Benzyl-2-morpholinopyrimidin-4-amine** (**2b**): The product was obtained after **2** coupling with morpholine (0.11 mL, 1.18 mmol) to afford an orange/light brown solid (0.20 g, 80%). mp: 93-95 °C. IR (film, CH_2Cl_2): 3434 cm^{-1} (NH). ^{1}H-NMR (300 MHz, $CDCl_3$): δ 7.87 (d, *J* = 6.0 Hz, 1H), δ 7.29-7.31 (m, 5H), δ 5.69 (d, *J* = 6.0 Hz, 1H), δ 4.91 (br s, 1H), δ 4.50 (d, *J* = 6.0 Hz, 2H), δ 3.70-3.75 (m, 8H). HREIMS Calcd for $C_{15}H_{18}N_4O$ (M^+) *m/z* 270.3296, observed 270.1605. Anal. Calcd for $C_{15}H_{18}N_4O$: C, 66.64; H, 6.71; N, 20.73. Found: C, 66.45; H, 6.72; N, 20.46.

***N*-Benzyl-2-thiomorpholinopyrimidin-4-amine** (**2c**): The product was obtained after **2** coupling with thiomorpholine (0.12 mL, 1.18 mmol) to afford a light brown solid (0.20 g, 77%). mp 85–87 °C. IR (film, $CDCl_3$): 3258 (NH) cm^{-1} (NH). ^{1}H-NMR (300 MHz, $CDCl_3$): δ 7.84 (d, *J* = 6.0 Hz, 1H), δ 7.24-7.33 (m, 5H), δ 5.66 (d, *J* = 6.0 Hz, 1H), δ 5.03 (br s, 1H), δ 4.47 (d, *J* = 6.0 Hz, 2H), δ 4.03-4.07 (m, 4H), δ 2.54-2.58 (m, 4H). HREIMS Calcd for $C_{15}H_{18}N_4S$ (M^+) *m/z* 286.3952, found m/z 286.1872. Anal. Calcd for $C_{15}H_{18}N_4S$: C, 62.91; H, 6.33; N, 19.56. Found: C, 62.62; H, 6.33; N, 19.31.

***N*-Benzyl-2-(4-methylpiperazin-1-yl)pyrimidin-4-amine** (**2f**): The product was obtained after coupling **2** with methylpiperazine (0.14 mL, 1.18 mmol) to afford a light yellow solid (0.22 g, 85%). mp: 150-153 °C. IR (film, CH_2Cl_2): 3454 cm^{-1} (NH). ^{1}H-NMR (300 MHz, $CDCl_3$): δ 7.86 (d, *J* = 6.0 Hz, 1H), δ 7.27-7.32 (m, 5H), δ 5.66 (d, *J* = 6.0 Hz, 1H), δ 4.87 (br s, 1H), δ 4.50 (d, *J* = 6.0 Hz, 2H), δ 3.77 (t, *J* = 6.0 Hz, 4H), δ 2.42 (t, *J* = 6.0 Hz, 4H), δ 2.31 (s, 3H). HREIMS calcd for $C_{16}H_{21}N_5$ (M^+) *m/z* 283.3714, found 283.1804.

Anal. Calcd for $C_{16}H_{21}N_5$•0.6 EtOAc: C, 65.74; H, 7.74; N, 20.83. Found: C, 65.64; H, 7.75; N, 20.67.

***N*-Benzyl-2-(4-methylpiperidin-1-yl)pyrimidin-4-amine** (**2g**): The product was obtained after coupling **2** with methylpiperidine (0.14 mL, 1.18 mmol) to afford a light pink solid (0.22 g, 85%). mp: 83-85 °C. IR (film, CH_2Cl_2): 3433 cm^{-1} (NH). ^{1}H-NMR (300 MHz, $CDCl_3$): δ 7.85 (d, *J* = 6.0 Hz, 1H), δ 7.28-7.32 (m, 5H), δ 5.61 (d, *J* = 6.0 Hz, 1H), δ 4.84 (br s, 1H), δ 4.63-4.67 (m, 2H), δ 4.50 (d, *J* = 6.0 Hz, 2H), δ 2.73-2.81 (m, 2H), δ 1.62-1.66 (m, 2H), δ 1.22-1.26 (m, 1H), δ 1.10-1.18 (m, 2H), δ 0.91 (d, *J* = 6.0 Hz, 3H). HREIMS Calcd for $C_{17}H_{22}N_4$ (M^+) *m/z* 282.3834, found 282.2376. Anal. Calcd for $C_{17}H_{22}N_4$; C, 72.31; H, 7.85; N, 19.84. Found: C, 72.18; H, 7.85; N, 19.60.

***N*-Benzyl-2-(4-isopropylpiperazin-1-yl)pyrimidin-4-amine** (**2h**): The product was obtained after coupling **2** with isopropylpiperazine (0.18 mL, 1.18 mmol) and was purified using a 3:1 EtOAc: hexanes SGCC to afford a white solid (0.14 g, 50%). mp: 103-105 °C. IR (film, CH_2Cl_2): 3438 cm^{-1} (NH). ^{1}H-NMR (300 MHz, $CDCl_3$): δ 7.85 (d, *J* = 6.0 Hz, 1H), δ 7.24-7.34 (m, 5H), δ 5.63 (d, *J* = 6.0 Hz, 1H), δ 4.93 (br s, 1H), δ 4.48 (d, *J* = 6.0 Hz, 2H), δ 3.73-3.76 (m, 4H), δ 2.62-2.71 (m, 1H), δ 2.50-2.53 (m, 4H), δ 1.03 (d, *J* = 6.0 Hz, 6H). HREIMS Calcd for $C_{18}H_{25}N_5$ (M^+) *m/z* 311.4246, found 311.2552. Anal. Calcd for $C_{18}H_{25}N_5$; C, 69.42; H, 8.09; N, 22.49. Found: C, 69.69; H, 8.31; N, 22.15.

***N*-Benzyl-2-(4-isopropylpiperidin-1-yl)pyrimidin-4-amine** (**2i**): The product was obtained after coupling **2** with isopropylpiperidine (0.18 mL, 1.18 mmol) and was purified using 3:1 ether: hexanes SGCC to afford a yellow solid (0.16 g, 55%). mp: 58-60 °C. IR (film, CH_2Cl_2): 3438 cm^{-1} (NH). ^{1}H-NMR (300 MHz, $CDCl_3$): δ 7.86 (d, *J* = 6.0 Hz, 1H), δ 7.22-7.32 (m, 5H), δ 5.61 (d, *J* = 6.0 Hz, 1H), δ 4.84 (br s, 1H), δ 4.71-4.75 (m, 2H), δ 4.49 (d, *J* = 6.0 Hz, 2H), δ 2.66-2.74 (m, 2H), δ 1.65-1.69 (m, 2H), δ 1.38-1.48 (m, 1H), δ 1.06-1.21 (m, 3H), δ 0.85-0.88 (m, 6H). HREIMS Calcd for $C_{19}H_{26}N_4$ (M^+) *m/z* 310.4365, found 310.3086. Anal. Calcd for $C_{19}H_{26}N_4$; C, 73.51; H, 8.44; N, 18.05. Found: C, 73.51; H, 8.57; N, 17.91.

***N*-Benzyl-2-(4-propylpiperazin-1-yl)pyrimidin-4-amine** (**2j**): The product was obtained after coupling **2** with *n*-propylpiperazine.2HBr (0.35 g, 1.18 mmol) and was purified using a 3:1 EtOAc: hexanes SGCC to

afford a light orange solid (0.16 g, 55%). mp: 93-95 °C. IR (film, CH_2Cl_2): 3436 cm^{-1} (NH). ^{1}H-NMR (300 MHz, $CDCl_3$): δ 7.85 (d, *J* = 6.0 Hz, 1H), δ 7.21-7.30 (m, 5H), δ 5.64 (d, *J* = 6.0 Hz, 1H), δ 4.93 (br s, 1H), δ 4.48 (d, *J* = 6.0 Hz, 2H), δ 3.71-3.75 (m, 4H), δ 2.39-2.42 (m, 4H), δ 2.27-2.30 (m, 2H), δ 1.49-1.56 (m, 2H), δ 0.87-0.91 (m, 3H). HREIMS Calcd for $C_{18}H_{25}N_5$ (M^+) *m/z* 311.4246, observed 311.2008. Anal. Calcd for $C_{18}H_{25}N_5$•0.6 H_2O; C, 67.09; H, 8.20; N, 21.73. Found: C, 67.11; H, 7.85; N, 21.55.

2-[4-(4-(Benzylamino)pyrimidin-2-yl)piperazin-1-yl]ethanol (**2k**): The product was obtained after coupling **2** with hydroxyethylpiperazine (0.15 mL, 1.18 mmol). Residue was re-dissolved in 1:1 EtOAc: DCM and was purified using a 3:1 EtOAc: hexanes SGCC to afford a brownish yellow solid (0.14 g, 50%). mp: 103-105 °C. IR (film, CH_2Cl_2): 3439 cm^{-1} (NH). ^{1}H-NMR (300 MHz, $CDCl_3$): δ 7.84 (d, *J* = 6.0 Hz, 1H), δ 7.24-7.34 (m, 5H), δ 5.65 (d, *J* = 6.0 Hz, 1H), δ 5.01 (br s, 1H), δ 4.48 (d, *J* = 6.0 Hz, 2H), δ 3.73-3.76 (m, 4H), δ 3.60-3.64 (m, 2H), δ 2.94 (s, 1H), δ 2.51-2.55 (m, 2H), δ 2.47-2.50 (m, 4H). HREIMS Calcd for $C_{17}H_{23}N_5O$ (M^+) *m/z* 313.3974, found 313.1637. Anal. Calcd for $C_{17}H_{23}N_5O$•0.3 DCM; C, 60.20; H, 6.78; N, 20.65. Found: C, 60.03; H, 6.89; N, 20.10.

***N*-Benzyl-2-[4-(2-methoxyethyl)piperazin-1-yl]pyrimidin-4-amine** (**2l**): The product was obtained after coupling **2** with methoxyethylpiperazine (0.18 mL, 1.18 mmol) to afford an orange semi-solid (0.17 g, 57%). mp: 63-65 °C. IR (film, CH_2Cl_2): 3433 cm^{-1} (NH). ^{1}H-NMR (300 MHz, $CDCl_3$): δ 7.82 (d, *J* = 6.0 Hz, 1H), δ 7.21-7.31 (m, 5H), δ 5.62 (d, *J* = 6.0 Hz, 1H), δ 5.06 (br s, 1H), δ 4.46 (d, *J* = 6.0 Hz, 2H), δ 3.74-3.77 (m, 4H), δ 3.48-3.52 (m, 2H), δ 3.32 (s, 3H), δ 2.54-2.58 (m, 2H), δ 2.45-2.48 (m, 4H). HREIMS Calcd for $C_{18}H_{25}N_5O$ (M^+) *m/z* 327.4240, found 327.2040.

***N*-Benzyl-2-(4-cyclohexylpiperazin-1-yl)pyrimidin-4-amine** (**2m**): The product was obtained after coupling **2** with cyclohexylpiperazine (0.21 g, 1.18 mmol) and was purified using a 3:1 EtOAc: hexanes SGCC to afford an orange solid (0.21 g, 66%). mp: 60-62 °C. IR (film, CH_2Cl_2): 3435 cm^{-1} (NH). ^{1}H-NMR (300 MHz, $CDCl_3$): δ 7.82 (d, *J* = 6.0 Hz, 1H), δ 7.21-7.32 (m, 5H), δ 5.61 (d, *J* = 6.0 Hz, 1H), δ 5.07 (br s, 1H), δ 4.46 (d, *J* = 6.0 Hz, 2H), δ 3.72-3.75 (m, 4H), δ 2.54-2.57 (m, 4H), δ 2.25 (s, 1H), δ 1.86 (br s, 2H), δ 1.75 (br s, 2H), δ 1.58-1.61 (m, 1H), δ 1.13-1.19 (m, 5H). HREIMS Calcd for $C_{21}H_{29}N_5$ (M^+) *m/z*

351.4885, found 351.2259. Anal. Calcd for $C_{21}H_{29}N_5$•0.5 DCM; C, 65.55; H, 7.68; N, 17.78. Found: C, 65.77; H, 7.70; N, 17.85.

1-[4-(4-(Benzylamino)pyrimidin-2-yl)piperazin-1-yl]ethanone (**2n**): The product was obtained after coupling **2** with acetylpiperazine (0.16 g, 1.18 mmol) to afford a yellowish white solid (0.25 g, 86%). mp: 150-153 °C. IR (film, CH_2Cl_2): 3437 cm^{-1} (NH). ^{1}H-NMR (300 MHz, $CDCl_3$): δ 7.87 (d, *J* = 6.0 Hz, 1H), δ 7.28-7.31 (m, 5H), δ 5.70 (d, *J* = 6.0 Hz, 1H), δ 4.93 (br s, 1H), δ 4.49 (d, *J* = 6.0 Hz, 2H), δ 3.72-3.79 (m, 4H), δ 3.61-3.64 (m, 2H), δ 3.44-3.48 (m, 2H), δ 2.11 (s, 3H). HREIMS Calcd for $C_{17}H_{21}N_5O$ (M^+) *m/z* 311.3815, found 311.1746. Anal. Calcd for $C_{17}H_{21}N_5O$•0.4 EtOAc; C, 64.46; H, 7.04; N, 20.21. Found: C, 64.43; H, 7.04; N, 20.15.

***Tert*-butyl 4-[4-(Benzylamino)pyrimidin-2-yl]piperazine-1-carboxylate** (**2o**): The product was obtained after coupling **7** with *tert*-butyl piperazine-1-carboxylate (0.23 g, 1.18 mmol). Product was purified using a 3:1 EtOAc: hexanes SGCC to afford a light yellowish solid (0.31 g, 90%). mp: 115-117 °C. IR (film, CH_2Cl_2): 3438 cm^{-1} (NH). ^{1}H-NMR (300 MHz, $CDCl_3$): δ 7.80 (d, *J* = 6.0 Hz, 1H), δ 7.21-7.30 (m, 5H), δ 5.65 (d, *J* = 6.0 Hz, 1H), δ 4.91 (br s, 1H), δ 4.49 (d, *J* = 6.0 Hz, 2H), δ 3.66-3.69 (m, 4H), δ 3.37-3.40 (m, 4H), δ 1.43 (s, 9H). HREIMS Calcd for $C_{20}H_{27}N_5O$ (M^+) *m/z* 369.4607, found 369.2163. Anal. Calcd for $C_{20}H_{27}N_5O_2$; C, 65.02; H, 7.37; N, 18.96. Found: C, 65.54; H, 7.33; N, 18.76.

***N*-Benzyl-2-[4-(4-chlorobenzyl)piperazin-1-yl]pyrimidin-4-amine** (**2q**): The product was obtained after coupling **2** with 4-chlorobenzylpiperazine (0.23 mL, 1.18 mmol). The sample was purified using a 9:1 EtOAc:DCM SGCC to afford a yellowish solid (0.20 g, 55%). mp: 88-90 °C. IR (film, CH_2Cl_2): 3437 cm^{-1} (NH). ^{1}H-NMR (300 MHz, $CDCl_3$) δ 7.85 (d, *J* = 6.0 Hz, 1H), δ 7.24-7.30 (m, 9H), δ 5.65 (d, *J* = 6.0 Hz, 1H), δ 4.87 (br s, 1H), δ 4.48 (d, *J* = 6.0 Hz, 2H), δ 3.73-3.76 (m, 4H), δ 3.47 (s, 2H), δ 2.41-2.44 (m, 4H). HREIMS Calcd for $C_{22}H_{24}ClN_5$ (M^+) *m/z* 393.9125, found 393.2443. Anal. Calcd for $C_{22}H_{24}ClN_5$; C, 67.08; H, 6.14; N, 17.78. Found: C, 67.44; H, 6.13; N, 17.68.

***N*-Benzyl-2-[4-(4-bromobenzyl)piperazin-1-yl]pyrimidin-4-amine** (**2r**): The product was obtained after coupling **2** with 4-bromobenzylpiperazine (0.30 g, 1.18 mmol) to afford a yellowish solid (0.20 g, 50%). mp: 90-93 °C. IR (film, CH_2Cl_2): 3434 cm^{-1} (NH). ^{1}H-NMR (300 MHz, $CDCl_3$) δ 7.85 (d, *J* = 6.0 Hz, 1H), δ 7.41-7.44 (m, 2H), δ 7.24-7.34 (m, 5H), δ 7.19-7.22 (m, 2H), δ 5.65 (d, *J* = 6.0 Hz, 1H), δ 4.87 (br s, 1H), δ 4.48 (d, *J* = 6.0 Hz, 2H), δ 3.73-3.76 (m, 4H), δ 3.45 (s, 2H), δ 2.41-2.44 (m, 4H). HREIMS Calcd $C_{22}H_{24}BrN_5$ (M^+) *m/z* 438.3635, found 438.2430. Anal. Calcd for $C_{22}H_{24}BrN_5$•0.2 EtOAc; C, 60.06; H, 5.66; N, 15.36. Found: C, 60.07; H, 5.65; N, 15.39.

***N*-Benzyl-2-[4-(4-fluorobenzyl)piperazin-1-yl]pyrimidin-4-amine** (**2s**): The product was obtained after coupling **2** with 4-fluorobenzylpiperazine (0.23 g, 1.18 mmol) to afford an orange semi-solid (0.22 g, 65%). IR (film, CH_2Cl_2): 3439 cm^{-1} (NH). ^{1}H-NMR (300 MHz, $CDCl_3$): δ 7.84 (d, *J* = 6.0 Hz, 1H), δ 7.26-7.29 (m, 7H), δ 6.96-7.02 (m, 2H), δ 5.63 (d, *J* = 6.0 Hz, 1H), δ 5.17 (br s, 1H), δ 4.47 (d, *J* = 6.0 Hz, 2H), δ 3.74-3.76 (m, 4H), δ 3.46 (s, 2H), δ 2.40 (t, *J* = 6.0 Hz, 4H). HREIMS Calcd for $C_{22}H_{24}FN_5$ (M^+) *m/z* 377.4579, found 377.1980. Anal. Calcd for $C_{22}H_{24}FN_5$•0.5 DCM; C, 64.36; H, 6.00; N, 16.68. Found: C, 63.95; H, 5.97; N, 16.54.

***N*-Benzyl-2-[4-(4-trifluoromethylbenzyl)piperazin-1-yl]pyrimidin-4-amine** (**2t**): The product was obtained after coupling **2** with 4-trifluoromethylbenzylpiperazine (0.25 mL, 1.18 mmol) to afford a yellowish orange solid (0.25 g, 64%). mp: 88-90 °C. IR (film, CH_2Cl_2): 3437 cm^{-1} (NH). ^{1}H-NMR (300 MHz, $CDCl_3$): δ 7.85 (d, *J* = 6.0 Hz, 1H), δ 7.55-7.58 (m, 2H), δ 7.44-7.47 (m, 2H), δ 7.24-7.34 (m, 5H), δ 5.65 (d, *J* = 6.0 Hz, 1H), δ 5.00 (br s, 1H), δ 4.48 (d, *J* = 6.0 Hz, 2H), δ 3.75-3.78 (m, 4H), δ 3.55 (s, 2H), δ 2.43-2.46 (m, 4H). HREIMS Calcd $C_{23}H_{24}F_3N_5$ (M^+) *m/z* 427.4654, found 427.2203. Anal. Calcd for $C_{23}H_{24}F_3N_5$; C, 64.62; H, 5.66; N, 16.38. Found: C, 64.39; H, 5.64; N, 16.12.

6.1.2.2. 2-Chlorobenzylamines (3a,f-h,m)

***N*-(2-Chlorobenzyl)-2-(pyrrolidin-1-yl)pyrimidin-4-amine** (**3a**): The product was obtained after coupling **3** with pyrrolidine (0.08 mL, 1.02 mmol) and was purified using a 9:1 EtOAc: MeOH SGCC to afford a

light brown semi-solid (0.16 g, 70%). ^{1}H-NMR (300 MHz, $CDCl_3$): δ 7.85 (d, *J* = 6.0 Hz, 1H), δ 7.34-7.41 (m, 2H), δ 7.17-7.23 (m, 2H), δ 5.63 (d, *J* = 6.0 Hz, 1H), δ 4.98 (br s, 1H), δ 4.61 (d, *J* = 6.0 Hz, 2H), δ 3.50-3.53 (m, 4H), δ 1.91-1.94 (m, 4H). HREIMS Calcd for $C_{15}H_{17}ClN_4$ (M^+) *m/z* 288.7753, observed 288.1145.

***N*-(2-Chlorobenzyl)-2-(4-methylpiperazin-1-yl)pyrimidin-4-amine** (**3f**): The product was obtained after coupling **3** with methylpiperazine (0.12 mL, 1.02 mmol) and was purified using a 9:1 EtOAc: MeOH SGCC to afford a beige solid (0.18 g, 72%). mp: 105-107 °C. ^{1}H-NMR (300 MHz, $CDCl_3$): δ 7.85 (d, *J* = 6.0 Hz, 1H), δ 7.33-7.38 (m, 2H), δ 7.17-7.22 (m, 2H), δ 5.65 (d, *J* = 6.0 Hz, 1H), δ 4.98 (br s, 1H), δ 4.59 (d, *J* = 6.0 Hz, 2H), δ 3.74-3.77 (m, 4H), δ 2.39-2.42 (m, 4H), δ 2.30 (s, 3H). HREIMS calcd for $C_{16}H_{20}ClN_5$ (M^+) *m/z* 317.8165, found 317.1403.

***N*-(2-Chlorobenzyl)-2-(4-methylpiperidin-1-yl)pyrimidin-4-amine** (**3g**): The product was obtained after coupling **3** with methylpiperidine (0.12 mL, 1.02 mmol) and was purified using a 9:1 EtOAc: MeOH SGCC to afford a light orange/yellow semi-solid (0.12 g, 50%). ^{1}H-NMR (300 MHz, $CDCl_3$): δ 7.85 (d, *J* = 6.0 Hz, 1H), δ 7.35-7.39 (m, 2H), δ 7.18-7.23 (m, 2H), δ 5.60 (d, *J* = 6.0 Hz, 1H), δ 4.95 (br s, 1H), δ 4.63-4.67 (m, 2H), δ 4.59 (d, *J* = 6.0 Hz, 2H), δ 2.73-2.81 (m, 2H), δ 1.62-1.66 (m, 2H), δ 1.22-1.26 (m, 1H), δ 1.10-1.18 (m, 2H), δ 0.91 (d, *J* = 6.0 Hz, 3H). HREIMS Calcd for $C_{17}H_{21}ClN_4$ (M^+) *m/z* 316.8284, found 316.1452.

***N*-(2-Chlorobenzyl)-2-(4-isopropylpiperazin-1-yl)pyrimidin-4-amine** (**3h**): The product was obtained after coupling **3** with isopropylpiperazine (0.16 mL, 1.02 mmol) and was purified using a 9:1 EtOAc: MeOH SGCC to afford a light brown solid (0.18 g, 65%). mp: 97-99 °C. ^{1}H-NMR (300 MHz, $CDCl_3$): δ 7.85 (d, *J* = 6.0 Hz, 1H), δ 7.32-7.38 (m, 2H), δ 7.16-7.21 (m, 2H), δ 5.64 (d, *J* = 6.0 Hz, 1H), δ 4.97 (br s, 1H), δ 4.59 (d, *J* = 6.0 Hz, 2H), δ 3.74-3.77 (m, 4H), δ 2.66-2.72 (m, 1H), δ 2.50-2.54 (m, 4H), δ 1.02 (d, *J* = 6.0 Hz, 6H). HREIMS Calcd for $C_{18}H_{24}ClN_5$ (M^+) *m/z* 345.8697, found 345.1729.

***N*-(2-Chlorobenzyl)-2-(4-cyclohexylpiperazin-1-yl)pyrimidin-4-amine** (**3m**): The product was obtained after coupling **3** with cyclohexylpiperazine (0.18 g, 1.02 mmol) and was purified using a 9:1 EtOAc: MeOH SGCC to afford an orange solid (0.21 g, 70%). mp: 56-58 °C. ^{1}H-NMR (300 MHz, $CDCl_3$): δ 7.85 (d, *J* = 6.0 Hz, 1H), δ 7.32-7.38 (m, 2H), δ 7.16-7.21 (m, 2H), δ 5.64 (d, *J* = 6.0 Hz, 1H), δ 4.97 (br s, 1H), δ 4.59 (d, *J* = 6.0 Hz, 2H), δ 3.72-3.76 (m, 4H), δ 2.55-2.59 (m, 4H), δ 2.26 (s, 1H), δ 1.88 (br s, 2H), δ 1.77 (br s, 2H), δ 1.58-1.61 (m, 1H), δ 1.13-1.19 (m, 5H). HREIMS Calcd for $C_{21}H_{29}N_5$ (M^+) *m/z* 385.9335, found 385.2027.

6.1.2.3. 3-Chlorobenzylamines (4a,f-h,m)

***N*-(3-Chlorobenzyl)-2-(pyrrolidin-1-yl)pyrimidin-4-amine** (**4a**): The product was obtained after coupling **4** with pyrrolidine (0.08 mL, 1.02 mmol) and was purified using a 9:1 EtOAc: MeOH SGCC to afford a light orange/brown solid (0.14 g, 61%). mp: 90-92 °C. ^{1}H-NMR (300 MHz, $CDCl_3$) δ 7.82 (d, *J* = 6.0 Hz, 1H), δ 7.27-7.31 (m, 1H), δ 7.13-7.21 (m, 3H), δ 5.69 (d, *J* = 6.0 Hz, 1H), δ 5.35 (br s, 1H), δ 4.50 (d, *J* = 6.0 Hz, 2H), δ 3.49-3.53 (m, 4H), δ 1.90-1.95 (m, 4H). HREIMS Calcd for $C_{15}H_{17}ClN_4$ 288.7753, observed 288.1134.

***N*-(3-Chlorobenzyl)-2-(4-methylpiperazin-1-yl)pyrimidin-4-amine** (**4f**): The product was obtained after coupling **4** with methylpiperazine (0.12 mL, 1.02 mmol) and was purified using a 9:1 EtOAc: MeOH SGCC to afford an off-white solid (0.20 g, 80%). mp: 98-100 °C. ^{1}H-NMR (300 MHz, $CDCl_3$) δ 7.86 (d, *J* = 6.0 Hz, 1H), δ 7.26-7.30 (m, 1H), δ 7.16-7.23 (m, 3H), δ 5.65 (d, *J* = 6.0 Hz, 1H), δ 4.94 (br s, 1H), δ 4.48 (d, *J* = 6.0 Hz, 2H), δ 3.75-3.78 (m, 4H), δ 2.41-2.44 (m, 4H), δ 2.31 (s, 3H). HREIMS Calcd for $C_{16}H_{20}ClN_5$ 317.8165, observed 317.1404.

***N*-(3-Chlorobenzyl)-2-(4-methylpiperidin-1-yl)pyrimidin-4-amine** (**4g**): The product was obtained after coupling **4** with methylpiperidine (0.12 mL, 1.02 mmol) and was purified using a 9:1 EtOAc: MeOH SGCC to afford an off-white solid (0.20 g, 80%). mp: 88-90 °C. ^{1}H-NMR (300 MHz, $CDCl_3$) δ 7.86 (d, *J* = 6.0 Hz, 1H), δ 7.27-7.30 (m, 1H), δ 7.19-7.26 (m, 3H), δ 5.62 (d, *J* = 6.0 Hz, 1H), δ 5.00 (br s, 1H), δ 4.60-4.64 (m, 2H),δ 4.48 (d, *J* = 6.0 Hz, 2H), δ 2.72-2.77 (m, 2H), δ 1.58-1.62 (m, 2H), δ 1.53-1.57 (m, 1H), δ

1.05-1.17 (m, 2H), δ 0.91 (d, *J* = 6.0 Hz, 3H). HREIMS Calcd for $C_{17}H_{21}ClN_4$ 316.8284, observed 316.1452.

***N*-(3-Chlorobenzyl)-2-(4-isopropylpiperazin-1-yl)pyrimidin-4-amine** (**4h**): The product was obtained after coupling **4** with isopropylpiperazine (0.16 mL, 1.02 mmol) and was purified using a 9:1 EtOAc: MeOH SGCC to afford a beige solid (0.15 g, 55%). mp: 105-107 °C. ^{1}H-NMR (300 MHz, $CDCl_3$) δ 7.86 (d, *J* = 6.0 Hz, 1H), δ 7.27-7.31 (m, 1H), δ 7.19-7.24 (m, 3H), δ 5.64 (d, *J* = 6.0 Hz, 1H), δ 4.90 (br s, 1H), δ 4.48 (d, *J* = 6.0 Hz, 2H), δ 3.74-3.80 (m, 4H), δ 2.69-2.73 (m, 1H), δ 2.50-2.56 (m, 4H), δ 1.05 (d, *J* = 6.0 Hz, 6H). HREIMS Calcd for $C_{18}H_{24}ClN_5$ 345.8697, observed 345.1724.

***N*-(3-Chlorobenzyl)-2-(4-cyclohexylpiperazin-1-yl)pyrimidin-4-amine** (**4m**): The product was obtained after coupling **4** with cyclohexylpiperazine (0.18 g, 1.02 mmol) and was purified using a 9:1 EtOAc: MeOH SGCC to afford a whitish solid (0.15 g, 59%). mp: 90-92 °C. ^{1}H-NMR (300 MHz, $CDCl_3$) δ 7.86 (d, *J* = 6.0 Hz, 1H), δ 7.28-7.32 (m, 1H), δ 7.19-7.24 (m, 3H), δ 5.64 (d, *J* = 6.0 Hz, 1H), δ 4.90 (br s, 1H), δ 4.48 (d, *J* = 6.0 Hz, 2H), δ 3.74-3.79 (m, 4H), δ 2.57-2.62 (m, 4H), δ 2.30 (br s, 1H), δ 1.89 (br s, 2H), δ 1.78 (br s, 2H), δ 1.59-1.60 (m, 1H), δ 1.15-1.22 (m, 5H). HREIMS Calcd for $C_{21}H_{28}ClN_5$ 385.9335, observed 385.2022.

6.1.2.4. 4-Chlorobenzylamines (5a,f-h,m)

***N*-(4-Chlorobenzyl)-2-(pyrrolidin-1-yl)pyrimidin-4-amine** (**5a**): The product was obtained after coupling **5** with pyrrolidine (0.08 mL, 1.02 mmol) and was purified using a 9:1 EtOAc: MeOH SGCC to afford a light orange/brown solid (0.15 g, 64%). mp: 129-131 °C. ^{1}H-NMR (300 MHz, $CDCl_3$) δ 7.84 (d, *J* = 6.0 Hz, 1H), δ 7.24-7.33 (m, 4H), δ 5.66 (d, *J* = 6.0 Hz, 1H), δ 5.12 (br s, 1H), δ 4.49 (d, *J* = 6.0 Hz, 2H), δ 3.50-3.54 (m, 4H), δ 1.90-1.94 (m, 4H). HREIMS Calcd for $C_{15}H_{17}ClN_4$ 288.7753, observed 288.1136.

***N*-(4-Chlorobenzyl)-2-(4-methylpiperazin-1-yl)pyrimidin-4-amine** (**5f**): The product was obtained after coupling **5** with methylpiperazine (0.12 mL, 1.02 mmol) and was purified using a 9:1 EtOAc: MeOH

SGCC to afford an off-white solid (0.22 g, 88%). mp: 135-137 °C. ^{1}H-NMR (300 MHz, $CDCl_3$) δ 7.86 (d, *J* = 6.0 Hz, 1H), δ 7.26-7.33 (m, 2H), δ 7.21-7.25 (m, 2H), δ 5.65 (d, *J* = 6.0 Hz, 1H), δ 4.90 (br s, 1H), δ 4.47 (d, *J* = 6.0 Hz, 2H), δ 3.76-3.79 (m, 4H), δ 2.43-2.46 (m, 4H), δ 2.33 (s, 3H). HREIMS Calcd for $C_{16}H_{20}ClN_5$ 317.8165 , observed 317.1410.

***N*-(4-Chlorobenzyl)-2-(4-methylpiperidin-1-yl)pyrimidin-4-amine** (**5g**): The product was obtained after coupling **5** with methylpiperidine (0.12 mL, 1.02 mmol) and was purified using a 9:1 EtOAc: MeOH SGCC to afford a light orange solid (0.20 g, 80%). mp: 86-88 °C. ^{1}H-NMR (300 MHz, $CDCl_3$) δ 7.85 (d, *J* = 6.0 Hz, 1H), δ 7.26-7.33 (m, 2H), δ 7.22-7.26 (m, 2H), δ 5.60 (d, *J* = 6.0 Hz, 1H), δ 4.89 (br s, 1H), δ 4.60-4.65 (m, 2H), δ 4.46 (d, *J* = 6.0 Hz, 2H), δ 2.72-2.80 (m, 2H), δ 1.62-1.66 (m, 2H), δ 1.56-1.61 (m, 1H), δ 1.03-1.09 (m, 2H), δ 0.91 (d, *J* = 6.0 Hz, 3H). HREIMS Calcd for $C_{16}H_{20}ClN_5$ 316.8284, observed 316.1449.

***N*-(4-Chlorobenzyl)-2-(4-isopropylpiperazin-1-yl)pyrimidin-4-amine** (**5h**): The product was obtained after coupling **5** with isopropylpiperazine (0.16 mL, 1.02 mmol) to afford a beige solid (0.25 g, 93%). mp: 120-122 °C. ^{1}H-NMR (300 MHz, $CDCl_3$) δ 7.85 (d, *J* = 6.0 Hz, 1H), δ 7.26-7.33 (m, 2H), δ 7.21-7.26 (m, 2H), δ 5.63 (d, *J* = 6.0 Hz, 1H), δ 4.89 (br s, 1H), δ 4.46 (d, *J* = 6.0 Hz, 2H), δ 3.74-3.77 (m, 4H), δ 2.70-2.74 (m, 1H), δ 2.52-2.55 (m, 4H), δ 1.05 (d, *J* = 6.0 Hz, 6H). HREIMS Calcd for $C_{18}H_{24}ClN_5$ 345.8697, observed 345.1724.

***N*-(4-Chlorobenzyl)-2-(4-cyclohexylpiperazin-1-yl)pyrimidin-4-amine** (**5m**): The product was obtained after coupling **5** with cyclohexylpiperazine (0.18 g, 1.02 mmol) and was purified using a 9:1 EtOAc: MeOH SGCC to afford an orange/brown solid (0.26 g, 86%). mp: 55-57 °C. ^{1}H-NMR (300 MHz, $CDCl_3$) δ 7.86 (d, *J* = 6.0 Hz, 1H), δ 7.26-7.30 (m, 2H), δ 7.21-7.25 (m, 2H), δ 5.64 (d, *J* = 6.0 Hz, 1H), δ 4.88 (br s, 1H), δ 4.46 (d, *J* = 6.0 Hz, 2H), δ 3.74-3.80 (m, 4H), δ 2.58-2.64 (m, 4H), δ 2.29-2.36 (m, 1H), δ 1.90 (br s, 2H), δ 1.79 (br s, 2H), δ 1.61-1.65 (m, 1H), δ 1.20-1.26 (m, 5H). HREIMS Calcd for $C_{21}H_{28}ClN_5$ 385.9335, observed 385.2035.

6.1.2.5. 2-Bromobenzylamines (6a,f-h,m)

***N*-(4-Bromobenzyl)-2-(pyrrolidin-1-yl)pyrimidin-4-amine (6a)**: The product was obtained after coupling **6** with pyrrolidine (0.07 mL, 0.87 mmol) and was purified using a 9:1 EtOAc: MeOH SGCC to afford a light yellow solid (0.12 g, 54%). mp: 122-124 °C. ^{1}H-NMR (300 MHz, $CDCl_3$) δ 7.78 (d, *J* = 6.0 Hz, 1H), δ 7.39-7.43 (m, 2H), δ 7.17-7.22 (m, 2H), δ 5.77 (d, *J* = 6.0 Hz, 1H), δ 5.06 (br s, 1H), δ 4.49 (d, *J* = 6.0 Hz, 2H), δ 3.46-3.53 (m, 4H), δ 1.91-1.98 (m, 4H). HREIMS Calcd for $C_{15}H_{17}BrN_4$ 333.2263, observed 332.0640.

***N*-(4-Bromobenzyl)-2-(4-methylpiperazin-1-yl)pyrimidin-4-amine (6f)**: The product was obtained after coupling **6** with methylpiperazine (0.10 mL, 0.87 mmol) and was purified using a 9:1 EtOAc: MeOH SGCC to afford an orange/brown solid (0.17 g, 70%). mp: 65-67 °C. ^{1}H-NMR (300 MHz, $CDCl_3$) δ 7.85 (d, *J* = 6.0 Hz, 1H), δ 7.40-7.45 (m, 2H), δ 7.15-7.23 (m, 2H), δ 5.70 (d, *J* = 6.0 Hz, 1H), δ 5.05 (br s, 1H), δ 4.45 (d, *J* = 6.0 Hz, 2H), δ 3.90-3.95 (m, 4H), δ 2.61-2.66 (m, 4H), δ 2.47 (s, 3H). HREIMS Calcd for $C_{16}H_{20}BrN_5$ 362.2675, observed 361.0903.

***N*-(4-Bromobenzyl)-2-(4-methylpiperidin-1-yl)pyrimidin-4-amine (6g)**: The product was obtained after coupling **6** with methylpiperidine (0.10 mL, 0.87 mmol) and was purified using a 9:1 EtOAc: MeOH SGCC to afford a light orange solid (0.12 g, 50%). mp: 85-87 °C. ^{1}H-NMR (300 MHz, $CDCl_3$) δ 7.82 (d, *J* = 6.0 Hz, 1H), δ 7.40-7.44 (m, 2H), δ 7.17-7.24 (m, 2H), δ 5.65 (d, *J* = 6.0 Hz, 1H), δ 5.03 (br s, 1H), δ 4.60-4.64 (m, 2H), δ 4.46 (d, *J* = 6.0 Hz, 2H), δ 2.75-2.83 (m, 2H), δ 1.63-1.71 (m, 2H), δ 1.57-1.61 (m, 1H), δ 1.07-1.12 (m, 2H), δ 0.91 (d, *J* = 6.0 Hz, 3H). HREIMS Calcd for $C_{17}H_{21}BrN_4$ 361.2794, observed 360.0953.

***N*-(4-Bromobenzyl)-2-(4-isopropylpiperazin-1-yl)pyrimidin-4-amine (6h)**: The product was obtained after coupling **6** with isopropylpiperazine (0.10 mL, 0.87 mmol) to afford an orangey/brown solid (0.18 g, 69%). mp: 115-117 °C. ^{1}H-NMR (300 MHz, $CDCl_3$) δ 7.85 (d, *J* = 6.0 Hz, 1H), δ 7.39-7.44 (m, 2H), δ 7.16-7.24 (m, 2H), δ 5.64 (d, *J* = 6.0 Hz, 1H), δ 4.90 (br s, 1H), δ 4.45 (d, *J* = 6.0 Hz, 2H), δ 3.60-3.66 (m,

4H), δ 2.59-2.66 (m, 4H), δ 2.30-2.37 (m, 1H), δ 1.06 (d, *J* = 6.0 Hz, 6H). HRMS Calcd for $C_{18}H_{24}BrN_5$ 390.3207, observed 389.1213.

***N*-(4-Bromobenzyl)-2-(4-cyclohexylpiperazin-1-yl)pyrimidin-4-amine** (**6m**): The product was obtained after coupling **6** with cyclohexylpiperazine (0.15 g, 0.87 mmol) and was purified using a 9:1 EtOAc: MeOH SGCC to afford an orange/brown solid (0.15 g, 60%). mp: 51-53 °C. ^{1}H-NMR (300 MHz, $CDCl_3$) δ 7.85 (d, *J* = 6.0 Hz, 1H), δ 7.39-7.44 (m, 2H), δ 7.16-7.24 (m, 2H), δ 5.64 (d, *J* = 6.0 Hz, 1H), δ 4.90 (br s, 1H), δ 4.45 (d, *J* = 6.0 Hz, 2H), δ 3.60-3.66 (m, 4H), δ 2.59-2.66 (m, 4H), δ 2.30-2.37 (m, 1H), δ 1.91 (br s, 2H), δ 1.79 (br s, 2H), δ 1.60-1.64 (m, 1H), δ 1.20-1.26 (m, 5H). HREIMS Calcd for $C_{21}H_{28}BrN_5$ 430.3845, observed 429.1529.

6.1.2.6. 4-Fluorobenzylamines (7a,f-h,m)

***N*-(4-Fluorobenzyl)-2-(pyrrolidin-1-yl)pyrimidin-4-amine** (**7a**): The product was obtained after coupling **7** with pyrrolidine (0.09 mL, 1.09 mmol) and was purified using a 9:1 EtOAc: MeOH SGCC to afford a white solid (0.14 g, 60%). mp: 120-122 °C. ^{1}H-NMR (300 MHz, $CDCl_3$) δ 7.81 (d, *J* = 6.0 Hz, 1H), δ 7.26-7.31 (m, 2H), δ 6.96-7.02 (m, 2H), δ 5.76 (d, *J* = 6.0 Hz, 1H), δ 5.43 (br s, 1H), δ 4.49 (d, *J* = 6.0 Hz, 2H), δ 3.51-3.55 (m, 4H), δ 1.91-1.95 (m, 4H). HREIMS Calcd for $C_{11}H_{17}FN_3$ 272.3207, observed 272.1437.

***N*-(4-Fluorobenzyl)-2-(4-methylpiperazin-1-yl)pyrimidin-4-amine** (**7f**): The product was obtained after coupling **7** with methylpiperazine (0.12 mL, 1.09 mmol) and was purified using a 9:1 EtOAc: MeOH SGCC to afford a light yellow solid (0.18 g, 71%). mp: 152-154 °C. ^{1}H-NMR (300 MHz, $CDCl_3$) δ 7.86 (d, *J* = 6.0 Hz, 1H), δ 7.24-7.29 (m, 2H), δ 6.96-7.02 (m, 2H), δ 5.68 (d, *J* = 6.0 Hz, 1H), δ 4.94 (br s, 1H), δ 4.48 (d, *J* = 6.0 Hz, 2H), δ 3.85-3.88 (m, 4H), δ 2.53-2.56 (m, 4H), δ 2.32 (s, 3H). HREIMS Calcd for $C_{16}H_{20}FN_5$ 301.3619, observed 301.1701.

***N*-(4-Fluorobenzyl)-2-(4-methylpiperidin-1-yl)pyrimidin-4-amine** (**7g**): The product was obtained after coupling **7** with methylpiperidine (0.12 mL, 1.09 mmol) and was purified using a 9:1 EtOAc: MeOH

SGCC to afford a light orange solid (0.17 g, 69%). mp: 90-92 °C. ^{1}H-NMR (300 MHz, $CDCl_3$) δ 7.53 (d, *J* = 6.0 Hz, 1H), δ 7.24-7.30 (m, 2H), δ 6.89-6.98 (m, 2H), δ 6.22 (d, *J* = 6.0 Hz, 1H), δ 5.07 (br s, 1H), δ 4.55-4.61 (m, 2H), δ 4.48 (d, *J* = 6.0 Hz, 2H), δ 2.90-2.98 (m, 2H), δ 1.71-1.76 (m, 2H), δ 1.09-1.23 (m, 3H), δ 0.93 (d, *J* = 6.0 Hz, 3H). HREIMS Calcd for $C_{17}H_{21}FN_4$ 300.3738, observed 300.1748.

***N*-(4-Fluorobenzyl)-2-(4-isopropylpiperazin-1-yl)pyrimidin-4-amine** (**7h**): The product was obtained after coupling **7** with isopropylpiperazine (0.12 mL, 1.09 mmol) to afford an orangey/brown solid (0.22 g, 85%). mp: 85-87 °C. ^{1}H-NMR (300 MHz, $CDCl_3$) δ 7.84 (d, *J* = 6.0 Hz, 1H), δ 7.23-7.28 (m, 2H), δ 6.96-7.02 (m, 2H), δ 5.68 (d, *J* = 6.0 Hz, 1H), δ 5.01 (br s, 1H), δ 4.45 (d, *J* = 6.0 Hz, 2H), δ 3.60-3.64 (m, 4H), δ 2.89-2.93 (m, 1H), δ 2.65-2.69 (m, 4H), δ 1.17 (d, *J* = 6.0 Hz, 6H). HREIMS Calcd for $C_{18}H_{24}FN_5$ 329.4151, observed 329.2025.

2-(4-Cyclohexylpiperazin-1-yl)-*N*-(4-fluorobenzyl)pyrimidin-4-amine (**7m**): The product was obtained after coupling **7** with cyclohexylpiperazine (0.18 g, 1.09 mmol) and was purified using a 9:1 EtOAc: MeOH SGCC to afford an orange/brown solid (0.25 g, 80%). mp: 50-52 °C. ^{1}H-NMR (300 MHz, $CDCl_3$) δ 7.85 (d, *J* = 6.0 Hz, 1H), δ 7.24-7.39 (m, 2H), δ 6.94-7.02 (m, 2H), δ 5.65 (d, *J* = 6.0 Hz, 1H), δ 4.90 (br s, 1H), δ 4.48 (d, *J* = 6.0 Hz, 2H), δ 3.80-3.84 (m, 4H), δ 2.62-2.66 (m, 4H), δ 2.34-2.39 (m, 1H), δ 2.02 (br s, 2H), δ 1.92 (br s, 2H), δ 1.60-1.64 (m, 1H), δ 1.14-1.18 (m, 5H). HREIMS Calcd for $C_{21}H_{28}FN_5$ 369.4789, observed 369.2341.

6.1.2.7. 4-Methylbenzylamines (8a,f-h,m)

***N*-(4-Methylbenzyl)-2-(pyrrolidin-1-yl)pyrimidin-4-amine** (**8a**): The product was obtained after coupling **8** with pyrrolidine (0.09 mL, 1.11 mmol) and was purified using a 9:1 EtOAc: MeOH SGCC to afford a yellow solid (0.11 g, 50%). mp: 90-92 °C. ^{1}H-NMR (300 MHz, $CDCl_3$) δ 7.75 (d, *J* = 6.0 Hz, 1H), δ 7.16-7.22 (m, 2H), δ 7.07-7.15 (m, 2H), δ 5.78 (d, *J* = 6.0 Hz, 1H), δ 4.48 (d, *J* = 6.0 Hz, 2H), δ 3.54-3.58 (m, 4H), δ 2.31 (s, 3H), δ 1.91-1.95 (m, 4H). HREIMS Calcd for $C_{16}H_{20}N_4$ 268.3568, observed 268.1688.

***N*-(4-Methylbenzyl)-2-(4-methylpiperazin-1-yl)pyrimidin-4-amine** (**8f**): The product was obtained after coupling **8** with methylpiperazine (0.12 mL, 1.11 mmol) and was purified using a 9:1 EtOAc: MeOH SGCC to afford a yellow solid (0.16 g, 63%). mp: 95-97 °C. ^{1}H-NMR (300 MHz, $CDCl_3$) δ 7.87 (d, *J* = 6.0 Hz, 1H), δ 7.18-7.23 (m, 2H), δ 7.05-7.11 (m, 2H), δ 5.64 (d, *J* = 6.0 Hz, 1H), δ 4.86 (br s, 1H), δ 4.44 (d, *J* = 6.0 Hz, 2H), δ 3.76-3.80 (m, 4H), δ 2.41-2.45 (m, 4H), δ 2.32 (s, 3H), δ 2.31 (s, 3H). HREIMS Calcd for $C_{17}H_{23}N_5$ 297.3980, observed 297.1949.

***N*-(4-Methylbenzyl)-2-(4-methylpiperidin-1-yl)pyrimidin-4-amine** (**8g**): The product was obtained after coupling **8** with methylpiperidine (0.12 mL, 1.11 mmol) and was purified using a 9:1 EtOAc: MeOH SGCC to afford a light yellow solid (0.12 g, 49%). mp: 96-98 °C. ^{1}H-NMR (300 MHz, $CDCl_3$) δ 7.86 (d, *J* = 6.0 Hz, 1H), δ 7.18-7.22 (m, 2H), δ 7.11-7.15 (m, 2H), δ 5.62 (d, *J* = 6.0 Hz, 1H), δ 4.80 (br s, 1H), δ 4.64-4.68 (m, 2H), δ 4.44 (d, *J* = 6.0 Hz, 2H), δ 2.72-2.80 (m, 2H), δ 2.32 (s, 3H), δ 1.62-1.66 (m, 2H), δ 1.52-1.59 (m, 1H), δ 1.10-1.17 (m, 2H), δ 0.92 (d, *J* = 6.0 Hz, 3H). HREIMS Calcd for $C_{18}H_{24}N_4$ 296.4100, observed 296.1997.

2-(4-Isopropylpiperazin-1-yl)-*N*-(4-methylbenzyl)pyrimidin-4-amine (**8h**): The product was obtained after coupling **8** with isopropylpiperazine (0.12 mL, 1.11 mmol) to afford an orangey/brown semi-solid (0.18 g, 65%). ^{1}H-NMR (300 MHz, $CDCl_3$) δ 7.85 (d, *J* = 6.0 Hz, 1H), δ 7.16-7.21 (m, 2H), δ 7.09-7.14 (m, 2H), δ 5.65 (d, *J* = 6.0 Hz, 1H), δ 4.85 (br s, 1H), δ 4.44 (d, *J* = 6.0 Hz, 2H), δ 3.79-3.83 (m, 4H), δ 2.71-2.75 (m, 1H), δ 2.52-2.56 (m, 4H), δ 2.31 (s, 3H), δ 1.03 (d, *J* = 6.0 Hz, 6H). HREIMS Calcd for $C_{19}H_{27}N_5$ 325.4512, observed 325.2271.

2-(4-Cyclohexylpiperazin-1-yl)-*N*-(4-methylbenzyl)-pyrimidin-4-amine (**8m**): The product was obtained after coupling **8** with cyclohexylpiperazine (0.18 g, 1.11 mmol) and was purified using a 9:1 EtOAc: MeOH SGCC to afford a light orange solid (0.21 g, 67%). mp: 55-57 °C. ^{1}H-NMR (300 MHz, $CDCl_3$) δ 7.85 (d, *J* = 6.0 Hz, 1H), δ 7.16-7.21 (m, 2H), δ 7.10-7.15 (m, 2H), δ 5.63 (d, *J* = 6.0 Hz, 1H), δ 4.84 (br s, 1H), δ 4.43 (d, *J* = 6.0 Hz, 2H), δ 3.74-3.78 (m, 4H), δ 2.57-2.61 (m, 4H), δ 2.32 (s, 3H), δ 2.25-2.31 (m,

1H), δ 1.88 (br s, 2H), δ 1.78 (br s, 2H), δ 1.60-1.64 (m, 1H), δ 1.19-1.24 (m, 5H). HRMS Calcd for $C_{22}H_{31}N_5$ 365.5150, observed 365.2570.

6.1.2.8. 4-Methoxybenzylamines (9a,f-h,m)

***N*-(4-Methoxybenzyl)-2-(pyrrolidin-1-yl)pyrimidin-4-amine** (**9a**): The product was obtained after coupling **9** with pyrrolidine (0.08 mL, 1.04 mmol) and was purified using a 9:1 EtOAc: MeOH SGCC to afford a yellow solid (0.14 g, 61%). mp: 96-98 °C. ^{1}H-NMR (300 MHz, $CDCl_3$) δ 7.86 (d, *J* = 6.0 Hz, 1H), δ 7.22-7.27 (m, 2H), δ 6.81-6.86 (m, 2H), δ 5.61 (d, *J* = 6.0 Hz, 1H), δ 4.85 (br s, 1H), δ 4.42 (d, *J* = 6.0 Hz, 2H), δ 3.77 (s, 3H), δ 3.49-3.53 (m, 4H), δ 1.90-1.94 (m, 4H). HREIMS Calcd for $C_{16}H_{20}N_4O$ 284.3562, observed 284.1646.

***N*-(4-Methoxybenzyl)-2-(4-methylpiperazin-1-yl)pyrimidin-4-amine** (**9f**): The product was obtained after coupling **9** with methylpiperazine (0.11 mL, 1.04 mmol) and was purified using a 9:1 EtOAc: MeOH SGCC to afford a yellow solid (0.18 g, 71%). mp: 105-107 °C. ^{1}H-NMR (300 MHz, $CDCl_3$) δ 7.86 (d, *J* = 6.0 Hz, 1H), δ 7.21-7.26 (m, 2H), δ 6.82-6.87 (m, 2H), δ 5.65 (d, *J* = 6.0 Hz, 1H), δ 4.83 (br s, 1H), δ 4.41 (d, *J* = 6.0 Hz, 2H), δ 3.75-3.81 (m, 7H), δ 2.43-2.47 (m, 4H), δ 2.32 (s, 3H). HREIMS Calcd for $C_{17}H_{23}N_5O$ 313.3974, observed 313.1895.

***N*-(4-Methoxybenzyl)-2-(4-methylpiperidin-1-yl)pyrimidin-4-amine** (**9g**): The product was obtained after coupling **9** with methylpiperidine (0.11 mL, 1.04 mmol) and was purified using a 9:1 EtOAc: MeOH SGCC to afford an off-white solid (0.11 g, 45%). mp: 84-86 °C. ^{1}H-NMR (300 MHz, $CDCl_3$) δ 7.85 (d, *J* = 6.0 Hz, 1H), δ 7.20-7.23 (m, 2H), δ 6.83-6.86 (m, 2H), δ 5.60 (d, *J* = 6.0 Hz, 1H), δ 4.78 (br s, 1H), δ 4.64-4.68 (m, 2H), δ 4.41 (d, *J* = 6.0 Hz, 2H), δ 3.78 (s, 3H), δ 2.73-2.80 (m, 2H), δ 1.62-1.66 (m, 2H), δ 1.56-1.62 (m, 1H), δ 1.11-1.19 (m, 2H), δ 0.92 (d, *J* = 6.0 Hz, 3H). HREIMS Calcd for $C_{18}H_{24}N_4O$ 312.4094, observed 312.1944.

2-(4-Isopropylpiperazin-1-yl)-*N*-(4-methoxybenzyl)pyrimidin-4-amine (**9h**): The product was obtained after coupling **9** with isopropylpiperazine (0.11 mL, 1.04 mmol) to afford a beige solid (0.13 g, 49%). mp: 128-130 °C. ^{1}H-NMR (300 MHz, $CDCl_3$) δ 7.85 (d, *J* = 6.0 Hz, 1H), δ 7.21-7.26 (m, 2H), δ 6.83-6.86 (m, 2H), δ 5.64 (d, *J* = 6.0 Hz, 1H), δ 4.82 (br s, 1H), δ 4.41 (d, *J* = 6.0 Hz, 2H), δ 3.74-3.78 (m, 7H), δ 2.67-2.73 (m, 1H), δ 2.51-2.55 (m, 4H), δ 1.03 (d, *J* = 6.0 Hz, 6H). HREIMS Calcd for $C_{19}H_{27}N_5O$ 341.4506, observed 341.2221.

2-(4-Cyclohexylpiperazin-1-yl)-*N*-(4-methoxybenzyl)pyrimidin-4-amine (**9m**): The product was obtained after coupling **9** with cyclohexylpiperazine (0.17 g, 1.04 mmol) and was purified using a 9:1 EtOAc: MeOH SGCC to afford an orange brown solid (0.20 g, 60%). mp: 51-53 °C. ^{1}H-NMR (300 MHz, $CDCl_3$) δ 7.85 (d, *J* = 6.0 Hz, 1H), δ 7.21-7.26 (m, 2H), δ 6.83-6.86 (m, 2H), δ 5.64 (d, *J* = 6.0 Hz, 1H), δ 4.81 (br s, 1H), δ 4.41 (d, *J* = 6.0 Hz, 2H), δ 3.71-3.78 (m, 7H), δ 2.58-2.62 (m, 4H), δ 2.28-2.32 (m, 1H), δ 1.89 (br s, 2H), δ 1.77 (br s, 2H), δ 1.60-1.64 (m, 1H), δ 1.16-1.23 (m, 5H). HREIMS Calcd for $C_{22}H_{31}N_5O$ 381.5144, observed 381.2533.

6.1.2.9. 3,4-Dimethoxybenzylamines (10a,f-h,m)

***N*-(3,4-Dimethoxybenzyl)-2-(pyrrolidin-1-yl)pyrimidin-4-amine** (**10a**): The product was obtained after coupling **10** with pyrrolidine (0.07 mL, 0.93 mmol) and was purified using a 9:1 EtOAc: MeOH SGCC to afford a beige solid (0.12 g, 55%). mp: 68-70 °C. ^{1}H-NMR (300 MHz, $CDCl_3$) δ 7.88 (d, *J* = 6.0 Hz, 1H), δ 6.78-6.88 (m, 3H), δ 5.63 (d, *J* = 6.0 Hz, 1H), δ 4.82 (br s, 1H), δ 4.43 (d, *J* = 6.0 Hz, 2H), δ 3.85 (s, 3H), δ 3.84 (s, 3H), δ 3.46-3.51 (m, 4H), δ 1.90-1.95 (m, 4H). HREIMS Calcd for $C_{17}H_{22}N_4O_2$ 314.3822, observed 314.1736.

***N*-(3,4-Dimethoxybenzyl)-2-(4-methylpiperazin-1-yl)pyrimidin-4-amine** (**10f**): The product was obtained after coupling **10** with methylpiperazine (0.10 mL, 0.93 mmol) and was purified using a 9:1 EtOAc: MeOH SGCC to afford a yellow solid (0.12 g, 50%). mp: 75-77 °C. ^{1}H-NMR (300 MHz, $CDCl_3$) δ 7.87 (d, *J* = 6.0 Hz, 1H), δ 6.79-6.88 (m, 3H), δ 5.66 (d, *J* = 6.0 Hz, 1H), δ 4.82 (br s, 1H), δ 4.44 (d, *J* =

6.0 Hz, 2H), δ 3.85 (s, 3H), δ 3.84 (s, 3H), δ 3.76-3.80 (m, 4H), δ 2.40-2.44 (m, 4H), δ 2.30 (s, 3H). HREIMS Calcd for $C_{18}H_{25}N_5O_2$ 343.4234, observed 343.2011.

***N*-(3,4-Dimethoxybenzyl)-2-(4-methylpiperidin-1-yl)pyrimidin-4-amine** (**10g**): The product was obtained after coupling **10** with methylpiperidine (0.10 mL, 0.93 mmol) and was purified using a 9:1 EtOAc: MeOH SGCC to afford a beige semi-solid (0.11 g, 46%). ^{1}H-NMR (300 MHz, $CDCl_3$) δ 7.86 (d, *J* = 6.0 Hz, 1H), δ 6.79-6.88 (m, 3H), δ 5.61 (d, *J* = 6.0 Hz, 1H), δ 4.79 (br s, 1H), δ 4.64-4.68 (m, 2H), δ 4.41 (d, *J* = 6.0 Hz, 2H), δ 3.85 (s, 3H), δ 3.84 (s, 3H), δ 2.72-2.79 (m, 2H), δ 1.63-1.67 (m, 2H), δ 1.55-1.61 (m, 1H), δ 1.10-1.19 (m, 2H), δ 0.92 (d, *J* = 6.0 Hz, 3H). HREIMS Calcd for $C_{19}H_{26}N_4O_2$ 342.4353, observed 342.2043.

***N*-(3,4-Dimethoxybenzyl)-2-(4-isopropylpiperazin-1-yl)pyrimidin-4-amine** (**10h**): The product was obtained after coupling **10** with isopropylpiperazine (0.10 mL, 0.93 mmol) to afford a light brown semi-solid (0.16 g, 60%). ^{1}H-NMR (300 MHz, $CDCl_3$) δ 7.86 (d, *J* = 6.0 Hz, 1H), δ 6.79-6.89 (m, 3H), δ 5.65 (d, *J* = 6.0 Hz, 1H), δ 4.83 (br s, 1H), δ 4.43 (d, *J* = 6.0 Hz, 2H), δ 3.85 (s, 3H), δ 3.84 (s, 3H), δ 3.76-3.80 (m, 4H), δ 2.64-2.70 (m, 1H), δ 2.51-2.56 (m, 4H), δ 1.04 (d, *J* = 6.0 Hz, 6H). HREIMS Calcd for $C_{20}H_{29}N_5O_2$ 371.4766, observed 371.2318.

2-(4-Cyclohexylpiperazin-1-yl)-*N*-(3,4-dimethoxybenzyl)pyrimidin-4-amine (**10m**): The product was obtained after coupling **10** with cyclohexylpiperazine (0.15 g, 0.93 mmol) and was purified using a 9:1 EtOAc: MeOH SGCC to afford an orangey brown solid (0.21 g, 71%). mp: 56-58 °C. ^{1}H-NMR (300 MHz, $CDCl_3$) δ 7.83 (d, *J* = 6.0 Hz, 1H), δ 6.79-6.89 (m, 3H), δ 5.65 (d, *J* = 6.0 Hz, 1H), δ 4.82 (br s, 1H), δ 4.42 (d, *J* = 6.0 Hz, 2H), δ 3.85 (s, 3H), δ 3.84 (s, 3H), δ 3.76-3.81 (m, 4H), δ 2.56-2.61 (m, 4H), δ 2.27-2.32 (m, 1H), δ 1.90 (br s, 2H), δ 1.78 (br s, 2H), δ 1.59-1.63 (m, 1H), δ 1.17-1.24 (m, 5H). HREIMS Calcd for $C_{23}H_{33}N_5O_2$ 411.5404, observed 411.2635.

6.1.2.10. 3,4,5-Trimethoxybenzylamines (11a,f-h,m)

2-(Pyrrolidin-1-yl)-*N*-(3,4,5-trimethoxybenzyl)pyrimidin-4-amine (**11a**): The product was obtained after coupling **11** with pyrrolidine (0.06 mL, 0.84 mmol) and was purified using a 9:1 EtOAc: MeOH SGCC to afford a beige solid (0.15 g, 67%). mp: 66-68 °C. ^{1}H-NMR (300 MHz, $CDCl_3$) δ 7.89 (d, *J* = 6.0 Hz, 1H), δ 6.55 (s, 2H), δ 5.64 (d, *J* = 6.0 Hz, 1H), δ 4.85 (br s, 1H), δ 4.43 (d, *J* = 6.0 Hz, 2H), δ 3.82 (s, 6H), δ 3.81 (s, 3H), δ 3.50-3.55 (m, 4H), δ 1.90-1.95 (m, 4H). HREIMS Calcd for $C_{18}H_{24}N_4O_3$ 344.4082, observed 344.1847.

***N*-(3,4,5-Trimethoxybenzyl)-2-(4-methylpiperazin-1-yl)pyrimidin-4-amine** (**11f**): The product was obtained after coupling **11** with methylpiperazine (0.09 mL, 0.84 mmol) and was purified using a 9:1 EtOAc: MeOH SGCC to afford a yellow solid (0.13 g, 54%). mp: 55-57 °C. ^{1}H-NMR (300 MHz, $CDCl_3$) δ 7.87 (d, *J* = 6.0 Hz, 1H), δ 6.54 (s, 2H), δ 5.66 (d, *J* = 6.0 Hz, 1H), δ 4.84 (br s, 1H), δ 4.42 (d, *J* = 6.0 Hz, 2H), δ 3.82 (s, 6H), δ 3.81 (s, 3H), δ 3.76-3.80 (m, 4H), δ 2.40-2.44 (m, 4H), δ 2.31 (s, 3H). HREIMS Calcd for $C_{19}H_{27}N_5O_3$ 373.4494, observed 373.2124.

***N*-(3,4,5-Trimethoxybenzyl)-2-(4-methylpiperidin-1-yl)pyrimidin-4-amine** (**11g**): The product was obtained after coupling **11** with methylpiperidine (0.09 mL, 0.84 mmol) and was purified using a 9:1 EtOAc: MeOH SGCC to afford a beige solid (0.12 g, 48%). mp: 65-67 °C. ^{1}H-NMR (300 MHz, $CDCl_3$) δ 7.85 (d, *J* = 6.0 Hz, 1H), δ 6.54 (s, 2H), δ 5.71 (d, *J* = 6.0 Hz, 1H), δ 4.78 (br s, 1H), δ 4.65-4.69 (m, 2H), δ 4.43 (d, *J* = 6.0 Hz, 2H), δ 3.83 (s, 6H), δ 3.82 (s, 3H), δ 2.78-2.86 (m, 2H), δ 1.64-1.70 (m, 2H), δ 1.58-1.63 (m, 1H), δ 1.07-1.16 (m, 2H), δ 0.92 (d, *J* = 6.0 Hz, 3H). HREIMS Calcd for $C_{20}H_{28}N_4O_3$ 372.4613, observed 372.2162.

2-(4-Isopropylpiperazin-1-yl)-*N*-(3,4,5-trimethoxybenzyl)pyrimidin-4-amine (**11h**): The product was obtained after coupling **11** with isopropylpiperazine (0.09 mL, 0.84 mmol) to afford a light orange solid (0.14 g, 54%). mp: 100-102 °C. ^{1}H-NMR (300 MHz, $CDCl_3$) δ 7.87 (d, *J* = 6.0 Hz, 1H), δ 6.45 (m, 2H), δ 5.65 (d, *J* = 6.0 Hz, 1H), δ 4.83 (br s, 1H), δ 4.42 (d, *J* = 6.0 Hz, 2H), δ 3.83 (s, 6H), δ 3.82 (s, 3H), δ 3.76-

3.80 (m, 4H), δ 2.64-2.70 (m, 1H), δ 2.53-2.57 (m, 4H), δ 1.03 (d, *J* = 6.0 Hz, 6H). HREIMS Calcd for $C_{21}H_{31}N_5O_3$ 401.5025, observed 401.2429.

2-(4-Cyclohexylpiperazin-1-yl)-*N*-(3,4,5-trimethoxybenzyl)pyrimidin-4-amine (**11m**): The product was obtained after coupling **11** with cyclohexylpiperazine (0.14 g, 0.84 mmol) and was purified using a 9:1 EtOAc: MeOH SGCC to afford an orange brown solid (0.20 g, 70%). mp: 56-58 °C. ^{1}H-NMR (300 MHz, $CDCl_3$) δ 7.85 (d, *J* = 6.0 Hz, 1H), δ 6.54 (s, 2H), δ 5.65 (d, *J* = 6.0 Hz, 1H), δ 4.83 (br s, 1H), δ 4.41 (d, *J* = 6.0 Hz, 2H), δ 3.83 (s, 6H), δ 3.82 (s, 3H), δ 3.75-3.80 (m, 4H), δ 2.58-2.62 (m, 4H), δ 2.24-2.29 (m, 1H), δ 1.89 (br s, 2H), δ 1.77 (br s, 2H), δ 1.59-1.63 (m, 1H), δ 1.15-1.22 (m, 5H). HREIMS Calcd for $C_{24}H_{35}N_5O_3$ 441.5664, observed 441.2744.

6.1.2.11. Benzo[*d*][1,3]dioxol-5-methylamines (12a,f-h,m)

***N*-(benzo[*d*][1,3]dioxol-5-ylmethyl)-2-(pyrrolidin-1-yl)pyrimidin-4-amine** (**12a**): The product was obtained after coupling **12** with pyrrolidine (0.07 mL, 0.99 mmol) and was purified using a 9:1 EtOAc: MeOH SGCC to afford a beige solid (0.11 g, 48%). mp: 60-62 °C. ^{1}H-NMR (300 MHz, $CDCl_3$) δ 7.86 (d, *J* = 6.0 Hz, 1H), δ 6.76-6.85 (m, 3H), δ 5.86 (s, 2H), δ 5.60 (d, *J* = 6.0 Hz, 1H), δ 4.82 (br s, 1H), δ 4.47 (d, *J* = 6.0 Hz, 2H), δ 3.49-3.53 (m, 4H), δ 1.91-1.95 (m, 4H). HREIMS Calcd for $C_{16}H_{18}N_4O_2$ 298.3397, observed 298.1436.

***N*-(benzo[*d*][1,3]dioxol-5-ylmethyl)-2-(4-methylpiperazin-1-yl)pyrimidin-4-amine** (**12f**): The product was obtained after coupling **12** with methylpiperazine (0.11 mL, 0.99 mmol) and was purified using a 9:1 EtOAc: MeOH SGCC to afford a light yellow solid (0.15 g, 60%). mp: 75-77 °C. ^{1}H-NMR (300 MHz, $CDCl_3$) δ 7.85 (d, *J* = 6.0 Hz, 1H), δ 6.80-6.89 (m, 3H), δ 5.92 (s, 2H), δ 5.64 (d, *J* = 6.0 Hz, 1H), δ 4.80 (br s, 1H), δ 4.48 (d, *J* = 6.0 Hz, 2H), δ 3.72-3.77 (m, 4H), δ 2.40-2.45 (m, 4H), δ 2.31 (s, 3H). HREIMS Calcd for $C_{17}H_{21}N_5O_2$ 327.3809, observed 327.1700.

***N*-(benzo[*d*][1,3]dioxol-5-ylmethyl)-2-(4-methylpiperidin-1-yl)pyrimidin-4-amine** (**12g**): The product was obtained after coupling **12** with methylpiperidine (0.11 mL, 0.99 mmol) and was purified using a 9:1 EtOAc: MeOH SGCC to afford a beige semi-solid (0.11 g, 46%). ^{1}H-NMR (300 MHz, $CDCl_3$) δ 7.85 (d, *J* = 6.0 Hz, 1H), δ 6.72-6.80 (m, 3H), δ 5.91 (s, 2H), δ 5.64 (d, *J* = 6.0 Hz, 1H), δ 4.78 (br s, 1H), δ 4.63-4.67 (m, 2H), δ 4.39 (d, *J* = 6.0 Hz, 2H), δ 2.73-2.80 (m, 2H), δ 1.62-1.67 (m, 2H), δ 1.56-1.61 (m, 1H), δ 1.08-1.18 (m, 2H), δ 0.92 (d, *J* = 6.0 Hz, 3H). HREIMS Calcd for $C_{18}H_{22}N_4O_2$ 326.3929, observed 326.1742.

***N*-(benzo[*d*][1,3]dioxol-5-ylmethyl)-2-(4-isopropylpiperazin-1-yl)pyrimidin-4-amine** (**12h**): The product was obtained after coupling **12** with isopropylpiperazine (0.11 mL, 0.99 mmol) to afford a beige solid (0.12 g, 45%). mp: 119-121 °C. ^{1}H-NMR (300 MHz, $CDCl_3$) δ 7.86 (d, *J* = 6.0 Hz, 1H), δ 6.74-6.84 (m, 3H), δ 5.91 (s, 2H), δ 5.63 (d, *J* = 6.0 Hz, 1H), δ 4.80 (br s, 1H), δ 4.39 (d, *J* = 6.0 Hz, 2H), δ 3.74-3.79 (m, 4H), δ 2.67-2.71 (m, 1H), δ 2.50-2.55 (m, 4H), δ 1.04 (d, *J* = 6.0 Hz, 6H). HREIMS Calcd for $C_{19}H_{25}N_5O_2$ 355.4341, observed 355.2007.

***N*-(benzo[*d*][1,3]dioxol-5-ylmethyl)-2-(4-cyclohexylpiperazin-1-yl)pyrimidin-4-amine** (**12m**): The product was obtained after coupling **12** with cyclohexylpiperazine (0.17 g, 0.99 mmol) and was purified using a 9:1 EtOAc: MeOH SGCC to afford an orangey brown solid (0.19 g, 63%). mp: 52-54 °C. ^{1}H-NMR (300 MHz, $CDCl_3$) δ 7.85 (d, *J* = 6.0 Hz, 1H), δ 6.72-6.80 (m, 3H), δ 5.90 (s, 2H), δ 5.62 (d, *J* = 6.0 Hz, 1H), δ 4.80 (br s, 1H), δ 4.39 (d, *J* = 6.0 Hz, 2H), δ 3.72-3.77 (m, 4H), δ 2.55-2.60 (m, 4H), δ 2.25-2.30 (m, 1H), δ 1.88 (br s, 2H), δ 1.77 (br s, 2H), δ 1.60-1.64 (m, 1H), δ 1.15-1.22 (m, 5H). HREIMS Calcd for $C_{22}H_{29}N_5O_2$ 395.4980, observed 395.2311.

6.1.2.12. Naphthalen-1ylmethylamines (13a-c,f-o)

***N*-(Naphthalen-1-ylmethyl)-2-(pyrrolidine)pyrimidin-4-amines** (**13a**): The product was obtained after coupling **13** with pyrrolidine (0.08 mL, 0.96 mmol) to afford a light brown solid (0.16 g, 70%). mp: 105-107 °C. IR (film, CH_2Cl_2): 3433 cm^{-1} (NH). ^{1}H-NMR (300 MHz, $CDCl_3$) δ 8.05 (d, *J* = 6.0 Hz, 1H), δ 7.78-7.91 (m, 3H), δ 7.38-7.51 (m, 4H), δ 5.64 (d, *J* = 6.0 Hz, 1H), δ 4.96 (d, *J* = 6.0 Hz, 2H), δ 4.79 (br s, 1H),

δ 3.53-3.57 (m, 4H), δ 1.91-1.95 (m, 4H). HREIMS Calcd $C_{19}H_{20}N_4$ (M^+) *m/z* 304.3889, found 304.2086. Anal. Calcd for $C_{19}H_{20}N_4$•0.2 H_2O; C, 74.02; H, 6.49; N, 18.18. Found: C, 74.09; H, 6.68; N, 18.19.

2-Morpholino-*N*-(naphthalen-1-ylmethyl)pyrimidin-4-amine (**13b**): The product was obtained after coupling **13** with morpholine (0.08 mL, 0.96 mmol) to afford a light yellow solid (0.18 g, 75%). mp: 170-172 °C. IR (film, CH_2Cl_2): 3437 cm^{-1} (NH). ^{1}H-NMR (300 MHz, $CDCl_3$): δ 8.01 (d, *J* = 6.0 Hz, 1H), δ 7.79-7.90 (m, 3H), δ 7.39-7.52 (m, 4H), δ 5.71 (d, *J* = 6.0 Hz, 1H), δ 4.92 (d, *J* = 6.0 Hz, 2H), δ 4.77 (br s, 1H), δ 3.69-3.77 (m, 8H). HREIMS Calcd $C_{19}H_{20}N_4O$ (M^+) *m/z* 320.3883, found 320.1825. Anal. Calcd for $C_{19}H_{20}N_4O$; C, 71.23; H, 6.29; N, 17.49. Found: C, 71.28; H, 6.37; N, 17.08.

***N*-(Naphthalen-1-ylmethyl)-2-thiomorpholinopyrimidin-4-amine** (**13c**): The product was obtained after coupling **13** thiomorpholine (0.10 mL, 0.96 mmol) to afford a yellowish brown solid (0.19 g, 76%). mp: 105-107 °C. IR (film, CH_2Cl_2): 3439 cm^{-1} (NH). ^{1}H-NMR (300 MHz, $CDCl_3$): δ 8.01 (d, *J* = 6.0 Hz, 1H), δ 7.73-7.87 (m, 3H), δ 7.39-7.51 (m, 4H), δ 5.68 (d, *J* = 6.0 Hz, 1H), δ 4.93 (d, *J* = 6.0 Hz, 2H), δ 4.82 (br s, 1H), δ 4.05-4.12 (m, 4H), δ 2.59-2.65 (m, 4H). HREIMS Calcd $C_{19}H_{20}N_4S$ (M^+) *m/z* 336.4539, found 336.2171. Anal. Calcd for $C_{19}H_{20}N_4S$; C, 67.83; H, 5.99; N, 16.65. Found: C, 67.78; H, 5.86; N, 16.50.

2-(4-Methylpiperazin-1-yl)-*N*-(naphthalen-1-ylmethyl)pyrimidin-4-amine (**13f**): The product was obtained after coupling **13** with methylpiperazine (0.11 mL, 0.96 mmol) to afford a yellow solid (0.23 g, 80%). mp: 118-120 °C. IR (film, CH_2Cl_2): 3436 cm^{-1} (NH). ^{1}H-NMR (300 MHz, $CDCl_3$): δ 8.03 (d, *J* = 6.0 Hz, 1H), δ 7.78-7.90 (m, 3H), δ 7.39-7.52 (m, 4H), δ 5.67 (d, *J* = 6.0 Hz, 1H), δ 4.94 (d, *J* = 6.0 Hz, 2H), δ 4.80 (br s, 1H), δ 3.81-3.85 (m, 4H), δ 2.41-2.45 (m, 4H), δ 2.32 (s, 3H). HREIMS Calcd $C_{20}H_{23}N_5$ (M^+) *m/z* 333.4301, found 333.1961. Anal. Calcd for $C_{20}H_{23}N_5$•0.5 EtOAc; C, 70.01; H, 7.21; N, 18.55. Found: C, 69.72; H, 7.25; N, 18.21.

2-(4-Methylpiperidin-1-yl)-*N*-(naphthalen-1-ylmethyl)pyrimidin-4-amine (**13g**): The product was obtained after coupling **13** with methylpiperidine (0.11 mL, 0.96 mmol). The residue was purified using a 3:1 ether: hexanes column to afford an off-white/light yellow semi-solid (0.14 g, 55%). IR (film, CH_2Cl_2):

3439 cm^{-1} (NH). ^{1}H-NMR (300 MHz, $CDCl_3$): δ 8.03 (d, *J* = 6.0 Hz, 1H), δ 7.78-7.91 (m, 3H), δ 7.38-7.53 (m, 4H), δ 5.62 (d, *J* = 6.0 Hz, 1H), δ 4.94 (d, *J* = 6.0 Hz, 2H), δ 4.75 (br s, 1H), δ 4.68-4.72 (m, 3H), δ 2.76-2.84 (m, 2H), δ 1.64-1.68 (m, 2H), 1.57-1.60 (m, 1H), 1.10-1.14 (m, 4H), 0.92 (d, *J* = 6.0 Hz, 3H). HREIMS Calcd $C_{21}H_{24}N_4$ (M^+) *m/z* 332.4421, found 332.2246. Anal. Calcd for $C_{21}H_{24}N_4$•0.5 EtOAc; C, 73.38; H, 7.50; N, 14.88. Found: C, 73.07; H, 7.52; N, 14.64.

2-(4-Isopropylpiperazin-1-yl)-*N*-(naphthalen-1-ylmethyl)pyrimidin-4-amine (**13h**): The product was obtained after coupling **13** with isopropylpiperazine (0.14 mL, 0.96 mmol). The residue was purified using a 3:1 EtOAc: hexanes column to afford a yellow semi-solid (0.16 g, 60%). IR (film, CH_2Cl_2): 3437 cm^{-1} (NH). ^{1}H-NMR (300 MHz, $CDCl_3$): δ 7.89 (d, *J* = 6.0 Hz, 1H), δ 7.78-7.87 (m, 3H), δ 7.41-7.53 (m, 4H), δ 5.66 (d, *J* = 6.0 Hz, 1H), δ 4.94 (d, *J* = 6.0 Hz, 2H), δ 4.79 (br s, 1H), δ 3.78-3.81 (m, 4H), δ 2.65-2.74 (m, 1H), δ 2.53-2.56 (m, 4H), δ 1.04 (d, *J* = 6.0 Hz, 6H). HREIMS Calcd $C_{22}H_{27}N_5$ (M^+) *m/z* 361.4833, found 361.2267. Anal. Calcd for: $C_{22}H_{27}N_5$•0.5 DCM; C, 66.90; H, 6.99; N, 17.34. Found: C, 66.68; H, 6.97; N, 17.26.

2-(4-Isopropylpiperidin-1-yl)-*N*-(naphthalen-1-ylmethyl)pyrimidin-4-amine (**13i**): The product was obtained after coupling **13** with isopropylpiperidine (0.14 mL, 0.96 mmol) to afford a light orange semi-solid (0.20 g, 75%). IR (film, CH_2Cl_2): 3438 cm^{-1} (NH). ^{1}H-NMR (300 MHz, $CDCl_3$): δ 8.02 (d, *J* = 6.0 Hz, 1H), δ 7.78-7.95 (m, 3H), δ 7.38-7.53 (m, 4H), δ 5.61 (d, *J* = 6.0 Hz, 1H), δ 4.92 (br s, 3H), δ 4.75-4.80 (m, 2H), δ 2.69-2.77 (m, 2H), δ 1.66-1.70 (m, 2H), δ 1.41-1.47 (m, 1H), δ 1.07-1.24 (m, 3H), δ 0.87-0.89 (d, *J* = 6.0 Hz, 6H). HREIMS Calcd for $C_{23}H_{28}N_4$ (M^+) *m/z* 360.4952, found 360.2317. Anal. Calcd for: $C_{23}H_{28}N_4$; C, 76.63; H, 7.83; N, 15.54. Found: C, 76.34; H, 7.80; N, 15.47.

***N*-(Naphthalen-1-ylmethyl)-2-(4-propylpiperazin-1-yl)-pyrimidin-4-amine** (**13j**): The product was obtained after coupling **13** with *n*-propylpiperazine.2HBr (0.29 g, 0.96 mmol) to afford a light brown solid (0.19 g, 70%). mp: 100-102 °C. IR (film, CH_2Cl_2): 3435 cm^{-1} (NH). ^{1}H-NMR (300 MHz, $CDCl_3$): δ 7.88 (d, *J* = 6.0 Hz, 1H), δ 7.75-7.85 (m, 3H), δ 7.40-7.52 (m, 4H), δ 5.66 (d, *J* = 6.0 Hz, 1H), δ 4.93 (d, *J* = 6.0 Hz, 2H), δ 4.80 (br s, 1H), δ 3.77-3.81 (m, 4H), δ 2.42-2.46 (m, 4H), δ 2.27-2.32 (m, 2H), δ 1.46-1.52 (m,

2H), δ 0.87-0.96 (m, 3H). HREIMS Calcd for $C_{22}H_{27}N_5$ (M^+) *m/z* 361.4833, found 361.2275.

2-[4-(4-[(Naphthalen-1-ylmethyl)amino]pyrimidin-2-yl)piperazin-1-yl]ethanol (**13k**): The product was obtained after coupling **13** with hydroxyethylpiperazine (0.12 mL, 0.96 mmol) to afford a brown solid (0.21 g, 78%). mp: 53-55 ^oC. IR (film, CH_2Cl_2): 3436 cm^{-1} (NH). ^{1}H-NMR (300 MHz, $CDCl_3$): δ 8.00 (d, *J* = 6.0 Hz, 1H), δ 7.77-7.88 (m, 3H), δ 7.37-7.51 (m, 4H), δ 5.66 (d, *J* = 6.0 Hz, 1H), δ 4.93 (br s, 3H), δ 3.77-3.80 (m, 4H), δ 3.60-3.64 (m, 2H), δ 2.50-2.56 (m, 6H). HREIMS Calcd for $C_{21}H_{25}N_5O$ (M^+) *m/z* 363.4561, found 363.2045.

2-[4-(2-Methoxyethyl)piperazin-1-yl]-*N*-(naphthalen-1-ylmethyl)pyrimidin-4-amine (**13l**): The product was obtained after coupling **13** with methoxyethylpiperazine (0.14mL, 0.96 mmol) to afford a dark brown semi-solid (0.20 g, 70%). IR (film, CH_2Cl_2): 3436 cm^{-1} (NH). ^{1}H-NMR (300 MHz, $CDCl_3$): δ 8.00 (d, *J* = 6.0 Hz, 1H), δ 7.77-7.87 (m, 3H), δ 7.37- 7.50 (m, 4H), δ 5.64 (d, *J* = 5.7 Hz, 1H), δ 4.92 (br s, 3H), δ 3.81-3.85 (m, 4H), δ 3.49-3.53 (m, 2H), δ 3.34 (s, 3H), δ 2.56-2.60 (m, 2H), δ 2.51-2.55 (m, 4H). HREIMS Calcd for $C_{22}H_{27}N_5O$ (M^+) *m/z* 377.4827, found 377.2214.

2-(4-Cyclohexylpiperazin-1-yl)-*N*-(naphthalen-1-ylmethyl)pyrimidin-4-amine (**13m**): The product was obtained after coupling **13** with cyclohexylpiperazine (0.16 g, 0.96 mmol) to afford a yellow solid (0.24 g, 80%). mp: 53-55 °C. IR (film, CH_2Cl_2): 3435 cm^{-1} (NH). ^{1}H-NMR (300 MHz, $CDCl_3$): δ 8.00 (d, *J* = 6.0 Hz, 1H), δ 7.74-7.87 (m, 3H), δ 7.37-7.51 (m, 4H), δ 5.63 (d, *J* = 6.0 Hz, 1H), δ 4.92 (br s, 3H), δ 3.76-3.80 (m, 4H), δ 2.56-2.60 (m, 4H), δ 2.26-2.31 (m, 1H), δ 1.80-1.90 (m, 2H), δ 1.67-1.77 (m, 2H), δ 1.59-1.63 (m, 1H), δ 1.17-1.23 (m, 5H). HREIMS Calcd for $C_{25}H_{31}N_5$ (M^+) *m/z* 401.5471, found 401.2948.

1-[4-(4-[(Naphthalen-1-ylmethyl)amino]pyrimidin-2-yl)piperazin-1-yl]ethanone (**13n**): The product was obtained after coupling **13** with acetylpiperazine (0.13 g, 0.96 mmol) to afford a light orange solid (0.18 g, 68%). mp: 70-72 °C. IR (film, CH_2Cl_2): 3437 cm^{-1} (NH). ^{1}H-NMR (300 MHz, $CDCl_3$): δ 8.00 (d, *J* = 6.0 Hz, 1H), δ 7.77-7.88 (m, 3H), δ 7.37-7.53 (m, 4H), δ 5.71 (d, *J* = 6.0 Hz, 1H), δ 4.94 (d, *J* = 6.0 Hz, 2H), δ 4.88 (br s, 1H), δ 3.72-3.78 (m, 4H), δ 3.58-3.62 (m, 2H), δ 3.40-3.44 (m, 2H), δ 2.07 (s, 3H).

HREIMS Calcd for $C_{21}H_{23}N_5O$ (M^+) *m/z* 361.4402, found 361.1899.

***Tert*-butyl 4-[4-([Naphthalen-1-ylmethyl]amino)pyrimidin-2-yl]piperazine-1-carboxylate** (**13o**): The product was obtained after coupling **13** with *tert*-butyl piperazine-1-carboxylate (0.18 g, 0.96 mmol). The residue was purified using a 3:1 EtOAc: hexanes column to afford a yellow solid (0.21 g, 68%). mp: 70-72 °C. IR (film, CH_2Cl_2): 3438 cm^{-1} (NH). ^{1}H-NMR (300 MHz, $CDCl_3$): δ 7.98 (d, *J* = 6.0 Hz, 1H), δ 7.84-7.76 (m, 3H), δ 7.36-7.50 (m, 4H), δ 5.66 (d, *J* = 6.0 Hz, 1H), δ 5.05 (br s, 1H), δ 4.91 (d, *J* = 6.0 Hz, 2H), δ 3.71-3.74 (m, 4H), δ 3.41-3.44 (m, 4H), δ1.45 (s, 9H). HREIMS Calcd for $C_{24}H_{29}N_5O_2$ (M^+) *m/z* 419.5194, observed 419.2325.

6.1.2.13. Diphenylmethylamines (14f-o)

***N*-Benzhydryl-2-(methylpiperazin-1-yl)pyrimidin-4-amine** (**14f**): The product was obtained after coupling **14** with methylpiperazine (0.17 mL, 1.14 mmol). The residue was purified using a 9:1 EtOAc: MeOH column to afford a yellow solid (0.17 g, 70%). mp: 128-130 °C. IR (film, $CDCl_3$): 3431 cm^{-1} (NH). ^{1}H-NMR (300 MHz, $CDCl_3$): δ 7.84 (d, *J* = 6.0 Hz, 1H), δ 7.27-7.36 (m, 10H), δ 5.93 (br s, 1H), δ 5.62 (d, *J* = 6.0 Hz, 1H), δ 5.15 (br s, 1H), δ 3.73-3.77 (m, 4H), δ 2.41-2.45 (m, 4H), δ 2.33 (s, 3H). HREIMS Calcd for $C_{22}H_{25}N_5$ (M^+) *m/z* 359.4674, found 359.2105.

***N*-Benzhydryl-2-(methylpiperidin-1-yl)pyrimidin-4-amine** (**14g**): The product was obtained after coupling **14** with methylpiperidine (0.17 mL, 1.14 mmol). The residue was purified using a 9:1 EtOAc: MeOH column to afford a light orange/yellow semi-solid (0.12 g, 50%). IR (film, $CDCl_3$): 3432 cm^{-1} (NH). ^{1}H-NMR (300 MHz, $CDCl_3$): δ 7.82 (d, *J* = 6.0 Hz, 1H), δ 7.26-7.35 (m, 10H), δ 5.94 (br s, 1H), δ 5.58 (d, *J* = 6.0 Hz, 1H), δ 5.17 (br s, 1H), δ 4.51-4.56 (m, 2H), δ 2.68-2.76 (m, 2H), δ 1.50-1.56 (m, 3H), δ 1.02-1.09 (m, 2H), δ 0.89 (d, *J* = 6.0 Hz, 3H). HREIMS Calcd for $C_{22}H_{26}N_5$ (M^+) *m/z* 358.4793, found 358.2155.

***N*-Benzhydryl-2-(4-isopropylpiperazin-1-yl)pyrimidin-4-amine** (**14h**): The product was obtained after coupling **14** with isopropylpiperazine (0.17 mL, 1.14 mmol). The residue was purified using a 9:1 EtOAc:

MeOH column to afford an off-white solid (0.16 g, 60%). mp: 103-105 °C. IR (film, $CDCl_3$): 3429 cm^{-1} (NH). ^{1}H-NMR (300 MHz, $CDCl_3$): δ 7.81 (d, *J* = 6.0 Hz, 1H), δ 7.24-7.34 (m, 10H), δ 5.94 (br s, 1H), δ 5.59 (d, *J* = 6.0 Hz, 1H), δ 5.22 (d, *J* = 6.0 Hz, 1H), δ 3.66-3.70 (m, 4H), δ 2.62-2.70 (m, 1H), δ 2.43-2.47 (m, 4H), δ 1.02 (d, *J* = 6.0 Hz, 6H). HREIMS Calcd for $C_{24}H_{29}N_5$ (M^+) *m/z* 387.5206, found 387.2414.

***N*-Benzhydryl-2-(4-isopropylpiperidin-1-yl)pyrimidin-4-amine** (**14i**): The product was obtained after coupling **14** with isopropylpiperidine (0.17 mL, 1.15 mmol). The residue was purified using a 3:1 EtOAc: DCM column to afford an orange semi-solid (0.13 g, 50%). IR (film, $CDCl_3$): 3427 cm^{-1} (NH). ^{1}H-NMR (300 MHz, $CDCl_3$δ 7.82 (d, *J* = 6.0 Hz, 1H), δ 7.27-7.36 (m, 10H), δ 5.96 (br s, 1H), δ 5.74 (br s, 1H), δ 5.60 (br s, 1H) δ 4.60-4.64 (m, 2H), δ 2.62-2.70 (m, 2H), δ 1.60-1.64 (m, 2H), δ 1.40-1.45 (m, 1H), δ 1.14-1.24 (m, 3H), δ 0.87 (d, *J* = 6.0 Hz, 6H). HREIMS Calcd for $C_{25}H_{30}N_4$ (M^+) *m/z* 386.5325, found 386.2462.

***N*-Benzhydryl-2-(4-propylpiperazin-1-yl)pyrimidin-4-amine** (**14j**): The product was obtained after coupling **14** with *n*-propylpiperazine.2HBr (0.34 g, 1.15 mmol). The residue was purified using a 9:1 EtOAc: MeOH column to afford an off-white semi-solid (0.15 g, 57%). IR (film, $CDCl_3$) 3423 cm^{-1} (NH). ^{1}H-NMR (300 MHz, $CDCl_3$): δ 7.83 (d, *J* = 6.0 Hz, 1H), δ 7.24-7.32 (m, 10H), δ 5.92 (br s, 1H), δ 5.61 (d, *J* = 6.0 Hz, 1H), δ 5.13 (d, *J* = 6.0 Hz, 1H), δ 3.68-3.72 (m, 4H), δ 2.39-2.42 (m, 4H), δ 2.29-2.34 (m, 2H), δ 1.50-1.55 (m, 2H), δ 0.87-0.92 (m, 3H). HREIMS Calcd for $C_{24}H_{29}N_5$ (M^+) *m/z* 387.5206, found 387.2434.

2-[4-(4-[Benzhydrylamino]pyrimidin-2-yl)piperazin-1-yl]ethanol (**14k**): The product was obtained after coupling **14** with hydroxyethylpiperazine (0.15 mL, 1.15 mmol) to afford a light yellow solid (0.17 g, 65%). mp: 155-157 °C. IR (film, $CDCl_3$): 3421 cm^{-1} (NH). ^{1}H-NMR (300 MHz, $CDCl_3$): δ 7.84 (d, *J* = 6.0 Hz, 1H), δ 7.27-7.34 (m, 10H), δ 5.93 (br s, 1H), δ 5.66 (d, *J* = 6.0 Hz, 1H), δ 5.19 (br s, 1H), δ 3.76-3.80 (m, 4H), δ 3.68 (t, *J* = 6.0 Hz, 2H), δ 2.62 (t, *J* = 6.0 Hz, 2H), δ 2.56-2.60 (m, 4H). HREIMS Calcd for $C_{23}H_{27}N_5O$ (M^+) *m/z* 389.4934, found 389.2217.

***N*-Benzhydryl-2-[4-(2-methoxyethyl)piperazin-1-yl]pyrimidin-4-amine (14l)**: The product was obtained after coupling **14** with methoxyethylpiperazine (0.17 mL, 1.15 mmol) to afford a light orange/yellow semi-solid (0.18 g, 65%). IR (film, $CDCl_3$): 3428 cm^{-1} (NH). ^{1}H-NMR (300 MHz, $CDCl_3$): δ 7.79 (d, *J* = 6.0 Hz, 1H), δ 7.25-7.30 (m, 10H), δ 5.93 (br s, 1H), δ 5.58 (d, *J* = 6.0 Hz, 1H), δ 5.28 (d, *J* = 6.0 Hz, 1H), δ 3.65-3.68 (m, 4H), δ 3.47-3.51 (m, 2H), δ 3.32 (s, 3H), δ 2.51-2.55 (m 2H), δ 2.40-2.43 (m, 4H). HREIMS Calcd for $C_{24}H_{29}N_5O$ (M^+) *m/z* 403.5200, found 403.2378. Anal. Calcd for: $C_{24}H_{29}N_5O$; C, 71.44; H, 7.24; N, 17.36. Found: C, 71.31; H, 7.15; N, 17.14.

***N*-Benzhydryl-2-(4-cyclohexylpiperazin-1-yl)pyrimidin-4-amine (14m)**: The product was obtained after coupling **14** with cyclohexylpiperazine (0.19 g, 1.15 mmol). The residue was purified using a 3:1 EtOAc: DCM column to afford a light yellow solid (0.17 g, 60%). mp: 53-55 °C. IR (film, $CDCl_3$): 3424 cm^{-1} (NH). H-NMR (300 MHz, $CDCl_3$) δ 7.83 (d, *J* = 6.0 Hz, 1H), δ 7.24-7.33 (m, 10H), δ 5.92 (br s, 1H), δ 5.61 (d, *J* = 6.0 Hz, 1H), δ 5.14 (br s, 1H), δ 3.64-3.68 (m, 4H), δ 2.49-2.52 (m, 4H), δ 2.27-2.32 (m, 1H), δ 1.81-1.86 (m, 2H), δ 1.75-1.80 (m, 2H) δ 1.60-1.64 (m, 1H), δ 1.21-1.27 (m, 5H). HREIMS Calcd for $C_{27}H_{33}N_5$ (M^+) *m/z* 427.5844, found 427.2733.

1-[4-(4-[Benzhydrylamino]pyrimidin-2-yl)piperazin-1-yl]ethanone (14n): The product was obtained after coupling **14** with acetylpiperazine (0.16 g, 1.15 mmol) to afford a light yellow solid (0.2 g, 76%). mp: 182-184 °C. IR (film, $CDCl_3$): 3429 cm^{-1} (NH). ^{1}H-NMR (300 MHz, $CDCl_3$) δ 7.81 (d, *J* = 6.0 Hz, 1H), δ 7.21-7.28 (m, 10H), δ 5.96 (br s, 1H), δ 5.68 (d, *J* = 6.0 Hz, 1H), δ 5.46 (d, *J* = 6.0 Hz, 1H), δ 3.64 (d, *J* = 6.0 Hz, 2H), δ 3.59 (d, *J* = 6.0 Hz, 2H), δ 3.49 (d, *J* = 6.0 Hz, 2H), δ 3.33 (d, *J* = 6.0 Hz, 2H), δ 2.04 (s, 3H) HREIMS Calcd for $C_{23}H_{25}N_5O$ (M^+) *m/z* 387.4775, found 387.2059. Anal. Calcd for: $C_{23}H_{25}N_5O$; C, 71.29; H, 6.50; N, 18.07. Found: C, 71.11; H, 6.52; N, 18.02.

***Tert*-butyl 4-[4-(Benzhydrylamino)pyrimidin-2-yl]piperazine-1-carboxylate (14o)**: The product was obtained after coupling **14** with *tert*-butyl piperazine-1-carboxylate (0.21 g, 1.15 mmol). The residue was purified using a 3:1 EtOAc: DCM column to afford an off-white solid (0.18 g, 60%). mp: 68-70 °C. IR (film, $CDCl_3$): 3442 cm^{-1} (NH). ^{1}H-NMR (300 MHz, $CDCl_3$): δ 7.81 (d, *J* = 6.0 Hz, 1H), δ 7.22-7.32 (m,

10H), δ 5.95 (br s, 1H), δ 5.63 (d, *J* = 6.0 Hz, 1H), δ 5.30 (d, *J* = 6.0 Hz, 1H), δ 3.58-3.62 (m, 4H), δ 3.31-3.35 (m, 4H), δ 1.45 (s, 9H). HREIMS Calcd for $C_{26}H_{31}N_5O_2$ (M^+) *m/z* 445.5566, found 445.2489. Anal. Calcd for: $C_{26}H_{31}N_5O_2$; C, 70.09; H, 7.01; N, 15.72. Found: C, 70.17; H, 7.02; N, 15.71.

6.1.2.14. Phenylethylamines (15a-c,f,g,n)

***N*-Phenethyl-2-(pyrrolidin-1-yl)pyrimidin-4-amines (15a)**: The product was obtained by coupling **15** with pyrrolidine (0.09 mL, 1.11 mmol) to afford a light yellowish brown solid (0.15 g, 65%). mp: 85-87 °C. IR (film, CH_2Cl_2): 3436 cm^{-1} (NH). ^{1}H-NMR (300 MHz, $CDCl_3$): δ 7.86 (d, *J* = 6.0 Hz, 1H), δ 7.18-7.32 (m, 5H), δ 5.59 (d, *J* = 6.0 Hz, 1H), δ 4.56 (br s, 1H), δ 3.55 (t, *J* = 6.0 Hz, 2H), δ 3.50 (t, *J* = 6.0 Hz, 4H), δ 2.86-2.91 (m, 2H), δ 1.90-1.93 (m, 4H). HREIMS $C_{16}H_{20}N_4$ (M^+) *m/z* 268.3568, found 268.2125. Anal. Calcd for $C_{16}H_{20}N_4$•0.5 H_2O; C, 69.29; H, 7.63; N, 20.2. Found: C, 69.51; H, 7.32; N, 20.11.

2-Morpholino-*N*-phenethylpyrimidin-4-amine (**15b**): The product was obtained after coupling **15** with morpholine (0.10 mL, 1.11 mmol) to afford a light brown solid (0.21 g, 86%). mp: 93-95 °C. IR (film, CH_2Cl_2): 3433 cm^{-1} (NH). ^{1}H-NMR (300 MHz, $CDCl_3$): δ 7.85 (d, *J* = 6.0 Hz, 1H), δ 7.18-7.32 (m, 5H), δ 5.65 (d, *J* = 6.0 Hz, 1H), δ 4.59 (br s, 1H), δ 3.68-3.75 (m, 8H), δ 3.55-3.59 (m, 2H), δ 2.86-2.90 (m, 2H). HREIMS Calcd $C_{16}H_{20}N_4O$ (M^+) *m/z* 284.3562, found 284.1725. Anal. Calcd for $C_{16}H_{20}N_4O$; C, 67.58; H, 7.09; N, 19.70. Found: C, 67.71; H, 7.14; N, 19.42.

***N*-Phenethyl-2-thiomorpholinopyrimidin-4-amine** (**15c**): The product was obtained after coupling **15** with thiomorpholine (0.11 mL, 1.11 mmol) to afford a brown solid (0.21 g, 81%). mp: 60-62 °C. IR (film, CH_2Cl_2): 3437 cm^{-1} (NH). ^{1}H-NMR (300 MHz, $CDCl_3$) δ 7.84 (d, *J* = 6.0 Hz, 1H), δ 7.18-7.30 (m, 5H), δ 5.61 (d, *J* = 6.0 Hz, 1H), δ 4.58 (br s, 1H), δ 3.98 (t, *J* = 6.0 Hz, 4H), δ 3.54 (t, *J* = 6.0 Hz, 2H), δ 2.86-2.90 (m, 2H), δ 2.61 (t, *J* = 6.0 Hz, 4H). HREIMS Calcd $C_{16}H_{20}N_4S$ (M^+) *m/z* 284.3562, found 284.1725. Anal. Calcd for $C_{16}H_{20}N_4S$; C, 63.97; H, 6.71; N, 18.65. Found: C, 64.12; H, 6.85; N, 18.46.

2-(4-Methylpiperazin-1-yl)-*N*-phenethylpyrimidin-4-amine (**15f**): The product was obtained after coupling **15** with methylpiperazine (0.12 mL, 1.11 mmol) to afford a light yellow solid (0.18 g, 69%). mp: 58-60 °C IR (film, CH_2Cl_2): 3436 cm^{-1} (NH). ^{1}H-NMR (300 MHz, $CDCl_3$): δ 7.85 (d, *J* = 6.0 Hz, 1H), δ 7.18-7.30 (m, 5H), δ 5.62 (d, *J* = 6.0 Hz, 1H), δ 4.57 (br s, 1H), δ 3.76-3.79 (m, 4H), δ 3.52-3.56 (m, 2H), δ 2.86-2.90 (m, 2H), δ 2.41-2.44 (m, 4H), δ 2.31 (s, 3H). HREIMS Calcd $C_{17}H_{23}N_5$ (M^+) *m/z* 297.3980, found 297.1958. Anal. Calcd for $C_{17}H_{23}N_5$•1.3 H_2O; C, 68.05; H, 7.67; N, 23.35. Found: C, 68.12; H, 7.82; N, 23.36.

2-(4-Methylpiperidin-1-yl)-*N*-phenethylpyrimidin-4-amine (**15g**): The product was obtained after coupling **15** with methylpiperidine (0.12 mL, 1.11 mmol) to afford a light brown solid (0.20 g, 79%). mp: 65-67 °C. IR (film, CH_2Cl_2): 3439 cm^{-1} (NH). ^{1}H-NMR (300 MHz, $CDCl_3$): δ 7.84 (d, *J* = 6.0 Hz, 1H), δ 7.18-7.33 (m, 5H), δ 5.57 (d, *J* = 6.0 Hz, 1H), δ 4.64-4.69 (m, 2H), δ 4.53 (br s, 1H), δ 3.52-3.56 (m, 2H), δ 2.86-2.90 (m, 2H), δ 2.73-2.82 (m, 2H), δ 1.63-1.68 (m, 3H), δ 1.33-1.40 (m, 1H), δ 1.08-1.16 (m, 3H), δ 0.92 (d, *J* = 6.0 Hz, 3H). HREIMS Calcd $C_{18}H_{24}N_4$ (M^+) *m/z* 296.4100, found 296.2380.

1-[4-(4-(Phenethylamino)pyrimidin-2-yl)piperazin-1-yl]ethanone (**15n**): The product was obtained after coupling **15** with acetylpiperazine (0.14 g, 1.11 mmol) to afford a yellow solid (0.24 g, 86%). mp: 150-152 °C. IR (film, CH_2Cl_2): 3437 cm^{-1} (NH). ^{1}H-NMR (300 MHz, $CDCl_3$): δ 7.85 (d, *J* = 6.0 Hz, 1H), δ 7.19-7.33 (m, 5H), δ 5.66 (d, *J* = 6.0 Hz, 1H), δ 4.61 (br s, 1H), δ 3.73-3.80 (m, 4H), δ 3.65 (t, *J* = 6.0 Hz, 2H), δ 3.55 (t, *J* = 6.0 Hz, 2H), δ 3.46-3.50 (m, 2H), δ 2.86-2.90 (m, 2H), δ 2.12 (s, 3H). HREIMS Calcd $C_{18}H_{23}N_5O$ (M^+) *m/z* 325.4081, found 325.1913. Anal. Calcd for $C_{18}H_{23}N_5$•0.6 EtOAc; C, 64.78; H, 7.41; N, 18.52. Found: C, 64.66; H, 7.43; N, 18.30.

6.1.3. General method to prepare derivatives 2-12u.

To a solution of 4-aminobenzylpiperidine and DIPEA (2.58-3.64 mmol, each) in 1 mL of *n*-BuOH kept in a PV with stirring, an intermediate **2-15** (0.20 g, 0.65-0.91 mmol) was added. The sealed PV was placed in an oil bath at 185-195 °C and stirred overnight (~ 14-16 hrs). Solution was neutralized with 6M

HCl, diluted with 15 mL EtOAc and washed successively with saturated $NaHCO_3$ and NaCl solution (1:3, 1 x 15 mL). The aqueous layer was washed with EtOAc (2 x 5 mL) and the organic layer was dried over anhydrous $MgSO_4$ then filtered. The solution was evaporated in vacuo and purified using 9:1 Acetone: MeOH SGCC and (if necessary) de-greased by boiling in hexanes for 5 min. then decanting the contaminated solvent and re-dried to afford either solid or semisolid orange/light brown products. Some physical and spectroscopy data are provided below.

***N*^{4}-Benzyl-*N*^{2}-(1-benzylpiperidin-4-yl)pyrimidine-2,4-diamine** (**2u**): The product was obtained after coupling **2** with 4-aminobenzylpiperidine (0.74 mL, 3.64 mmol) (0.20 g, 59%). mp: 88-90 °C. IR (film, CH_2Cl_2): 3438 cm^{-1} (NH). ^{1}H-NMR (300 MHz, $CDCl_3$): δ 7.78 (d, *J* = 6.0 Hz, 1H), δ 7.21-7.34 (m, 10H), δ 5.66 (d, *J* = 6.0 Hz, 1H), δ 4.92 (br s, 2H), δ 4.46 (d, *J* = 6.0 Hz, 2H), δ 3.76-3.82 (m, 1H), δ 3.48 (s, 2H), δ 2.76-2.80 (m, 2H), 2.09-2.16 (m, 2H), 1.95-1.99 (m, 2H), 1.42-1.55 (m, 2H). HREIMS Calcd $C_{23}H_{27}N_5$ (M^+) *m/z* 373.4940, found 373.2008. Anal. Calcd for $C_{23}H_{27}N_5$•DCM; C, 62.88; H, 6.38; N, 15.28. Found: C, 62.88; H, 6.38; N, 15.28.

***N*^{2}-(1-Benzylpiperidin-4-yl)-*N*^{4}-(2-chlorobenzyl)pyrimidine-2,4-diamine** (**3u**): The product was obtained after coupling **3** with 4-aminobenzylpiperidine (0.64 mL, 3.15 mmol) (0.16 g, 51%). mp: 65-67 °C. ^{1}H-NMR (300 MHz, $CDCl_3$): δ 7.78 (d, *J* = 6.0 Hz, 1H), δ 7.17-7.36 (m, 9H), δ 5.67 (d, *J* = 6.0 Hz, 1H), δ 4.99 (br s, 1H), δ 4.73 (br s, 1H) δ 4.57 (d, *J* = 6.0 Hz, 2H), δ 3.75-3.79 (m, 1H), δ 3.48 (s, 2H), δ 2.76-2.80 (m, 2H), 2.09-2.16 (m, 2H), 1.95-1.99 (m, 2H), 1.42-1.55 (m, 2H). HREIMS Calcd $C_{23}H_{26}ClN_5$ (M^+) *m/z* 407.9390, found 407.1872.

***N*^{2}-(1-Benzylpiperidin-4-yl)-*N*^{4}-(3-chlorobenzyl)pyrimidine-2,4-diamine** (**4u**): The product was obtained after coupling **4** with 4-aminobenzylpiperidine (0.64 mL, 3.15 mmol) (0.16 g, 51%). mp: 62-63 °C. ^{1}H-NMR (300 MHz, $CDCl_3$) δ 7.77 (d, *J* = 6.0 Hz, 1H), δ 7.17-7.30 (m, 9H), δ 5.68 (d, *J* = 6.0 Hz, 1H), δ 5.00 (br s, 1H), δ 4.81 (br s, 1H), δ 4.46 (d, *J* = 6.0 Hz, 2H), δ 3.73-3.79 (m, 1H), δ 3.49 (s, 2H), δ 2.77-2.81 (m, 2H), δ 2.09-2.16 (m, 2H), δ 1.97-2.01 (m, 2H), δ 1.44-1.54 (m, 2H). HREIMS Calcd $C_{23}H_{26}ClN_5$ (M^+) *m/z* 407.9390, found 407.1877.

***N*^{2}-(1-Benzylpiperidin-4-yl)-*N*^{4}-(4-chlorobenzyl)pyrimidine-2,4-diamine** (**5u**): The product was obtained after coupling **5** with 4-aminobenzylpiperidine (0.64 mL, 3.15 mmol) (0.17 g, 54%). mp: 64-66 °C. ^{1}H-NMR (300 MHz, $CDCl_3$) δ 7.77 (d, *J* = 6.0 Hz, 1H), δ 7.25-7.30 (m, 5H), δ 7.16-7.23 (m, 4H), δ 5.66 (d, *J* = 6.0 Hz, 1H), δ 5.00 (br s, 1H), δ 4.87 (br s, 1H), δ 4.44 (d, *J* = 6.0 Hz, 2H), δ 3.73-3.79 (m, 1H), δ 3.50 (s, 2H), δ 2.77-2.81 (m, 2H), δ 2.09-2.16 (m, 2H), δ 1.97-2.01 (m, 2H), δ 1.44-1.54 (m, 2H). HREIMS Calcd $C_{23}H_{26}ClN_5$ (M^+) *m/z* 407.9390, found 407.1879.

***N*^{2}-(1-Benzylpiperidin-4-yl)-*N*^{4}-(4-bromobenzyl)pyrimidine-2,4-diamine** (**6u**): The product was obtained after coupling **6** with 4-aminobenzylpiperidine (0.54 mL, 2.68 mmol) (0.14 g, 48%). mp: 59-61 °C. ^{1}H-NMR (300 MHz, $CDCl_3$) δ 7.76 (d, *J* = 6.0 Hz, 1H), δ 7.55-7.58 (m, 2H), δ 7.21-7.26 (m, 5H), δ 7.14-7.17 (m, 2H), δ 5.66 (d, *J* = 6.0 Hz, 1H), δ 4.99 (br s, 2H), δ 4.43 (d, *J* = 6.0 Hz, 2H), δ 3.74-3.80 (m, 1H), δ 3.50 (s, 2H), δ 2.77-2.81 (m, 2H), δ 2.09-2.16 (m, 2H), δ 1.97-2.01 (m, 2H), δ 1.44-1.54 (m, 2H). HREIMS Calcd $C_{23}H_{26}BrN_5$ (M^+) *m/z* 452.3900, found 451.1361.

***N*^{2}-(1-Benzylpiperidin-4-yl)-*N*^{4}-(4-fluorobenzyl)pyrimidine-2,4-diamine** (**7u**): The product was obtained after coupling **7** with 4-aminobenzylpiperidine (0.68 mL, 3.37 mmol) (0.15 g, 45%). mp: 61-63 °C. ^{1}H-NMR (300 MHz, $CDCl_3$) δ 7.79 (d, *J* = 6.0 Hz, 1H), δ 7.28-7.31 (m, 2H), δ 7.21-7.27 (m, 5H), δ 6.96-7.02 (m, 2H), δ 5.65 (d, *J* = 6.0 Hz, 1H), δ 4.90 (br s, 1H), δ 4.71 (d, *J* = 6.0 Hz, 1H), δ 4.43 (d, *J* = 6.0 Hz, 2H), δ 3.75-3.80 (m, 1H), δ 3.49 (s, 2H), δ 2.77-2.81 (m, 2H), δ 2.09-2.16 (m, 2H), δ 1.97-2.01 (m, 2H), δ 1.44-1.54 (m, 2H). HREIMS Calcd $C_{23}H_{26}FN_5$ (M^+) *m/z* 391.4844, found 391.2165.

***N*^{2}-(1-Benzylpiperidin-4-yl)-*N*^{4}-(4-methylbenzyl)pyrimidine-2,4-diamine** (**8u**): The product was obtained after coupling **8** with 4-aminobenzylpiperidine (0.69 mL, 3.42 mmol) (0.17 g, 50%). mp: 60-62 °C. ^{1}H-NMR (300 MHz, $CDCl_3$) δ 7.77 (d, *J* = 6.0 Hz, 1H), δ 7.25-7.30 (m, 5H), δ 7.19-7.23 (m, 2H), δ 7.10-7.15 (m, 2H), δ 5.65 (d, *J* = 6.0 Hz, 1H), δ 4.88 (br s, 2H), δ 4.42 (d, *J* = 6.0 Hz, 2H), δ 3.76-3.82 (m, 1H), δ 3.49 (s, 2H), δ 2.77-2.81 (m, 2H), δ 2.31 (s, 3H), δ 2.09-2.16 (m, 2H), δ 1.97-2.01 (m, 2H), δ 1.44-1.54 (m, 2H). HREIMS Calcd $C_{24}H_{29}N_5$ (M^+) *m/z* 387.5206, observed 387.2415.

***N*^{2}-(1-Benzylpiperidin-4-yl)-*N*^{4}-(4-methoxybenzyl)pyrimidine-2,4-diamine** (**9u**): The product was obtained after coupling **9** with 4-aminobenzylpiperidine (0.65 mL, 3.20 mmol) (0.15 g, 45%). mp: 55-57 °C. ^{1}H-NMR (300 MHz, $CDCl_3$) δ 7.79 (d, *J* = 6.0 Hz, 1H), δ 7.21-7.30 (m, 7H), δ 6.83-6.86 (m, 2H), δ 5.65 (d, *J* = 6.0 Hz, 1H), δ 4.81 (br s, 1H), δ 4.68 (d, *J* = 6.0 Hz, 1H), δ 4.38 (d, *J* = 6.0 Hz, 2H), δ 3.77 (s, 3H), δ 3.49 (s, 2H), δ 2.77-2.81 (m, 2H), δ 2.10-2.17 (m, 2H), δ 1.96-2.00 (m, 2H), δ 1.66-1.72 (m, 1H), δ 1.42-1.52 (m, 2H). HRMS Calcd for $C_{24}H_{29}N_5O$ 403.5200 , observed 403.2361.

***N*^{2}-(1-Benzylpiperidin-4-yl)-*N*^{4}-(3,4-dimethoxybenzyl)pyrimidine-2,4-diamine** (**10u**): The product was obtained after coupling **10** with 4-aminobenzylpiperidine (0.58 mL, 2.86 mmol) (0.14 g, 45%). mp: 52-54 °C. ^{1}H-NMR (300 MHz, $CDCl_3$) δ 7.80 (d, *J* = 6.0 Hz, 1H), δ 7.27-7.31 (m, 5H), δ 6.79-6.86 (m, 3H), δ 5.67 (d, *J* = 6.0 Hz, 1H), δ 4.83 (br s, 1H), δ 4.76 (br s, 1H), δ 4.39 (d, *J* = 6.0 Hz, 2H), δ δ 3.85 (s, 3H), δ 3.84 (s, 3H), δ 3.49 (s, 2H), δ 2.77-2.81 (m, 2H), δ 2.11-2.18 (m, 2H), δ 1.97-2.01 (m, 2H), δ 1.55-1.62 (m, 1H), δ 1.44-1.51 (m, 2H). HRMS Calcd for $C_{25}H_{31}N_5O_2$ 433.5459, observed 433.2472.

***N*^{2}-(1-Benzylpiperidin-4-yl)-*N*^{4}-(3,4,5-trimethoxybenzyl)pyrimidine-2,4-diamine** (**11u**): The product was obtained after coupling **11** with 4-aminobenzylpiperidine (0.52 mL, 2.58 mmol) (0.14 g, 45%). mp: 63-65 °C. ^{1}H-NMR (300 MHz, $CDCl_3$) δ 7.80 (d, *J* = 6.0 Hz, 1H), δ 7.29-7.34 (m, 5H), δ 6.51 (s, 2H), δ 5.67 (d, *J* = 6.0 Hz, 1H), δ 4.84 (br s, 1H), δ 4.77 (br s, 1H), δ 4.40 (d, *J* = 6.0 Hz, 2H), δ 3.83 (s, 6H), δ 3.82 (s, 3H), δ 3.49 (s, 2H), δ 2.78-2.82 (m, 2H), δ 2.11-2.18 (m, 2H), δ 1.97-2.01 (m, 2H), δ 1.55-1.62 (m, 1H), δ 1.45-1.52 (m, 2H). HRMS Calcd for $C_{26}H_{33}N_5O_3$ 463.5719, observed 463.2578.

***N*^{4}-(Benzo[*d*][1,3]dioxol-5-ylmethyl)-*N*^{2}-(1-benzylpiperidin-4-yl)pyrimidine-2,4-diamine** (**12u**): The product was obtained after coupling **12** with 4-aminobenzylpiperidine (0.61 mL, 3.03 mmol) (0.14 g, 45%). mp: 56-58 °C. ^{1}H-NMR (300 MHz, $CDCl_3$) δ 7.77 (d, *J* = 6.0 Hz, 1H), δ 7.22-7.30 (m, 5H), δ 6.70-6.77 (m, 3H), δ 5.90 (s, 2H), δ 5.63 (d, *J* = 6.0 Hz, 1H), δ 5.01 (br s, 1H), δ 4.78 (d, *J* = 6.0 Hz, 1H), δ 4.35 (d, *J* = 6.0 Hz, 2H), δ 3.47 (s, 2H), δ 2.76-2.80 (m, 2H), δ 2.09-2.15 (m, 2H), δ 1.95-1.99 (m, 2H), δ 1.74-1.79 (m, 1H), δ 1.44-1.54 (m, 2H). HRMS Calcd for $C_{24}H_{27}N_5O_2$ 417.5035, observed 417.2175.

6.1.4. General method to prepare derivative 2d

4-(4-(benzylamino)pyrimidin-2-yl)thiomorpholine-1-oxide

To a mixture of *N*-benzyl-2-thiomorpholinopyrimidin-4-amine (**2c**) (0.20 g, 0.70 mmol) in 3 mL of 1,4-dioxane, kept at 0 °C (ice-bath), *m*CPBA (0.19 g, 1.12 mmol) in 1 mL 1,4-dioxane was added dropwise. The reaction is allowed to stir on the ice-bath for 5 minutes and then was kept at r.t for 3 hrs. DCM was added to the mixture to aid in the 1,4-dioxane in vacuo evaporation. The residue was re-dissolved in a 3:1 EtOAc and DCM and successfully washed with a concentrated $NaHCO_3$ and NaCl solution (1:2, 1 x 15 mL). Aqueous layer was washed with EtOAc (3 x 15 mL) and the combined organic layer was dried over anhydrous $MgSO_4$ and filtered. The organic layer was evaporated in vacuo and the resulting solid residue was further purified using 3:1 EtOAc: hexanes SGCC to afford a light yellow solid (0.16 g, 75%). mp: 78-80 °C. IR (film, CH_2Cl_2): 3439 cm^{-1} (NH). ^{1}H-NMR (300 MHz, $CDCl_3$): δ 7.87 (d, *J* = 6.0 Hz, 1H), δ 7.24-7.35 (m, 5H), δ 5.74 (d, *J* = 6.0 Hz, 1H), δ 4.99 (br s, 1H), δ 4.49 (d, *J* = 6.0 Hz, 2H), δ 4.37 (t, *J* = 6.0 Hz, 1H), δ 4.32 (t, *J* = 6.0 Hz, 1H), 4.10-4.19 (m, 2H), 2.69-2.73 (m, 4H). HREIMS Calcd $C_{15}H_{18}N_4OS$ (M^+) *m/z* 302.3946, found 302.1259. Anal. Calcd for $C_{15}H_{18}N_4OS$•0.3 DCM; C, 56.05; H, 5.72; N, 17.09. Found: C, 56.38; H, 5.74; N, 17.22.

6.1.5. General method to prepare derivative 2e

4-(4-(benzylamino)pyrimidin-2-yl)thiomorpholine 1,1-dioxide

To a mixture of *N*-benzyl-2-thiomorpholinopyrimidin-4-amine (**7c**) (0.20 g, 0.70 mmol) in 5 mL of MeOH, kept at 0 °C (ice-bath), potassium peroxymonosulphate (0.23 g, 1.54 mmol) in 0.5 mL of H_2O was added dropwise. The reaction was allowed to stir on the ice-bath for 5 minutes, then heated at 70-75 °C for 1hr and finally moved to r.t for 4hrs. MeOH was evaporated in vacuo and the residue was re-dissolved in 3:1 EtOAc: DCM and successfully washed with a concentrated $NaHCO_3$ and NaCl solution (1:2, 1 x 15 mL). Aqueous layer was washed with EtOAc (3 x 15 mL) and the combined organic layer was dried over anhydrous $MgSO_4$ and filtered. The organic layer was evaporated in vacuo and the resulting solid residue was further purified using 3:1 EtOAc: hexanes SGCC to afford a light orange solid (0.17 g, 75%). mp: 65-67 °C. IR (film, CH_2Cl_2): 3464 cm^{-1} (NH). ^{1}H-NMR (300 MHz, $CDCl_3$): δ 7.87 (d, *J* = 6.0 Hz, 1H), δ 7.25-

7.35 (m, 5H), δ 5.79 (d, *J* = 6.0 Hz, 1H), δ 5.14 (br s, 1H), δ 4.49 (d, *J* = 6.0 Hz, 2H), δ 4.21-4.25 (m, 4H), δ 2.88-2.92 (m, 4H). HREIMS Calcd $C_{15}H_{10}N_4O_2S$ (M^+) *m/z* 318.3946, found 318.1310. Anal. Calcd for $C_{15}H_{18}N_4O_2S$•0.2 DCM; C, 51.95; H, 5.28; N, 15.94. Found: C, 52.04; H, 5.34; N, 15.71.

6.1.6. General method to prepare derivatives **2p**, **13p** and **14p**

To a mixture of **2o**, **13o** or **14o** (0.20 g, 0.45-0.54 mmol) in 4 mL of DCM, kept at 0 ^oC (ice-bath), TFA (4 mL, 53.83 mmol) was added dropwise. The reaction was allowed to stir on the ice-bath for 5 minutes and then was kept at r.t for 2 hrs. DCM and TFA were evaporated in vacuo with the aid of toluene and the residue was re-dissolved in 3:1 EtOAc: DCM and successfully washed with a concentrated $NaHCO_3$ and NaCl solution (1:1, 1 x 15 mL). Aqueous layer was washed with EtOAc (3 x 15 mL) and the combined organic layer was dried over anhydrous $MgSO_4$ and filtered. The organic layer was evaporated in vacuo to afford a solid or semi-solid product. Some physical and spectroscopy data are provided below.

***N*-benzyl-2-(piperazin-1-yl)pyrimidin-4-amine** (**2p**): The product was a light yellow solid (0.11 g, 75%). mp: 70-72 °C. IR (film, CH_2Cl_2): 3438 cm^{-1} (NH). ^{1}H-NMR (300 MHz, $CDCl_3$): δ 7.86 (d, *J* = 6.0 Hz, 1H), δ 7.24-7.34 (m, 5H), δ 5.66 (d, *J* = 6.0 Hz, 1H), δ 4.91 (br s, 1H), δ 4.49 (d, *J* = 6.0 Hz, 2H), δ 3.73-3.76 (m, 4H), 3.09 (s, 1H), δ 2.88-2.91 (m, 4H). HREIMS Calcd $C_{15}H_{19}N_5$ (M^+) *m/z* 269.3449, found 269.1953.

***N*-(naphthalen-1-ylmethyl)-2-(piperazin-1-yl)pyrimidin-4-amine** (**13p**): The product was a yellow semi-solid (0.06 g, 60%). IR (film, CH_2Cl_2): 3438 cm^{-1} (NH). ^{1}H-NMR (300 MHz, $CDCl_3$) δ 7.98 (d, *J* = 6.0 Hz, 1H), δ 7.84-7.87 (m, 3H), δ 7.36-7.50 (m, 4H), δ 5.66 (d, *J* = 6.0 Hz, 1H), δ 5.05 (d, *J* = 6.0 Hz, 1H), δ 4.90 (d, *J* = 6.0 Hz, 2H), δ 3.95-4.01 (m, 4H), δ 3.07-3.13 (m, 4H). HREIMS Calcd for $C_{19}H_{21}N_5$ (M^+) *m/z* 319.4035, found 319.1785.

***N*-Benzhydryl-2-(piperazin-1-yl)pyrimidin-4-amine** (**14p**): The product was an orange/yellow semi-solid (0.07 g, 60%). IR (film, $CDCl_3$): 3426 cm^{-1} (NH). ^{1}H-NMR (300 MHz, $CDCl_3$): δ 7.84 (d, *J* = 6.0 Hz, 1H), δ 7.25-7.32 (m, 10H), δ 5.90 (br s, 1H), δ 5.80 (br s, 1H), δ 5.41 (br s, 1H), δ 3.94-3.98 (m, 4H), δ 2.98-

3.02 (m, 4H). HREIMS Calcd for $C_{21}H_{23}N_5$ (M^+) *m/z* 345.4408, found 345.1954.

6.2. Biochemistry

6.2.1. Cholinesterase Assay

The assay utilizes *h*AChE (product number C3389; Sigma-Aldrich, St. Louis, MO) and equine serum BuChE (product number C1057; Sigma-Aldrich, St. Louis, MO) along with tacrine.HCl (item number 70240; Cayman Chemical, Ann Arbor, MI), bis(7)-tacrine (item number 10005836; Cayman Chemical, Ann Arbor, MI), donepezil.HCl.H_2O (product number D6821; Sigma-Aldrich, St. Louis, MO) and galanthamine.HBr (product number G1660; Sigma, St. Louis, MO) as reference agents. Derivative stock solutions were dissolved in a minimum volume of DMSO (1%) and diluted using a 50 mM Tris–HCl, pH 8.0, 0.1 M NaCl, 0.02 M $MgCl_2.6H_2O$ buffer solution. In a standard 96-well plate, 160 µL 5,5'-dithiobis(2-nitrobenzoic acid) (1.5 mM DTNB prepared in buffer), 50 µL of *h*AChE (0.22 U/mL prepared in 50 mM Tris–HCl, pH 8.0, 0.1% w/v bovine serum albumin, BSA) or 50 µL of BuChE (0.06 U/mL prepared in 50 mM Tris–HCl, pH 8.0, 0.1% w/v BSA) were incubated with the various concentrations of test compounds (0.001–100 µM, 10 µL) at r.t for 5 min followed by the addition of 30 µL of the respective substrates (15 mM AThC or BuThC). The absorbance was measured at different time intervals (0-3 min) at a wavelength of 405 nm using a BioTek ELx800 microplate reader and percent inhibition was calculated by the comparison of compound treated to various control incubations that included 1% DMSO. The concentration of the test compound causing 50% inhibition (IC_{50}, µM) was calculated from the concentration-inhibition response curve on logarithmic scale (duplicate to quadruplicate determinations).

6.2.2. $A\beta_{1-40}$ Aggregation Assay

The *h*AChE-induced aggregation assay from Dr. Yang's group was previously reported in Ref. 121. The HFIP salt of $A\beta_{1-40}$ was purchased from Anaspec, Inc. (Cat. 64128-1), human recombinant AChE lyophilized powder and ThT were purchased from Sigma Aldrich (Cat. C1682 and T3516; respectively) and the *h*AChE-induced assay was run using propidium iodide (Cat. P4170; Sigma Aldrich) as a control. $A\beta_{1-40}$ was dissolved in DMSO (1 mL/mg) and sonicated for 30 min to obtain a 232 µM solution. *h*AChE

was dissolved in 215 mM sodium phosphate buffer (pH 8.0) to obtain a 4.69 μM solution. For the *h*AChE-induced assay, 4 μL of $A\beta_{1-40}$ were incubated with 20 μL of *h*AChE to give a final concentration of 23.2 μM of $A\beta_{1-40}$ and 2.35 μM of *h*AChE (10:1 ratio). For co-incubation experiments, 16 μL of test samples in 215 mM sodium phosphate buffer pH 8.0 solution (6% DMSO) (final concentration 100 μM) were used. For the self-induced assay, 4 μL of $A\beta_{1-40}$ was incubated with 16 μL of test samples in 215 mM sodium phosphate buffer pH 8.0 solution (6% DMSO) (final concentration 100 μM). The black Costar ®, clear bottom 96-well plates were incubated at room temperature for 24 hrs followed by the addition of 150 μL of 15 μM of thioflavin T in 50 mM glycine-NaOH buffer (pH 8.5). The plate was gently rocked for 2 min. and the fluorescence was monitored at 446 nm (excitation) and 490 nm (emission) using a Molecular Devices SpectraMax spectrofluorometer. The fluorescence intensities in the presence and absence of inhibitors before and after the incubation period were compared and the percentage of inhibition was calculated with equation: 100% control value (i.e. no inhibitor) - $[(IF_i - IF_o)]$ where IF_i and IF_o are the fluorescence intensities in the presence of ThT and absence of ThT before 24 hrs incubation, respectively.

6.2.3. β-secretase Assay

The instructions outlined in the PanVera ® BACE-1 screening kit (part # P2985; Madison, WI) were followed as directed with no deviations. Test samples were screened at various concentrations (0.1, 1, 10, 50 and 100 μM) to obtain an IC_{50} value along with donepezil (product number D6821; Sigma-Aldrich, St. Louis, MO) and a peptidic derivative (product number 565749; EMD-Merck) as reference agents. The results were an average of duplicate readings ($n = 2$).

6.2.4. MTT Assay

The cell viability assay from Dr. Yang's group (UCSD) was previously reported in Ref. 121 and the proceeding method was carried out Dr. Beazely's group (UW). The SH-SY5Y neuroblastoma cells were plated at density of 4×10^5 per mL in 96-well plates with complete growth media consisting of DMEM and Ham's F12 in a 1:1 ratio, supplemented with 2.5 mM glutamate and 10% fetal bovine serum at 37 °C in 5% CO_2. The cells were incubated overnight and treated with the test samples at a 40 μM concentration, for 24 hr at 37 °C ($n = 4$). The MTT in an amount equal to 10% of the culture medium volume was added to each

well and the cells were cultured for additional 3 hr at 37 °C in 5% CO_2. After incubation, the resulting formazan crystals were solubilized with MTT reagent solution (10% Triton X-100 and 0.1 N HCl in anhydrous isopropanol) in each well and the absorbance was recorded at 570 nm. All results were expressed as a percent reduction of MTT relative to untreated controls.

6.3. Computational Chemistry

Docking experiments were performed using Discovery Studio Client v2.5.0.9164 (2005-09), Accelrys Software Inc. The X-ray crystal structure coordinates for *h*AChE, *h*BuChE and *h*BACE-1 were obtained from the RCSB Protein Data Bank (PDB: 1B41, 1P0I, 1FKN) and hydrogens were added. The ligand molecules were constructed using the *Build Fragment* tool and energy minimized for 1000 iterations reaching a convergence of 0.01 kcal/mol Å. Docking experiments were carried out using the *Libdock* command in the receptor-ligand interactions protocol of Discovery Studio and the energy-minimized ligands after defining a 10-12 Å sphere radius subset within the enzyme. The Chemistry at HARvard Macromolecular Mechanics (CHARMM) force field, was employed for all docking purposes. The ligand-enzyme assembly was then subjected to a molecular dynamics (MD) simulation using *Simulation* protocol at a constant temperature of 300 K with a 100 step equilibration for over 1000 iterations and a time step of 1 fs using a distance dependent dielectric constant 4*r*. The optimal binding orientation of the ligand-enzyme assembly obtained after docking was further minimized for 1000 iterations using the conjugate gradient method until a convergence of 0.001 kcal/mol Å was reached after which $E_{\text{intermolecular}}$ (kcal/mol) of the ligand−enzyme assembly was evaluated and the distances measured.

• References •

1. Selkoe, D. J. Alzheimer's disease: Genes, proteins and therapy. *Physiol. Rev.* **2001**, *81*, 741-767.
2. Suh, W. H.; Suslick, K. S.; Suh, Y. H. Therapeutic agents for Alzheimer's disease. *Curr. Med. Chem.* **2005**, *5*, 259-269.
3. Klafki, H. W.; Staufenbiel, M.; Kornhuber, J.; Wiltfang, J. Therapeutic approaches to Alzheimer's disease. *Brain* **2006**, *129*, 2840-2855.
4. Hirono, N.; Hashimoto, M.; Yasuda, M.; Kazui, H.; Mori, E. Accelerated memory decline in Alzheimer's disease with apolipoprotein ε4 allele. *J. Neuropsychiatry Clin. Neurosci.* **2003**, *15*, 354-358.
5. Poirier, J. Apolipoprotein E in animal models of CNS injury and in Alzheimer's disease. *Trends Neurosci.* **1994**, *17*, 525-530.
6. Thies, W.; Bleiler, L. Alzheimer's association report – 2011 Alzheimer's disease facts and figures. *Alzheimer's & Dementia* **2011**, *7*, 208-244.
7. Maurer, K.; Volk, S.; Gerbaldo, H. Auguste D and Alzheimer's disease. *Lancet* **1997**, *349*, 1546-1549.
8. Selkoe, D. J. Alzheimer's disease is a synaptic failure. *Science* **2002**, *298*, 789-791.
9. Mohamed, T.; Rao, P. P. N. Alzheimer's disease: Emerging trends in small molecule therapies. *Curr. Med. Chem.* **2011**, *In Press*.
10. Lim, G. P.; Yang, F.; Chu, T.; Chen, P.; Beech, W.; Teter, B.; Tran, T.; Ubeda, O.; Hsiao Ashe, K.; Frautschy, S. A.; Cole, G. M. Ibuprofen suppresses plaque pathology and inflammation in a mouse model for Alzheimer's disease. *J. Neurosci.* **2000**, *20*, 5709-5714.
11. Hartmann, T. Cholesterol, Aβ and Alzheimer's disease. *Trends Neurosci.* **2001**, *24*, S45-S48.
12. Gasparini, L.; Xu, H. Potential roles of insulin and IGF-1 in Alzheimer's disease. *Trends Neurosci.* **2003**, *26*, 404-406.
13. Hirohata, M.; Ono, K.; Naiki, H.; Yamada, M. Non-steroidal anti-inflammatory drugs have anti-amyloidogenic effects for Alzheimer's β-amyloid fibrils in vitro. *Neuropharmacol.* **2005**, *49*, 1088-1099.

References – cont'd

14. Felician, O.; Sandson, T. A. The neurobiology and pharmacotherapy of Alzheimer's disease. *J. Neuropsychiatry Clin. Neurosci.* **1999**, *11*, 19-31.
15. Aboukhatwa, M.; Dosanjh, L.; Luo, Y. Antidepressants are a rational complementary therapy for the treatment of Alzheimer's disease. *Mol. Neurodegen.* **2010**, *5*, 1-17.
16. Frank-Cannon, T. C.; Alto, L. T.; McAlpine, F. E.; Tansey, M. G. Does neuroinflammation fan the flame in neurodegenerative diseases? *Mol. Neurodegen.* **2009**, *4*, 47-59.
17. Sayre, L. M.; Perry, G.; Smith, M. A. Oxidative stress and neurotoxicity. *Chem. Res. Toxicol.* **2008**, *21*, 172-188.
18. Zhao, X.; Marszalec, W.; Toth, P. T.; Huang, J.; Yeh, J. Z.; Narahashi, T. In vitro galantamine-memantine co-application: Mechanism of beneficial action. *Neuropharmacol.* **2006**, *51*, 1181-1191.
19. Matharu, B.; Gibson, G.; Parsons, R.; Huckerby, T. N.; Moore, S. A.; Cooper, L. J.; Millichamp, R.; Allsop, D.; Austen, B. Galantamine inhibits β-amyloid aggregation and cytotoxicity. *J. Neurol. Sci.* **2009**, *280*, 49-58,
20. Aisen, P. S.; Davis, K. L. The search for disease-modifying treatment for Alzheimer's disease. *Neurology* **1997**, *48*, S35-S41.
21. Scarpini, E.; Schelterns, P.; Feldman, H. Treatment for Alzheimer's disease; current status and new perspectives. *Lancet Neurol.* **2003**, *2*, 539-547.
22. Gauthier, S.; Poirier, J. Current and future management of Alzheimer's disease. *Alzheimer's Dement.* **2008**, *4*, S48-S50.
23. Salloway, S.; Mintzer, J.; Weiner, M. F.; Cummings, J. L. Disease-modifying therapies in Alzheimer's disease. *Alzheimer's Dement.* **2008**, *4*, 65-79.
24. Melnikova, I. Therapies for Alzheimer's disease. *Nat. Rev. Drug Disc.* **2007**, *6*, 341-342.
25. Currier, S. F.; Mautner, H. G. On the mechanism of action of choline acetyltransferase. *Proc. Natl. Acad. Sci. USA* **1974**, *71*, 3355-3358.
26. Francis, P. T.; Rameriz, M. J.; Lai, M. K. Neurochemical basis for symptomatic treatment of Alzheimer's disease. *Neuropharmacol.* **2010**, *59*, 221-229.

References – cont'd

27. Terry Jr., A. V.; Buccafusco, J. J. The cholinergic hypothesis of age and Alzheimer's disease – Related cognitive deficits: Recent challenges and their implications for novel drug development. *J. Pharmacol. Exper. Therap.* **2003**, *306*, 821-827.

28. Wilcock, G. K.; Esiri, M. M.; Bowen, D. M.; Smith, C. C. T. Alzheimer's disease: Correlation of cortical choline acetyltransferase activity with the severity of dementia and histological abnormalities. *J. Neurol. Sci.* **1982**, *57*, 407-417.

29. Kurz, A.; Perneczky, R. Novel insights for the treatment of Alzheimer's disease. *Progress Neuropsychopharmacol. Biol. Psych.* **2011**, *35*, 373-379.

30. Mihalak, K. B.; Carroll, F. I.; Luetje, C. W. Varenicline is a partial agonist at α4β2 and a full agonist at α7 neuronal nicotinic receptors. *Mol. Pharmacol.* **2006**, *70*, 801-806.

31. Merchant, C.; Tang, M. X.; Albert, S.; Manly, J.; Stern, Y.; Mayeux, R. The influence of smoking on the risk of Alzheimer's disease. *Neurology* **1995**, *52*, 1408-1413.

32. Massoulie, J.; Pezzementi, L.; Bon, S.; Krejci, E.; Vallette, F. M. Molecular and cellular biology of cholinesterases. *Prog. Neurobiol.* **1993**, *41*, 31-91.

33. Soreq, H.; Seidman, S. Acetylcholinesterase – new roles for an old actor. *Nat. Rev. Neurosci.* **2001**, *2*, 294-302.

34. Darvesh, S.; Hopkins, D. A.; Geula, C. Neurobiology of butyrylcholinesterase. *Nat. Rev. Neurosci.* **2003**, *4*, 131-138.

35. Chatonnet, A.; Lockridge, O. Comparison of butyrylcholinesterase and acetylcholinesterase. *Biochem. J.* **1989**, *260*, 625-634.

36. Vellom, D. C.; Radic, Z.; Li, Y.; Pickering, N. A.; Camp, S.; Taylor, P. Amino acid residues controlling acetylcholinesterase and butyrylcholinesterase specificity. *Biochemistry* **1993**, *32*, 12-17.

37. Greig, N. H.; Utsuki, T.; Ingram, D. K.; Wang, Y.; Pepeu, G.; Scali, C.; Yu, Q.; Mamczarz, J.; Holloway, H. W.; Giordano, T.; Chen, D.; Furukawa, K.; Sambamurti, K.; Brossi, A.; Lahiri, D. K. Selective butyrylcholinesterase inhibition elevates brain acetylcholine, augments learning and lowers Alzheimer β-amyloid peptide in rodent. *Proc. Natl. Acad. Sci. USA* **2005**, *102*, 17213-17218.

References – cont'd

38. Vellom, D. C.; Radic, Z.; Li, Y.; Pickering, N. A.; Camp, S.; Taylor, P. Amino acid residues controlling acetylcholinesterase and butyrylcholinesterase specificity. *Biochemistry* **1993**, *32*, 12-17.

39. Camps, P.; Formosa, X.; Galdeano, C.; Gomez, T.; Munzo-Torrero, D.; Scarpellini, M.; Viayna, E.; Badia, A.; Clos, M. V.; Camins, A.; Pallas, M.; Bartolini, M.; Mancini, F.; Andrisano, V.; Estelrich, J.; Lizondo, M.; Bidon-Chanal, A.; Luque, F. J. Novel donepezil-based inhibitors of acetyl- and butyrylcholinesterase and acetyl cholinesterase-induced β-amyloid aggregation. *J. Med. Chem.* **2008**, *51*, 3588-3598.

40. Bourne, Y.; Radic, Z.; Kolb, H. C.; Sharpless, K. B.; Taylor, P.; Marchot, P. Structural insights into conformational flexibility at the peripheral site and within the active center gorge of AChE. *Chem, Biol. Interact.* **2005**, *157-158*, 159-165.

41. Taylor, P.; Radic, Z. The cholinesterases: From genes to proteins. *Annu. Rev. Pharmacol. Toxicol.* **1994**, *34*. 281-320.

42. Shen, T.; Tai, K.; Henchman, R. H.; McCammon, J. A. Molecular dynamics of acetylcholinesterase. *Acc. Chem. Res.* **2002**, *35*, 332-340.

43. Barak, D.; Ordentlich, A.; Kaplan, D.; Kronman, C.; Velan, B.; Shafferman, A. Lessons from functional analysis of AChE covalent and noncovalent inhibitors for design of AD therapeutic agents. *Chem. Biol. Interact.* **2005**, *157-158*, 219-226.

44. Dickerson, T. J.; Beuscher IV, A. E.; Rogers, C. J.; Hixon, M. S.; Yamamoto, N.; Xu, Y.; Olson. A. J.; Janda, K. D. Discovery of acetyl cholinesterase peripheral anionic site ligands through computational refinement of a directed library. *Biochemistry* **2005**, *44*, 14845-14853.

45. Harel, M.; Schalk, I.; Ehret-Sabatier, L.; Bouet, F.; Goeldner, M.; Hirrth, C.; Axelsen, P. H.; Silman, I.; Sussman, J. L. Quaternary ligand binding to aromatic residues in the active-site gorge of acetylcholine esterase. *Proc. Natl. Acad. Sci. USA* **1993**, *90*, 9031-9035.

46. Inestrosa, N. C.; Dinamarca, M. C.; Alvarez, A. Amyloid-cholinesterase interactions – implications for Alzheimer's disease. *FEBS* **2008**, *275*, 625-632.

References – cont'd

47. Inestrosa, N. C.; Alvarez, A.; Perez, C. A.; Moreno, R. D.; Vincete, M.; Linker, C.; Casanueva, O. I.; Soto, C.; Garrido, J. Acetylcholinesterase accelerates assembly of amyloid-β-peptides into Alzheimer's fibrils: Possible role of the peripheral site of the enzyme. *Neuron* **1996**, *16*, 881-891.

48. Belluti, F.; Rampa, A.; Piazzi, L.; Bisi, A.; Gobbi, S.; Bartolini, M.; Andrisano, V.; Cavalli, A.; Recanatini, M.; Valenti, P. Cholinesterase inhibitors: Xanthostigmine derivatives blocking the acetyl cholinesterase-induced β-amyloid aggregation. *J. Med. Chem.* **2005**, *48*, 4444-4456.

49. Nicolet, Y.; Lockridge, O.; Masson, P.; Fontecilla-Camps, J. C.; Nachon, F. Crystal structure of human butyrylcholinesterase and of its complexes with substrate and products. *J. Biol. Chem.* **2003**, *278*, 41141-41147.

50. Greig, N. H.; Utsuki, T.; Ingram, D. K.; Wang, Y.; Pepeu, G.; Scali, C.; Yu, Q.; Mamczarz, J.; Holloway, H. W.; Giordano, T.; Chen, D.; Furukawa, K.; Sambamurti, K.; Brossi, A.; Lahiri, D. K. Selective butyrylcholinesterase inhibition elevates brain acetylcholine, augments learning and lowers Alzheimer β-amyloid peptide in rodent. *Proc. Natl. Acad. Sci. USA* **2005**, *102*, 17213-17218.

51. Darvesh, S.; Hopkins, D. A.; Geula, C. Neurobiology of butyrylcholinesterase. *Nat. Rev. Neurosci.* **2003**, *4*, 131-138.

52. Allderdice, P. W.; Gardner, H. A. R.; Galutira, D.; Lockridge, O.; Ladu, B. N.; McApline, P. J. The cloned butyrylcholinesterase (BCHE) gene maps to a single chromosome site, 3q26. *Genomics* **1991**, *11*, 452-454.

53. Giacobini E. Comparison of the structures of butyrylcholinesterase and acetylcholinesterase. In Giacobini E. (ed.), Butyrylcholinesterase: Its function and inhibitors, Martin Dunitz, London, **2003**, 42-44.

54. Nicolet, Y.; Lockridge, O.; Masson, P.; Fontecilla-Camps, J. C.; Nachon, F. Crystal structure of human butyrylcholinesterase and of its complexes with substrate and products. *J. Biol. Chem.* **2003**, *278*, 41141-41147.

References – cont'd

55. Saxena, A.; Redman, A. M. G.; Jiang, X.; Lockridge, O.; Doctor, B. P. Differences in active-site gorge dimensions of cholinesterases revealed by binding of inhibitors to human butyrylcholinesterase. *Chem. Biol. Interact.* **1999**, *119–120*, 61–69.

56. Teller, J. K.; Russo, C.; Debusk, L. M.; Angelini, G.; Zaccheo, D.; Dagna-Bricarelli, F.; Scartezzini, P.; Bertolini, S.; Mann, D. M. A.; Tabaton, M.; Gambetti, P. Presence of soluble amyloid-β peptide precedes amyloid plaque formation in Down's syndrome. *Nat. Med.* **1996**, *2*, 93-95.

57. Koo, E. H.; Lansbury Jr., P. T.; Kelly, J. W. Amyloid diseases: Abnormal protein aggregation in neurodegeneration. *Proc. Natl. Acad. Sci. USA* **1999**, *96*, 9989-9990.

58. Barger, S. W.; Horster, D.; Furukawa, K.; Goodman, Y.; Krieglstein, J.; Mattson, M. P. Tumor necrosis factors α and β protect neurons against amyloid β-peptide toxicity: Evidence for involvement of a κB-binding factor and attenuation of peroxide and Ca^{2+} accumulation. *Proc. Natl. Acad. Sci. USA* **1995**, *92*, 9328-9332.

59. Tarr, P. E.; Roncarati, R.; Pelicci, G.; Pelicci, P. G.; D'Adamio, L. Tyrosine phosphorylation of the β-amyloid precursor protein cytoplasmic tail promotes interaction with Shc. *J. Biol. Chem.* **2002**, *277*, 16798-16804.

60. Mattson, M. P. Pathways towards and away from Alzheimer's disease. *Nature* **2004**, *430*, 631-640.

61. Zheng, H.; Koo, E. H. The amyloid precursor protein: Beyond amyloid. *Mol. Neurodegener.* **2006**, *1*, 5-16.

62. Suh, Y.; Checler, F. Amyloid precursor protein, presenilins, and α-synuclein: Molecular pathogenesis and pharmacological applications in Alzheimer's disease. *Pharmacol. Rev.* **2002**, *54*, 469-525.

63. Selkoe, D. J. Physiological production of the β-amyloid protein and the mechanism of Alzheimer's disease. *Trends Neurosci.* **1993**, *16*, 403-409.

64. Cerpa, W. F.; Barria, M. I.; Chacon, M. A.; Suazo, M.; Gonzalez, M.; Opazo, C.; Bush, A. I.; Inestrosa, N. C. The N-terminal copper-binding domain of the amyloid precursor protein protects against Cu^{2+} neurotoxicity in vivo. *FASEB J.* **2004**, *18*, 1701-1703.

References – cont'd

65. Priller, C.; Bauer, T.; Mitteregger, G.; Krebs, B.; Kretzschmar, H. A.; Herms, J. Synapse formation and function is modulated by the amyloid precursor protein. *J. Neurosci.* **2006**, *26*, 7212-7221.

66. Wang, H.; Barreyro, L.; Provasi, D.; Djemil, I.; Torres-Arancivia, C.; Filizola, M.; Ubarretxena-Belandia, I. Molecular determinants and thermodynamics of the amyloid precursor protein transmembrane domain implicated in Alzheimer's disease. *J. Mol. Biol.* **2011**, *408*, 879-895.

67. Dahmas, S. O.; Hoefgen, S.; Roeser, D.; Schlott, B.; Guhrs, K.; Than, M. E. Structure and biochemical analysis of the heparin-induced E1 dimer of the amyloid precursor protein. *Proc. Natl. Acad. Sci. USA* **2010**, *107*, 5381-5386.

68. Ohkawara, T.; Nagase, H.; Koh, C.; Nakayama, K. The amyloid precursor protein intracellular domain alters gene expression and induces neuron-specific apoptosis. *Gene* **2011**, *475*, 1-9.

69. Hardy, J. Amyloid, the presenilins and Alzheimer's disease. *Trends Neurosci.* **1997**, *20*, 154-159.

70. Pakaski, M.; Kalman, J. Interactions between the amyloid and cholinergic mechanisms in Alzheimer's disease. *Neurochem. Inter.* **2008**, *53*, 103-111.

71. Hemming, M. L.; Elias, J. E.; Gygi, S. P.; Selkoe, D. J. Identification of β-secretase (BACE1) substrates using quantitative proteomics. *PLoS ONE* **2009**, *4*, e8477.

72. Citron, M. β-Secretase inhibition for the treatment of Alzheimer's disease – promise and challenge. *Trends Pharm. Sci.* **2004***, 25*, 92-97.

73. Skovronsky, D. M.; Lee, V. M-Y. β-Secretase revealed: Starting gate for race to novel therapies for Alzheimer's disease. *Trends Pharm. Sci.* **2000**, *21*, 161-163.

74. Parvathy, S.; Hussain, I.; Karran, E. H.; Turner, A. J.; Hooper, N. M. Cleavage of Alzheimer's amyloid precursor protein by α-secretase occurs at the surface of neuronal cells. *Biochemistry* **1999**, *38*, 9728-9734.

75. Lichtenthaler, S. F.; Haass, C. Amyloid at the cutting edge: Activation of α-secretase prevents amyloidogenesis in an Alzheimer's disease mouse model. *J. Clin. Investig.* **2004**, *113*, 1384-1387.

References – cont'd

76. Sinha, S. The metabolism of the amyloid precursor protein and its relevance to Alzheimer's disease. *Prespect. Drug Discov. Design* **1994**, *2*, 363-369.

77. Ghosh, A. K.; Gemma, S.; Tang, J. β-secretase as a therapeutic target for Alzheimer's disease. *Neurotherapeutics* **2008**, *5*, 399-408.

78. Vassar, R. BACE-1: The β-secretase enzyme in Alzheimer's disease. *J. Mol. Neurosci.* **2004**, *23*, 105-113.

79. Howlett, D. R.; Simmons, D. L.; Dingwall, C.; Christie, G. In search of an enzyme: the β -secretase of Alzheimer's disease is an aspartic proteinase. *Trends Neurosci.* **2000**, *23*, 565-570.

80. Citron, M. β-Secretase inhibition for the treatment of Alzheimer's disease – promise and challenge. *Trends Pharm. Sci.* **2004***, 25*, 92-97.

81. Skovronsky, D. M.; Lee, V. M-Y. β-Secretase revealed: Starting gate for race to novel therapies for Alzheimer's disease. *Trends Pharm. Sci.* **2000**, *21*, 161-163.

82. Rajamani, R.; Reynolds, C. H. Modeling the protonation states of the catalytic aspartates in β-secretase. *J. Med. Chem.* **2004**, *47*, 5159-5166.

83. Spronk, S. A.; Carlson, H. A. The role of tyrosine 71 in modulating the flap conformations of BACE-1. *Proteins: Struct., Funct. and Bioinform.* **2011**, *79*, 2247-2259.

84. Stockley, J. H.; O'Neil, C. Understanding BACE1: essential protease for amyloid-β production in Alzheimer's disease. *Cell Mol. Life Sci.* **2008**, *65*, 3265-3289.

85. Shimizu, H.; Tosaki, A.; Kaneko, K.; Hisano, T.; Sakurai, T.; Nukina, N. Crystal structure of an active form of BACE1, an enzyme responsible for amyloid-β protein production. *Mol. Cell. Biol.* **2008**, *28*, 3663-3671.

86. Hong, L.; Turner III, R. T.; Koelsch, G.; Shin, D.; Ghosh, A. K.; Tang, J. Crystal structure of memapsin 2 (β-secretase) in complex with an inhibitor OM00-3. *Biochemistry* **2002**, *41*, 10963-10967.

87. Bell, K. F. S.; Zheng, L.; Fahrenholz, F.; Cuello, A. C. ADAM-10 over-expression increases cortical synaptogenesis. *Neurobiol. Aging* **2008**, *29*, 554-565.

References – cont'd

88. Randall, A. D.; Witton, J.; Booth, C.; Hynes-Allen, A.; Brown, J. T. The functional neurophysiology of the amyloid precursor protein (APP) processing pathway. *Neuropharmacol.* **2010**, *59*, 243-267.

89. Zhou, S.; Zhou, H.; Walian, P. J.; Jap, B. K. Regulation of γ-secretase activity in Alzheimer's disease. *Biochemistry* **2007**, *46*, 2553-2563.

90. Fraering, P. C.; Ye, W.; LaVoie, M. J.; Ostaszewski, B. L.; Selkoe, D. J.; Wolfe, M. S. γ-secretase substrate specificity can be modulated directly via interaction with a nucleotide-binding site. *J. Biol. Chem.* **2005**, *280*, 41987-41996.

91. Wolfe, M. S. The γ-secretase complex: Membrane-embedded proteolytic ensemble. *Biochemistry* **2006**, *45*, 7931-7939.

92. Raurell, I.; Codina, M.; Casagolda, D.; Valle, B.; Baulida, J.; Herreros, A. G.; Dunach, M. Gamma-secretase-dependant and independent effects of presenilin1 on β-catenin·Tcf-4 transcriptional activity. *PLoS ONE* **2008**, *3*, e4080.

93. Small, D. H.; Klaver, D. W.; Foa, L. Presenilins and the γ-secretase: Still a complex problem. *Mol. Brain* **2010**, *3*, 7-12.

94. Beel, A. J.; Barrett, P.; Schnier, P. D.; Hitchcock, S. A.; Bagal, D.; Sanders, C. R.; Jordan, J. B. Nonspecificity of binding of γ-secretase modulators to the amyloid precursor protein. *Biochemistry* **2003**, *48*, 11837-11839.

95. Munoz, F. J.; Inestora, N. C. Neurotoxicity of the acetylcholinesterase amyloid-β-peptide aggregates in dependant on the type of Aβ-peptide and the AChE concentration present in complexes. *FEBS Lett.* **1999**, *450*, 205-209.

96. Hu, X.; Crick, S. L.; Bu, G.; Frieden, C.; Pappu, R. V.; Lee, J. Amyloid seeds formed by cellular uptake, concentration, and aggregation of the amyloid-beta peptide. *Proc. Natl. Acad. Sci. USA* **2009**, *106*, 20324-20329.

97. Schmidt, M.; Sachse, C.; Richter, W.; Xu, C.; Fandrich, M.; Grigorieff, N. Comparison of Alzheimer Aβ(1-40) and Aβ(1-42) amyloid fibrils reveals similar protofilament structures. *Proc. Natl. Acad. Sci. USA* **2009**, *106*, 19813-19818.

References – cont'd

98. Karr, J. W.; Akintoye, H.; Kaupp, L. J.; Szalai, V. A. N-terminal deletions modify the Cu^{2+} binding site in amyloid-β. *Biochemistry* **2005**, *44*, 5478-5487.

99. Chen, T.; Wang, X.; He, Y.; Zhang, C.; Wu, Z.; Liao, K; Wang, J.; Guo, Z. Effects of cyclen and cyclam on zinc(II)- and copper(II)-induced amyloid β-peptide aggregation and neurotoxicity. *Inorg. Chem.* **2009**, *48*, 5801-5809.

100. Smith, D. P.; Ciccotosto, G. D.; Tew, D. J.; Fodero-Tavoletti, M. T.; Johanssen, T.; Masters, C. L.; Barnham, K. J.; Cappi, R. Concentration dependent Cu^{2+} induced aggregation and dityrosine formation of the Alzheimer's disease amyloid-β peptide. *Biochemistry* **2007**, *46*, 2881-2891.

101. Nakamura, M.; Shishido, N.; Nunomura, A.; Smith, M. A.; Perry, G.; Hayashi, Y.; Nakayama, K.; Hayashi, T. Three histidine residues of amyloid-β peptide control the redox activity of copper and iron. *Biochemistry* **2007**, *46*, 12737-12743.

102. Sarell, C. J.; Syme, C. D.; Rigby, S. E. J.; Viles, J. H. Copper(II) binding to amyloid-β fibrils of Alzheimer's disease reveals a picomolar affinity: Stoichiometry and coordination geometry are independent of Aβ oligomeric form. *Biochemistry* **2009**, *48*, 4388-4402.

103. Ha, C.; Ryu, J.; Park, C. B. Metal ions differentially influence the aggregation and deposition of Alzheimer's β-amyloid on a solid template. *Biochemistry* **2007**, *46*, 6118-6125.

104. Scott, L. E.; Orvig, C. Medicinal inorganic chemistry approaches to passivation and removal of aberrant metal ions in disease. *Chem. Rev.* **2009**, *109,* 4885-4910.

105. Zatta, P.; Drago, D.; Bolognin, S.; Sensi, S. L. Alzheimer's disease, metal ions and metal homeostatic therapy. *Trends Pharm. Sci.* **2009**, *30*, 346-355.

106. Bush, A. I. The metallobiology of Alzheimer's disease. *Trends Neurosci.* **2003**, *26*, 207-214.

107. Francis, P. T.; Ramirez, M. J.; Lai, M. K. Neurochemical basis for symptomatic treatment of Alzheimer's disease. *Neuropharmacol.* **2010**, *59*, 221-229.

108. Proctor, C. J.; Gray, D. A. GSK3 and p53 – is there a link in Alzheimer's disease? *Mol. Neurodegen.* **2010**, *5*, 7-21.

References – cont'd

109. Cruz, J. C.; Tseng, H.; Goldman, J. A.; Shih, H.; Tsai, L. Aberrant Cdk5 activation by p25 triggers pathological events leading to neurodegeneration and neurofibrillary tangles. *Neuron* **2003**, *40*, 471-483.

110. Liu, M.; Choi, S.; Cuny, G. D.; Ding, K.; Dobson, B. C.; Glicksman, M. A.; Auerbach, K.; Stein, R. L. Kinetic studies of Cdk5/p25 kinase: Phosphorylation of tau and complex inhibition by two prototype inhibitors. *Biochemistry* **2008**, *47*, 8367-8377.

111. Li, T.; Paudel, H. K. Glycogen synthase kinase 3β phosphorylates Alzheimer's disease–specific Ser^{396} of microtubule-associated protein tau by a sequential mechanism. *Biochemistry* **2006**, *45*, 3125-3133.

112. Hoey, S. E.; Williams, R. J.; Perkinton, M. S. Synaptic NMDA receptor activation stimulates α-secretase amyloid precursor protein processing and inhibits amyloid-β production. *J. Neurosci.* **2009**, *29*, 4442-4460.

113. Frank-Cannon, T. C.; Alto, L. T.; McAlpine, F. E.; Tansey, M. G. Does neuroinflammation fan the flame in neurodegenerative diseases? *Mol. Neurodegen.* **2009**, *4*, 47-59.

114. Medeiros, R.; Figueiredo, C. P.; Pandolfo, P.; Duarte, F. S.; Prediger, R. D. S.; Passos, G. F.; Calixto, J. B. The role of TNF-α signaling pathway on COX-2 upregulation and cognitive decline induced by β-amyloid peptide. *Behaviour. Brain Res.* **2010**, *209*, 165-173.

115. Pratico, D.; Zhukareva, V.; Yao, Y.; Uryu, K.; Funk, C. D.; Lawson, J. A.; Trojanowski, J. Q.; Lee, V. M-Y. 12/15-lipooxygenase is increased in Alzheimer's disease. *Am. J. Pathol.* **2004**, *164*, 1655-1662.

116. Tobinick, E. L.; Gross, H. Rapid cognitive improvement in Alzheimer's disease following peri-spinal etanercept administration. *J. Neuroinflamm.* **2008**, *5*, 2-11.

117. McGeer, P. L.; Rogers, J.; McGeer, E. G. Inflammation, anti-inflammatory agents and Alzheimer's disease: The last 12 years. *J. Alz. Dis.* **2006**, *9*, 271-276.

References – cont'd

118. Lee, L. L.; Ha, H.; Chang, Y.; Delisa, M. P. Discovery of amyloid-beta aggregation inhibitors using an engineered assay for intracellular protein folding and solubility. *Protein Sci.* **2009**, *18*, 277-286.

119. Garino, C.; Tomita, T.; Pietrancosta, N.; Laras, Y.; Rosas, R.; Herbette, G.; Maigret, B.; Quelever, G.; Iwatsubo, T.; Kraus, J. Naphthyl and coumarinyl biarylpiperazine derivatives as highly potent human β-secretase inhibitors. Design, synthesis and enzymatic BACE-1 and cell assays. *J. Med. Chem.* **2006**, *49*, 4275-4285.

120. Mohamed, T.; Rao, P. P. N. Design, synthesis and evaluation of 2,4-disubstituted pyrimidines as cholinesterase inhibitors. *Bioorg. Med. Chem. Lett.* **2010**, *20*, 3606-3609.

121. Mohamed, T.; Zhao, X.; Habib, L. K.; Yang, J.; Rao, P. P. N. Design, synthesis and structure-activity relationship (SAR) studies of 2,4-disubstituted pyrimidine derivatives: Dual activity as cholinesterase and Aβ-aggregation inhibitors. *Bioorg. Med. Chem.* **2011**, *19*, 2269-2281.

122. Mohamed, T.; Yeung, J. C. K.; Rao, P. P. N. Development of 2-Substituted *N*-(Naphth-1-ylmethyl)- and *N*-Benzhydryl-Pyrimidin-4-Amines as Dual Cholinesterase and Aβ-Aggregation Inhibitors: Synthesis and Biological Evaluation. *Bioorg. Med. Chem. Lett.* **2011**, *In Press*.

123. Ellman, G. L.; Courtney, K. D.; Andres, V. Jr.; Featherstone, R. M. A new and rapid colorimetric determination of acetylcholinesterase activity. *Biochem. Pharmacol.* **1961**, *7*, 88-95.

124. Bourhim, M.; Kruzel, M.; Srikrishnan, T.; Nicotera, T. Linear quantification of Aβ aggregation using Thioflavin T: Reduction in fibril formation by colostrinin. *J. Neurosci. Methods* **2007**, *160*, 264-268.

125. Khurana, R.; Coleman, C.; Ionescu-Zanetti, C.; Carter, S. A.; Krishna, V.; Grover, R. K.; Roy, R.; Singh, S. Mechanism of thioflavin T binding to amyloid fibrils. *J. Struc. Biol.* **2005**, *151*, 229-238.

126. Biancalana, M.; Koide, S. Molecular mechanism of Thioflavin-T binding to amyloid fibrils. *Biochim. Biophys. Acta* **2010**, *1804*, 1405-1412.

127. Mosmann, T. Rapid colorimetric assay for cellular growth and survival: Application to proliferation and cytotoxicity assays. *J. Immunol. Methods* **1983**, *65*, 55-63.

References – cont'd

128. Matharu, B.; Gibson, G.; Parsons, R.; Huckerby, T. N.; Moore, S. A.; Cooper, L. J.; Millichamp, R.; Allsop, D.; Austen, B. Galantamine inhibits β-amyloid aggregation and cytotoxicity. *J. Neurol. Sci.* **2009**, *280*, 49.